Development of In-Situ sensors for Nutrients in Marine Waters

DISSERTATION

ZUR ERLANGUNG DES DOKTORGRADES

DER MATHEMATISCH - NATURWISSENSCHAFTLICHEN FAKULTÄT

DER CHRISTIAN-ALBRECHTS-UNIVERSITÄT ZU KIEL

VORGELEGT VON

Mahmoud Fatehy Abdalqader Altahan

Kiel, August 2022

GUTACHTER

Prof. Eric P. Achterberg

1. Gutachter: Prof. Dr. Eric P. Achterberg

2. Gutachterin : Prof. Dr. Sylvia Sander

Datum for Disputation: 25.10.2022

Achknowldements and dedication

I would like to express my special thanks to Prof. Dr. Eric Achterberg, who gave me the opportunity to work on this project. I believe that this work would not have been accomplished without his support, encouragement, mentoring, and valuable advice.

I would like to thank Dr. Mario Esposito for his patience and wise advice during the laboratory work and also during the field expedition. I believe that I gained many of my experiences during this work from valuable discussions with him.

I would like to thank all members of AG Achterberg for their helpfulness and cooperation.

Finally, but not least, I would like to dedicate this work to my family, especially my father and my mother's soul, my brother, my wife and my child Ziad for their endless love and support in my life.

Summary

In recent decades, the demand for autonomous on-site and in-situ chemical monitoring in natural waters has increased. The reason is that real-time monitoring facilitates high resolution data collection which allows us to improve our mechanistic and quantitative understanding of biogeochemical processes. Monitoring provides spatially or temporally well-resolved data, which cannot be obtained by conventional sampling and analysis using classical laboratory methods.

In particular, I focussed on the development, improvement, and deployment of autonomous analysers for on-site monitoring of nutrients that have shown promise for further application in field monitoring either on shore or in the water column (in-situ). Macronutrients include nitrate, nitrite, phosphate, and silicic acid. These macronutrients are important for primary production, and silicic acid is essential for the hard tissue of siliceous phytoplankton (e.g., diatoms). The importance of macronutrients for photosynthesis means that their supply rates have major implications for the functioning of phytoplankton communities, which are considered an carbon dioxide sink in the ocean. The analysis of macronutrients is still more difficult than physical parameters such as salinity and temperature or dissolved oxygen. In addition, analysis of macronutrients in a complex matrix such as seawater can be challenging because their concentrations are typically low, in the range from nanomolar to micromolar. This thesis reports on the development of an electrochemical approach for the determination of orthophosphate in estuarine and seawater, reporting the initial investigations of our technique with a further application in an automated analyser which uses a bipotentiostat approach to enhance data quality. In addition, the improvement of on-site determination of macronutrients (including phosphate (PO_4^{3-}), nitrate plus nitrite ($\Sigma(NO_3^- + NO_2^-)$), and silicic acid (H_4SiO_4)) with a long-term application in estuarine and coastal water is reported.

The main findings are as follows:

- A carbon paste electrode modified with ammonium molybdate in a 10:1 ratio was successfully used in square wave voltammetry (SWV) with optimized conditions for PO_4^{3-} under acidic conditions (pH 0.8) after pre-treatment by cyclic voltammetry into sodium hydroxide solution Laboratory-based characterizations showed a a good correlation between the peak current and PO_4^{3-} concentration in a calibration plot into artificial seawater with a corresponding detection limit of 0.003 μM. The exclusion of H_4SiO_4 as the main interferent of PO_4^{3-} in seawater was also demonstrated through optimisation of pH.

- The validation of the proposed method was demonstrated by the analysis of discrete samples collected during a research cruise with a CTD rosette sampler. Comparison with the concentration obtained using a colorimetric analyser with air segmented flow resulted in a correlation coefficient of 0.75.

- Our new electrochemical method was further developed for use in an automaed on-site sensor for PO_4^{3-} in seawater using a portable bi-potentiostat. The bi-potentiostat was used with two working electrodes sharing the same reference and auxiliary electrodes; the first working electrode was a molybdate/CPE and the second working electrode was a CPE. The bi-potentiostat allowed us to correct for matrix interferences and variations in working electrode sensitivity.

- Data processing was automated using a Python script. The laboratory-based characterization yielded two discrete linear ranges, a low range (0.02-0.2 μM) and a high range (0.5-3 μM), with a limit of detection of 0.014 μM. Another application was the on-line determination of PO_4^{3-} in seawater during a research cruise in the German Bight (Southwestern North Sea) in the discharge plume of the Elbe River. A good correlation (Pearson correlation coefficient of 0.91) was obtained by comparison with discretely collected samples which were analysed with a colorimetric laboratory analyser.

- A multi-macronutrient analyser (AutoLAB, developed by EnvironTech LLC, USA) was improved by optimising the measurement protocols for PO_4^{3-} and H_4SiO_4 and introducing the application of the vanadium chloride reduction method for the analysis of $\Sigma(NO_3^- + NO_2^-)$. Data processing with optical correction, which depends on the light intensity passed through the analyte sample before reagent addition, contributes significantly to the correction of matrix effects. Laboratory-based characterization showed a wide linear range up to 100 μM, demonstrating the broad applicability of the Analyser under the optimized protocol for various aquatic environments. The limits of detection (LOD) obtained were 0.18 μM, 0.15 μM, 0.45 μM, and 0.35 μM for PO_4^{3-}, H_4SiO_4, NO_3^-, and NO_2^-, respectively.

- Validation of the AutoLAB Analyser with our improved protocol was performed by analysis of certified reference material (CRM, Kanso, Japan), and field tests were conducted for 46 days on a pontoon on the Kiel Inner Fjord. Good correlation was obtained for 443, 440, and 409 field-collected data points for PO_4^{3-}, $\Sigma(NO_3^- + NO_2^-)$, and H_4SiO_4, respectively, with discrete samples collected and analysed in the laboratory using a colorimetric analyser based on a reference standard.

Overall, this dissertation contributes to the field of nutrient analysis in seawater (estuaries and the open ocean) by describing a simple electrochemical autonomous analyser for a single nutrient and

also the improvement and application of a commercial multi-nutrient analyser. The work details an improved measurement routine with the first application of the vanadium chloride reduction assay for nitrate, which overcomes the drawbacks of the cadmium column application. Autonomous on-site monitoring facilitates us to establish a large data set for nutrients in seawater and contributes to a better understanding of biogeochemical processes.

Zusammenfassung

In den letzten Jahrzehnten hat die Nachfrage nach autonomer chemischer Vor-Ort- und In-situ-Überwachung in natürlichen Gewässern zugenommen. Der Grund dafür ist, dass die Überwachung in Echtzeit eine hochauflösende Datenerfassung ermöglicht, die es uns erlaubt, unser mechanistisches und quantitatives Verständnis der biogeochemischen Prozesse zu verbessern. Die Überwachung liefert räumlich oder zeitlich gut aufgelöste Daten, die mit herkömmlichen Probenahmen und Analysen mit klassischen Labormethoden nicht gewonnen werden können.

Ich habe mich insbesondere auf die Entwicklung, Verbesserung und den Einsatz von autonomen Analysegeräten für die Vor-Ort-Überwachung von Nährstoffen konzentriert, die sich als vielversprechend für die weitere Anwendung bei der Feldüberwachung entweder an Land oder in der Wassersäule (in-situ) erwiesen haben. Zu den Makronährstoffen gehören Nitrat, Nitrit, Phosphat und Kieselsäure. Diese Makronährstoffe sind wichtig für die Primärproduktion, und die Kieselsäure ist für das harte Gewebe des kieselhaltigen Phytoplanktons (z. B. Kieselalgen) unerlässlich. Die Bedeutung der Makronährstoffe für die Photosynthese bedeutet, dass ihre Versorgungsraten große Auswirkungen auf das Funktionieren der Phytoplanktongemeinschaften haben, die als Kohlendioxidsenke im Ozean gelten. Die Analyse von Makronährstoffen ist immer noch schwieriger als physikalische Parameter wie Salzgehalt und Temperatur oder gelöster Sauerstoff. Darüber hinaus kann die Analyse von Makronährstoffen in einer komplexen Matrix wie dem Meerwasser eine Herausforderung darstellen, da ihre Konzentrationen in der Regel niedrig sind und im Bereich von nanomolar bis mikromolar liegen.

In dieser Arbeit wird über die Entwicklung einer elektrochemischen Methode zur Bestimmung von Orthophosphat in Ästuar- und Meerwasser berichtet, wobei die ersten Untersuchungen unserer Technik mit einer weiteren Anwendung in einem automatischen Analysator, der einen Bi-Potentiostat-Ansatz zur Verbesserung der Datenqualität verwendet, vorgestellt werden. Darüber hinaus wird über die Verbesserung der Vor-Ort-Überwachung von Makronährstoffen (einschließlich Phosphat (PO_4^{3-}), Nitrat und Nitrit ($\Sigma(NO_3^- + NO_2^-)$) und Kieselsäure (H_4SiO_4)) mit einer Langzeitanwendung in Ästuarwasser berichtet.

Die wichtigsten Ergebnisse sind wie folgt:

- Eine mit Ammoniummolybdat im Verhältnis 10:1 modifizierte Kohlenstoffpastenelektrode wurde erfolgreich in der Rechteckvoltammetrie (SWV) mit optimierten Bedingungen für PO43- unter sauren Bedingungen (pH 0,8) nach Vorbehandlung mit zyklischer Voltammetrie (CV)

eingesetzt. Laborbasierte Charakterisierungen zeigten einen linearen Bereich in künstlichem Meerwasser mit einer entsprechenden Nachweisgrenze von 0,003 µM. Der Ausschluss von H_4SiO_4 als Hauptinterferent von PO_4^{3-} in Meerwasser wurde auch durch die Optimierung des pH-Werts nachgewiesen.

- Die Validierung der vorgeschlagenen Methode wurde durch die Analyse von diskreten Proben demonstriert, die während einer Forschungsfahrt mit einem CTD-Rosetten-Sammler gesammelt wurden. Der Vergleich mit der Konzentration, die mit einem kolorimetrischen Analysator mit luftgeteilter Strömung ermittelt wurde, ergab einen Korrelationskoeffizienten von 0,75.

- Unsere neue elektrochemische Methode wurde für den Einsatz in einem automatischen Vor-Ort-Sensor für PO_4^{3-} in Meerwasser unter Verwendung eines tragbaren Bi-Potentiostaten weiterentwickelt. Der Bi-Potentiostat wurde mit zwei Arbeitselektroden verwendet, die sich dieselben Referenz- und Hilfselektroden teilen; die erste Arbeitselektrode war ein Molybdat/CPE und die zweite Arbeitselektrode war ein CPE. Der Bi-Potentiostat ermöglichte die Korrektur von Matrixinterferenzen und Schwankungen der Empfindlichkeit der Arbeitselektrode.

- Die Datenverarbeitung wurde mithilfe eines Python-Skripts automatisiert. Die laborgestützte Charakterisierung ergab zwei diskrete lineare Bereiche, einen niedrigen Bereich (0,02-0,2 µM) und einen hohen Bereich (0,5-3 µM), mit einer Bestimmungsgrenze von 0,014 µM. Eine weitere Anwendung war die Online-Bestimmung von PO_4^{3-} in Meerwasser während einer Forschungsfahrt in der Nordsee in der Abflussfahne des Flusses Elbe. Eine gute Korrelation (Pearson-Korrelationskoeffizient von 0,91) wurde durch den Vergleich mit diskret gesammelten Proben erzielt, die mit einem kolorimetrischen Laboranalysator analysiert wurden.

- Ein Multi-Makronährstoff-Analysator (AutoLAB, entwickelt von EnvironTech LLC, USA) wurde verbessert, indem die Messprotokolle für PO_4^{3-} und H_4SiO_4 optimiert und die Anwendung der Vanadiumchlorid-Reduktionsmethode für die Analyse von $\Sigma(NO_3^- + NO_2^-)$ eingeführt wurden. Die Datenverarbeitung mit optischer Korrektur, die von der Lichtintensität abhängt, die vor der Reagenzienzugabe durch die Analytprobe geleitet wird, trägt wesentlich zur Korrektur von Matrixeffekten bei. Die laborgestützte Charakterisierung ergab einen breiten linearen Bereich bis zu 100 µM, was die breite Anwendbarkeit des Analysators unter dem optimierten Protokoll für verschiedene aquatische Umgebungen belegt. Die erzielten Bestimmungsgrenzen lagen bei 0,18 µM, 0,15 µM, 0,45 µM und 0,35 µM für PO_4^{3-}, H_4SiO_4, NO_3^- bzw. NO_2^-.

- Die Validierung des AutoLAB-Analysegeräts mit unserem verbesserten Protokoll erfolgte durch die Analyse von zertifiziertem Referenzmaterial (CRM, Kanso, Japan), und es wurden 46 Tage lang

Feldtests auf einem Ponton auf der Kieler Innenförde durchgeführt. Eine gute Korrelation wurde für 443, 440 und 409 im Feld gesammelte Datenpunkte für PO_4^{3-}, $\Sigma(NO_3^- + NO_2^-)$ bzw. H_4SiO_4 mit diskreten Proben erzielt, die im Labor mit einem kolorimetrischen Analysator auf der Grundlage eines Referenzstandards gesammelt und analysiert wurden.

Insgesamt leistet diese Dissertation einen Beitrag zum Bereich der Nährstoffanalyse im Meerwasser (Ästuare und offener Ozean), indem sie einen einfachen elektrochemischen autonomen Analysator für einen einzelnen Nährstoff sowie die Verbesserung und Anwendung eines kommerziellen Multinährstoff-Analysators beschreibt. Die Arbeit beschreibt eine verbesserte Messroutine mit der ersten Anwendung des Vanadiumchlorid-Reduktionstests für Nitrat, der die Nachteile der Anwendung der Cadmiumsäule überwindet. Die autonome Vor-Ort-Überwachung ermöglicht es uns, einen großen Datensatz für Nährstoffe im Meerwasser zu erstellen und trägt zu einem besseren Verständnis der biogeochemischen Prozesse bei.

Table of Contents

Acronyms

1
12-Molybdophosphaeric acid (12-MPA) 51
A
absorbed light (I) 50
ammonia (NH_3) 10
ammonium (NH_4^+) 10
amperes (A) 41
AnaLyseur CHIMique In SiTu (ALCHEMIST) 35
B
brucite ($Mg(OH)_2$) 25
C
carbon paste electrode (CPE) 61
certified reference materials (CRM) 34
cetyltrimethylammonium bromide (CTAB) 26
charge transfer resistance (RCT) 42
clockwise (CW) 46
counterclockwise (CC) 46
cyclic voltammetry (CV(
D
digital output pin (DIO) 47
digital-to-analogue converter (DAC) 46
dihydrogen phosphate ($H_2PO_4^-$) 24
dinitrogen (N_2) 14
Direct headspace (HS) 30
Dissimilatory nitrate reduction (DNRA) 14
Dissimilatory Nitrate Reduction to Ammonium (DNRA) 9
dissolved organic nitrogen (DON) 10, 15
Dissolved organic phosphorus compounds (DOP) 16
dissolved reactive phosphate (DRP) 24
double layer capacitor (Cdl) 42
double-beam spectrophotometer (DBS) 44
double-electrochemical cell detector ECD) 87
E
Electrochemical impedance spectroscopy (EIS) 42
electrolyte resistance (RS) 42
F
flow injection analysis (FIA) 33
frequency (*f*). 42
field-emission scanning electron microscope (FE-SEM) 60
G
gas chromatography-mass spectrophotometry (GC-MS) 30
germanium (Ge) 22
Graphical User Interface (GUI) 49
H
hydrazine (N_2H_2) 14
hydrogen phosphate (HPO_4^{2-}) 24
hydrogen reference electrode (HRE) 41
hydrophilic-lipophilic balance (HLB) 26
hydroxyl ions (OH^-) 31
hydroxylamine (NH_2OH) 14
I
incident light (I_o) 50
integrated syringe pump-based environmental water Analyser (iSEA) 26
Ion Chromatography (IC) 30
ion-selective membrane electrodes (ISEs) 30
L
light emitting diodes (LEDs) 36
limit of determination LOD 23
liquid waveguide capillary flow cell (LWCFC) 24
Loop Flow Analysis (LFA) 36
M
magnesium-induced coprecipitation (MAGIC) 25
main control unit (MCU) 56
Micro Loop Flow Analysis (μLFA) 36
micro total analysis systems (μTAS) 26
molybdate (MoO_4^{2-}) 24
molybdophosphoric acid (MPA) 44
N

N-1-naphthylethylenediamine dichloride (NEDD) 28
nitrate (NO_3^-) 10
nitric oxide (NO) 11
nitrite (NO_2^-) 10
nitrite plus nitrate $\Sigma(NO_3^- + NO_2^-)$ 28
Nitrogen gas (N_2) 9
nitrous oxide (N_2O) 13
O
octadodcylsilane (ODS) 30
orthophosphoric acid (H_3PO_4) 24
ortho-silicic acid (H_4SiO_4) 24
oxidized form (Oxid.) 42
oxygen molecules (O_2) 11
P
particulate inorganic phosphorus (PIP) 17
Particulate Nitrogen (PN) 9
particulate organic nitrogen (PON) 10
particulate organic phosphorus (POP) 17
phosphomolybdate blue (PMB) 24
Phosphorus (P) 16
polarization resistance (RP) 42
poly (methyl methacrylate) (PMMA) 35
polyetheretherketone (PEEK) 35
potential (E). 41
R
reduced form (Redu) 42
relative standard deviation (RSD) 26
reverse flow injection Analyser (rFIA) 54
S
saturated calomal reference electrode (SCE) 41
screen-printed electrode (SP) electrode 27
serial clock pin (SCL) 47
serial data pin (SDA) 47
serial peripheral system (SPS) 56
silicomolybdenum-blue complex (SiMB) 33
silicon (Si). 22
single-beam spectrophotometer (SBS) 44
Sodium dodecyl sulphate (SDS) 25
sodium ions (Na+) 31
solid phase extraction (SPE) 26
Spectrophotometric Elemental Analysis System (SEAS) 29
square wave voltammetry (SWV) 27
step potential (EStep) 42
Submarinegroundwater discharge (SGD) 17
sulfanilamide (SAM) 28
T
total sulfide (ΣS) 35
transmittance (T). 50
triethyloxonium tetrafluoroborate (TEOT) 30
V
volts (V) 41
W
Warburg impedance (ZW) 42

1 Introduction

The objective of this chapter is to provide an overview of the biogeochemistry of major macronutrients such as phosphate, silicic acid, nitrate, and nitrite in marine waters and the analytical methods used to quantify them. In this chapter, the following three points have been addressed:

1. The role of macronutrients in oceanic biogeochemical cycles.
2. Analytical methods for the determination of macronutrients in marine water.
3. Automated systems for *on-site* and *in situ* monitoring of nutrients in marine waters.

To achieve these goals, the role of macronutrients in controlling oceanic primary productivity will be described. We will focus on the various analytical approaches that have been developed for analyses of macronutrients at low and high concentrations. The use of various automated macronutrient Analysers reported in literature or available commercially for *on-site* and in-situ monitoring in the ocean will be described.

1.1 Biogeochemistry of Macronutrients

Nutrient enrichment causes excessive algal growth and consequently a variety of problems in aquatic systems, including loss of biodiversity, fish kills, and hypoxia. The increasing inputs of macronutrients into the marine ecosystem causes eutrophication as it exceeds the natural uptake capacity of ecosystems (e.g., algae and weeds). As organic material from algal blooms is decomposed, there is a decrease in oxygen levels in the water column, resulting in for example dead zones as in the Gulf of Mexico(Rabalais, Turner, and Wiseman Jr 2002). As a result of the decrease in oxygen levels, organisms in the ecosystem die, drinking water would become contaminated in freshwater systems, green macroalgae would be promoted, harmful algal blooms may form and seagrasses would decline (van Beusekom 2018).

The importance of nitrogen, phosphorus, and silicon and their biological cycling in the ocean is widely reported. Nitrate and phosphate are the required nutrients for almost all phytoplankton (Paytan and McLaughlin 2007). Silicon plays an important role for diatoms (a key type of siliceous phytoplankton), which contribute to about 40% of the global primary production. In the oceans, diatoms have a major impact on the sequestration of inorganic carbon (Tréguer and De La Rocha

2013). In oligotrophic regions of the open oceans, primary production is limited by N and P scarcity. Silicic acid (the dissolved phase of silicon) may be depleted to low levels, limiting diatom production and thus carbon export from the surface mixed layer.(Zehr and Kudela 2011).

1.1.1 Global Nitrogen Cycling

Nitrogen is the fourth most abundant element in biomass and is a vital element for life. Nitrogen is involved in the formation of many vital biomacromolecules, such as nucleic acid, proteins, and dyes. Fixed nitrogen, which is considered the biologically available form of nitrogen, is the major limiting nutrient in most Earth surface environments (Elser et al. 2007). The most important features of the biogeochemical nitrogen cycle is that it is controlled by redox reactions, as shown in **Figure 1.1**. Nitrogen can exist in various organic forms, such as amide or amine groups, which can be in various oxidation states. Various N species can act as electron acceptors or electron donors in energy metabolism processes, further enhancing their role in marine chemistry (Zehr and Kudela 2011).

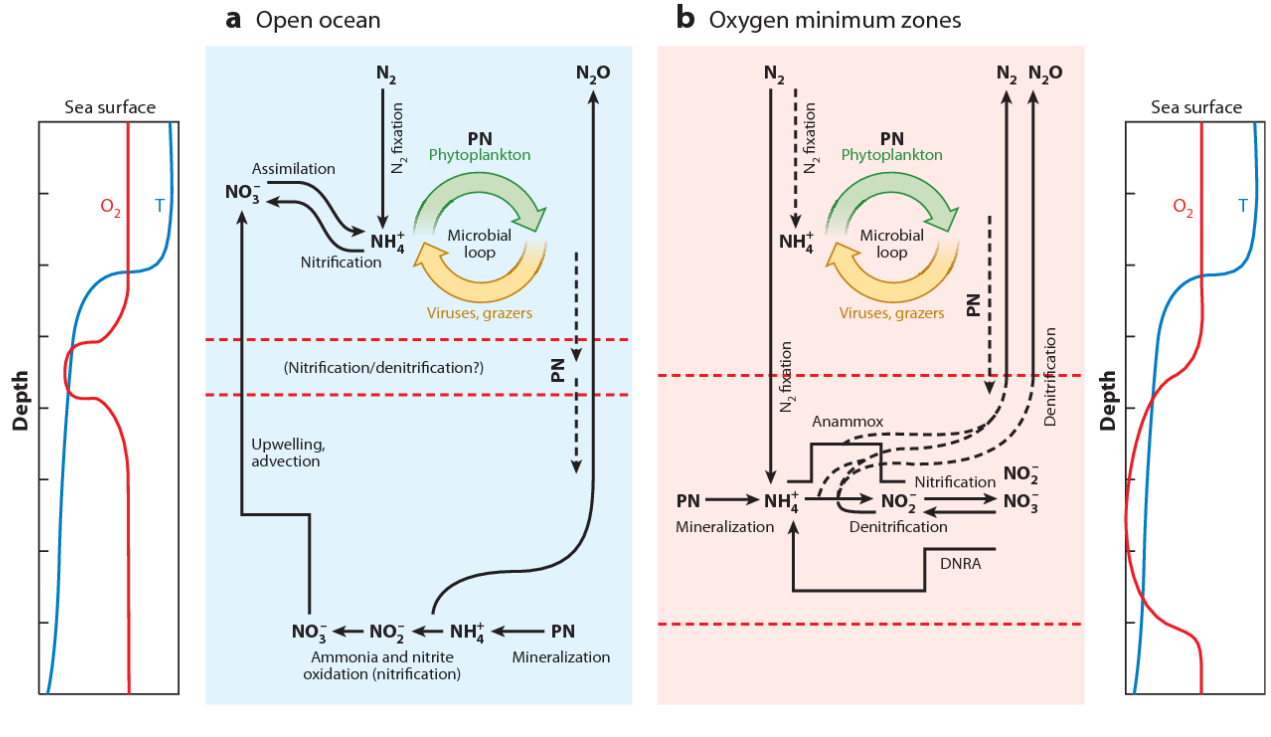

Figure 1.1 Schematic diagrams showing the main components of the nitrogen cycle and comparing them in (a) the open ocean as a typical oceanic water column and (b) oxygen minimum zones Particulate Nitrogen (PN), Dissimilatory Nitrate Reduction to Ammonium (DNRA) (Zehr and Kudela 2011).

Redox speciation

Nitrogen gas (N_2) is the most abundant N form in seawater. N_2 is inaccessible to most marine microbes because of the strong triple bonds between the two nitrogen atoms. Nitrogen fixation can only be accomplished by a group of a few microbes, the nitrogen fixers, which have the ability to break the triple bonds. As a result, the nitrogen can be converted into other fixed N forms.

There are the following different forms of fixed nitrogen;

- dissolved inorganic nitrogen (DIN) (e.g., nitrite (NO_2^-), nitrate (NO_3^-), ammonia or ammonium (NH_3 or NH_4^+)
- dissolved organic nitrogen (DON) (e.g. Urea, amino aicd, humic acid, nucleic acid and alky or quaternary amines)
- particulate organic nitrogen (PON).

The most abundant form of fixed nitrogen is DON, except in the open ocean below ca. 400 m depth where DIN is predominantly in the NO_3^- form. All the forms containing nitrogen either fixed or non-fixed are presented in **Table 1**.

Table 1.1 Common N-containing species in the global nitrogen cycle **(Zhang, Ward, and Sigman 2020)**

Form	Molecular formula	Redox state
Ammonium, ammonia	NH_4^+, NH_3	-3
Organic N	R-NH_3	-3
Hydrazine	N_2H_4	-2
Hydroxylamine	NH_2OH	-1
Dinitrogen*	N_2	0
Nitrous oxide*	N_2O	+1
Nitric oxide	NO	+2
Nitrite, nitrous oxide	NO_2^-, HNO_2	+3
Nitrogen dioxide	NO_2	+4
Nitrate, nitric acid	NO_3^-, HNO_3	+5

The asterisk symbol * points to the non-fixed nitrogen species

1.1.1.1 Nitrogen Transformations

The amounts of nitrogen available for various life functions are mainly controlled by the biogeochemical processes involving N species (**Figure 1.1, 1.2**). These processes are catagorized into two aspects. The first aspect contributes to the input/output of the "budget" of fixed nitrogen.

This input refers to biological nitrogen fixation, which either destroys or creates forms of fixed nitrogen, with the largest contribution coming from various human activities and a smaller contribution from enrichment by lightning from near-surface rocks. The second is the cycling of fixed nitrogen species, including the conversion of one form to another and the transfer of these forms from one region to another without altering nitrogen reservoirs (i.e., no creation or destruction of N-fixed forms). Some examples of anthropogenic activities include the igention of fossil fuels, the widespread exploitation of N-rich fertilizers, and the increase in legume agriculture, which dramatically increases bioavailable N inputs to terrestrial and coastal ecosystems (Fowler et al. 2013; Fowler, Steadman, Stevenson, Coyle, Rees, Skiba, Sutton, Cape, Dore, and Vieno 2015).

I. Input processes

A. Biological Nitrogen Fixation

It is actually known that nitrogen fixation is the only biological pathway for the formation of fixed nitrogen. This is because of the high stability of triple bond in N_2. Only few organisms in the ocean are able to break this bond. The process requires a high energy input. Biological nitrogen fixation is facilitated by the enzyme nitrogenase (Bulen and LeComte 1966; Hoffman et al. 2014). It is a multicomponent enzyme that requires iron and usually molybdenum (Seefeldt, Hoffman, and Dean 2009). Iron is the essential cofactor, so nitrogen fixation is directly dependent on iron availability. The reaction is exergonic, has a high activation energy, and is inactivated by the presence of oxygen. This type of metabolism occurs in an environment where the level of active nitrogen is too low. 8 electrons and 16 ATP molecules are required to reduce one mole of nitrogen (Raymond et al. 2004; Boyd and Peters 2013).

$$\mathbf{N_2 + 8\,H_2 + 8\,e^- + 16\,ATP \rightarrow 2\,NH_3 + H_2 + 16\,ADP + 16\,P_i} \qquad \textbf{Equation 1.1}$$

The reduced nitrogen atoms produced in this reaction are then incorporated into biomolecules via anabolic reactions. Most nitrogen fixation processes occur in the open ocean, with some contribution from benthic nitrogen fixation, bringing the annual total biological nitrogen fixation to 258 Tg N (Fowler, Steadman, Stevenson, Coyle, Rees, Skiba, Sutton, Cape, Dore, and Vieno 2015). This process occurs largely in (sub)tropical surface waters and is supported by cyanobacteria (e.g., *Tricbodesmium*) (Karl et al. 1997).

B. Abiotic sources

In addition to biological nitrogen fixation, nitrogen fixed by natural or anthropogenic activities can enter the ocean via the microbial nitrogen cycle once these compounds are deposited in the ocean.

In the atmosphere, Lighting is considered as an important source of fixed nitrogen. Lightning processes are associated with high temperatures that lead to dissociation of oxygen molecules (O_2) and subsequent formation of oxygen radicals that react with nitrogen (N_2) to form nitric oxide (NO)(this is known as the Zel'dovich mechanism)(Zeldvich 1946). The annual production of fixed nitrogen by lightning is estimated to be 5 ± 3 Tg N(Schumann and Huntrieser 2007). Another natural source of fixed nitrogen is volcanic activity, which results in thermal fixation of nitrogen. The annual emission of volcanic ammonia has been estimated at 0.9 Tg N(Paulot et al. 2015). Hydrothermal vents are another natural pathway for fixed nitrogen, where reduction of N_2 to NH_3 occurs at high temperatures through mineral-catalyzed reactions(Brandes et al. 1998).

Anthropogenic activities are the other main sources of abiotic sources. Anthropogenic sources of fixed nitrogen include the Haber-Bosch process for fertilizer production, in which N_2 and H_2 react under high temperature and pressure using a ferrite catalyst to form NH_3 (Hoffman et al. 2014). The most recent estimate of annual nitrogen fixation by the Haber-Bosch process is 160 Tg N(Fowler, Steadman, Stevenson, Coyle, Rees, Skiba, Sutton, Cape, Dore, and Vieno 2015). The use of fossil fuels for electricity generation, transportation, and heating produces nitogen oxides as byproducts. The annual production from fossil fuels was estimated at 40 Tg N(Fowler, Steadman, Stevenson, Coyle, Rees, Skiba, Sutton, Cape, Dore, and Vieno 2015). The total annual anthropogenic production of fixed nitrogen is 269 Tg N, with a value almost equal to that of biological nitrogen fixation (Zhang, Ward, and Sigman 2020).

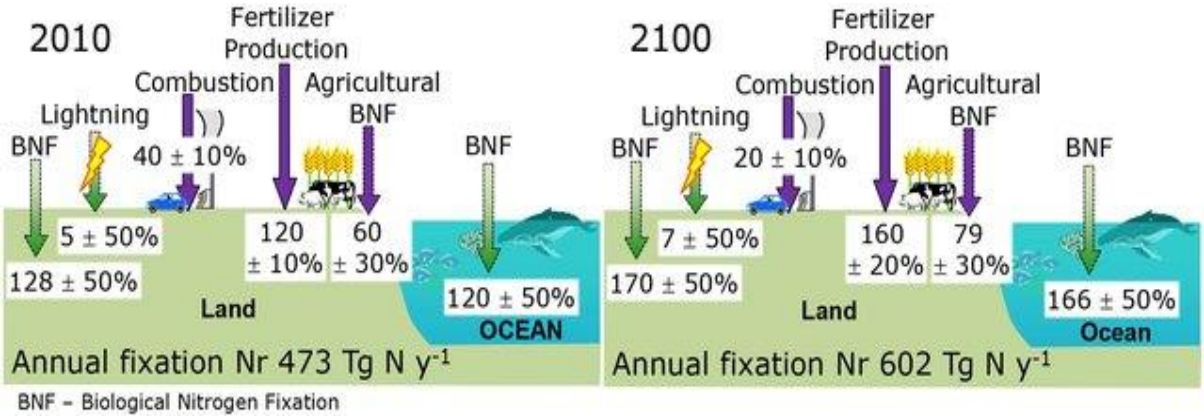

Figure 1.2 Global biological nitrogen fixation (BNF) in natural terrestrial and ocean ecosystems and by lighting (green arrows) and anthropogenic nitrogen fixation as a consequence of various activities (e.g., agriculture, combustion, and industrial processes (fertiliser production)) for 2010,

with an estimate for 2100 (Fowler, Steadman, Stevenson, Coyle, Rees, Skiba, Sutton, Cape, Dore, Vieno, et al. 2015).

II. Internal cycling

A. Nitrogen Assimilation

Nitrogen assimilation is the process by which external organic and inorganic species enter the cell and are used to produce organic nitrogen. These processes are found in plants, phytoplankton and microbes (Xu, Fan, and Miller 2012; Glibert et al. 2016). There are two pathways of nitrogen assimilation, the ammonium assimilation pathway and the nitrate assimilation pathway. During ammonium assimilation pathway, ammonium is first transported and diffused into the cell, where it is subsequently converted into amino acids by two enzymes, glutamine synthetase and glutamate synthetase. (Leigh and Dodsworth 2007). The assimilation of nitrate is metabolically more complex because several enzymes are involved in this process. Nitrate reduction to nitrite is mediated by nitrate reductase, which is followed by nitrite reduction to ammonium, mediated by the enzyme nitrite reductase, which undergoes the ammonium assimilation process by the same pathway (Glibert et al. 2016). In environments with low N concentrations, the preferred form of fixed nitrogen for assimilation is ammonium over nitrate because the redox state of N in ammonium and N in amino acids is similar. Due to the ease of assimilation of ammonium into organic biomass, accumulation of ammonium in the environment is rarely observed. This can only occur with the absence of autotrophic bacteria or chemical oxidants in a dark and anoxic environment (Berges and Mulholland 2008).

B. Nitrification

The nitrification process is that in which ammonium is oxidized in presence of oxygen to nitrate. Nitrification usually carried out by a group of specialized nitrifying chemoautotrophic microbes. In biomass, nitrate and ammonium provide both energy and nitrogen. Under low oxygen level (i.e., anoxic environment), as a byproduct of the nitrification process, nitrous oxide (N_2O) (greenhouse gas) is released (Stein 2019). Ammonia is oxidized to nitrite with oxygen in the presence of ammonia oxidizing bacteria (e.g., Thaumarchaeon *Nitrosomonas*) and archaea (e.g., Thaumarchaeon *Nitrosopumilus*). In the presence of nitrite oxidizing bacteria (e.g. protobacteria Nitrobacter, *Nitrospina*), nitrite is aerobically oxidized with oxygen to nitrate. Only Comammox, a group of protobacteria, has the ability to completely oxidize ammonia to nitrate. (Van Kessel et al. 2015). Several fungi and heterotrophic bacteria are able to oxidize inorganic or organic reduced nitrogen forms to nitrite and to nitrate. The process is called heterotrophic nitrification.

C. Mineralization

The mineralization process, which could also be called remineralization, involves the release of inorganic nitrogen species such as ammonium and nitrate. This occurs through the recycling of organic nitrogen macromolecules derived from the biomass which are usually in the form of PON The process refers to the release of ammonium into the environment, first decomposing the biomass PON into DON either by physical decomposition, solubilization, or splitting at the C-C bond, followed by deamination of the proteins and nucleotide macromolecules. The process is generally associated with excretion by recycling and bacterial degradation of macromolecular organic matter. The process is mediated by heterotrophic bacteria (e.g., prokaryotes and eukaryotes) (Schlesinger and Bernhardt 2013).

D. Dissimilatory Nitrate Reduction to Ammonium (DNRA)

Dissimilatory nitrate reduction to ammonium, in which nitrate is primarily reduced to nitrite, with nitrate act as an electron acceptor, nitrite then eventually reduced to ammonium. The process is mediated by a variety of prokaryotes and eukaryotic microbes (Kuypers, Marchant, and Kartal 2018; Kamp et al. 2015). DNRA is carried out by a number of microbes that compete for nitrate and organic matter with the microbes required for the denitrification process (the process is described in the following subsection). The microbes performing dissimilatory nitrate reduction and denitrification (will be discussed in the next sub-section) compete for nitrate and organic matter. At higher organic C/nitrate ratio, dissimilatory nitrate reduction is favoured and vice versa at lower ratios, denitrification will favour (King and Nedwell 1985; Kelso et al. 1997).

E. Dissimilatory Nitrate Reduction to Ammonium (DNRA)

Dissimilatory nitrate reduction to ammonium, in which nitrate is primarily reduced to nitrite, with nitrate act as an electron acceptor, nitrite then eventually reduced to ammonium. The process is mediated by a variety of prokaryotes and eukaryotic microbes (Kuypers, Marchant, and Kartal 2018; Kamp et al. 2015). DNRA is carried out by a number of microbes that compete for nitrate and organic matter with the microbes required for the denitrification process (the process is described in the following subsection). The microbes performing dissimilatory nitrate reduction and denitrification (will be discussed in the next sub-section) compete for nitrate and organic matter. At higher organic C/nitrate ratio, dissimilatory nitrate reduction is favoured and vice versa at lower ratios, denitrification will favour (King and Nedwell 1985; Kelso et al. 1997).

III. Output processes

A. Denitrification

The process of denitrification is the primary process by which the fixed nitrogen is lost from the marine system. It is the process by which fixed nitrogen is converted back to N2. The complete denitrification process involves several steps in which complete reduction to N_2 occurs, converting nitrate to nitrite, then to NO, to N_2O , and finally to N_2 (Nevison et al. 2016). Most denitrification processes are carried out by aerobic and heterotrophic bacteria, in which nitrate serves as a terminal electron acceptor for respiration in a low oxygen concentration environment (Robertson and Kuenen 1984).

B. Anammox (Anaerobic ammonium oxidation)

Anammox is the second route of the loss of fixed Nitrogen in low oxygen environment. Anammox bacteria (phylum *Planctomycetes*) oxidize NH_4^+ using NO_2^- as an electron acceptor ending in the production of N_2 as the final product. Anammox was discovered as a biological process into the enrichment area from wastewater treatment plants. The net reaction oxidizes ammonium using nitrite and resulting in the production of N_2 and NO_3^- under anaerobic conditions. In the biogeochemical pathways, nitrite is reduced firstly to NO by nitrite reductase and then to hydroxylamine (NH_2OH) which is readily reacted with NH_4^+ with the assistance of Hydrazine synthase enzyme to form hydrazine (N_2H_2). Hydrazine is then oxidized to N_2 by the assistance of hydrazine dehydrogenase (Fuerst 2005).

1.1.1.2 Distribution of Nitrogen

Nitrate is an inorganic species and the most abundant form of fixed nitrogen in the ocean. The concentration of NO_3^- varies greatly in the ocean and is much higher in deep waters than in surface waters (above 100 m)(Capone et al. 2008). This is a consequence of the internal cycling of NO_3^-, in which phytoplankton in the sunlit surface ocean consume NO_3^- for organic biomass production (i.e., photosynthesis). The organic N produced from nitrate is transported to depth as largely sinking particles. The organic N biomass is then remineralized to ammonium by respiration and bacterial degradation and subsequently oxidised to nitrite and nitrate (McElroy 2007; Karl and Lukas 1996). In surface waters of the open ocean, nitrate concentrations are close to the limit of quantification due to phytoplankton feeding. Nitrate concentrations in ocean surface waters exhibit spatial variations, resulting in ecological and biogeochemical zonation. Nitrates can be brought to the surface by upwelling, convection, and mixing, resulting in high nitrate concentrations in surface waters comparable to those in deep waters, e.g., in high latitude regions, along the equator, and along some coasts (Martin, Fitzwater, and Gordon 1990; Mitchell et al.

1991). In most tropical and subtropical regions, nitrate is drawn into surface waters where there is little mixing without upwelling, and the rate of nitrate supply in these regions is low. In the interior of the ocean, there is a strong gradient in nitrate concentration, largely due to ocean circulation. Deep water from the North Atlantic flows into the Indian and Pacific Oceans and accumulates nitrate, which leads to concentrations ranging from 20 μM in the deep North Atlantic to 45 μM in the deep Pacific through remineralization of organic matter (McElroy 2007). In contrast, ammonium concentrations were 1000 times lower than nitrate concentrations. Ammonium concentrations ranged from 0 to hundreds of nanomoles. Ammonium is rapidly formed by decomposition of organic matter and then released into the sunlit euphotic zones and the dark aphotic zone at average concentrations of 300 nM and 10 nM, respectively (Paulot et al. 2015; Capone et al. 2008). As mentioned earlier, ammonium accumulates to hundreds of nanomoles in the dark and reducing (anoxic) environments in coastal and estuarine waters. This is not the case in suboxic zones, where ammonium is rapidly consumed by annamox (as described in the subsection above)(Zhang, Ward, and Sigman 2020). Nitrite is an important species in the nitrogen cycle. The average concentrations in the euphotic and aphotic zones are 100 nM and 6 nM, respectively. Nitrite concentrations are significantly high in the regions where the production and consumption processes showed unbalanced behaviour, e.g., nitrite had a concentration up to 10 μM in the oxygen-minimal zones, a concentration of 0.2 to 1.5 μM nitrite at the base of the euphotic zone, and a concentration of 0.25 μM in the surface water of some polar regions (Zakem et al. 2018). The second most abundant form of fixed nitrogen in the ocean is DON, whose concentration at the surface (more than 4 μM) is lower than the concentration in deep waters (about 2 μM and below) (Letscher et al. 2013). In subtropical surface waters, DON is the largest pool of nitrogen. The higher molecular weight DON is mainly composed of amides, amines and N-acetylated sugars. After production in surface waters, DON consumes in surface waters (in the upper 100 m) or in the shallower coastal waters of the ocean thermocline (100-500 m depth) (Follett et al. 2014).

1.1.2 Global Phosphorus Cycling

Phosphorus (P) is the 11th most abundant element in the Earth's crust, with approximately 0.1 % by mass (Bricker 1972). It is a crucial macronutrient for all living organisms and controls primary production in a range of marine systems in the world's oceans (Mather et al. 2008; Elser et al. 2007). Phosphorus is found in seawater in either dissolved or particulate form, through the uptake by phytoplankton in surface waters. Dissolved organic phosphorus compounds (DOP) account for a significant and diverse proportion of dissolved phosphorus species in seawater and are

entirely due to the decay of marine organisms. Sugar phosphates, phospholipids, phosphonucleotides and their hydrolysed products, and phosphate esters (O-P bonds) and more stable aminophosphonic acids (C-P bonds) form an important part of the DOP compounds (Karl and Björkman 2015). Dissolved inorganic phosphate normally occurs in seawater as ionized products of H_3PO_4 such as $H_2PO_4^-$, HPO_4^{2-}, and PO_4^{3-}. The phosphorus cycle (**Figure 1.3**) is similar to the nitrogen cycle, with inputs by humans from land, through the discharge of sewage or the extensive use of plant fertilizers. The cycle of phosphorus is not as complicated as that of nitrogen.

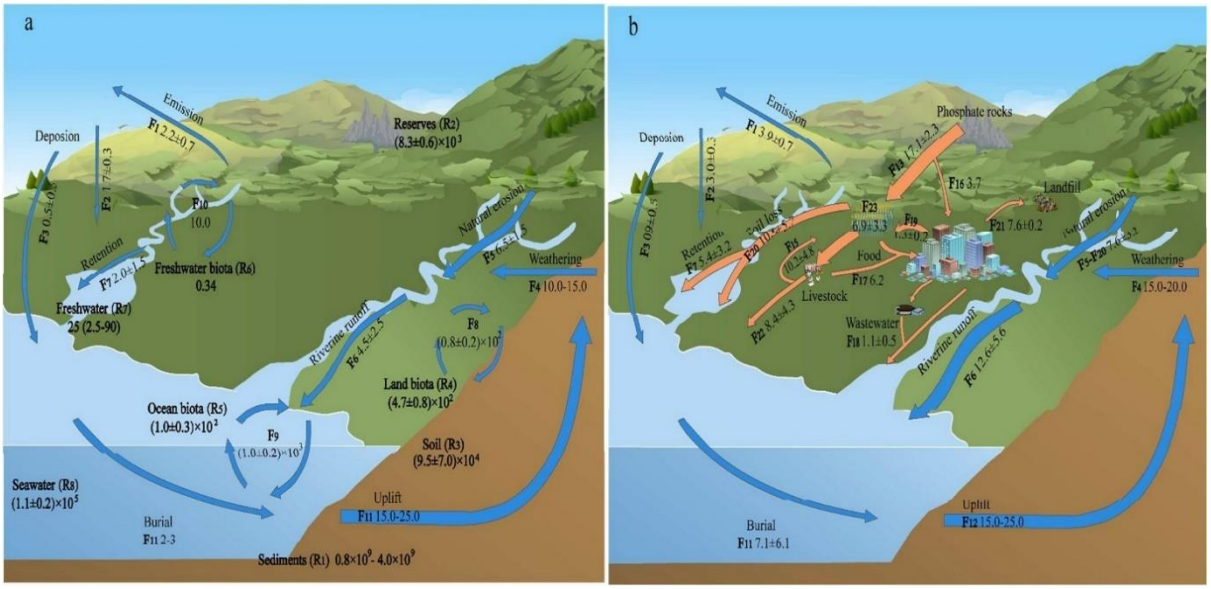

Figure 1.3 A schematic representation of the global phosphorus cycle (Yuan et al. 2018) in (a) background state and (b) human-modified state. The bubbled arrows indicate the flow of phosphorus from land to ocean and vice versa, while the orange arrows in (b) indicate the flow of phosphorus entering the natural ecosystem due to human anthropogenic activities. The bold black dots in (a) refer to phosphorus stocks in Tg P, which is also true for phosphorus flux (F).

1.1.2.1 Sources and distribution of Phosphorous

Phosphorus occurs in the form of inorganic phosphate minerals and organic phosphate derivatives which exist in the rock and soils. The most common naturally occurring phosphorus containing minerals in the earth's crust is Apatite ($[Ca_5(PO_4)_3X]$, X= F, Cl, OH)(Holzer, Frants, and Pasquier 1992). There are many sources of phosphorus inputs to the ocean. The primary source of phosphorus to the ocean is via continental weathering. Phosphorus is transported via riverine influx in either dissolved or particulate phase. Other source is the atmospheric deposition via aerosols, and mineral dust.

A. Continental Weathering

The major source of phosphorus to the marine environment is continental weathering (Glenn, Prévôt-Lucas, and Lucas 2000; Bricker 1972). Phosphorus is transported to the ocean by rivers, either in particulate or dissolved form. Particulate phosphorus from rivers exists in two phases: particulate inorganic phosphorus (PIP) and particulate organic phosphorus (POP). Estimates of annual river inputs have been reported as (27-49) $\times 10^{10}$ mol for PIP and 2.9×10^{10} mol for POP. Glenn et. al.(Glenn, Prévôt-Lucas, and Lucas 2000) estimated annual river fluxes using average river discharge and pre-anthropogenic DIP concentration of 0.23-0.32 μM to be 0.8-1.5 $\times 10^{10}$ mol for DIP and 0.6×10^{10} mol for DOP. Most of the phosphorus is associated with inorganic particles in rivers, with phosphorus occurring in apatite grains and other minerals, and also adsorbed to iron/manganese oxide. These particles rapidly deposit in estuarine sediments and coastal shelf and do not contribute to the oceanic phosphorus pool available to marine life. Phosphate from freshwaters tends to be adsorbed onto clay particles where iron and aluminum oxychloride are present on the surface. This deposited phosphate tends to be desorbed in estuarine water as salinity increases. The total phosphorus desorbed from the clay particles was estimated to be 2-3 times higher than that entering the ocean via the rivers. The DOP from the rivers may be trapped in flocculation processes in estuarine waters (Bolin and Cook 1983), and may be photohydrolyzed and remineralized (Hedges 1992). It has been estimated that 10-30% of phosphorus from rivers is accessible to oceanic phosphorus cycles for biological uptake. One quarter of the reactive phosphorus is trapped in estuarine sediments and never reaches the open ocean (Glenn, Prévôt-Lucas, and Lucas 2000).

B. Submarine groundwater discharge (SGD)

One of the nutrients sources to the coastal nutrient cycling is submarine ground water (Moore et al. 2000). Nutrients from SGD can compete nutrients input from riverine influx. In the coastal groundwater system, nitrogen/phosphorous (N/P) ratios exceed those in the river system and are higher than the Redfield ratio (Paytan et al. 2006). The increase nutrients input via SGD may drive the N-limitation coastal systems toward the P-limitation (Slomp and Van Cappellen 2004).

C. Aeolian inputs

Aerosols associated with the aeolian dust particles are one of the sources of phosphorus to the ocean with annual input was estimated to be 3.2×10^{10} mol representing about 5 % of the total pre-anthropogenic phosphorus input to the ocean (Duce et al. 1991). The atmospheric phosphorus in mineral dust exists in both organic and inorganic phases in equal proportions. The inorganic

portions in the aerosols are usually bound with iron oxides and may be associated with calcium, magnesium, aluminum. Generally, the inorganic portions are weakly soluble (Ridame and Guieu 2002). For the anthropogenic phosphorous, this may be associated with more soluble fractions. The flux of the atmospheric phosphorous to the ocean varies with space and time, with a daily flux in the Mediterranean of 0.9 μmol/m^2 (Ridame and Guieu 2002), 0.1 – 0.3 μmol/m^2 in the Atlantic Ocean and 0.08 – 0.4 μmol/m^2 in the Pacific Ocean (Mackey et al. 2012).

D. Anthropogenic sources

Most phosphates are lost from farmland through erosion and agriculture (i.e., crop production). Over the years, the use of phosphate fertilizers has increased. Many tons of phosphate rock are mined each year for fertilizer production. Much of the phosphorus from fertilizers and other human activities such as sewage, livestock, and paper manufacturing are washed into rivers, groundwater, and estuaries and make their way to the ocean. This results in a total annual phosphorus flux to rivers estimated at (57 - 100) × 10^{10} moles (Carpenter et al. 1998; Bennett, Carpenter, and Caraco 2001).

E. Marine sediments

Phosphorus enters marine sediments primarily as sinking particles. Sediments are considered the main deposit in the oceanic phosphorus cycle. Phosphorus is particularly associated with metal oxides and hydroxides. The total annual amount of phosphorus buried in open ocean sediments is estimated to be in the range of (9.3 - 34) × 10^{10} mol (Filippelli and Delaney 1996). Most of the buried phosphorus is the reactive component, while the non-reactive component is deposited on continental shelves. The reactive phosphorus is determined from sequential extraction of marine sediments in which P is present in organic form are loosely sorbed and associated with iron oxides present in authigenic minerals, e.g., calcium fluorapatite and rare earth element phosphate minerals (Rasmussen 1996). Reactive phosphorus is biologically available or associated with biologically related phosphorus components in the water column before burial. The relative contribution of specific sinks to phosphorus in sediments depends on the redox conditions in the sediment (i.e., the abundance of oxidizing and reducing agents). Under oxic conditions, surface sediments are rich in iron (III) and manganese, where large amounts of phosphorus are taken up by adsorption or mineral formation, whereas under anoxic conditions the sediment is depleted and phosphorus is bound to calcium minerals (Ingall and Jahnke 1994).

However, phosphorous in sediment can be released to the pore water and then contribute to the phosphorus cycle in the water column. DIP depth profiles in the oceans investigate a nutrient

trend as surface waters depleted due to the intense biological uptake in the euphotic zone and increase with the depth by the regeneration process i.e., conversion of organic phosphorus fractions to DIP. In the open ocean, the maximum values occur near 1000 m (the same depth as the oxygen minimum layer). In the Atlantic Ocean, the maximum values are 1.5 μM while in the pacific values of 3.2 μM can occur. Within deep waters, an increase concentration of DIP is also exhibited with increasing the age of the deep water due to the continuous cumulative accumulation of the sinking particles and their regeneration. At present, in the North Atlantic the deep water that forms flow through deep water basins to the North Pacific, this process takes place in 1500 years. Thus, the waters in the deep Pacific is older than the waters in the North Pacific this leads to increase the concentration of DOP and DIP in the Pacific than in the Atlantic Ocean (Broecker and Peng 1982).

1.1.2.2 Transformations of Phosphorous

Phosphorus occurs in the ocean either in dissolved form (filtered through the 0.45-μm filter) or as particles (retained on the 0.45-μm filter). The dissolved fraction may be inorganic phosphorus, generally soluble orthophosphate, and may be organic phosphorus compounds or macromolecular colloidal phosphorus. The particulate fraction includes live and dead plankton, phosphorus adsorbed on particles, and amorphous phosphorus phases. In both the dissolved and particulate fractions, phosphorus may be present in inorganic form (orthophosphate, pyrophosphate, polyphosphate, and phosphate-containing minerals) or in organic form (P-esters, P-diesters, and phosphonates) (Cotner Jr and Wetzel 1992; Paytan and McLaughlin 2007). In general, the particulate and dissolved phases undergo continuous transformations. The dissolved fraction, i.e. orthophosphate, is assimilated by phytoplankton via photosynthesis and leads to the formation of organic phosphorus compounds.

Regarding dissolved phosphorus in the ocean, marine phytoplankton and autotrophic bacteria take up phosphorus in the form of PO_4^{3-} and HPO_4^{2-} from the water column for their metabolic needs. Heterotrophic bacteria are able to convert DOP to DIP. Autotrophic bacteria and phytoplankton are able to hydrolyze organic phosphorus compounds when inorganic dissolved phosphorus is insufficient for their metabolic needs. Most of the DIP uptake occurred in the sunlit upper zone of the water column (euphotic zone), where the photosynthesis takes place (Cotner and Biddanda 2002).

1.1.3 Global Silicon Cycling

Silicon is the second most abundant element on Earth and is considered one of the most important macronutrients in the sea. Silicon is essential for the growth of diatoms and some sponges and is utilised by radiolarians. (Deshmukh, Ma, and Bélanger 2017). The estimated residence times of silicon in the modern ocean are 15000 years (Treguer et al. 1995) to 17000 years (Laruelle et al. 2009) over a period when the silicon cycle is in equilibrium in coastal areas. The marine silicon cycle (**Figure 1-4**) has been assumed to be unaffected by human activities, although recent studies indicate that the silica cycle is strongly influenced by anthropogenic inputs, e.g., dams that lead to a decrease in dissolved silica in estuaries and rivers (Ittekkot et al. 2012; Bernard et al. 2011).

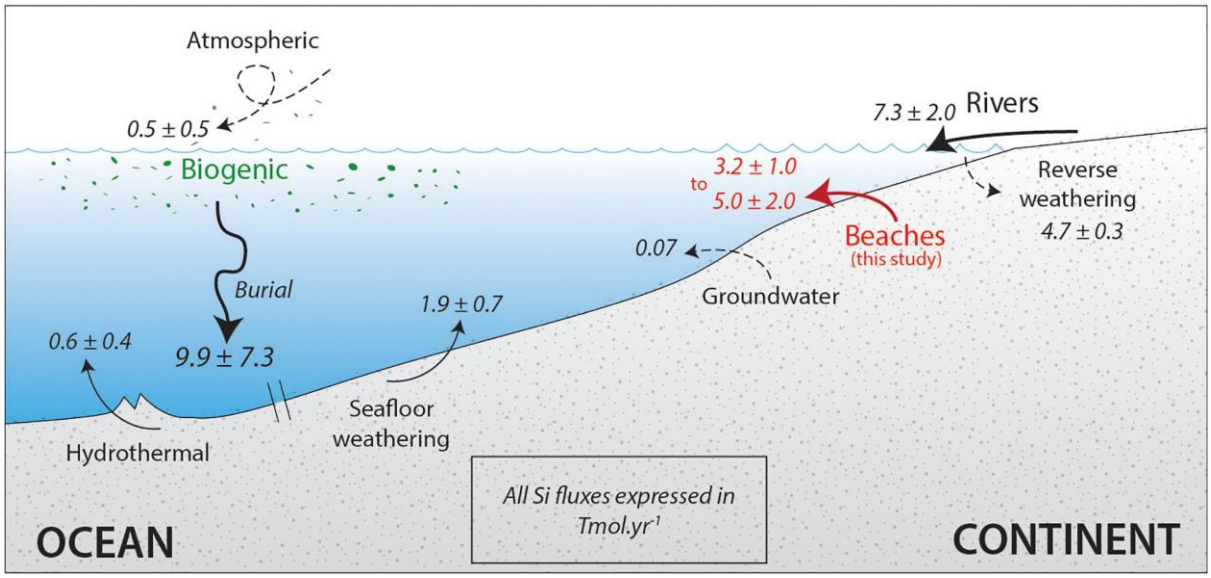

Figure 1.4 Global oceanic silicon cycles (sources and sinks) revised from (Fabre et al. 2019), inspired by (Tréguer and De La Rocha 2013). Values for groundwater discharge are from (Rahman, Aller, and Cochran 2017) and for reverse weathering from (Ehlert et al. 2016).

1.1.3.1 Sources and distribution of silicon

There are several external sources of silicic acid input to the ocean, most of which are ultimately due to weathering of the Earth's crust. The net annual input of dissolved silicic acid to the ocean is estimated to be 9.4 ± 4.7 Tmol Si, which is divided into several components: dissolved silicic acid from rivers, biogenic silicon from rivers, submarine groundwater discharge, aeoline inputs, hydrothermal input, and lithogenic sediment and basalt dissolution (Tréguer and De La Rocha 2013).

A. Continental inputs

Dissolved silicic acid enters the global ocean primarily through chemical weathering of continental rocks. Dissolved silicon, like silicic acid and biogenic dissolved silicon, enters coastal waters (e.g., estuaries) via river discharges or submarine runoff from groundwater. Two important processes that affect the net flux of dissolved silicic acid to estuaries are the trapping of biogenic silicon and the reverse weathering process that occurs in estuarine water and river runoff. Silicic acid is transported to estuaries via rivers, with an estimated 60% of total river discharges to the ocean (39080 km3/year) currently having a discharge-weighted average silicic acid concentration of 158 μM (Dürr et al. 2011). The gross annual input of silicic acid via river discharges was estimated to be 6.2 ± 1.8 Tmol Si (Tréguer and De La Rocha 2013). Particulate silicon (either lithogenic or biogenic) is also transported to estuaries via river discharges, and the annual flux was estimated to be 147 ± 44 Tmol Si. Particulate silicon consists of two phases, one of which is sparingly soluble (lithogenic component) and the other of which is readily soluble (amorphous, largely biogenic component); these include phytoliths, freshwater diatoms, and sponge spherules. Although dissolution of the particulate silicon results in an insignificant input of dissolved silicic acid to the ocean, the dissolved silicic acid in the ocean would be removed by reverse weathering as the amorphous silicic acid is converted to clay minerals in marginal sediments. The total gross annual input of amorphous silicic acid to coastal waters via river discharges was estimated to be 7.3 ± 2 Tmol Si (Tréguer and De La Rocha 2013). The silicon from the river discharge may be incorporated into the biogenic silicon in diatom blooms fed by nutrients from the river and then transported to the sediments. The silicon from the river runoff can be incorporated into the biogenic silicon in diatom blooms fed by nutrients from the river and then transported to the sediments. The silicon from the river, either in particulate or dissolved form, triggers diagenetic reactions that result in the formation of authigenic silicate minerals and the degradation of the newly formed dissolved silicon. Reverse weathering generally occurs in deltaic areas such as the Amazon (Michalopoulos and Aller 2004), Mississippi (Presti and Michalopoulos 2008), Gulf of Papua, and French Guinea (Tréguer and De La Rocha 2013). Reverse weathering results in greater deposition of silicon in non-tropical deltaic environments than previously thought. The input of dissolved silica to the ocean from submarine inflow can be substantial in some places and is comparable to inflow from surface rivers (Kim et al. 2005). For example, in the Bay of Bengal, the annual input of dissolved silica via submarine bottom inflow was estimated to be 0.093 Tmol Si, which is 66% of the input of dissolved silica from the Ganges-Brahmaputra River to the ocean (Georg et al. 2009).

B. Aeolian inputs

Knowledge of dust fluxes and dissolution rates is required to estimate the aeolian input of dissolved silica. The annual rate of dry deposition of particulate lithogenic silicon to the ocean has been estimated to be between 2.8 and 4.6 Tmol Si. This localized mainly in the North Atlantic as a result of downwelling from the Sahara Desert and also in the western North Pacific as a result of downwelling from the Gobi Desert (Tegen and Kohfeld 2006). The dissolution of silica from dust fluxes cannot be readily estimated because it is very difficult to know how much will dissolve due to the large differences in solubility of the various lithogenic and biogenic dust constituents. For example, the solubility of Saharan dust, which is primarily quartz, ranges from 0.02% to 1.1% (Baker et al. 2006). bout 10% of the silicon may be soluble in the feldspar dust, and even more may be soluble in the biogenic silicon of the dust. Wet deposition by rainwater also yields silica with values ranging from 0 to 6.7 mmol Si/m^2 year in the Mediterranean Sea near Corsica (Treguer et al. 1995) and from 2.55 to 2.6 mmol Si/m^2 year in the Yellow Sea and East China Sea (Zhang, Zhang, and Liu 2005).

C. Hydrothermal inputs

Deep-sea hydrothermal fluxes consist of high-temperature inputs (350 ± 30 °C) from for example mid-ocean ridges (axial component of the flux) and low temperature inputs (below 75°C) from ridges flanks (diffuse off-axis component). These inputs are highly variable and different, where the reactions occur at high temperatures leads to the leaching of silicon from the ocean crust, this cause high dissolved silicic acid liberated into the hydrothermal fluids, while the cooling of these fluids removes dissolved silicic acid via clay precipitation like smectite (Wheat and McManus 2005). The estimation of the budgets based on the germanium to silicon (Ge/Si) ratios was used to determine the hydrothermal dissolved silicic acid inputs (Treguer et al. 1995), where the annual input was estimated to be 0.2 ± 0.1 Tmol Si, while this estimation ignores the non-opaline germanium sink into the ocean while biasing this estimation (King, Froelich, and Jahnke 2000). The correction of this estimate result into an annual input of 0.6 ± 0.4 Tmol Si where the annual rate of non-opaline sink of 6-7 Mmol Ge was estimated (Tréguer and De La Rocha 2013).

D. Low-temperature dissolution of terrigenous and seafloor basalt

Another external source of dissolved silicic acid in the ocean is the dissolution at low temperatures of basalt and terrigenous silicon deposited in seafloor sediments. The annual budget included 0.4 ± 0.3 Tmol Si from seafloor basalt (Wollast and Mackenzie 1983). Benthic discharges of 10-20

mmol Si/m2.yrar were reported for the biogenic, silicon -poor seafloor of the southern Angola Basin (Van Bennekom and Berger 1984) and Sargasso Sea (Sayles et al. 1996).

1.1.3.2 The biogeochemical fluxes

Siliceous organisms produce biogenic silicon in the photic zone. Some of this flux is transported to the deep sea. The biogenic silicon exported that sinks into the deep sea is dissolved, producing silicic acid. The remaining biogenic silicon amasses at the sediment-water interface and serves as a silicon reservoir (Nelson et al. 1995). The gross annual production of biogenic silicon was estimated to be 240 ± 40 Tmol Si. This production was attributed to diatoms, although the contribution of protists (e.g., silicoflagellates and radiolarians) is poorly known. In the coastal zone, diatoms are the largest contributor to the total phytoplankton and provide large-scale support to fisheries. Comparing the average annual silicon production in the major upwelling areas of the ocean (6 Tmol Si) to about 12 times the production in the coastal regions on the eastern boundary outside the upwelling areas (with an annual average of 74 Tmol) (Shipe and Brzezinski 2001). Average annual primary production is 380 g C/m2 in coastal waters on the western boundary (estimated to represent 5% of the surface area of the world ocean) (Longhurst et al. 1995). Brezezinski et al. estimated total biogenic silicon production at 136 Tmol Si (Brzezinski 1985). Unlike in coastal areas, diatoms in the open ocean do not contribute significantly to the silicon cycle. The net annual production of biogenic silicon in subtropical eddies in the North Atlantic and North Pacific is 13 Tmol Si (Brzezinski et al. 2011). Comparing the silicon cycle in the subarctic Pacific with that in the Southern Ocean. Nelson et al. estimate that slightly less than two-thirds of the biogenic silicon production was dissolved in surface waters in the upper 2000 m, leading to an estimate of gross annual production of the subarctic gyre of 10 Tmol Si, based on an annual export production of 0.575 Tmol Si (Nelson et al. 2002). In the Southern Ocean, gross annual production was originally estimated to be about 50 Tmol Si. This estimate has been corrected to 80 ± 18 Tmol Si, which represents one-third of the total primary production of biogenic silicon (Pondaven et al. 2000).

1.2 Analytical methods of nutrients

The importance of nutrient measurements in oceanographic research is well known. Marine chemists are very interested in the methods of monitoring of nutrients in marine waters. Quantification of nutrients (phosphates, silicic acid, nitrate and nitrite) is a major challenge for

marine chemists. Several methods and approaches have been introduced to achieve lower limit of determination (LOD) values and to develop ultrasensitive deployable monitoring tools.
Optimizing chemistry is very important, but new research in the field of chemistry is very limited because it is already very well researched, so different approaches are already being used:
- Magnification of the detected spectrophotometric signal (i.e., absorbance) by increasing the path length of the absorption cell (long waveguide capillary).
- Preconcentration of the analyte or reaction mixture before detection via spectrophotometry.
- Optimisation of the optical system to improve the signal-to-noise ratio.
- Research into new approaches with sensitive electrochemical detection systems.

1.2.1 Analysis of Phosphate

1.2.1.1 Spectrophotometric measuring of phosphate

I. Blue method assay

The most common spectrophotometric method for phosphate determination is the phosphomolybdate blue (PMB) assay (Estela and Cerdà 2005; Motomizu and Li 2005; Patey et al. 2008; Murphy and Riley 1962b). PMB is generally based on the reaction of dissolved reactive phosphate (DRP) (phosphate forms passing through a 0.45-μm membrane filter and reacting with reagents (Auflitsch et al. 1997; Legiret, Sieben, Woodward, Bey, et al. 2013)) with molybdate reagent, whereby a yellow coloured phosphomolybdate complex is formed, which is subsequently reduced with a reducing agent such as L-ascorbic acid, stannous chloride, or hydrazine to form a blue coloured phosphomolybdate complex that shows two absorption peaks at 720 nm and 880 nm, with the absorption maximum at 880 nm (Adeloju 2013). DRP includes orthophosphate and small proportions of acid-hydrolyzable and condensed phosphorus compounds, orthophosphoric acid (H_3PO_4), dihydrogen phosphate ($H_2PO_4^-$), and hydrogen phosphate (HPO_4^{2-}), all of which are soluble and whose occurrence in seawater is pH-dependent, with H_3PO_4 being the dominant form under acidic conditions. The main interfering factor in seawater for the molybdate method is H_4SiO_4, since H_4SiO_4 (ortho-silicic acid) has the same tendency as DRP (due to its similar ionic structure) to react with molybdate and form a silicomolybdate complex with a peak at the same wavelength of 880 nm. To overcome this problem, strongly acidic conditions are required for the PMB method. (Zhang, Fischer, and Ortner 1999) have shown that to minimize interference from H_4SiO_4, a proton/molybdate (H^+/MoO_4^{2-}) ratio of 60-80 is required, which can be achieved at a pH of 0.4-0.9.

Several automated flow injection systems have been developed for phosphate determination based on the PMB method. These include Analysers with air segments and some connected to a capillary flow cell with a liquid conductor, and several microfluidic-based Analysers. Although several other techniques have been developed in recent years, such as chemiluminescence, first introduced by Zui et al. (Zui and Birks 2000), almost all recently published (in the last decade) analysers for phosphate in the aquatic environment (especially for nanomolar detection levels) are based on the PMB method.

a. Liquid waveguide capillary (LWC)

Zhang et al. used an automated segmented gas flow in conjunction with a liquid waveguide capillary flow cell (LWCFC) of 2 m to increase the path length because, according to Lambert-Beer's law, the magnitude of absorbance is directly proportional to the optical path length, molar absorptivity of the organic chromophore, and concentration of the analyte (equation 1.2) (Zhang and Chi 2002). Since the molar absorptivity of PMA is relatively low (10^3 to 5×10^4 L mol^{-1} cm^{-1}), the increase in the sensitivity of the method is directly related to the increase in the path length.

$$A = \varepsilon b C \qquad \textbf{Equation 1.2}$$

A is the absorbance (unitless), ε is the molar absorptivity in $M^{-1}.cm^{-1}$,b is the path length of the flow cell in cm and C is the concentration in M.

Sodium dodecyl sulphate (i.e., sodium sulphate decahydrate) (SDS) was added to ascorbic acid to achieve lower baseline noise with uniform flow. (Gimbert, Haygarth, and Worsfold 2007) used a flux injection manifold of 1 m LWCFC with a miniature fibre optic spectrophotometer with LOD of 10 nM based on the molybdenum blue method, which used a tin (II) chloride reduction step. Excellent sensitivity is achieved, which is 100 times higher than the conventional flow injection cell of 1 cm pathlength. A comparison was made between the proposed method using LWC and the reference method using a flow cell with 1 cm path length. For the proposed method, calibration was performed for a linear range between 10 nM and 1 μM with the following regression equation: Absorbance unit (y) = 0.7264 concentration in μM (x) + 0.0076 and LOD of 10 nM. For the reference method, a calibration plot was made over a linear range of 2 - 30 μM with the regression equation Absorbance unit (y) = 0.0125 concentration in μM (x) - 0.004, with a LOD value of 1 μM (100 times more than with the proposed method).

The interferences from silicic acid were excluded by the addition of tartaric acid (as a masking agent). Grasshoff et al. reported a novel reverse flux injection coupled with a 2 m liquid waveguide

capillary (Grasshoff, Kremling, and Ehrhardt 2009). A univariate experimental design was used to optimise the experimental conditions, including injection volume, flow rate, and mixing coil length with a linear range of 0 – 165 Nm and a LOD value of 0.5 Nm. Interference from silicic acid up to 240 μM and from arsenate up to 53.3 Nm, which is not a major problem due to the slow rate of the reaction between arsenate and molybdate.

b. Magnesium induced co-precipitation method (MAGIC)

Karl et al. introduced the method of magnesium-induced coprecipitation (MAGIC) (Karl and Tien 1992). The method is based on the quantitative removal of phosphorus from a solution by the in vitro formation of brucite [$Mg(OH)_2$], initiated by NaOH addition. The precipitate is collected by centrifugation for 60 min and hydrolysed by 8 M HCl, dried at 80°C and ashed (450°C for 3 h). Rimmelin et al. re-examined the MAGIC method for low phosphate concentrations in seawater (Rimmelin and Moutin 2005). The centrifugation was significantly shortened from 60 to 10 min. With a 25-fold enrichment, the method was able to determine phosphate in the nanomolar range (detection limit 0.8 Nm with a precision of 0.5 Nm). Li et al. conducted comparative studies between the MAGIC and LWCFC and the coupling of these methods, and conducted three experiments for comparison. The first was the comparison between the two methods by the standard addition series of P concentrations, the second was the application of the two methods for the analysis of natural seawater without P addition and the comparison and the third experiment was to study the effect of the addition of DOP as an interference on the determination of dissolved reactive phosphate. In these experiments, two fractions of DOP (ß-glycerophosphate pentahydrate and phytic acid) were studied, and the results of the estimation of both MAGIC and LWCFC showed a small contribution of both fractions to the calibration diagram (100 - 500 nM PO_4^{3-}).They coupled both methods and achieved a detection limit (LOD) of about 0.3 nM, while the LOD for individuals of about 3.5 nM for MAGIC and of about 1.5 nM for LWCFC with the same set of standard solutions.

c. Solid phase extraction precipitation method (SPE)

Liang et al. used a solid phase extraction (SPE) technique on Sep-Pak C18 sorbent to enrich PMB complexes paired with cetyltrimethylammonium bromide (CTAB) for nanomolar phosphate determination (Liang et al. 2007). The pre-concentrated PMA-CTAB was eluted with 0.5 M H_2SO_4 in ethanol. A standard linear calibration of 3.2 and 48.5 Nm with a detection limit of 1.57 Nm and a recovery of 96.4%. The relative standard deviation (RSD) of 4.52 % was determined over 8 days for a concentration of 32.4 Nm Ma et al. instead used a hydrophilic-lipophilic balance (HLB) SPE

cartridge to preconcentrate PMB without any additives . (Ma, Yuan, and Liang 2008). Using the technique of sequential injection analysis, Ma et al. succeeded in extracting PMA that formed at room temperature and eluted rapidly through a solution of 0.15 M NaOH, which was then determined using a spectrophotometer at 740 nm. A detection limit of 1.4 nM, recovery of 94.4% and RSD of 2.5% were obtained at a concentration of 31 nM. In 2016, (Ma, Yuan, and Yuan 2017) integrated their approach into an automated portable Analyser for underway automated analysis of nanomolar phosphate. A detection limit of 1 nM and an RSD of 5.4% (n=180) were obtained. The analysis time was 4-7 minutes/sample. The system was successfully deployed in continuous use during a two-week cruise in the South China Sea. (Deng et al. 2020) continued their work on building a system for nanomolar and micromolar determination of phosphate, using an automated integrated syringe pump-based environmental water Analyser (*i*SEA) with a 3-cm Z-type flow cell. A detection limit of 1.7 nM and RSDs of 3 - 5.7% (n = 11-120) were obtained.

II. **Yellow method assay**

Kitson et al. first reported the yellow molybdovanadophosphoric acid method (Kitson and Mellon 1944). The method was based on the addition of a solution of excess molybdate to an acidic solution mixture of vanadate and orthophosphate to form a yellow molybdovanadophosphoric acid complex.(Sequeira et al. 2002) presented the fabrication of micro total analysis systems (μTAS) or lab-on-a-chip for autonomous monitoring systems. The systems were built for the colorimetric determination of phosphate based on the yellow molybdovanadophosphoric acid, with the yellow coloured complex having an absorption maximum at 380 nm. (Bowden and Diamond 2003) reported the applicability of the molybdovanadophosphoric acid method to the microfluidic manifold for phosphate determination in terms of reagent lifetime and reaction mixture stability. With reagent stability over a 7-week period, absorbance measurements showed an RSD of 3.62% and an RSD of 3.507% for two batches tested. Legiret et al. reported a high-performance, autonomous microfluidic-based Analyser using the yellow molybdovanadophosphoric acid method for DRP determination onboard ships (Legiret, Sieben, Woodward, Abi Kaed Bey, et al. 2013). The research group preferred the yellow method over the blue method in terms of reagent stability. The reagents for the yellow method were more stable than those for the blue method for 1 year. Using a flow cell with 25 mm path length, a LOD value of 52 nM was obtained. Discrete water samples were collected during deployment and analysis via a reference phosphate auto Analyser and compared well with in situ data. Although the LOD is well suited for coastal waters, its application is still limited in oligotrophic zones in the open ocean where phosphate concentrations are typically much lower than 50 nM, especially in surface waters.

1.2.1.2 Electrochemical determination of phosphates

Electrochemistry offers a competitive alternative to wet chemical spectrophotometric techniques for field applications. It allows miniaturization, and features minimum power consumption, and short reaction time, making it easier to integrate into prototypes for in situ monitoring. Several electroanalytical methods and working electrodes have been described, using either solid electrodes (Udnan et al. 2005; Jońca, León Fernández, et al. 2011; Barus et al. 2016) or screen-printed electrodes(Talarico et al. 2015; Kolliopoulos, Kampouris, and Banks 2015) that can be pre-loaded with reagents (Cinti et al. 2016; Wei et al. 2021). Almost all electroanalytical methods are based on phosphomolybdate chemistry and use various electrochemical techniques, e.g., amperometry (Udnan et al. 2005), voltammetry (cyclic voltammetry) (Kolliopoulos, Kampouris, and Banks 2015), and pulsed techniques such as differential pulse voltammetry (DPV) (Jońca et al. 2013) and square wave voltammetry (SWV) (Barus et al. 2016).

Electrochemical determination of orthophosphate based on phosphomolybdate chemistry involves the reaction of phosphate under highly acidic conditions (pH $\leq$ 1), with molybdate reagent, which is either present in solution, pre-loaded onto the working electrode surface (especially screen-printed electrode (SPE)) or hydrolyzed from a molybdenum electrode to form a phosphomolybdate complex which is readily reduced by cathodic reduction. The measurement is characterized by two oxidation peaks and two anodic peaks which are related to the oxidation and reduction states of molybdenum. Of all the electroanalytical techniques reported to date, very few electrochemical prototypes have been reported that allow in situ field application.

Reagentless techniques recently reported by (Jońca, Fernández, et al. 2011; Jońca et al. 2013; Barus et al. 2016) coud be integtrated into full automated analyser with low power consumption for in-situ monitoring of orthophosphate in marine water. The technique is based on the formation of molybdate and protons as a result of oxidation of the molybdenum electrode. Molybdate then reacts with phosphate to form a phosphatemolybdate complex, which can be detected electrochemically. The two major challenges are to avoid interference from silicic acid, which has the same affinity to react with molybdate and form a silicomolybdate complex, and to develop an appropriately sensitive electrochemical detection method. As described in the literature, the ratio of proton to molybdate (H^+/MoO_4^{2-}) must be equal to 70 to prevent the formation of a silicomolybdate complex. This prompted the authors to apply a three-compartment design using a non-proton exchange membrane (Jońca et al. 2013).

Amperometric detection using a rotating gold electrode with an LOD of 0.11 µM and differential pulse voltammetric detection using a static gold electrode with an LOD 0.19 µM were used for

phosphate determination, the latter being more attractive for in situ use due to its lower energy requirement.

DPV has some limitations for in situ application, which are the complexity of parameter optimization and the lack of repeatability. This prompted Barus et al. (Barus et al. 2016) to report on the use of square-wave voltammetry for open-cell applications in a small prototype (<400 μL).

1.2.2 Analysis of nitrates/nitrites

1.2.2.1 Spectrophotometric measuring of nitrates/nitrites

Almost all spectrophotometric methods for nitrite and nitrate analysis are based on the classical Griess reagent method (Griess and Bemerkungen 1879). The Griess reagent method is based primarily on the reaction of nitrite with sulfanilamide (SAM) to form a diazonium salt, which then reacts with a coupling agent N-1-naphthylethylenediamine dichloride (NEDD) to form a pink product. The resulting azo dye is detectable with a spectrophotometer at a maximum wavelength of 540 nm. Nitrate is usually reduced to nitrite via a copper-plated cadmium column and more recently via vanadium chloride at moderately high temperature and then determined via a Griess reagent assay (Moorcroft, Davis, and Compton 2001).

a. Liquid waveguide capillary (LWC)

Li et al. developed a shipboard deployable device for simultaneous monitoring of nitrite plus nitrate ($\Sigma(NO_3^- + NO_2^-)$) and phosphate in the nanomolar range, for which the flow injection system was coupled with two waveguide capillary flow cells (Li, Hansell, and Zhang 2008). The LOD was about 2 nM. The system was deployed over the western Florida continental shelf and in oligotrophic regions as far north as the Sargasso Sea. (Adornato et al. 2005) developed a system using a multiple pump, cartridge heater, 15 cm path length flow cell, and multiple wavelength spectrophotometer. They called the system the Spectrophotometric Elemental Analysis System (SEAS). SEAS with a sampling frequency of 0.4 to 0.75 Hz was capable of collecting ancillary data from separate instruments; 2 nutrient Analysers, a CTD, fluorometer, PAR (Photosynthetically Active Radiation) sensor. SEAS can detect nitrate over a wide linear concentration range from 2 nM to 20 μM. (Feng et al. 2013) reported the quantification of nitrate and nitrite simultaneously applying a reverse flow injection analysis in conjunction with a long path capillary flow cell. A dual-beam detection mode was selected to eliminate light source drift and interference from the sample matrix. The method had a limit of quantitation of 0.6 nM over a wide concentration range of 2-500 nM for both nitrate and nitrite. They chose reverse flow injection analysis instead of normal

analysis to improve sensitivity in terms of lower reagent consumption and lower sample dispersion.

b. Solid phase extraction precipitation method (SPE)

Chen et al. reported the determination of nitrite in the nanomolar range by a sequential injection method based on the Griess reagent method, in which the product of pink azo dye is preconcentrated by adsorption on Sep-Pak C18 cartridge (Chen et al. 2008). The pre-concentrated azo dye was eluted with a solution of 26.6% (v/v) ethanol and 0.108 M H_2SO_4 after being alternately rinsed with water and 28% (v/v) ethanol. The eluted product was detected using a spectrophotometer at 543 nm. Calibration curves of 0.71- 42.9 nM and 35.7- 429 nM were obtained using two sample volumes of 150 ml and 15 ml, respectively. The detection limit of 0.1 nM was reached with a filling volume of 150 ml. 4 samples were collected per hour. Solid-phase extraction method based on HLB cartridge was first used by Zhang et al. using a cadmium column for nitrate reduction in LWCC (Zhang et al. 2010). The detection limit is 0.3 nM and 1.5 nM for nitrite and nitrate, respectively.

c. Microfluidic Sensor

Sieben et al. reported the design and fabrication of a microfluidic flow system and the description of the absorption cells and detection system (Sieben et al. 2010). The microfluidic system was successfully used to determine nitrite and other chemicals in seawater, as discussed in the previous and following sections. By using microfluidic chips manufactured of tinted poly(methyl methacrylate) with a custom-built syringe pump (with 3 syringes), 15 valves, and three absorption cells, a LOD of 25 nM and 20 nM was achieved for NO_3^- and NO_2^-, respectively (Beaton et al. 2012). Because of their small size and minimum power consumption, these analysers are well suited for use on autonomous underway vehicles (AUVs) and gliders. These micro-Analysers showed suitable analytical performance and durability during field-testing in coastal waters (e.g., 26 days of field-testing in Southampton waters).

1.2.2.2 Ion Chromatography (IC)

Kodamatani et al. reported a method for simultaneous determination of nitrite and nitrate based on ion pair chromatographic separation (Kodamatani et al. 2011). The separation is performed by a short column of octadodcylsilane (ODS) with a mobile phase of 10 mM borate buffer - methanol (99.5: 0.5) (v/v) pH 10 containing 5 mM lauryltrimethylammonium chloride and 50 mM NaBr. Detection was by UV irradiation followed by chemical luminescence. A calibration curve of 0.1 - 20 μM NO_2^- and 1 - 200 μM NO_3^- was obtained and LOD values of 0.05 μM NO_2^- and 0.4 μM NO_3^-. For 7 identical replicate injections of 0.5 μM NO_2^- and 5 μM NO_3^-, a precision of 2.7% and

2.1%, respectively, was obtained. For two seawater samples spiked with 2 μM NO_2^- and 20 μM NO_3^-, recoveries of 58% and 75%, respectively, were obtained. The recoveries improved to values of 84% and 87%, respectively, when diluted tenfold. This indicates that the method is not yet mature enough to be used directly for seawater analysis and further studies should be conducted.

1.2.2.3 Gas Chromatography-Mass spectrophotometry (GC-MS)

Pagliano et al. proposes a quantification of nitrate and nitrite in seawater combining derivatization of triethyloxonium tetrafluoroborate (TEOT) with direct headspace (HS) gas chromatography-mass spectrophotometry (GC-MS) (Pagliano et al. 2011). TEOT undergoes an O-alkylation reaction with nitrite and nitrate to form the corresponding ethyl esters, which are readily detectable using GC-MS. The method was proposed for the simultaneous determination of nitrite and nitrate in seawater in the micromolar range. Validation was performed by determining nitrate and nitrite in certified reference material for nutrients (NRC, Canada). A percentage of 10% was considered for the chemical conversion of nitrite to nitrate. Interconversion was evaluated and corrected by using isotope-enriched internal standards. Pagliano et al. continued their work using negative chemical ionization to further improve sensitivity, yielding a detection limit of 150 ng L^{-1} for NO_2^- and 600 ng L^{-1} for NO_3^- (Pagliano et al. 2012). Optimizations were made and alkaline conditions were selected to minimize the conversion of nitrite to nitrate and to avoid the exchange of oxygen between the analytes and the water solvent.

1.2.2.4 Electrochemical measuring of nitrates/nitrites

Electrochemical determination of nitrite and nitrate in seawater presents some challenges. Many attempts have been made to quantify nitrite and nitrate by electrochemical quantification on ion-selective membrane electrodes (ISEs) for potentiometric sensors. The potentiometric sensors determine the analytical quantity of interest (i.e., the concentration of some components in the solution) by the potential difference between two connected electrodes. The signal from the potentiometric sensors is based on the Nernst equation

$$E = E^0 + \frac{RT}{nF}\ln[a_i] \qquad \textbf{Equation 1.3}$$

Where E is the potential difference between the ion selective (indicator) electrode and reference electrode in V, E^0 is the standard potential in V, a_i is the activity of the target ion, R is the gas constant (8.314 $J.K^{-1}$), T is the temperature in kelvin, n is the number of electrons, F is the Faraday constant (96500 C/mol). The commercially available ISEs have not been deployed directly for nitrate and nitrite determination into non-spiked seawater. The challenges that face the direct

application of potentiometric membrane ISEs is the high concentration of chloride (Cl^-) ions in the seawater causing a high interfering error. As mentioned by Cuartero et al, in the potentiometric detection of nitrate in seawater, the chloride ions present in the matrix deposit reversibly on the surface of the silver working electrode as AgCl, releasing the sodium ions to the external solution, while the reverse reaction occurs at the counter/reference electrode; this was evident by calculating the LOD of NO_3^- in a solution containing 600 mM NaCl and a solution containing 1 mM NaCl, which were 10 μM NO_3^- and 1 μM NO_3^- (Cuartero, Crespo, and Bakker 2015). The potentiometric determination of nitrite is the same challenge as that of nitrate, with the addition of hydroxyl ions (OH^-) as interfering ions. Pankratova reported the coupling of an inline sample acidification unit for a significant improvement in the potentiometric determination of nitrite in seawater. Pankratova et al. reported calibration curves performed in a solution of 1 mM NaCl at pH 8.2 and pH 5.5, and the same for a solution of 0.6 M NaCl. At pH 8, LOD values of 13 μM and 40 μM were reported in a solution of 1 mM and 0.6 mM NaCl, respectively. At pH 5.5, LOD values of 0.38 μM and 16 μM were reported in a solution of 1 mM and 0.6 mM NaCl, respectively (Pankratova et al. 2017). Cuartero et al. reported the fabrication of a microfluidic thin film flat cell in which direct determination of nitrate was performed by in-line coupling with the electrochemical desalting unit. The desalination unit functioned by electrolytically depositing Cl^- from a thin film solution onto the silver working electrode as AgCl, and the Na^+ was released to the external solution through a permselective membrane (Cuartero, Crespo, and Bakker 2015). The potentiometric detection unit with a total volume of 13 μL consisted of the solid selective electrode (working electrode) was made for nitrate determination, where lipophilic carbon nanotubes were deposited on a glass carbon electrode, and a miniaturised Ag/AgCl reference electrode in the reverse direction. After successful reduction of Cl^- concentration from 600 mM to 2.5 mM, the 80 μL of desalted sample was transferred to the detection cell. With a response time of 5 s, a detection limit of 0.5 μM NO_3^- was determined. (Cuartero et al. 2018) reported the in-situ deployment of the proposed system in Arcachon Bay, France, with a 2-hour sampling frequency, integrating the desalination and acidification modules into the submerged system for potentiometric detection of nitrate and nitrite after removal of Cl^- and OH^- from the seawater matrix.

Wang et al. demonstrated MoboSens, a mobile phone sensing platform that performs electrochemical voltammetric measurements by using audio jack of smartphone (Wang et al. 2015). He used this sensor to measure nitrate concentration using few microliters liquid sample in the field along with providing geospatial map locations through wireless network.

1.2.3 Analysis of Silicic acid

1.2.3.1 Spectrophotometric measuring

Silicic acid is usually determined spectrophotometrically by the reaction of silicic acid with molybdenum salt in an acid medium to form a yellow-coloured silicomolybdenum complex (β-molybdic acid), which can be detected directly or is generally reduced by ascorbic acid with the assistance of Oxalic acid to form a blue coloured silicomolybdenum complex (α-molybdic acid) which has two peaks in the absorption spectrum at 660 and 820 nm, with the highest absorption at 820 nm. In 1955, Mullin et al. first proposed the colorimetric determination of silicon based on the hydrocyanic acid method. Mullin et al. introduced the blue method for the determination of silica, which overcame the shortcomings of the yellow method such as 1) the colour of the reaction mixture is stable for only about 5 minutes, 2) the absorption maximum overlaps with that of the molybdate solution used for complexation, 3) the method is not suitable for the determination of low silicon contents. (less than 0.1 mg/L)(Mullin and Riley 1955). Truesdale et al. first reported the automatic determination of silicic acid in natural fresh water via means of reduction of silicomolybdic acid to blue molybdenum complex using a reducing agent (tin(II) chloride)(Truesdale and Smith 1976). In 1983, Thomsen et al. reported the determination of silicic acid in seawater by flow injection analysis where he firstly reported the usage of oxalic acid which transform the excess molybdate to a nonreducible form as well as suppresses the interference from phosphate by decomposing phosphomolybdic acid Finally, the stannous chloride and ascorbic acid were tested as reductants(Thomsen, Johnson, and Petty 1983). The following sections summarise the approaches used for trace level analysis of silicic acid.

a. Liquid waveguide capillary (LWC)

In 2009, Amornthammarong and Zhang used 8-way distribution valves equipped by one syringe pump connected with 2 m liquid core waveguide (LWC) tube. Poly vinyl alcohol was added to the solution in order to prevent the reprecipitation into the ammonium molybdate. No refractive index effects seemed with this method but some small effects due to change of the salinity appeared during the analysis of seawater samples but these can be corrected. Despite the long analysis time (~15 min sample^{-1}) and the length of LCW (2 m), the working linear range was 0.1- 10 μM and the LOD was 100 nM (Amornthammarong and Zhang 2009). In 2012, Ma and Byrne (Ma and Byrne 2012a) combined both the flow injection analysis (FIA) with LCW of 160 cm. The FIA method depends on the injection of small volume of the sample inside the detector with the stream of the reagents, the advantages of those systems represented into its merits of simplicity, acquiescence to

automation and high sample throughout rate and low risk of contamination (Grasshoff, Kremling, and Ehrhardt 2009). This method showed LOD value of 10 nM and the interference effect of phosphate is diminished by the addition of 50 g L^{-1} oxalic acid prior to the formation of the yellow phosphomolybdic complex and then it was reduced with ascorbic acid. Seawater matrix and salinity effects were examined and minimized through on-line dilution with reagents. The linear range in this method was 0.1 to 5 μM which can be raised to higher concentration range on-line without alteration in the instrument' hardware (either with using alternative analytical wavelength or changing the flow rate). This engineered set-up facilitates the on-line measurement of silicic acid either for determination of silicic acid in ultra-pure waters (industrial activities) or shipboard/underway monitoring in sea water (oceanographic science).

b. Solvent extraction

Brzezinski and Nelson investigated a solvent – extraction method for nanomolar concentrations of silicic acid, this approach depends on the extraction of β-silicomolybdic complex in n-butanol, after the mixing of silicic acid and molybdenum under low pH conditions and then the reduction by *p*-methylaminophenol sulphate or sulphite. The silicomolybdenum blue complex (SiMB) can then be detected colourimetrically in a cuvette of 10 cm at a wavelength of 820 nm. This method enhances the sensitivity of traditional aqueous method by 30 times and improve the precision by 10 times. However, this approach is labor intensive and highly consumable of organic solvents, the sensitivity is 70 % in sea water compared with that into seawater due to the salt effect error (Brzezinski and Nelson 1986).

c. Magnesium induced co-precipitation method (MAGIC)

MAGIC depends in general on the concentrate the analyte before the routine measurement by adsorption to $Mg(OH)_2$ precipitate. In 2007 Rimmelin-Maury et al. adapted this method for silicic acid determination. First, NaOH is added to water samples, then the sample is preconcentrated by centrifugation and then dissolution by dilute acid (0.025 M HCl) and then analysis by classical calorimetrically at 820 nm. At 12.5 times for preconcentration of silicic acid in compared with the conventional methods with improvement by 10-fold for the precision and the detection limit. But MAGIC is a highly labor-intensive method and it requires 2 h waiting for colour formation into preconcentrated silicic acid solution (Rimmelin-Maury, Moutin, and Quéguiner 2007).

1.2.3.2 Chromatographic determination

Ion exclusion chromatography (IEC) based method was introduced as an alternative to classical colourimetric quantification of silicic acid in 1997 by Akiharu Hioki et al. to seperate silicic acid

from sulphide and chloride ions inside the solution, in combination with highly sensitive, selective and ultra-accurate inductively coupled plasma (ICP). The authors reached a LOD value of 80 nM, this value is not appropriate for oligotrophic oceanic analysis although it was enough for certified reference materials (CRM) (Hioki, Lam, and McLaren 1997). Furthermore, in 2000 Bin-Liu et al present an IEC method connected with conductivity-detector instead of using ICP in order to reduce the cost of the instrument and a long concentrations range was detected from 0.1 to 1000 μM (Li and Chen 2000). This method is more expensive and, in most cases, it is required a well experienced person who can deal with those well-establish techniques.

1.2.4 Deployable Analysers

The technologies that allow monitoring of macronutrients under environmental conditions (i.e., *on-site* and *in-situ*) are urgently needed to measure short-term fluctuations as well as long-term trends. Most of them are commercially available and some have only recently been described in the literature. Three major analytical technologies have been employed wet chemical techniques, optical (ultraviolet) sensors and electrochemical techniques.

- Hydrocycle-PO_4, Sea-Bird

The HydroCycle Phosphate Sensor (Snazelle 2018a) is a wet chemical sensor developed by Sea-Bird Scientific (Philomath, Oregon, United States) for the continuous measurement of soluble orthophosphate in the environment. The HydroCycle measures orthophosphate based on the blue phosphomolybdate complex method. The Analyser has a reagent cartridge containing a mixed reagent of acid molybdenum and antimony, a reagent cartridge containing ascorbic acid, and a reagent cartridge containing a 5.3 μM phosphate standard solution. The sensor uses a simple copper screen with 0.11-inch pores and 5-10-micron on-board filters to reduce sediment uptake. Power is supplied via a six-pin cable for RS -232 communication and via an 8-pin cable for SD -12 communication. The Analyser weighs 7.6 kg (with reagents) and has a height of 56 cm and a diameter of 18 cm with a rated depth of 200 m. The Analyser is designed for vertical use and does not work well in horizontal orientation.

- ANAIS

The autonomous nutrient Analyser ANAIS (Autonomous Nutrient Analzyer In-Situ) (Thouron et al. 2003) has been produced for monitoring nitrate, silicic acid and phosphate and can be deployed at depths of up to 1000 m. The chemistry is based on spectrophotometric detection by using solenoid driven diaphragm pumps to inject the sample, standards and reagents through a

thermostatic manifold with micro-conduit and flow injection. Microchannels are engraved into two poly (methyl methacrylate) (PMMA) plates for phosphate and nitrate and two polyetheretherketone (PEEK) plates for silicic acid. The measurement protocol involves three steps over 13 minutes, including sample stream purging, reagent introduction, and absorbance detection. The chemistry used is based on the Griess reagent test using a cadmium column for nitrate reduction, the silicomolybdate blue method is based on the use of acid molybdenum reagent, oxalic acid and ascorbic acid, the phosphomolybdate blue method is based on the use of acid molybdenum reagent with the further reduction via a stannous chloride solution (9 % (wt/v), hydrazine sulfate (0.26 % (wt/v), concentrated H_2SO_4 (2.8 % (v/v)) in autoclaved deionized water) . The Analyser is placed in an equipressure tank filled with oil. The Analyser showed a linear concentration range up to 40 μM nitrate, 150 μM silicic acid and 0.5 μM phosphate with detection limits of 0.1, 0.5 and 0.1 μM and an accuracy of 1, 1 and 3 %, respectively.

- ALCHEMIST

ALCHIMST (AnaLyseur CHIMique In SiTu) (Le Bris et al. 2000) is a submersible chemical Analyser developed by Bris et al. based on colourimetric determination and flow injection analysis (FIA) for in situ determination of $\Sigma(NO_3^-+NO_2^-)$ and total sulfide (ΣS) to be used in deep-sea hydrothermal environments. ALCHEMIST consists of three main modules: Hydraulics, Spectrophotometry and Electronics. An electronic package manages the power supply and serial communication between the computer and spectrophotometric and hydraulic modules. Two PMAA flow cells (3 cm path length) with two spectrophotometric detection cells with two wavelengths. The solutions are mixed and transferred to the spectrophotometric module via a peristaltic pump, two injection valves and two selection valves with six ports in the hydraulic modules. Chemical analysis was based on the Griess method for $\Sigma(NO_3^-+NO_2^-)$, which is based on the reduction of nitrate on a copper-plated cadmium column, and the method used for ΣS was adapted to FIA from method developed by Sakamoto-Arnold et al.(Sakamoto-Arnold, Johnson, and Beehler 1986) Detection limits of 0.8 μM for ΣS and 0.5 μM for $\Sigma(NO_3^-+NO_2^-)$ were obtained.

- Microfluidics technologies

Lab-on-Chip (microfluidic technologies) was manufactured by Clearwater Senor Ltd. (Southampton, England). The product is based on the development of in situ technology invented by the National Oceanography Centre and the University of Southampton. Five devices have been produced for pH (Yin et al. 2021), $\Sigma(NO_3^-+NO_2^-)$(Beaton et al. 2012), PO_4^{3-} (Grand et al. 2017), H_4SiO_4 (Cao et al. 2017) and iron ((Geißler et al. 2017). The sensor consists mainly of an

optofluidic chip combining both microfluidics and optics. The delivery of reagents, standards and seawater samples is assisted by pumps and electromechanical valves that allow mixing of the analyte solution with the reagent in the mixing chamber. The chip was made of a dark-tinted PMMA that reduces light drift effect, stray light and ambient light. The width of the channels is 150 μm, in which pockets for light emitting diodes (LEDs), waveguides, photodiodes, and the printed circuit boards (PCBs) were placed. The main PCB contains the microprocessor and almost all the function commands read from the sensor. Typically, the sensor has a height of 56 cm with the reagent housing and a diameter of 20 cm. A LOD of 20 nM for $\Sigma(NO_3^-+NO_2^-)$, 40 nM for PO_4^{3-}, 20 nM for ferric (II) and ferrous (III), 0.75 μM for silicic acid, and a precision of 0.001 for pH. These sensors have been deployed more than 200 times on the smallest and lowest performance platforms, including floating profiles and sea gliders. They have been deployed at physically and geographically extreme depths of about 4800 meters, in ice-covered and sedimented proglacial meltwaters, rivers and estuaries.

- WIZ and NPA

SYSTEA SpA (Anagni, Lazio, Italy) manufactured two types of in situ probes: Nutrient Probe Analyser (NPA) and WIZ (Bodini et al. 2015; Moscetta et al. 2009), based on a patented Loop Flow Analysis (LFA) and Micro Loop Flow Analysis (μLFA). The Analysers were used for sequential quantification of four parameters in one cycle (30 minutes for a complete cycle with four parameters). The Analysers are characterized by their small size and contain both the reagent container and the analysis unit. The reagents are connected to the analysis unit via an "umbilical cord", which contains ten fluid lines for the supply of reagents and standard solutions. In the lid there are various hydraulic connections for water samples and the inflow of deionized water as well as the outflow of the waste. When using the waterproof electrical connection, 12 V continuous current is required as a power source and communication is via RS -232 serial connection.

- NuLAB

The NuLAB was developed by Green Eyes LLC (Easton, United States) for the automated determination of nutrient concentrations ($\Sigma(NO_3^-+NO_2^-)$, PO_4^{3-}, H_4SiO_4, and NH_4^+) through four individual channels ('Green Eyes, LLC'),. Each channel consisted of a syringe that injects and withdraws an accurate volume of sample, standard, and reagent for mixing and rinsing; a six-port rotary valve that connects the reagents, standards, detectors, and water sample to the syringe; and a colourimetric detector consisting of LED that transmits light through the flow cell (2 mm for low sensitivity (i.e., high concentration range) and 10 mm for high sensitivity (i.e., low

concentration range) and measures the transmitted light at the end with a photodiode. The detection limits for the high sensitivity detector were 0.2 μM for $\Sigma(NO_3^-+NO_2^-)$, 0.15 μM for NO_3^-, 0.2 μM for PO_4^{3-}, 0.3 μM for H_4SiO_4, and 0.3 μM for NH_4^+.

- SUNA

SUNA was developed in 2008 as the smaller and freshwater shallow version of in-situ ultraviolet spectrophotometer (ISUS) which was reported by Johnson et al. (Johnson and Coletti 2002). Ultraviolet measurement of dissolved nitrate ions was performed at a wavelength below 240 nm. The ISUS consists of major components including a continuous wave deuterium light source (Hereaus Fiberlight), optical fibre coupled retroreflectance probes, a second fibre connected to the UV light source to monitor the sensitivity of the light source, the high-resolution UV photodiode array spectrophotometer, and a lower power large memory controller. The probe body is made of PEEK and is designed to withstand a pressure of 200 bar and a temperature of 280°C. The main difference between SUNA and ISUS is that for SUNA the fibre optic probe was replaced by a continuous quartz chamber and the single board computer used for ISUS was replaced by a microcontroller for nitrate measurement (MacIntyre et al. 2009). For SUNA, a depth range of 2000 mm was demonstrated with a corrosion-protected aluminium housing. A LOD of 2.4 μM was achieved at 10 mm path length (Bai et al. 2014).

-OPUS

One of the ultraviolet spectrophotometers for nitrate is OPUS (Trios), it is a submersible device used both in the surface and deep sea (Nehir et al. 2021). The instrument uses a light source consisting of a xenon flash lamp with 256-channel high-end miniature spectrophotometer and a reference photodiode. The light is emitted by a xenon lamp and directed into a flow cell containing the sample. It is then recorded by a spectrophotometer over a wavelength range of 200 - 360 nm with an integration time of 256 ms. The reference diode is used to monitor the light intensity of the xenon lamp. The analyser components are housed in a stainless-steel case for surface water up to 300 m or in a titanium case for use in deep waters up to 6000 m. OPUS has been set to a continuous sampling mode for measurement with a 30 s time interval. A time interval of 3 s can be achieved with a custom-made controller. OPUS offers an accuracy of about 2 μM NO_3^- and a short-term precision of 0.4 μM NO_3^-.

-ANESIS

An automated electrochemical sensor for in situ determination of silicic acid in marine waters was presented by (Barus et al. 2018) and validated in 2021 (Legrand et al. 2021). The Analyser design is based on two electrochemical cells with a volume of 376 µL for the complexation cell and a volume of 94 µL for the detection cell. The NKE Instrumentation design is a cylindrical sensor made of anodized aluminum with a weight of 2.2 kg in air, a diameter of 90 mm and a height of 250 mm without the connector. The bottom of the sensor with the connector and the electrochemical cells is made of PEEK parts. Solenoid pumps were used to deliver the solutions to the complexation cell and then the reaction mixture to the detection cell. The enclosure was validated up to 60 bars (600 m). The molybdenum electrode used for reagent formation (molybdenum and proton discharge) is located at the bottom of the complexation cell. In the complexation cell, the silver wire reference electrode and titanium grid are located behind the Nafion membrane. For the detection cell, three electrodes - a gold working electrode, a silver reference electrode and a platinum counter electrode - all with the same diameter of 2 cm are placed in the same PEEK piece with epoxy resin. The sensor was equipped with temperature and pressure sensors. The sensor was deployed on a mooring off Coquimbo, Chile, and also combined on a PROVOR profiling float in the Mediterranean sea off Villefranche-sur-Mer, France. In 2021, the analyser was deployed in the Thau Lagoon (Mediterranean Sea) at a depth of 1.6 m.

1.2.5 Limitation of deployable nutrients Analyser

Despite the availability of numerous operational macronutrient Analysers and significant technological advances in recent years, there are still a range of challenges that hinder the proper use of the equipment. This prevents a better understanding of nutrient distribution in real time and does not contribute to better comparability with data obtained from discrete samples collected at sampling sites and analysed with various laboratory-based Analysers.

Few real-time analysers for monitoring multiple macronutrients in natural water are known in the literature or on the market, including WIZ and NPA from Systea, Italy, and NuLAB from GreenEyes LLC, USA, but there is no report on the long-term use of these analysers in seawater. Also, there is no report of field testing of electrochemical sensors for PO_4^{3-} in autonomous prototypes in seawater.

Overall, almost all deployable Analysers suffer from the following drawbacks (Daniel, Laës-Huon, Barus, Beaton, Blandfort, Guigues, Knockaert, Munaron, Salter, Woodward, et al. 2020):

- the low reliability compared to laboratory-based reference Analysers

- sensitivity (i.e., detection limit) is insufficient for nutrient analysis in some marine research areas (e.g., open ocean, oligotrophic areas).
- Complications in data interpretation due to deviation of calibration plots before and after deployment as a result of various problems normally encountered during deployment, such as biofouling and sensor drift.

1.3 Thesis objectives and outline

The overall aim of this work is to find a suitable analytical protocol for the analysis of macronutrients in seawater in order to describe their behaviour and distribution in estuarine and coastal waters. The importance of macronutrients in the aquatic environment, as they control primary production and thus the global carbon cycle, necessitates the provision of real-time monitoring tools to detect both spatial and temporal changes. These instruments should provide macronutrient concentrations with high precision. The general research questions and objectives underlying this work are as follows

- Fabrication of a new electrochemical sensor for PO_4^{3-} based on the phosphomolybdate method.
- Adaptation of the analytical method for good, accurate and repeatable performance and characterization of the working electrode surface morphology.
- Validation of the proposed method through the analysis of real seawater samples analysed with a colorimetric reference instrument.
- Integration of the proposed method into an autonomous analyser and further validation during real-time field experiments.
- Improve the performance of a commercial analyser for real-time monitoring of macronutrients and implement the new vanadium chloride nitrate reduction assay in a field macronutrient analyser for the first time.
- Validation of the analyser with our proposed protocol by field deployment in highly dynamic estuarine water in the Kiel Fjord.

The dissertation consists of six chapters. This chapter, Chapter 1, is the introduction. Chapter 2 introduces the reader to the basic knowledge assumed in the following chapters through a detailed description of the techniques and instrumentation used (AutoLAB Analyser) and the description of the prototype designed, which is not discussed further in the following chapters. Chapters 3, 4, and 5 were written as manuscripts that have been published or are prepared for submission to

scientific journals. Chapter 3 and Chapter 4 present our proposed protocol for the electrochemical determination of phosphate in seawater.

In Chapter 3, describe the first step to fabricate a carbon paste modified electrode and develop the proposed protocol. An attempt was made to describe the mechanism of the reactions that occur and to investigate the effects of different analytical conditions, as well as the ability of the proposed sensor to overcome the interfering effect of silicic acid as a common interfering ion of phosphate in seawater. The evaluation was performed on discrete samples collected during a research cruise in the North Sea and analysed in the laboratory, with a comparison to the analytical methods used by the reference laboratory and to other hydrographic data collected by CTD sensors. This chapter was published in the Journal of Electrochemical Society (DOI: https://doi.org/10.1149/1945-7111/ac3b03).

Chapter 4 addresses the application of the electrochemical method proposed in Chapter 3 in a prototype flow injection Analyser with an *on-site* application on a pontoon in a research cruise in North Sea. Chapter 5 focuses on the improvement of an *on-site* Analysers for macronutrients (phosphate, nitrite, nitrate, and silicic acid) in natural water. A new vanadium chloride reduction method was used for nitrate analysis with the classic Griess reagent method, and the classic blue method for phosphate and the classic blue method for silicic acid. An improved analytical protocol was fully described and applied to the Analyser. The evaluation was based on a long-term deployment campaign conducted in Kiel Fjord in May and June 2021 and the results show the ability of the Analyser to describe the dynamics of macronutrients in the fjord through ancillary data collected from other sensors deployed at the same time at the research site. This chapter has been published in Sensors (DOI: https://doi.org/10.3390/s22093479).

2 Materials and Method

2.1 Voltammetry

All voltammetric techniques have in common that in all of them a potential (E) in volts (V) is applied, which can be considered as an excitation signal for a working electrode, and as a consequence a current (I) in amperes (A) flows through the electrochemical cell. In the voltammetric techniques, the change in potential or current is observed over a period of time (t).

All voltammetric techniques are performed in an electrochemical cell. It is typically a three-electrode system with a working (indicator) electrode, a counter (or auxiliary) electrode, and the reference electrode (hydrogen reference electrode (HRE) ($Pt(s)|H^+|H_2$); saturated calomal reference electrode (SCE) ($Cl^-(4M)|Hg_2Cl_2|Hg^+|Pt$); or silver/silver chloride reference electrode ($Ag^{(0)}|AgCl|KCl$ (3M)). The potential of the working electrode is controlled with respect to the reference electrode. The working electrode is the electrode on whose surface the reaction takes place, and the electrode generally represents the interface across which the charge is transferred. The reduction and oxidation processes generally occur on the surface of the working electrode, which corresponds to mass transfer under the required applied potential and results in the generation of the current to be monitored.

A typical voltammetric cell usually consists of an analyte dissolved in a solvent, an ionic electrolyte, and three electrode chambers. The reference electrode should have a reversible half-reaction with Nernst behaviour that keeps the potential constant over time, and it should be easy to fabricate and maintain. The most common reference electrodes are silver/silver chloride (Ag/AgCl, 3.0 M KCl) with a potential of 0.210 V vs. HRE at 25°C and SCE (Hg/Hg2Cl2, KCl) with a potential of 0.241 V vs. HRE at 25°C. The counter electrode (also called auxiliary electrode) is used to apply the current to the working electrode through the connection to the electrolyte. It is usually made of an inert metal or noble metal or graphite to protect it from dissolution. The working electrodes differ according to geometry and material.

The potentiostat is an instrument that allows you to apply a specific potential and monitor the current. Most voltammetric techniques are dynamic and require a modulated potential according to a predefined waveform that can be flexibly and accurately controlled by the potentiostat.

The cyclic voltammetry technique is based on linear potential scanning according to the triangular waveform, where the excitation potential switches the potential between two values and is then called the switching potential.

Square wave voltammetry is a type of pulsed voltammetry technique that reduces the non-Faradic current (charging current) in the direction of the Faradic current, which increases the sensitivity of this technique among the various voltammetry techniques. Square wave voltammetry is a large amplitude differential technique that depends on a symmetrical square wave in which the current is measured twice at the beginning and end of the pulse. This technique is controlled by three components: amplitude in mV (height of the potential pulse), step potential in mV (staircase-shaped potential ramp), and frequency in Hz (reciprocal of the duration of a potential cycle), where the scan rate (υ)is measured in mV.s-1 from the value of the step potential (E_{Step}) and the frequency (f).

$$\upsilon = \boldsymbol{E_{Step}\, X\, f} \qquad \textbf{Equation 2.1}$$

2.2 Electrochemical Impedance Spectroscopy

Electrochemical impedance spectroscopy (EIS) is one of the earliest techniques used in electrochemistry for about a century. EIS is typically used to describe all possible electrochemical reactions at electrode/electrolyte interfaces in terms of components of equivalent electrical circuit diagrams. The current flow in an electrochemical cell is the result of a chemical reaction (i.e., the Faradic components),

$$\boldsymbol{Oxid. + ne^{-} \rightarrow Redu.} \qquad \textbf{Equation 2.2}$$

where n is the number of electrons transferred, Oxid. is the oxidized form, and Redu. is the reduced form: the current flow also depends on some other components unrelated to the measurement reaction (i.e., non-Faradic components)? The transfer of charge in an electrochemical cell result in Faradic and non-Faradic components. One of the Faradaic components is the polarization resistance (R_P), the so-called activation barrier, which the electrons of the reaction (5) must overcome to pass the interface. At any electrode potential, the activation barrier is called polarization resistance while at the standard electrode potential, this component is named as the charge transfer resistance (R_{CT}). One of the other Faradaic components is the uncompensated solution resistance (i.e., electrolyte resistance) (R_S). One of the non-Faradaic components is the current generated by charging the double layer capacitor (C_{dl}). Another class of impedances is the Warburg impedance (Z_W), which is important for electroanalytical chemistry because charge transfer occurs when mass transport of reactants and products occurs at the interface, and then affects the rate of electron transfer. The rate of electron transfer depends on how fast the reactants (oxidants) are consumed and how fast the reducing agents are produced

near the electrode surface. This shows up as a peak current in a voltammogram or a current plateau in a polarogram. All of these components are shown in an equivalent electrical circuit first proposed by Randles and shown in **Figure 2.1**. Many attempts have been made to improve techniques (e.g., normal pulse, square wave and differential pulse voltammetry) that compensate for the influence of non-Faradic double layer charging current which affected traditional voltammetric techniques at different extents based on the experimental conditions applied (e.g., cyclic voltammetry and linear sweep).

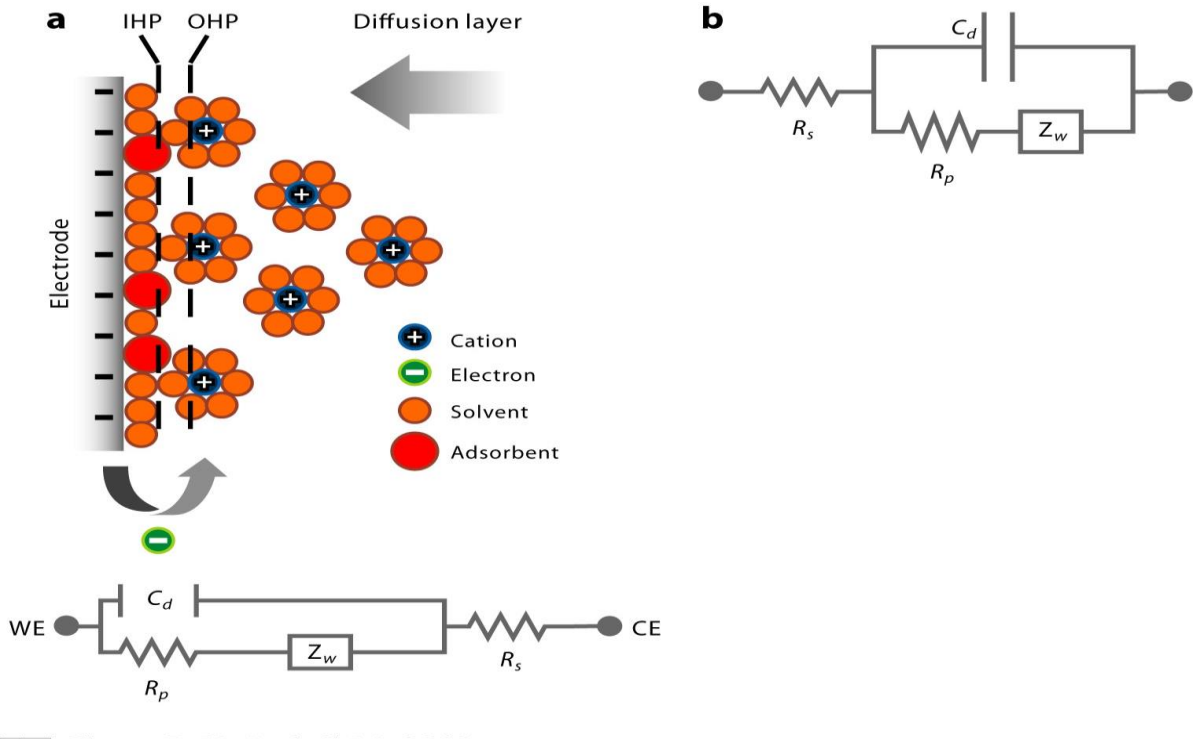

Figure 2.1 (a) the electrified surface where the electrode surface is negatively charged with counter cations are place in alignment along the electrified surface, where IHP is inner Helmholtz plane and OHP is outer Helmholtz plane (upper) and the equivalent electrical circuit combine all interface components (bottom), CE is the counter electrode and WE is the working electrode. (b) idealized Randles equivalent electrical circuit (Chang and Park 2010).

2.3 Electrochemical determination of PO_4^{3-} based on phosphomolybdate method

The common analytical method for the electrochemical determination of phosphate is to treat the sample with an acidic molybdate solution to convert orthophosphate to the Keggin anions ($PMo_{12}O_{40}^{3-}$) followed by reduction. The chemistry of the Keggin anions is very complicated. The

formation, stability and spectrum of the isomers depend on a number of experimental conditions(Nagul et al. 2015), in particular pH, while the method suffers from a number of interfering factors that have the same ionic structure (e.g. silicic acid), which facilitates their tendency to react with molybdate to form the Keggin ion (Ilangovan and Chandrasekara Pillai 1997; Jońca et al. 2012).

Overall, almost all electrochemical methods for the determination of phosphate using the phosphomolybdate method are based on the electrochemical reduction of the phosphomolybdate complex previously formed in the solution after the reaction of the molybdate ion with orthophosphate under acidic conditions. This electrochemical determination of phosphate based on the molybdate assay is carried out via a series of electrochemical reactions such as (1) reduction of molybdophosphoric acid (MPA) to molybdenum blue, (2) oxidation of molybdenum blue that has been electrochemically pre-reduced and adsorbed on the electrode, and (3) electroreduction of molybdovanadophosphate.

2.4 Dual-electrodes electrochemical cell

A bi-potentiostat in dual-channel mode is an approach in which the potentiostat operates with a dual-channel in which the measurement is made on 2 working electrodes that share the same counter electrode and reference electrode.

The bi-potentiostat techniques have two modes:

- The standard mode where one technique is applied to the first channel while fixed potential is applied to the second channel.

- The scanning mode where the same technique with the same potential sweep is applied for both channels.

The bi-potentiostat technique is comparable to the dual-beam spectrophotometry technique in which the incident light beam is split into two parts, one of which passes through the cuvette cell containing the analyte sample and the other of which passes through the cuvette cell containing the reference blank solution, and the detector measures the ratio between the two beams in real time. The advantages of the double-beam spectrophotometer (DBS), which corrects for solvent blank absorbance, over the single-beam spectrophotometer (SBS): the DBS has the advantage of correcting for variations in the light beam from the lamp (i.e., the light source). These variations are either in stray light, beam intensity variation, or electronic noise and can be corrected as soon

as it is done in real time. Although SBS provides higher sensitivity than DBS because the light is consistently brighter or because a smaller number of optical components results in higher light transmission and noise reduction, the benefits of using DBS outweigh the higher sensitivity of SBS. Modern advances in optics and electronics have led to the increasing adoption of dual beam systems.

In the same way, our approach for phosphate analysis depends on the use of a dual-mode bi-potentiostat (Metrohm DropSens, Netherlands), where one working electrode is made of the carbon paste containing the required reagent (i.e., molybdate reagent) and acts as a reagent-based electrode at this point, while the second working electrode contains only the carbon paste and acts as a bare electrode.

We have adapted our proposed setup to perform the same function as DBS, where the same potential sweep is applied to both the reagent-based electrode and the bare electrode, and this correction can help correct for interferences from the natural water matrix. The proposed setup can also correct for the changes in the surface area of the working electrodes that affects the signal obtained. This can be done by subtracting the voltammogram of the bare electrode from that of the reagent-based electrode.

2.5 Electrochemical Flow Injection Analyser (FIA)

The flow injection Analyser (FIA) is a most important instrument for automation of chemical analyses in a laboratory. This is because a range of measurements in a chemical laboratory involve liquid materials and a number of the following operations: handling of solutions, detection of analytes, data acquisition, data processing and calculation of results (Ruzicka and Hansen 1988). The FIA gives us the ability to transfer routine chemical analysis that has been developed or improved to the laboratory for use in field measurement under environmental conditions. The FIA setup shown in **Figure 2.2** consists of four components arranged in sequence: Standard and reagent solution containers, solution supply (peristaltic pump), sample selection (switching valve), detection unit (a potentiostat as detector and an electrochemical flow cell). The reagents, standards and deionized water for washing were continuously delivered to the flow cell via the peristaltic pump.

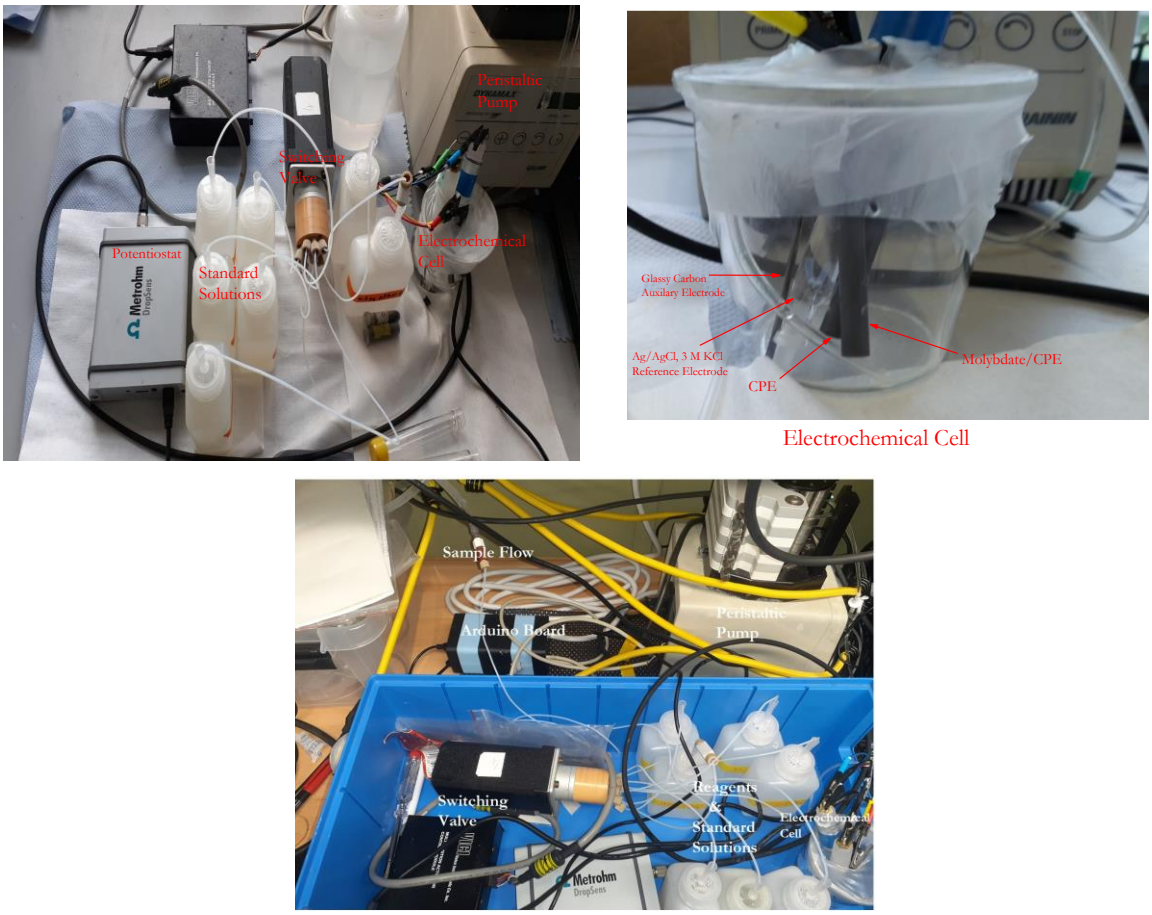

Figure 2.2 Electrochemical flow injection Analyser with 10-position switching valve with control module box, peristaltic pump, μStat 400 Metrohm DropSense potentiostat and an electrochemical cell with two working electrodes.

The operation of the DYNAMAX RP -1 peristaltic pump (Rainin Instrument Co., US) was automated with a home-built controller box and programmed with a Python script. The DYNAMAX RP -1 peristaltic pump has a connector with 8 pins as follows: Pins 1 and 2 to set the pump speed with a voltage range of 0 → 5 V (stopped → 100% speed), pins 3 and 4 to set the stop/run mode, and pins 5 and 6 to set the pump direction with electrical levels of +5 V (open) and 0 V (closed). Pins 7 and 8 are available for an output of +5 V, while pins 2, 4, 6 and 8 are available for ground connections. Pumping state ON / OFF and clockwise (CW) and counterclockwise (CC) pumping direction were configured via 4-relay module 5V (AZ -delivery, Germany).

As shown in Figure 2.4, Relay 1 sets the pumping state and Relay 2 sets the pumping direction by opening and closing pins 5 and 6. A 12-bit digital-to-analogue converter (DAC) (MCP4725,

Microchip technology Inc., USA) was used to control the pump speed by setting the relative pump speed with a reference voltage for the output of the pump. An output voltage of +5 V from pins 7 and 8, with +5 V working voltage provided by pin 8 and ground connections from pin 7, and with an input on pins 1 and 2 with an input voltage of 0 - 5 V.

The DAC is connected to the Arduino UNO R3 board to establish the 12C communication protocol by connecting to the Arduino pins (serial data pin (SDA) Ardunio A4 and serial clock pin (SCL) Arduino A5). To power the three components (**Figure 2.3**, bottom left 1,2 and 3), an Arduino UNO R3 board (Smart Projects Co., Italy) was used, which also runs the software and receives the serial commands and converts them into signals for the peristaltic pump and potentiostat. The Arduino board also helps establish serial communication with the potentiostat via an I/O cable (DRP-SV-IO cable 400 and DB9 connector, Metrohm Dropsense, Netherlands), where the board reads the output of the potentiostat via an analogue input pin (Arduino A0) connected to the digital output pin (DIO 2) of the potentiostat. Since the maximum voltage readout signal that the potentiostat can sense is in the range of 0 (low level) – 3.3 V (high level), the logic level converter 8 canal (AZ -delivery, Germany) was used to convert the digital Ios from the +5V of the Arduino board to +3.3 V to Metrohm, and the connection was made between pin 3 in the Arduiono board and the digital input (DIO1) of the potentiostat. The configuration of the peripherals in Metrohm's Dropview interface is shown in **Figure 2.3.** (top), with digital IO1 as the digital input and the active level set to low level (0 V) while the measurements are running, which is also true for digital IO2 as the digital output. The USB-B cable connection was used for RS232 communication to control the pump, switch the valve, and send the signal to the potentiostat via a homemade Python script with the graphical user interface shown in **Figure 2.4**.

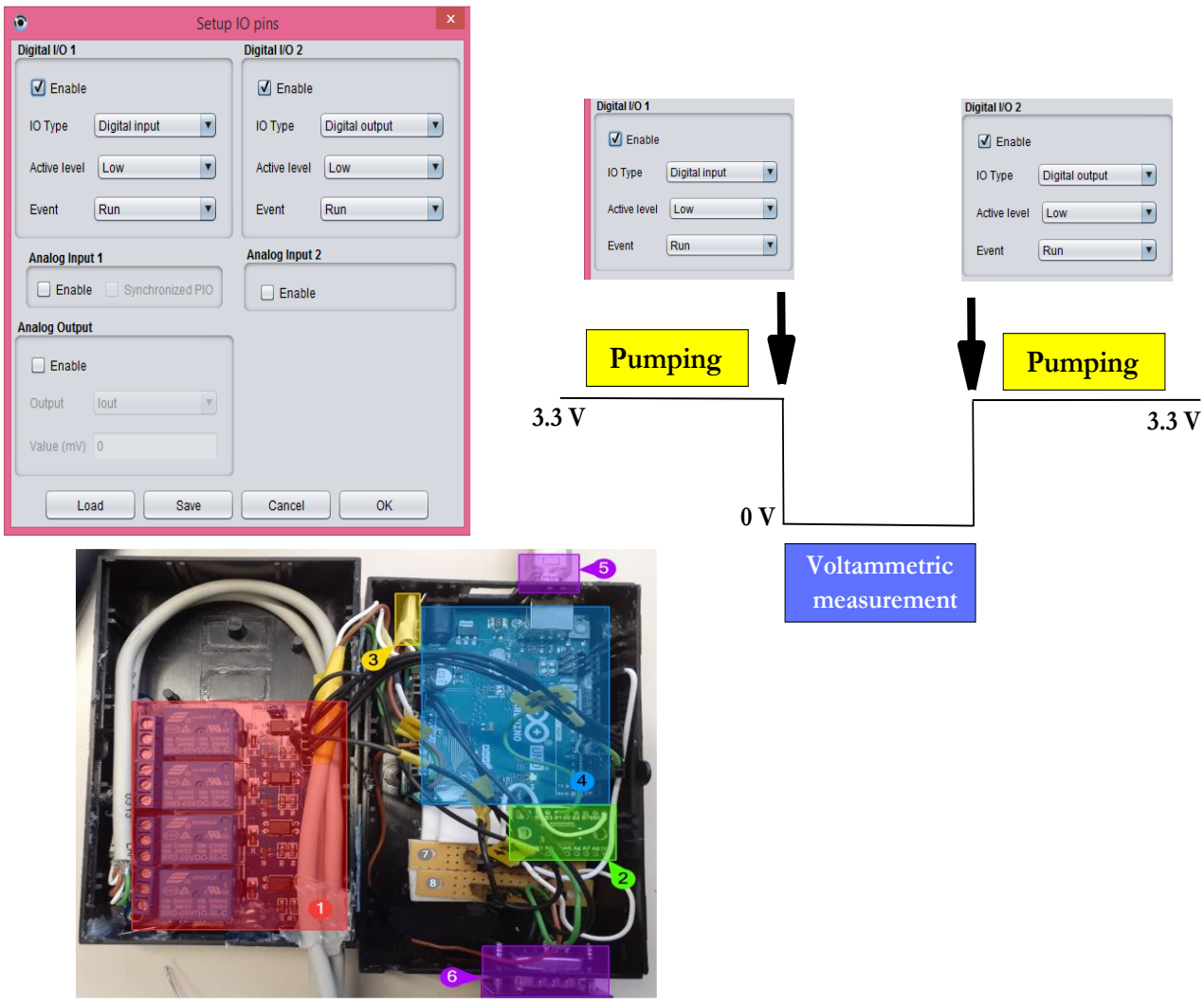

Figure 2.3 Dropview window for setting up IO pins with the setup of two digital I/O (input and output) (top left), the schematic diagram of our proposed principle for setting up synchronization between the peristaltic pump and the potentiostat (top right), and bottom left overview of the controller box components (1) 4-relay module 5V with optocoupler, (2) AZ -supply 8-channel logic level converter, (3) Adafruit 12-bit 12C DAC, (4) Arduino UNO R3, (5) USB B connector, and (6) DB9 connector.

For each measurement, a measurement routine is required, which can be called via Electrochemical FIA.exe. The graphical user interface (**Figure 2.4**) gives you full control over all components of the manifold. You can either edit them individually or run them in a loop for a specified number of cycles, repeating each step several times. For example, you can set the pump time, the pump speed, the pump direction and the receiving and sending of signals to the potentiostat.

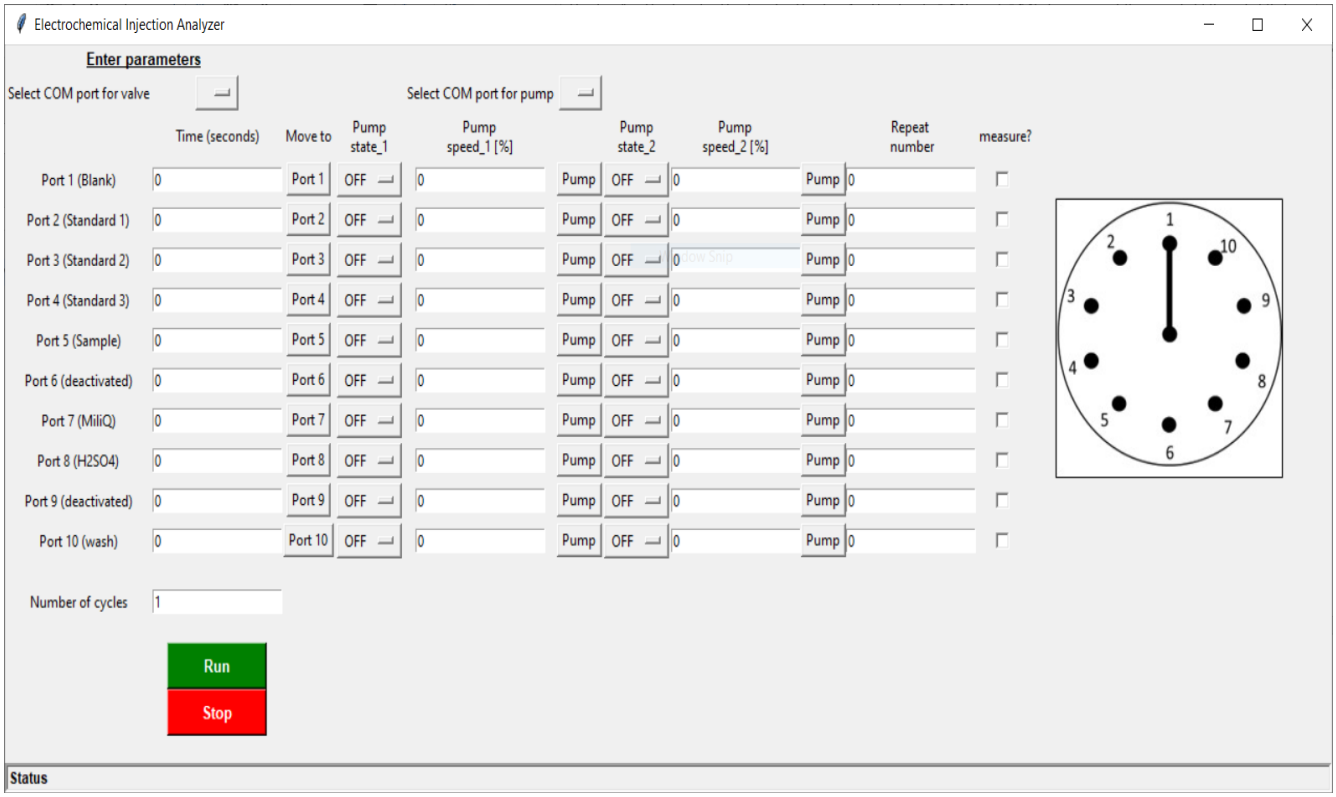

Figure 2.4 'Electrochemical FIA.exe' Graphical User Interface (GUI) to program the peristaltic pump and to control the Potentiostat.

2.6 Spectroscophotometry

Spectrophotometry is the oldest technique for the determination of nutrients. Spectrophotometry involves the transfer of energy through the absorption of radiation. For a given excitation process, the molecule can absorb light from electromagnetic radiation in the ultraviolet/visible range (from 180 nm to 800 nm) with the amount corresponding to a frequency required for transfer to the excitation leve). A spectrophotometer is an instrument that allows the determination of the amount of light that can be absorbed by molecules, and this facilities the analysis and quantification of molecules. The intensity of the absorbed light varies exponentially with the intensity of the incident light and the absorption coefficient according to the following equation

$$I = I_0 \times e^{-\varepsilon b C} \qquad \textbf{Equation 2.3}$$

Where ε is the molar absorptivity (extinction coefficient) in $L.mole^{-1}.cm^{-1}$, b is the path length in cm, and C is the concentration of the solute in $mol.L^{-1}$.

According to the Beer-Lambert law (**Equation 1.2**), the concentration of the solute is directly proportional to the absorbance. The colourimeter allows light to pass through a cuvette containing a sample of the solution that can absorb the incident beam. When the light beam of a certain intensity (I_o) falls through a coloured solution, part of the light can be absorbed (I_a) and the rest is transmitted (I_b), which can pass through the sample and hit the detector. The following equation can describe the incident light.

$$\boldsymbol{I_o = I_a + I_b} \qquad \textbf{Equation 2.4}$$

The transmittance (T) is the ratio between the amount of incident light (I_o) and the amount of absorbed light (I) and is expressed by the following formula

$$\boldsymbol{T = I/I_o} \qquad \textbf{Equation 2.5}$$

The transmittance (T) can be related to the absorption by the following equation.

$$\boldsymbol{Absorbance\ (A) = -\log T = -\log(I/I_o)} \qquad \textbf{Equation 2.6}$$

Lambert's law has some limitations that usually occur at higher absorbance values (high analyte concentrations). Absorbance is not linear with concentration at high absorbance values and this relates to the concentration of the analyte and also to the length of the cuvette (flow cell).

2.6.1 Spectrophotometric determination of PO_4^{3-}

The PMB (phosphomolybdate blue) method was first mentioned by Scheele in 1783 and by Berzelius in 1826 (Müller and Serain 2000). The PMB reactions proceed in two stages; the first stage involves the formation of the Kegging ion around the analyte (yellow coloured phosphomolybdate complex) and the second stage involves reduction with ascorbic acid to form a deeply coloured complex. The PMB method requires a strongly acidic solution, a reducing agent, and molybdate. In previous work it was found that a pH of 0-1 is very important to obtain the best colour intensity (Nagul et al. 2015).

$$PO_4^{-3} + 12MoO_4^{-2} + 27\ H^+ \rightarrow H_3PO_4(MoO_3)_{12} + 12\ H_2O$$

yellow

Phosphomolybdate

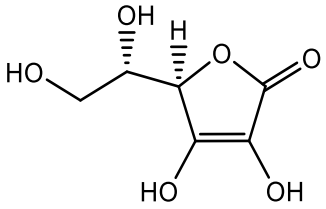

$H_3Pmo^{(VI)}{}_{12}O_{40}$ + L(+)Asorbic Acid (Reductant) → $[H_4Pmo^{(VI)}8Mo^{(V)}{}_4O_{40}]^{-3}$ Blue coloured complex

Scheme 1. The chemical reactions describe the phosphomolybdate blue method assay for spectrophotometric determination of phosphate.

As shown in Scheme 1, orthophosphate (PO_4^{3-}) is one of the tetrahedral ions with the form XO4 and has the ability to form the Keggin ions $[X^{n+}Mo_{12}O_{40}]^{-(8-n)}$, where X is the heteroatom. The key factors affecting this chemistry are: molybdate concentration, degree of protonation (i.e., concentration of acid), and a range of chemical conditions (e.g., presence of reducing agents (either organic or/and metallic reducing agents and/or temperature). (Nagul et al. 2015) described the mechanisms of the molybdate blue reaction in detail. The coordination chemistry of molybdenum is complicated and the degree of intensity of the blue colour of the complex depends on the Mo (IV) speciation, or in other words, on the ability to form the appropriate amount of the suitable reduced product without additional reduction procedures. 12-Molybdophosphaeric acid (12-MPA) is the most accessible form for reduction. It depends not only on pH, but also on the degree of protonation (Cruywagen et al. 2002; Pettersson, Andersson, and Oehman 1986), which can be defined as the number of protons that can be bound to molybdate in a solution.

$$\mathbf{p}\left(\mathbf{MoO_4^{2-}}\right) + \mathbf{qH^+} \leftrightharpoons [(\mathbf{MoO_4})_\mathbf{p}\mathbf{H}_q]^{-(2p-q)} \qquad \textbf{Equation 2.7}$$

As shown in Equation 8, where p is the number of molybdate molecules that have the ability to combine with q (number of protons that have the ability to combine with molybdate), the degree of protonation of molybdate ions is defined as the ratio of p/q, where q is the amount of total proton ions added to the solution minus the amount of free proton ions after complexation (i.e., not bound with molybdate ions). The degree of protonation was estimated to be ≥ 2, can be achieved at a pH ≤ 0.9 and a concentration of 10 mM Mo (IV) to ensure that the product is 12-MPA overall and not a mixture of 12-MPA alongside its hydrolysis product 11-MPA, which is so difficult to reduce (van Veen et al. 1986).

12-MPA has two stereoisomers, the α-isomer and the β-isomer. The α-isomer is the more stable, unreduced form of 12-MPA and with a 60° rotation, the β-isomer can be obtained (López et al. 2001). Isomerization of the α-isomer to the β-isomer can occur within minutes. While the

reduction starts, the isomerization of the α-isomer to the β-isomer starts. Tanaka et al. used voltammetric data to demonstrate the presence of the α-isomer and the β-isomer at a percentage of 1:1 10 minutes after the onset of reduction of pure α-12-MPA (Tanaka, Unoura, and Itabashi 1982). Heating favoured α → β isomerization (Launay, Massart, and Souchay 1974) in the presence of an organic (nonmetallic) reducing agent (e.g., tartaric acid); a metallic reducing agent (e.g., antimony Sb or tin Sn) has the ability to change the composition of the phosphomolybdate complex. Reduction of the α-isomer to the β-isomer can only occur in the presence of organic reducing agent or hydrazine (i.e., nonmetallic reducing agents) with heating and shows two spectral peaks with a clear absorption maximum at a wavelength of 880 nm and a discernible shoulder at 660 nm.

In the presence of a metallic reducing agent such as tin (Sn in the form of $SnCl_2$) which was preferred as a reducing agent due to its fast kinetics without the need for heating, a mixture of the three species of pure phosphomolybdate and its mono- and di-Sn complexes with absorption peaks at 820 nm, 720 nm and 620 nm, respectively, was shown when $SnCl_2$ was used for the blue method (Massart, Fournier, and Souchay 1968). The presence of Sb accelerates the reduction of 12-MPA by ascorbic acid without the need for a heating step. The reduction is completed within about 10 minutes (Murphy and Riley 1962b), which can be reduced to 1.5 minutes with excess ascorbic acid (Drummond and Maher 1995).

2.6.2 Spectrophotometric determination of NO_3^- and NO_2^-

The Griess reagent method was first proposed by (Griess 1879), it based mainly on the reaction of SAM with the coupling agent NEDD in presence of nitrites and hydrochloric acid. The resultant pink azo-dye can be detected at 540 nm. The method in my work is based on the reaction of the analyte solution with a reaction mixture of Griess reagent and Vanadium chloride reagent and with incubation under moderate temperature (40-60°C) for a definite time because the rate of the reaction is very slow to reduce NO_3^- to NO_2^- (the active specie to react with Griess reagent).

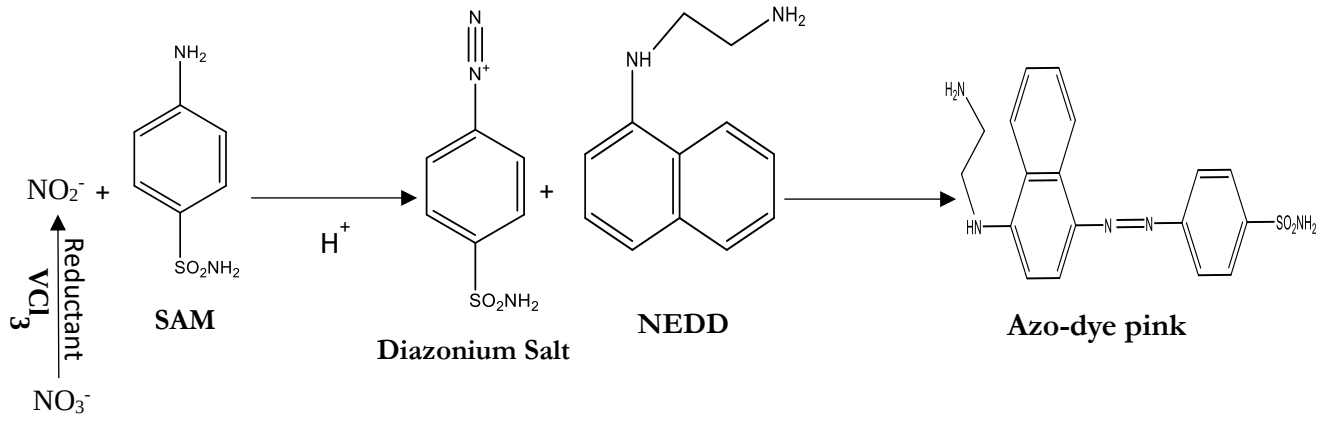

Scheme 2. The chemical reactions describe the Griess reagent assay for spectrophotometric determination of nitrate and nitrite.

The Griess reagent method is a stable part of the chemistry of most dyes. As shown in Scheme 1, nitrite reacts with an aromatic amine to give the corresponding diazonium salt, which then reacts with another aromatic amine or phenol to give the diazo compound as the final product. Intensely coloured "azo dyes" depend on the choice of appropriate aromatic amines. In the determination of nitrite, colour development is rapid, very sensitive and very simple, so it can be used for any inexpensive analytical instrument. The same method can be used to detect nitrate after stoichiometric reduction to nitrite. Several attempts have been made to find a suitable reduction procedure for nitrate to nitrite. For several decades, the widely used method has been reduction after passing through the copper-coated cadmium column (Morris and Riley 1963; Wood, Armstrong, and Richards 1967). The reduction of nitrate on a Cu-Cd reduction column has several disadvantages. The high toxicity of cadmium is a concern, and the preparation and regeneration of the column are time-consuming and associated with a high probability of inconsistencies after the regeneration procedure for long-term use (Pai et al. 2021). Among all the proposed methods, the vanadium chloride reduction method emerges as an excellent potential method to replace the Cu-Cd reduction method. In 1980, Cox first proposed the vanadium chloride reduction (Cox 1980), which was then described in detail by Braman and Hendrix. They used the vanadium ion (III) to reduce nitrate to nitric oxide (NO) under heated conditions (80-90°C), and the signal from NO was then recorded via chemiluminescence (Braman and Hendrix 1989). A significant modification was reported by Miranda et al. where the reduction of nitrate was achieved after incubation at 37 °C for 30 min in the presence of 5% HCl. This study proves the importance of HCl and moderate temperature to achieve better sensitivity of the method when H_3PO_4 was used

and incubation was performed at room temperature for 30 min to achieve a low limit of quantification of 3 μM NO_3^-(Miranda, Espey, and Wink 2001). However, instead of using NO, Miranda et al. reported the Griess method assay, in which the nitrite formed is captured to form the pink azo dye, which is detected spectrophotometrically, and this assay was then used in several studies. The proposed assay was adapted to be used manually(Schnetger and Lehners 2014b; García-Robledo, Corzo, and Papaspyrou 2014), on flow injection Analysers (FIA) (Wang et al. 2016), reverse flow injection Analyser (rFIA) (Lin et al. 2019) or finally on syringe-integrated pump (or sequential injection Analysers (SIA))(Fang et al. 2019).

2.6.3 Spectrophotometric determination of H_4SiO_4

The most common spectrophotometric determination method for silicic acid is the reaction with molybdenum salts in an acidic solution to form a silicomolybdate complex. First, a yellow silicomolybdate complex is formed, followed by a reduction with oxalic acid and ascorbic acid to form the blue-coloured silicomolybdate complex (**Scheme 3**). The blue silicomolybdate complex (SiMB) method constitutes the standard protocol for the determination of silicic acid.

$$H_4SiO_4 + 12MoO_4^{-2} + 5\ H^+ \rightarrow H_3SiO_4(MoO_3)_{12} + 12\ H_2O$$

yellow

Silicomolybdate

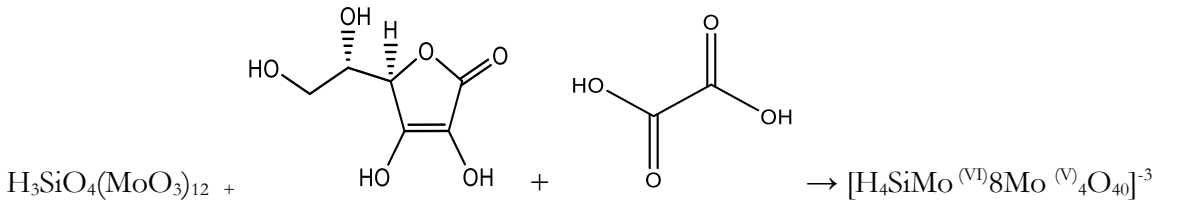

Scheme 3. The chemical reactions describe the silicomolybdate blue method assay for spectrophotometric determination of silicic acid.

There were two stereoisomers of the silicomolybdate complex, the α-isomer and the β-isomer, and their abundance in solution is strongly dependent on pH. The α-isomer was present at pH 3.5 – 4.5 and the β-isomer at pH 0.8 – 2.5 (Hansen and Koroleff 1999). Studies by (Ma and Byrne 2012b) showed that the highest signal of the complex was obtained at a concentration of 0.1 M H_2SO_4.

Several reducing agents were tested to form the blue coloured complex. Tin chloride ($SnCl_2$) was used, but despite its faster kinetics and the fact that the reduction can be performed with little temperature effect, ascorbic acid was preferred for routine analysis. In view of the ease of reagent preparation, improved linearity and lower blank values (Thomsen, Johnson, and Petty 1983). In general, the absorbance of the blue silicomolybdate complex can be increased with increasing ascorbic acid concentration (Ma and Byrne 2012b). Oxalic acid should be included in the method to eliminate interference from orthophosphate competing with silicic acid to react with molybdate to form the Keggin ion. This is because the use of oxalic acid prevents the excessive reduction of excess molybdate and thus suppresses the formation of the phosphomolybdate complex.

2.7 AutoLAB Analyser

AutoLab Analyser was manufactured by EnvironTech LLC for *on-site* determination of macronutrients (PO_4^{3-}, Σ (NO_3^- + NO_2^-) and H_4SiO_4) based on an automated syringe pump flow injection Analyser (FIA) and wet-chemistry colourimetric method.

2.7.1 Hardware

The AutoLAB is a multinutrient Analyser that consists of a multinutrient analysis module, an electronic recording device, and bottles for the reagents and standards. Like many conventional nutrient analysis modules, it consists of four devices: a 16-way rotary valve, three colorimetric detectors, and a syringe and syringe motor to control its movement (**Figure 2.5**)

The colourimeters consist of a narrow capillary flow cell with the LEDs as the light sources at one end and a photodiode detector at the other end. An additional photodiode detector was placed next to the light source to monitor the light intensity. The colourimeters were industrially manufactured from high quality glass with small pores incorporated to allow seawater and analyte solution to enter the flow cell and equalize. The inlet of the colourimeter is connected to the valve via a small plastic tube. For example, for nitrate, a green, high-intensity LED with a peak wavelength of 567 nm. The detector is a silicon photodiode with a peak sensitivity at a wavelength of 560 nm. Thus, the sensitivity of the photodiode was more than 50% in the bandwidth of 440-660 nm. The colourimeter was encapsulated in black polyurethane to minimize light interference from the environment, and the electrical connections were made inside the capsule to an opening in the bottom of the colourimeter housing. The output signal in microamps was transmitted to the input stage of the electronics via the analog interface.

The electronics housing contains a number of electronic modules, including the main control unit (MCU), the motor drivers, and the detector interface. The motor drivers and detector interface are individual intelligent devices that have their own microprocessor that is operated and configured through the connections with the MCU. The peripheral devices are arranged in a "bus". When 4 busses are used and each bus can hold about 12 devices, the bus arrangement is called a serial peripheral system (SPS), where the detectors and motors are called SPS devices and each device has its own address. In Table 2.1 we have given the SPS address for each SPS device.

Table 2.1 SPS address

No.	**SPS devices**	**SPS address**
1	Nitrate detector	14
2	Silicic acid detector	14
3	Phosphate detector	1A
4	Syringe Motor	00
5	Valve Motor	01

AutoLAB is controlled and operated by a programmable interface, configured using the built-in command set and a scripting language called Eco-Script, which is stored on a memory card where all results are saved and can be retrieved after recovery. It is possible to set a waiting time between sample analyses. During this time, the AutoLAB is latent and operates in power saving mode. The AutoLAB is programmed and controlled via a communication link to any computer running terminal emulation software (e.g., Tera Term), where the communication port settings are as follows Baud rate: 19200, Data bits: 8, Parity: No and Stop bits: 1.

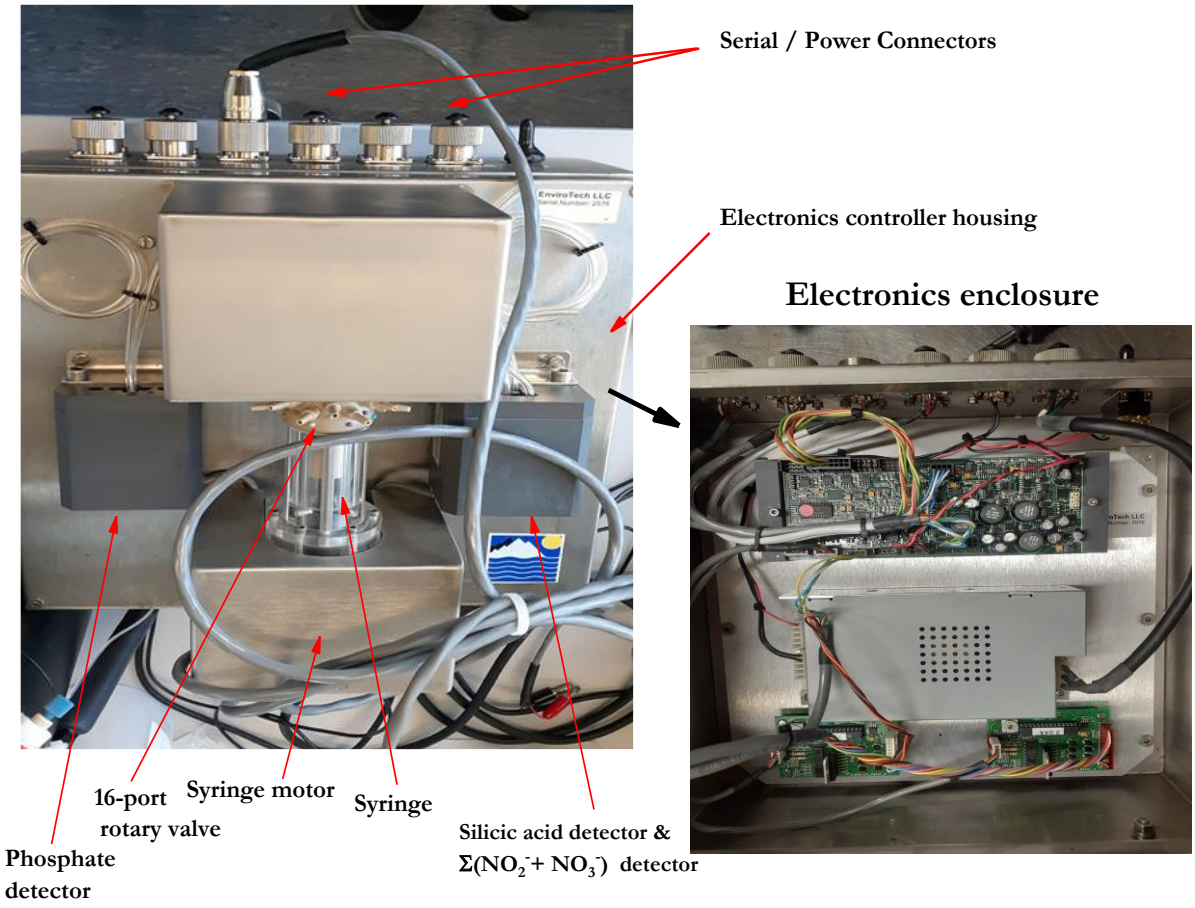

Figure 2.5 Hardware of AutoLAB showing all the components.

2.7.2 User Interface

The Eco-Script language is run on a PC where it can be stored on a memory card and then the AutoLAB can continue to run with the PC. Eco-Script is a very simple language designed for remote and unattended data acquisition. A set of commands is assembled into a script. In principle, at least one script is required to give instructions to AutoLAB, but multiple scripts can be uploaded in sequence. This can be done manually by the user or you can call each other into a single script. As an example, we have shown in script 1 the nitrate analysis of the blank solution we modified, describing each step and the procedure. Two drives were configured; the first is the script drive and the other is the data driver where the results can be retrieved by the following command

```
/store/cf/data/ extract /store/cf/data/ graph
```

Script 1. Describing of blank measurement for nitrate analysis

```
# no3b
# Nitrate Blank

execute "/store/cf/scripts/init"                    # ensure that all SPS devices are
                                                    connected
transmit 0, "Home rotary and linear motors\r\n"
execute "/store/cf/scripts/align"                   # align the rotory valve to the inlet
                                                    position
execute "/store/cf/scripts/p-waste"                 # switch the valve to port 4 and
execute "/store/cf/scripts/i4500"                   ensure that the syringe is completely
                                                    injected (zero position)
transmit 0,"Start NO3-Blank\r\n"
# Inlet                                             # switch the valve to port 7 and
execute "/store/cf/scripts/p-nobs1"                 draw up the blank soln.
execute "/store/cf/scripts/r2700"                   # switch the valve to port 4 and
execute "/store/cf/scripts/p-waste"                 inject 340 μL to discharge air
execute "/store/cf/scripts/i700"                    bubbles

# NO3 detector                                      # switch the valve to port 16 (nOx
execute "/store/cf/scripts/p-detn"                  detector) and inject the blank soln. to
execute "/store/cf/scripts/i2000"                   the detector

transmit 0,"Standard blank\r\n"
wait 3000
# Set detector light intensity                      # send instructions for SPS 14 (nOx
execute "/store/cf/scripts/setn-""                  detector) to set the light intensity


# Blank                                             # select device (nOx detector)
device clear                                        # add the data and time
deviceport 14, sps                                  # add a light "source" channel
device add, [vIn]                                   # add a light "colour" channel
device add, [So0]                                   # add a temperature channel
device add, [Co0]                                   # take the reading, store it in a
device add, [cTemperature]                          specific folder and display the data
burst 1000,1"[Bb-NO3]"/store/cf/data,noburst,display # the54oltameo command turn off
device clear                                        the nOx detector
digitalio 14, clear                                 # turn on the heater into the
                                                    phosphate detector and set it to the
                                                    maximum temperature
execute"/store/cf/scripts/setp-"                    # draw up the blank soln. from the
                                                    nOx detector
transmit 0,"Get Blank–-"
execute"/store/cf/scripts/r144"

transmit 0,"Get VCl3–-"                             # switch the rotary to the port 5
transmit 0," reduce NO3>>NO2–-"                     # withdraw the mixed griess reagent
execute"/store/cf/scripts/p-Gr"
execute"/store/cf/scripts/r36"                      # mix the reagent with the blank soln.
execute"/store/cf/scripts/p-det"
repeat 2
```

```
execute“/store/cf/scripts/i45”                    # insert the reaction mixture to the
execute“/store/cf/scripts/r45”                    phosphate detector
end
execute“/store/cf/scripts/p-det”                  # wait 30 minutes for reduction of
execute“/store/cf/scripts/i180”                   NO3- to NO2-

repeat 30                                         # draw up the reaction mixture to the
wait 60000                                        phosphate detector
end

execute“/store/cf/scripts/r180”                   # wait 2 minutes to cool the reaction
execute“/store/cf/scripts/p-det”                  mixture

transmit 0,“ develop\r\”                          # discharge 110 μL of reaction
repeat 2                                          mixture for air bubbles discharge
wait 60000                                        # inject the rest to the nOx detector
end

execute“/store/cf/scripts/p-wast”
execute“/store/cf/scripts/i22”
execute“/store/cf/scripts/p-det”                  # send instructions for SPS 14 (nOx
execute“/store/cf/scripts/i157”                   detector) to set the light intensity

transmit 0"Blank reaction\r\"
wait 3000                                         # select device (nOx detector)
                                                  # add the data and time
execute“/store/cf/scripts/setn-”                  # add a light “source” channel
                                                  # add a light “colour” channel
                                                  # add a temperature channel
device clear                                      # take the reading, store it in a
deviceport 14, sps                                specific folder and display the data
device add, [vIn]                                 # Turn off the nOx detector
device add, [So0]
device add, [Co0]
device add, [cTemperature]
burst 1000,1"[Rb-NO3]"/store/cf/data, noburst,display
device clear
digitalio 14, clear
# EOF
```

3 NaOH Pretreated molybdate-carbon paste electrode for the determination of phosphate in seawater by square wave voltammetry with impedimetric evaluation

Mahmoud Fatehy Altahan[1,2], Eric P. Achterberg[1] , Asmaa Galal Ali[3], Magdi Abdel-Azzem[3]

Published in *Journal of Electrochemical Society, IOP publishing*

DOI: 10.1149/1945-7111/ac3b03

[1] Chemical Oceanography Department, GEOMAR Helmholtz for Ocean Research Kiel, Kiel 24148, Germany.

[2] Central Laboratory for Environmental Quality Monitoring, National Water Research Center, El-Qanater El- Khairia 13621, Egypt.

[3] Electrochemistry Laboratory, Chemistry Department, Faculty of Science, Menoufia University, Shibin El-Kom 32511, Egypt.

Abstract

Phosphate (PO_4^{3-}) is an important nutrient for phytoplankton growth and at high loadings can result in water quality deteriorations. Autonomous PO_4^{3-} measurements are required for monitoring purposes, and are best achieved using sensitive, portable and low-cost techniques. Here we describe a new electrochemical sensor for PO_4^{3-} detection in seawater. The electrochemical quantification of PO_4^{3-} typically depends on the reaction between molybdate and PO_4^{3-} under acidic conditions to form a phosphomolybdic complex, which is electrochemically active. In this work, we prepared a carbon paste electrode (CPE) modified with molybdate and pretreated in 0.1 M NaOH using cyclic voltammetry (CV). The modified CPE was employed for the determination of PO_4^{3-} in artificial seawater (35 g/L NaCl) acidified with sulfuric acid to pH 0.8. The analytical conditions, including pH, waiting time for complexation, square wave amplitude and frequency, were optimized. An additional cleaning step (cyclic voltammetry (CV)) of 10 cycles in 0.1 M NaOH at −0.5 to 0.5 V was required between PO_4^{3-} determinations to dissolve the phosphomolybdic complex formed on the surface of the working electrode. EIS results confirmed that the molybdate-modified CPE (molybdate/CPE) exhibited a R_{ct} toward PO_4^{3-}, and showed an improved analytical performance for different concentrations of PO_4^{3-}. A calibration plot in the range of 0.01–5 μM with a limit of detection (LOD) of 0.003 μM was obtained. The proposed electrode demonstrated good precision (4.3% and 5.8%) for concentrations of 5 and 0.2 μM, respectively. The proposed method was employed to analyse PO_4^{3-} in seawater samples on a research cruise in the North Sea, with results in close agreement to those obtained using conventional colorimetric measurements.

3.1 Introduction

Phosphate (PO_4^{3-}) is a key nutrient necessary for the growth of marine phytoplankton. Its availability determines the primary production and species composition of phytoplankton in coastal and oceanic waters. Surplus nutrient inputs, including phosphate, from anthropogenic sources lead to excessive algal growth and the subsequent depletion of oxygen caused by the remineralization of sinking dead algal biomass; this phenomenon is called eutrophication. Phytoplankton blooms may also cause the release of algal toxins that can have serious impacts on ecosystem and human health (Salomon and Markus 2018; Bricker et al. 2008). Therefore, monitoring the concentrations of PO_4^{3-} in marine waters is important to assess water quality (Karl 2014). Generally, colorimetric techniques are used for the analysis of PO_4^{3-} in natural waters. The methods involve the complexation of PO_4^{3-} by molybdenum ions with the aid of antimony tartrate ($C_{12}H_{12}O_{18}Sb_2$) in the presence of a reducing agent to form the blue phosphomolybdate ($H_4pMo_8^{VI}Mo_4^{V}O_{40}$), which demonstrates a maximum absorbance at a wavelength of 880 nm (Nagul et al. 2015). Alternatively, in the presence of vanadate ions, PO_4^{3-} can react with molybdate ions to form the yellow vanadomolybdophosphoric acid ($H_4PVMo_{11}O_{40}$), which is calorimetrically detected at a wavelength of 385 nm (Warwick, Guerreiro, and Soares 2013). Various wet chemical in-situ monitoring instruments, including lab-on-a-chip sensors, have been developed based on the blue or yellow methods and deployed for PO_4^{3-} analysis in marine waters over periods up to several weeks (Grand et al. 2017; Legiret, Sieben, Woodward, Abi Kaed Bey, et al. 2013). However, these wet chemical techniques are limited by the consumption rate of reagents and instability of some reagents, e.g., ascorbic acid.

For field measurements, electrochemistry offers an excellent alternative to wet chemical approaches as it facilitates miniaturization, minimal power and reagent consumption, and reduced response times. For chemical oceanography, electrochemical devices have been developed for potentiometric pH monitoring (McLaughlin et al. 2017), amperometric measurement of dissolved oxygen (DO) (Revsbech et al. 2009), trace metal speciation analysis using voltammetry (Howell et al. 2003; Braungardt et al. 2009; Achterberg and Braungardt 1999; Illuminati et al. 2019), and conductivity/salinity measurements.

Several electroanalytical methods have been developed to detect PO_4^{3-}, and they offer a range of advantages. They do not require ascorbic acid as a reductant, and are fast and cost-effective, and do not require interventions related to turbidity interferences in the sample (Berchmans, Issa, and Singh 2012). In addition, using electroanalytical methods, it is possible to create a portable Analyser

that could be used for field analysis of PO_4^{3-}. Over the last few decades, a number of electrochemical sensors have been reported that detect PO_4^{3-} in fresh or marine water by sensing phosphomolybdate complexes and utilizing cathodic reduction processes instead of a reductant.

The various electrochemical techniques for PO_4^{3-} analysis include amperometry, as reported by Udnan et al. (Udnan et al. 2005). These workers used a glassy carbon electrode to detect PO_4^{3-} based on the reduction reaction with acidic molybdate, and applied flow injection amperometry for fresh and sea water samples. Amperometry was also utilized by Janca et al. (Jońca, León Fernández, et al. 2011), where self-production of molybdate ions inside the electrochemical cell was performed via the direct electrolysis of a molybdenum electrode. However, amperometry is complex because it requires the use of a rotating disk electrode, which makes it more complicated for field monitoring (Jońca, Comtat, and Garçon 2013a). Cyclic voltammetry has been utilized with a modified screen-printed electrode for the quantification of PO_4^{3-} in mineral and river waters (Cinti et al. 2016). Despite the simplicity and speed offered by cyclic voltammetry, the sensitivity is insufficient for the measurement of PO_4^{3-} in seawater, where the concentration ranges from a few nanomolar to 5 μM.

In contrast, pulsed techniques offer enhanced sensitivity and access to a wide range of time scales and background suppression options (Kounaves 1997; Allen and Larry 2001). One of these techniques is differential pulse voltammetry (DPV), which was utilized in an autonomous, reagentless electrochemical method with a limit of detection (LOD) of 0.19 μM (Jońca, Comtat, and Garçon 2013a). However, it is difficult to optimize the parameters and achieve adequate repeatability with DPV.

Another pulsed technique, square wave voltammetry (SWV), combines the best aspects of several pulsed techniques and exhibits a better sensitivity than DPV (Allen and Larry 2001). SWV was first utilized by Barus (Barus et al. 2016), who used a static gold electrode as working electrode with a molybdenum electrode to electrolytically generate molybdate with a LOD of 0.05 μM. The waiting time for complexation was 60 min, and an LOD value of 0.01 μM was achieved with a 30 min waiting time. Although the waiting time could be reduced to 5 min by separating the compartments for detection and complex formation, a LOD was not reported for the linear range.

Recently, several modified electrodes have been prepared for PO_4^{3-} analysis. Kumar et. al. (Kumar et al. 2021) reported a wearable polyaniline/coconut shell carbon/poly(vinylidene fluoride-co-hexafluoropropylene) sensor preloaded with ammonium heptamolybdate for the amperometric determination of PO_4^{3-} in river water samples. It showed a wide detection range (10-114 μM), but the LOD (0.6 μM) was not sufficiently low for analysis of natural waters. Wei et. al. (Wei et al.

2021) developed a modified screen printing electrode for DPV analysis of PO_4^{3-} in turbid coastal waters, with a linear detection range of 0.2 to 150 μM and a LOD of 0.05 μM.

A carbon paste electrode (CPE) was utilized for measuring PO_4^{3-} by Guanghan et al. (Guanghan et al. 1999a), where a phosphomolybdic anion film was formed on the electrode surface using cyclic voltammetry in a solution containing PO_4^{3-} and molybdate. Then, the electrode was used to detect PO_4^{3-} via cyclic voltammetry with an LOD of 0.04 μg/mL (~0.4 μM). However, this study neglected the interference from silicic acid, which is the primary compound that interferes with PO_4^{3-} quantification in seawater using the molybdate chemistry.

The main challenge for utilizing electrochemistry for in-situ and real time determination of PO_4^{3-} is the lack of a direct and highly sensitive electrochemical sensor, which should be able to detect PO_4^{3-} in seawater, down to the nanomolar concentrations.

The aim of this work is to establish a rapid and sensitive electrochemical sensor for measuring PO_4^{3-} in seawater. For this, molybdate is added to a CPE to facilitate rapid formation of phosphomolybdate complexes, which can then be electrochemically detected using SWV or electrochemical impedance spectroscopy (EIS). The interference problems caused by silicic acid and a surfactant (Triton X-100) are investigated, and an application to natural seawater samples collected during a research cruise in the North Sea is presented. A comparison with the classical colourimetric method is also provided.

3.2 Experimental

3.2.1 Reagents and calibration standards

All the reagents were prepared using deionized (DI) water (resistivity >18.2 MΩ·cm, MilliQ, Millipore) and reagent grade salts. A thorough cleaning procedure was used to prepare all glassware and plasticware prior to use; they were rinsed with DI water and then soaked in a 10% HCl (v/v) (~1.2 M) bath (reagent grade, Carl Roth) for at least 24 h; finally, they were again rinsed with DI water. All of the calibration standards for PO_4^{3-} and silicic acid were prepared in artificial seawater with a salinity of 35, which was prepared using sodium chloride (NaCl, Merck) at 35 g/L. Stock solutions of 1 mM PO_4^{3-} (KH_2PO_4, Merck) and 1 mM silicic acid ($Na_2SiO_3 \cdot 5H_2O$, Merck) were prepared by dissolving the salts in DI water.

3.2.2 Seawater sampling

Natural seawater samples were collected using rosette Niskin bottles on a CTD rosette frame (Multi water sampler SlimLine 6, Hydro-Bios, Germany) during a MOSES Stern 5 cruise in the North Sea (September 2020). The from was equipped with sensors for continuous acquisition of hydrographic data (Temperature, Salinity, pH, depth and dissolved oxygen). Seawater samples were filtered using a cartridge filter (0.2 μm pore size, Sartorius Sartobran P300) and collected in 50 mL polypropylene tubes for colourimetric nutrient measurements and 125 mL low-density polyethylene tubes for electrochemical measurements. The seawater samples were frozen at sea and analysed upon return to the land-based laboratory.

3.2.3 Colorimetric measurements

The colorimetric analysis of seawater samples was performed using a nutrient auto-analyser (QuAAtro, SEAL Analytical) by applying the classical molybdenum blue method for PO_4^{3-} (Murphy and Riley 1962b; Legiret, Sieben, Woodward, Abi Kaed Bey, et al. 2013; Hydes et al. 2010) and silicic acid (Motomizu and Li 2005), and applying the Griess reagent method for nitrite (NO_2^-) and with the assistance of a cadmium column (Seal Analytical) for nitrate (NO_3^-) (Moorcroft, Davis, and Compton 2001). The baseline was established using artificial seawater that was prepared from NaCl. The detection limit was calculated as three times the standard deviation of the lowest concentration during the analytical run, which was 0.005 μM for PO_4^{3-}, 0.155 μM for H_4SiO_4, 0.028 μM for $\Sigma(NO_2^- + NO_3^-)$ and 0.004 μM for NO_2^-.

3.2.4 Apparatus

A potentiostat (μ-Autolab III, Metrohm, Netherlands) was employed for CV and SWV. A conventical three-electrode cell was utilized; it contained a working electrode (CPE, BASi, USA), a counter electrode (platinum wire, diameter 0.5 mm, Metrohm, Netherlands), and a reference electrode (Ag/AgCl, 3 M KCl, Metrohm, Netherlands). All potentials were reported against the reference electrode. EIS measurements were performed on a Model VersaSTAT 4 potentiostat (Princeton Applied Research, Oak Ridge, TN, USA), and all data were processed using EC-Lab software (Bio-Logic, USA), which was also employed to fit and interpret the experimental results according to the equivalent circuit. Surface morphology analysis and elemental mapping of the molybdate/CPE were conducted using Field-emission scanning electron microscope (FE-SEM)

(Gemini Ultra55 Plus, Zeiss, Germany) attached with an energy dispersive x-ray instrument (EDX) (X-act, Oxford Instruments, UK).

3.2.5 Preparation of the modified electrodes

The construction of the molybdate/CPE involved several steps. First, 0.7 g of graphite powder (particle size <20 μm, Sigma Aldrich, USA) was mixed with 0.3 g of paraffin oil (Sigma Aldrich, USA) in a mortar for 10 min to form a uniform carbon paste. Then, 0.1 g of ammonium molybdate tetrahydrate [$(NH_4)_6Mo_7O_{24}\cdot 4H_2O$] (≥ 99%, Sigma Aldrich, USA) was mixed with the resulting carbon paste (CP) in the mortar. The obtained mixture was pressed into the hole at the end of an electrode holder (BASi, USA) to prepare a modified molybdate/CPE. Subsequently, any excess electrode material was removed by polishing with a piece of filter paper (Whatman, England). The resulting modified CPE was rinsed with DI water and immersed in a solution of 0.1 M NaOH; then, CV was performed from −0.5 to 0.5 V for 10 scanning cycles at a scan rate of 0.1 V/s. Finally, the modified electrode was rinsed again with DI water, and then, it was used for measuring PO_4^{3-}.

3.2.6 Electrochemical measurements

Phosphate was measured using the modified electrode with SWV and a potential range of −0.2 to +0.8 V with a SW frequency of 150 Hz, a SW amplitude of 50 mV, and a step potential of 1 mV. All solutions were acidified using sulfuric acid (H_2SO_4, 98%, Merck) to reach a pH value of 0.8 prior to analysis. EIS measurements were performed from 0.25 Hz to 10 kHz for artificial seawater and from 0.1 Hz to 10 kHz only with the CP electrode.

3.3 Results and discussion

3.3.1 Electrochemical pretreatment of molybdate/CPE

The chemistry of molybdenum is complex because of its wide range of potential oxidation states (−2 to +5) and coordination numbers (0 to 8). The stability and behavior of the different valent compounds of molybdenum are pH-dependent (Pourbaix 1974). The electrochemical oxidation of molybdenum has been performed under various conditions (Wang, Li, and He 1998; Bojinov, Betova, and Raicheff 1995; Hull 1972). However, there are a limited number of studies on the

electrochemical behaviour of molybdenum electrodes in a basic medium and our understanding of the products obtained under these conditions is still limited.

The molybdate/CPE underwent CV in a solution of 0.1 M NaOH, and repetitive scanning was used to assess the formation of MoO_4^{2-}. A possible formation pathway is indicated by the following equations (Saji and Lee 2012; Hull 1972):

$$\mathbf{Mo + 2\,OH^- \rightarrow Mo(OH)_2^+ + + 3e^-} \qquad \textbf{Equation 3.1}$$

$$\mathbf{Mo(OH)_2^+ + 6\,OH^- \rightarrow MoO_4^{2-} + 4\,H_2O + 3e^-} \qquad \textbf{Equation 3.2}$$

After 10 consecutive CV sweeps in NaOH, the charge-transfer steps yielded the final Mo(VI) species MoO_4^{2-} on the working electrode surface. After this treatment with NaOH, the modified electrode was immersed in a solution of artificial seawater containing PO_4^{3-}, where the phosphomolybdate complex was formed under acidic conditions. After repeating the same procedure in 0.1 M H_2SO_4, the molybdate/CPE did not indicate any clear voltammetric peaks, even over 1 μM PO_4^{3-} concentrations in the solution.

3.3.2 SWV of PO_4^{3-}

Phosphate cannot be detected directly because it is an electrochemically inactive species. However, it can be electrochemically interrogated in a highly acidic medium in the presence of molybdate ions, where it can form a phosphomolybdate complex, which is also known as the Keggin ion (Equation 3) (Guanghan et al. 1999b).

$$\mathbf{7H_2PO_4 + 12\,MoO_4^{2-} + 72H^+ \rightarrow 7[PMo_{12}^{(VI)}O_{40}]^{3-} + 36H_2O} \qquad \textbf{Equation 3.3}$$

This approach suffers from cross interference from silicic acid, which has the same affinity for molybdate to form a silicomolybdate complex. The interference can be reduced by altering the ratio of H^+ to MoO_4^{2-} to between 60 and 80, and adjusting the pH to between 0.4 and 0.9 (Directive 2000; Jońca, Comtat, and Garçon 2013a). In the current study, the pH of the electrolyte medium was adjusted using sulfuric acid to pH 0.8. Under these conditions, SWV was performed from −0.2 to 0.8 V. **Figure 3.1** shows the SWVs of 0.5 μM PO_4^{3-} in artificial seawater in acidic conditions at the molybdate/CPE before and after the treatment with NaOH. Without the NaOH pre-treatment, five oxidation peaks at −0.12 V, 0.03 V, 0.1 V, 0.28 V, and 0.5 V (peaks I to V, respectively) were observed, which are likely related to the formation of different phosphomolybdate polymeric structures generated by the coupling between molybdate ions and PO_4^{3-}(Ilangovan and Chandrasekara Pillai 1997; Jońca et al. 2012). At various PO_4^{3-} concentrations, the relationship between the peak current for all the various peaks and the PO_4^{3-}

concentration was not linear which was likely caused by the adsorption of phosphomolybdate polymers onto the working electrode surface (Rong and Anson 1996). In contrast, the molybdate/CPE that had been pre-treated with consecutive CVs in NaOH showed a different electrochemical behaviour toward PO_4^{3-} ions. The voltammograms show two oxidation peaks at 0.21 V and 0.58 V, corresponding to peak I and II, respectively. These two peaks are related to the electrooxidation of Mo(II) to Mo(IV) and Mo(IV) to Mo(VI), respectively (Kolliopoulos, Kampouris, and Banks 2015). The current of the peak at 0.21 V increases with increasing concentration of PO_4^{3-}, demonstrating a good electrochemical behaviour.

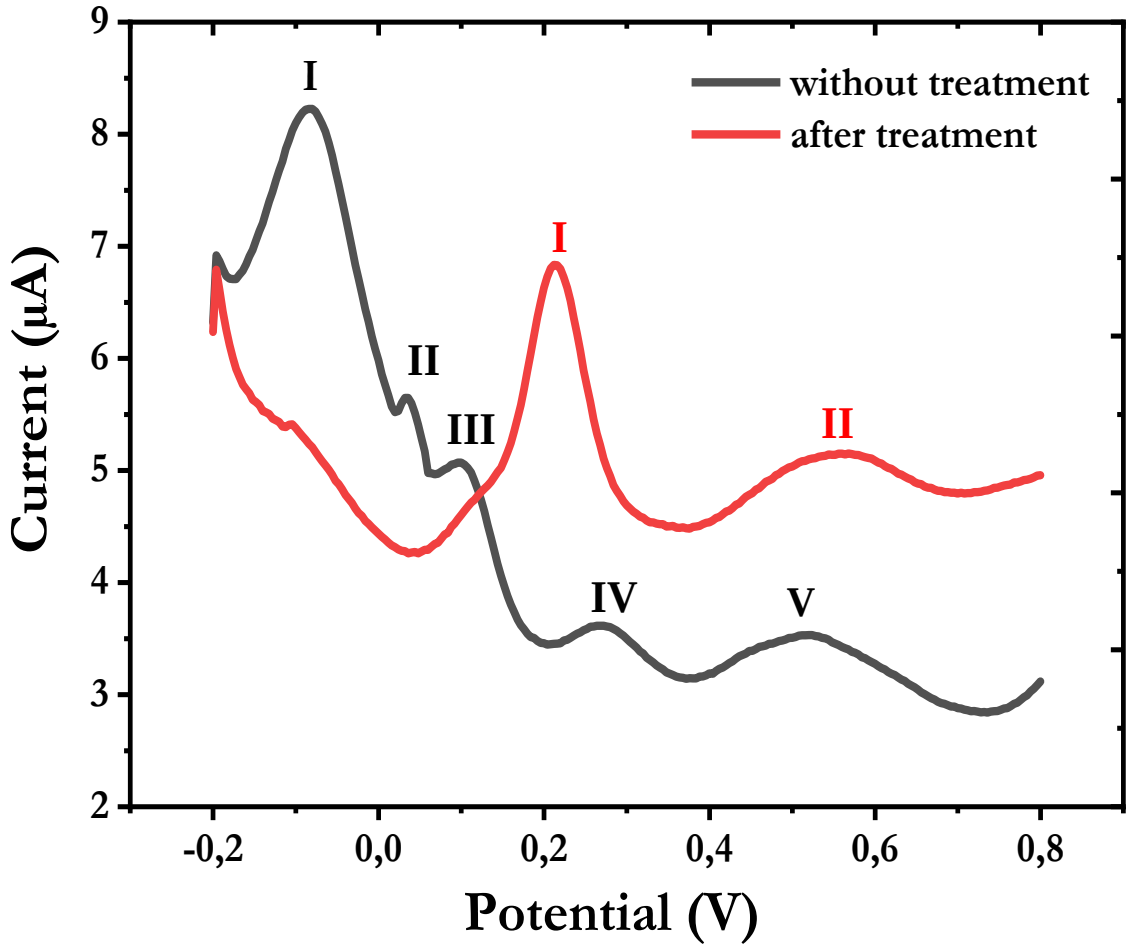

Figure 3.1 Comparison between square wave voltammograms of the pretreated (red line) and the untreated (black line) molybdate / CPE in a solution of 35 g/L NaCl (pH 0.8) containing 0.5 µM PO_4^{3-} with square wave frequency 150 Hz, 50 mV square wave amplitude, 1 mV step potential and 75 s quiet time. The pretreatment was performed by CV for 10 scanning cycles in 0.1 M NaOH from–- 0.5 V to 0.5 V at a scan rate of 0.1 V/s.

3.3.3 Surface morphology and X-ray analysis

The structure and surface morphology of the molybdate/CPE before and after pretreatment by CV in 0.1 M NaOH, and after SWV in a solution of artificial seawater (pH 0.8) containing 1 μM PO_4^{3-}, were studied using FE-SEM as shown in **Figure 3.2**. The components present on the surface were also confirmed by EDX spectra and show the distribution of the components in the studied region by elemental mapping analysis (**Figure 3.2), (Figure S1.1**). **Figure 3.2, A** shows an image of molybdate/CPE at low magnification (100 μm), where the carbon paste can be seen as a pattern of irregular sheets, while molybdate oxide can be seen on the image at high magnification (20 μm) as a white spot surrounded by a dark graphite network. The selected spot contains about 95.7% carbon, 3.42% oxygen and 0.85% molybdenum. **Figure 3.2, B** shows the increase in thickness of the molybdate oxide structure, which appears as a dense white spot after modification by CV in 0.1 M NaOH. The EDX showed the increase in molybdate oxide with about 1.51% molybdenum, 8.51% oxygen and 89.9% carbon. This explains the improvement in the electrochemical sensor performance by the pretreatment step in NaOH solution. After SWV in a solution of 35 g/L (pH 0.8) containing 1 μM PO_4^{3-}, the molybdate/CPE exhibited a thick white spot of molybdenum oxide in which PO_4^{3-} was present, as shown in **Figure 3.2, C**, which was indicated by the mapping analysis where phosphorus appeared as orange dots in the spot of molybdenum oxide (**Figure S1.1, J**). This indicates the formation of a Keggin-type phosphomolybdate complex on the molybdate/CPE pretreated with NaOH. However, the phosphorus content cannot be seen in the EDX spectra because the phosphorus concentration was extremely low compared to other components (C, Mo, O) physically embedded in the paste, while PO_4^{3-} comes from a solution of 1 μM.

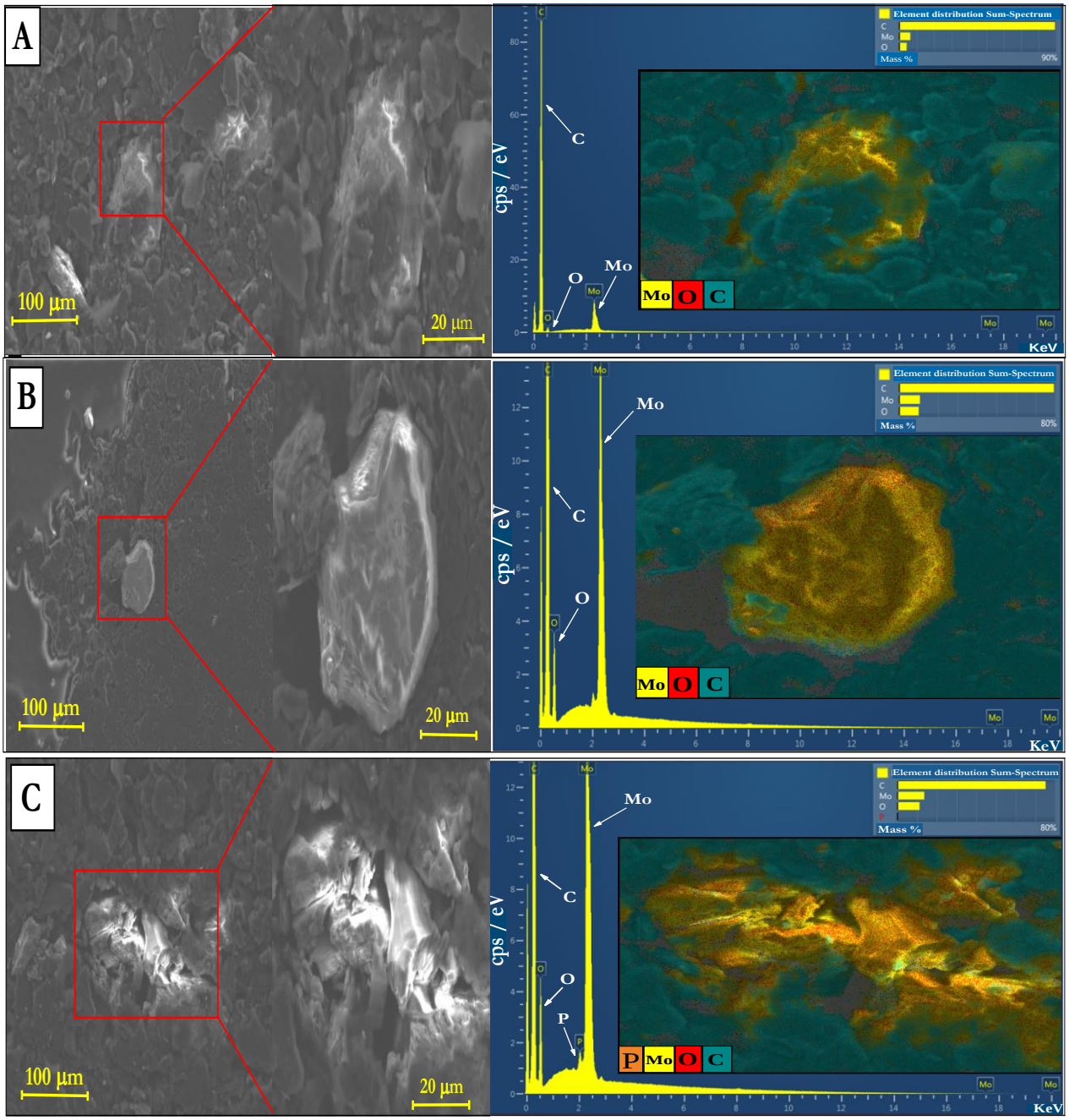

Figure 3.2 Field emission-scanning electron microscope images with different magnifications, energy dispersive x-ray spectrum and elemental mapping analysis showing the distribution of C, Mo, O and P for (A) molybdate / CPE without modification, (B) after CV of molybdate / CPE

in 0.1 M NaOH and (C) after SWV of molybdate / CPE in a solution of 30 g/L NaCl (pH 0.8) with 1 M PO_4^{3-}.

3.3.4 Optimization of analytical conditions

The analytical method was optimized by investigating the influence on the signal of different analytical conditions, including pH of the medium, quiet time before measurement, and square wave parameters, including frequency and amplitude.

The sensitivity of the electrochemical measurement of PO_4^{3-} based on the molybdate method is strongly affected by pH. In addition, the selectivity of the method is influenced by the acid concentration as an optimized pH value is essential to exclude the interference by silicic acid, which is present in seawater at concentrations ranging from ~0.5 to 200 μM. To illustrate the pH dependency, the peak current of 0.01 μM PO_4^{3-} in artificial seawater at the molybdate/CPE was recorded in the pH range from 4.6 to 0.3 (**Figure S1.2, A)**. It was observed that when the pH decreased, the peak current increased, reaching a maximum peak current of 4.4 μA at pH 0.8 and pH 0.6. To minimise the amount of sulfuric acid needed to acidify the sample prior to the analysis, pH 0.8 was chosen as the optimal pH value.

The quiet time is the period between the insertion of the working electrode into the electrolyte and the commencement of the potential scan. After transferring the electrodes from a very basic medium (0.1 M NaOH, pH ~12.6) to a highly acidic medium (pH 0.8), setting a quiet time before generating phosphomolybdate complexes during the PO_4^{3-}measurement allows for adequate mixing of PO_4^{3-} ions with molybdate ions on the working electrode surface. The quiet time was varied from 0 to 300 seconds and the resulting voltammetric behaviour was recorded for 0.01 μM PO_4^{3-} in artificial seawater (pH 0.8) **(Figure S1.2, B**). Increased peak currents were observed when the quiet time was increased from 0 s (0.3 μA) to 90 s (2.2 μA). This behaviour is likely caused by an increased amount of PO_4^{3-} ions adsorbed on the surface of the molybdate/CPE after prolonging the quiet time. At longer quiet times, no further enhancement was observed, probably due to saturation of the working electrode surface with adsorbed PO_4^{3-} ions before analysis. Thus, 90 s of quiet time was found to be suitable for the PO_4^{3-} determination.

A square-shaped potential pulse is employed in SWV that is produced periodically with a staircase potential ramp. In addition, SWV combines three components that can be optimized to increase the sensitivity and performance of the method. The components include the staircase potential modulation or step potential (E_{step}) and the height of the potential pulse or square wave amplitude,

which is larger than the step potential (both are measured in mV). The period of one potential cycle is described by its reciprocal or frequency (f) in Hertz (Hz). Here, the effect of varying two square wave components (amplitude and frequency) on the peak current values at a constant step potential value (1 mV) was studied. The influence of the square wave amplitude on the peak current of 0.01 μM PO_4^{3-} was evaluated from 10 to 100 mV (**Figure S1.1, C**), and it was observed that the peak current increased at higher square wave amplitudes up to 50 mV to generate a maximum value of 2.05 μA. At amplitudes higher than 50 mV, the peak currents decreased to 1.8 μA and 1.6 μA for 75 mV and 100 mV, respectively. Thus, 50 mV was determined to be the optimal square wave amplitude, where higher values resulting in a slight decrease of the peak current. The scan rate (ν) for SWV is assigned in terms of the step potential and frequency ($\nu = E_{step} \times f$)/mV·s^{-1}. To study the influence of the square waveform scan rate on the peak current, the frequency was varied from 10 to 200 Hz (**Figure S1.1, D**) while holding the step potential constant at 1 mV to reduce the peak noise (at higher than 1 mV, a distortion of the peak voltammogram was observed). The peak current was found to increase linearly with frequency until 150 Hz. Therefore, the optimum frequency, i.e., the scan rate, was approximately 150 Hz with a related peak current value of 4.5 μA, and at higher scan rates, the peak current decreased slightly to 4 μA at a frequency of 200 Hz.

3.3.5 Impedimetric performance

Electrochemical impedance spectroscopy was used to analyze the properties of the analytical method by accounting for the possible positions of all components in the electrochemical cell (resistors, conductors, capacitors) and their influences on the movement of ions and electrons by applying alternating current signals and recording the response as a function of frequency. The resulting electrical output signals were sinusoidal at different times (phase-shifted) as a function of the voltage. EIS can be evaluated using two approaches: Nyquist plot and Bode plot. The Nyquist plot compares the imaginary impedance component (out-of-phase, Z_{Im}) against the real impedance (in-phase, Z_{Re}) at each applied frequency. The Bode plot compares the logarithm of the absolute impedance |Z| and the phase-shift against the logarithm of the applied frequency (Prodromidis 2010). To test the impedimetric responses of the bare electrode, CPE, and molybdate/CPE, EIS was performed in a solution containing 0.1 μM PO_4^{3-} in artificial seawater at a pH of 0.8 at both electrodes.

The Nyquist and Bode plots are shown in **Figure S1.3 (A, B)**, and a modified Randles equivalent circuit was used to fit the experimental data (**Figure S1.3 A, inset**). The data fit using this circuit

are represented by solid lines in the EIS spectra. A good match was observed between the experimental and fitted data. The equivalent circuit used to model the data is associated with the resistive and capacitive components. The components of the circuit are as follows: solution resistance R_s, double layer capacitance Y_o1, capacitance of the film Y_o2, charge-transfer resistance R_{ct}, film resistance R_f, and Warburg impedance W_s1. All of the fitting data are listed in **Table S1.1**. The suitability of the model circuit is indicated by the sum of the weighted error, or X^2, where a smaller value of X^2 indicates a good fit of the experimental data (Boukamp 1986). It was found that for the CPE and molybdate/CPE, the variation in the value of R_s was not high because the values of R_s only depend on the ionic strength of the electrolyte solution and the distance between the auxiliary and working electrodes in the electrochemical cell (Dijksma et al. 2002), and the ionic strength of the electrolyte solution remained constant (0.1 μM PO_4^{3-} in artificial seawater at pH 0.8). Y_o1 is the double layer capacitance on the interface between the electrode and its surrounding electrolyte. The double layer is formed as ions in the solution are deposited on the electrode surface. This value depends on many variables (e.g., electrode potential, ionic concentration, electrode roughness). The deviation of Y_o1 from perfect capacitance (n = 1) is due to the relatively small value of its components for both cases (n = 0.9287 for CPE) and (n = 0.8234 for molybdate/CPE). The relatively high value of n for molybdate/CPE indicates the capacitive nature of the proposed sensor toward PO_4^{3-}. The Y_o2 and W_s1 values generally relate to the diffusion of ions from the electrolyte solution to the surface of the electrode. The low values for both variables in molybdate/CPE as compared to CPE indicate that the proposed sensor is more diffusive for PO_4^{3-} than CPE. Among these variables, R_{ct} is the most essential element because it is related to the kinetics of the charge-transfer reaction at the interface. The measured values of $1.838 \times 10^6\ \Omega$ for CPE and 1.173 Ω for molybdate/CPE indicate fast kinetics of electrons in the presence of PO_4^{3-} at the modified electrode, while the decrease in R_f indicates lower resistance of the electrode film layer toward PO_4^{3-}.

Following analysis of the equivalent circuit and comparison of the influence of CPE and molybdate/CPE on the impedimetric signal of the electrolyte containing PO_4^{3-}, the response of the sensor to the presence of PO_4^{3-} in various electrolyte solutions was assessed. EIS was performed on molybdate/CPE for different concentrations of PO_4^{3-} in artificial seawater to evaluate its analytical performance. A series of EIS experiments were performed where the molybdate/CPE was exposed to increasing concentrations of PO_4^{3-}. The experimental data for the determination of PO_4^{3-} are represented by the corresponding Nyquist plot shown in **Figure 3.3A**. The data were fitted according to the modified Randles equivalent circuit presented in **Figure 3.3B** with the same components used in the equivalent circuit in **Figure 3.12**, with the

exception of a constant phase element that was used rather than a capacitor for the film capacitance. The data in **Figure 3.3C** indicate a gradual decrease in the impedimetric signal in terms of the R_{ct} value, which is likely due to the release of electrons during the reaction of PO_4^{3-} ions with molybdate ions as part of the complexation process. The proposed sensor exhibited a linear relationship between R_{ct} value and PO_4^{3-} concentration in the range of 0.1 to 1 μM with a sensitivity of −431.35 Ω·μM^{-1} and a coefficient of detection (R^2) of 0.982.

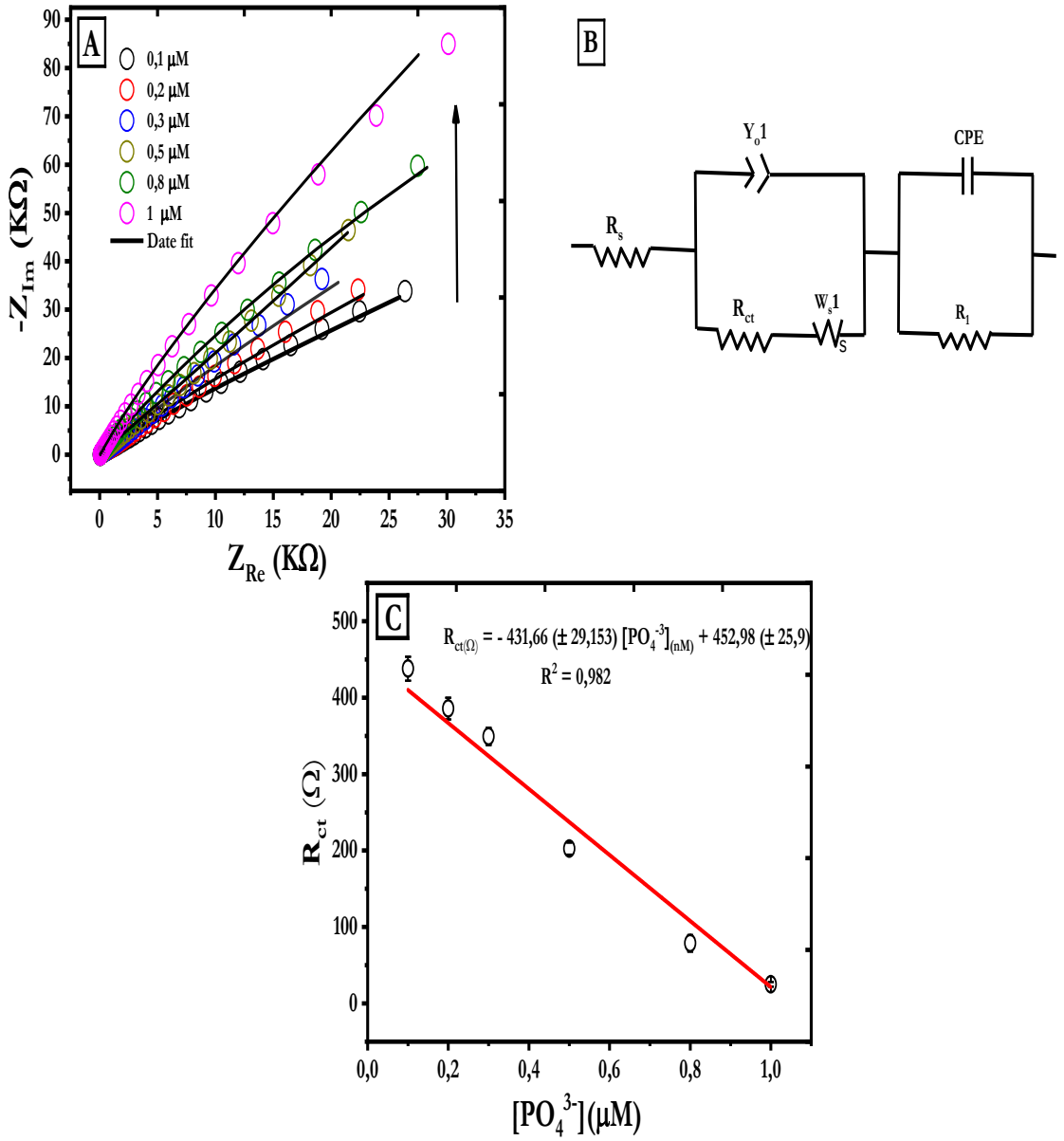

Figure 3.3 (A) Nyquist plots (Z(real) vs. −Z(imaginary)) obtained for molybdate/CPE for 0.1, 0.2, 0.3, 0.5, 0.8, and 1 μM PO_4^{3-}, each in 35-g/L NaCl solution (pH 0.8). The circles denote the experimental data, whereas the solid lines represent the data measured using the modified Randles

equivalent circuit in (B) used to fit the experimental data to extrapolate impedance parameters. (C) The calibration curve for various PO_4^{3-} concentrations at the charge-transfer resistance (R_{ct}). The data points are expressed as a mean ± SD of three replicated measurements, and the fitted curve represents the linear regression.

3.3.6 Analytical performance

Square wave voltammetry was employed for the quantitative measurement of PO_4^{3-} in artificial seawater (35 g/L NaCl) under acidic conditions (pH 0.8), including a washing step using CV for 10 cycles in NaOH between the measurements. The square wave voltammograms were recorded under the optimized conditions using a range of PO_4^{3-} concentrations (0.01, 0.02, 0.05, 0.1, 0.2, 0.4, 1, 2, 3, and 5 μM) (**Figure 3.4**). The data demonstrate a fairly linear relationship between the PO_4^{3-} concentration and peak current values at the molybdate/CPE. Two regimes of linear behaviour was observed. The first was over a concentration range of 0.01 to 0.4 μM PO_4^{3-} with a slope of 13.9704 $\mu A \cdot \mu M^{-1}$ (R^2 = 0.99039), and the second linear regime was over a concentration range from 1 to 5 μM PO_4^{3-} with a slope of 0.3025 $\mu A \cdot \mu M^{-1}$ (R^2 = 0.9904). The separation of the data into two discrete linear ranges reflects the adsorption of the phosphomolybdate complex onto the electrode surface at high concentrations of PO_4^{3-}, similar to the behaviour reported previously for electrochemical PO_4^{3-} sensors (Barus et al. 2016; Kolliopoulos, Kampouris, and Banks 2015; Bai et al. 2014). This behaviour was attributed to the formation of a polymer film of the phosphomolybdate complex at high concentrations of PO_4^{3-} (Choi and Kim 2009; Wang and Dong 1996; Rong and Anson 1996), where the polymer film may act as an insulator to impede the electron transfer through the electrode surface. The LOD was calculated to be 0.003 μM based on the IUPAC recommendation (Long and Winefordner 1983) defined as three times the standard deviation of the analysis of blank solutions (n = 20), divided by the slope of the linear fit (slope of the calibration curve 0.01–0.4 μM PO_4^{3-}).

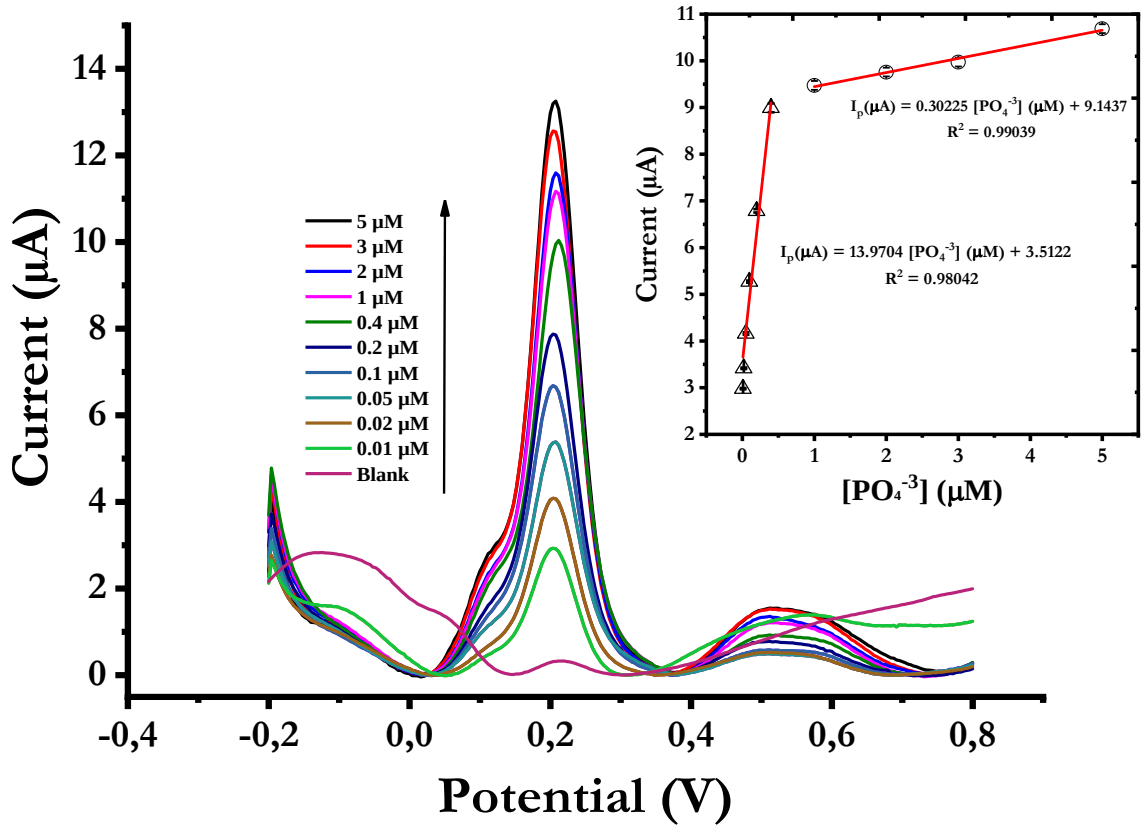

Figure 3.4 Square wave voltammograms of different PO_4^{3-} concentrations (0.01, 0.02, 0.05, 0.1, 0.2, 0.4, 1, 2, 3, and 5 µM) on molybdate/CPE in 35 g/L NaCl (pH 0.8), frequency of 150 Hz, and amplitude of 50 mV, with the calibration curve shown in the inset that is related to the regression equations and R^2 value. (**Error bar *n* = 5**).

Table 3.1 Summary of comparison of the molybdate/CPE modified electrode with those reported previously in the literature (Huang 2017; Satoh et al. 2017; Topcu et al. 2018; Li, Shang, and Qin 2016; Talarico et al. 2015; Cinti et al. 2016; Ogabiela et al. 2015; Cui et al. 2014; Kolliopoulos, Kampouris, and Banks 2015; Barus et al. 2016). The proposed sensor was found to have a higher sensitivity, with only a screen-printed electrode reported by Kolliopoulos et al. in 2015 demonstrated a similar LOD for the quantification of PO_4^{3-} after complexation with molybdate in solution.

Table 3.1 Electrochemical determination of PO_4^{3-} using different working electrodes.

Electrode	Technique	Linear range (µM)	LoD (µM)	Reference
PANI	Amperometric	1-100	1	(Huang 2017)

Bis(DBPS)methane/PVC	Potentiometric	0.5-5 × 10^3	0.5	(Satoh et al. 2017)
Chitosan-clay/PVC	Potentiometric	1- 1× 10^4	0.6	(Topcu et al. 2018)
Cu-BPMP	Potentiometric	3-50	0.5	(Li, Shang, and Qin 2016)
CBNPs-SPE	Amperometric	1-80	0.1	(Talarico et al. 2015)
CB/SPE	Amperometric	0.5-100	0.4	(Cinti et al. 2016)
AuNWs	Amperometric	12.5-1 × 10^3	0.1	(Ogabiela et al. 2015)
AuNWs/Pt	Amperometric	48-1.4 × 10^3	45	(Cui et al. 2014)
SPE	CV (Ammonium Molybdate tetra hydrate)	0.005- 0.2	0.003	(Kolliopoulos, Kampouris, and Banks 2015)
Au electrode	SWV (Electrolytic produced Molybdate + NaCl)	0.1-1	0.05	(Barus et al. 2016)
Molybdate / CPE	SWV	0.01–- 5	0.003	This work

PANI = polyaniline, DBPS = Bis(dibromophenylstannyl)methane, PVC = polyvinyl chloride, BPMP = 2,6-bis(bis(2- pyridylmethyl)aminomethyl)-4-methylphenol, CB = carbon black nanoparticles, SPE = screen printed electrode, AuNWs = Gold-nanowires array

3.3.7 Reproducibility and stability of the modified electrode

The fabricated molybdate /CPE exhibited excellent repeatability (**Figure 3.5)** for SWV responses toward 0.2 and 5 μM PO_4^{3-}. The electrode was tested via 10 repetitive measurements of PO_4^{3-} employing the same sensor in the same solution, and the precision was determined by the relative

standard deviation (RSD). For 0.2 μM PO_4^{3-}, an RSD value of 5.76% was obtained, and for 5 μM PO_4^{3-}, an RSD value of 4.32% was measured. The reproducibility of the sensor electrode was tested using five different sets of electrochemically fabricated electrodes, which generated an RSD value of 5.46% for 5 μM PO_4^{3-} and exhibited a good reproducibility with an independently fabricated electrode. The stability of the electrode was evaluated using the SWV responses recorded over five days (the modified electrode was stored at room temperature between uses), and an RSD value of 7.26% was obtained, possibly caused by the decrease of the signal over time, which may be improved by adapting the storage conditions. Overall, the electrochemically-modified electrode demonstrates good stability, reproducibility, and reparability characteristics for PO_4^{3-} analysis.

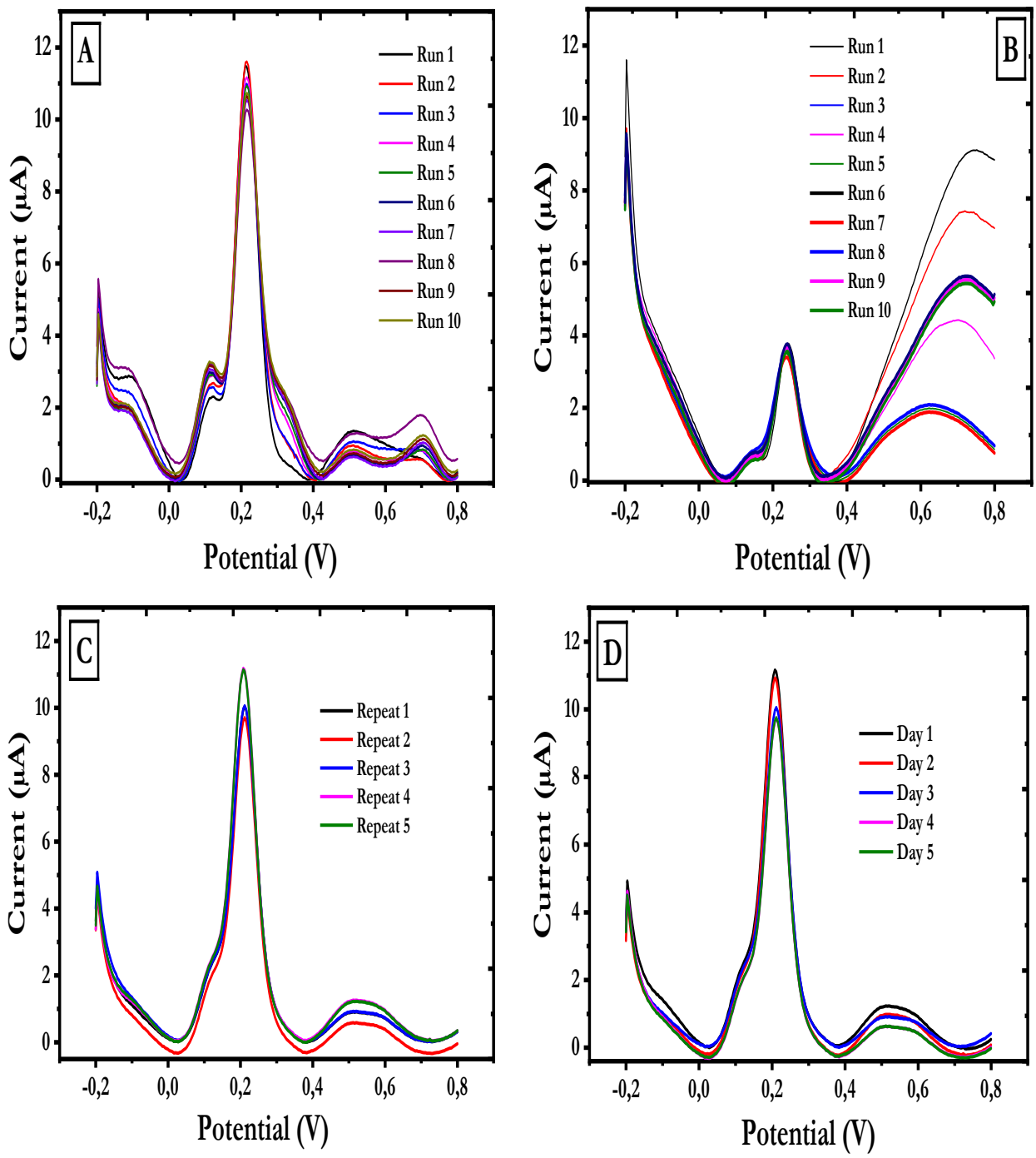

Figure 3.5 Repeatability of molybdate/CPE sensor toward PO_4^{3-}detection. (A) Square-wave voltammograms of 5 µM PO_4^{3-}, (B) square-wave voltammograms of 0.2 µM PO_4^{3-} in 30-g/L NaCl, pH 0.8. Ten repetitive measurements were reordered at every 100 intervals over 20 min with 10 scanning cyclic voltammograms into 0.1-M NaOH after each measurement. (C) Reproducibility of molybdate/CPE to 5 µM PO_4^{3-} into artificial seawater (pH 0.8) with five fabricated electrodes. (D) Operative stability to 5 µM PO_4^{3-} into artificial seawater with stored molybdate/CPE (at room

temperature) over five days. The SWV potential ranges from −0.2 V to 0.8 V (vs. Ag–AgCl) using a 150 Hz frequency, an amplitude of 50 mV, and step potential of 1 mV.

3.3.8 Interferences on PO_4^{3-} analysis

A surfactant is identified as a molecule containing both a hydrophobic head and end. Because of their unique chemical structure, surfactants affect the electrochemical process of substances by modifying the electrode-solution interface properties (Shankar, Swamy, and Chandrashekar 2012). Triton X-100 is a highly hydrophobic nonionic surfactant with an average of 95 ethoxy groups. In this study, Triton X-100 was selected because of its outstanding tendency to be adsorbed on the working electrode surface (Kowalcze and Jakubowska 2018). The potential interference from Triton X-100 was assessed by varying the surfactant concentration in a solution of artificial seawater that was spiked with 0.01 μM PO_4^{3-} (**Figure 3.6A**). The addition of 1 mg/L Triton X-100 resulted in a decrease of the peak current compared to the 0.01 μM PO_4^{3-} standard solution, and a PO_4^{3-} underestimation of ~9%. For a solution containing 2 mg/L Triton X-100, the peak current decrease resulted in a PO_4^{3-} underestimation of ~7%. At 3 mg/L Triton X-100, the peak current was similar to a surfactant-free solution, but beyond 3 mg/L the peak current increased until 8 mg/L resulting in a PO_4^{3-} overestimation of ~14%. At concentrations higher than 8 mg/L, a stronger interference was observed with an overestimation of ~40% and ~55% for 9 mg/L and 10 mg/L Triton X-100, respectively. The level of nonionic surfactants in natural waters is typically between 0.1 and 0.5 mg/L (Cosović and Vojvodić 1982). Although there was an interference effect on the peak current measurement of PO_4^{3-} due to Triton X-100, the linearity of the response was not influenced, as shown in **Figure 3.6B**, where a calibration curve was established over the linear range of 0.01–0.05 μM PO_4^{3-} in a solution spiked with 10 mg/L Triton, with the regression equation, I_p (μA) = 24.9586 [PO_4^{3-}] (μM) + 0.84751 and an R^2 value of 0.994.

There is an interference in seawater by silicic acid on the determination of PO_4^{3-} Silicic acid competes with PO_4^{3-} to react with molybdate ions because of their similar ionic structure. To overcome this problem, the concentration of molybdate ions and protons (H^+) should be regulated in order to obtain an appropriate H^+ to MoO_4^{2-} ratio. Zhang et al. (Zhang, Fischer, and Ortner 1999) demonstrated that it is possible to avoid the interference from silicic acid by conducting the analysis at a pH between 0.4 and 0.9 . We verified this assumption by testing various loading concentrations of silicic acid from 10 to 50 μM were tested at a constant concentration of PO_4^{3-} (0.05 μM) in a solution of artificial seawater (pH 0.8) (**Figure 3.6C**). The peak current of the standard PO_4^{3-} solution with and without silicic acid was measured after each addition, and the signal change did not exceed 7% with an increase of the silicic acid concentrations up to 50 μM,

indicating the capability of the proposed method to exclude silicic acid interferent during real seawater analysis. The peak intensities are reported on the calibration curve between 0.01 and 0.2 μM PO_4^{3-} (**Figure 3.6D**, red dots), and the results demonstrate that silicic acid does not interfere in the PO_4^{3-} concentration determination.

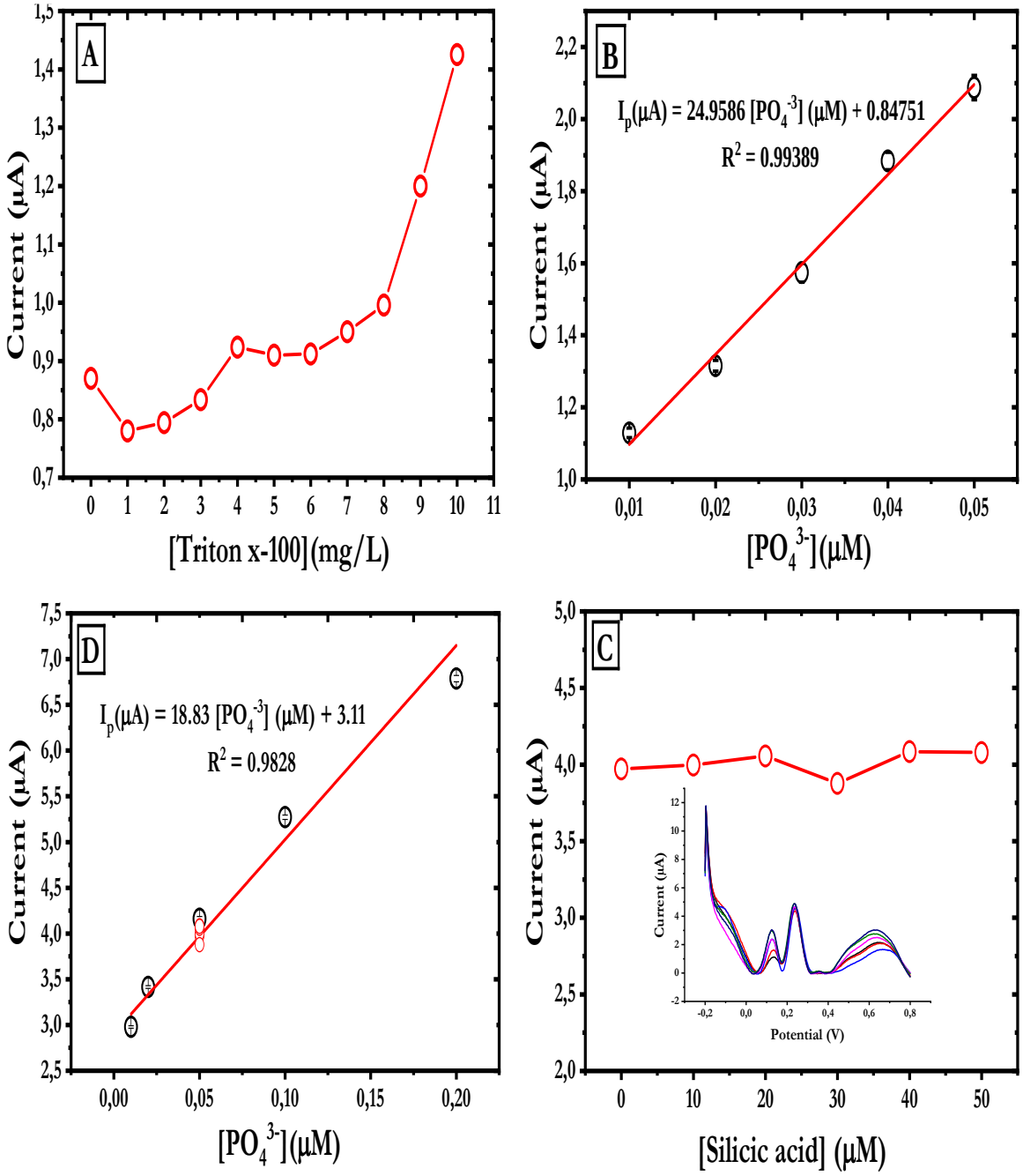

Figure 3.6 Interference effect from A) the nonionic surfactant Triton X-100 on the peak current of 0.01 μM PO_4^{3-} in 30 g/L NaCl (pH 0.8). B) Calibration curve constructed from 0.01, 0.02, 0.03, 0.04, and 0.05 μM PO_4^{3-} containing 10 ppm of Triton X-100 with the related regression equation and R^2. C) The interference study of silicic acid at concentrations of 0, 10, 20, 30, 40, and 50 μM in

a solution containing 0.05 μM PO_4^{3-} in artificial sea water. mD) Calibration curve from SWVs at PO_4^{3-} concentrations of 0.01, 0.02, 0.05, 0.1, 0.2 μM at the peak at 0.2 V, including the peak current of 0.05 μM PO_4^{3-} containing different concentrations of silicic acid.

3.3.9 Analysis of coastal seawater samples

As a demonstration of the proposed method to natural samples, discrete samples were collected at different stations in the North Sea between the coast and Helgoland Island (**Figure 3.7).** The research was conducted in the German Bight in the outflow plume of the Elbe River. The North Sea is a shallow, semi-enclosed shelf sea of the North Atlantic (Otto et al. 1990). In the North Sea, two water bodies can be distinguished. The northern and central parts are under oceanic influence with surface salinities under 34. The southern part is well mixed and receives oceanic water from the British Channel (Otto et al. 1990). In the coastal water, salinity is lower at 30 because of strong riverine influences (Reuter et al. 2009). The Elbe River is one of the larger rivers discharging into the North Sea, with a length of 1.094×10^3 km and a catchment area of 148.268×10^3 km^2, categorized as the fourth largest catchment area of Central Europe (Carstens et al. 2004). The Elbe River is subject to high anthropogenic influences, and it represents the most frequent shipping route to Hamburg (50,000 vessels move through the river yearly). The Elbe River is considered one of the most heavily polluted rivers in Europe with low dissolved oxygen levels, organic matter enrichment, nutrient enrichment because of human activities, and navigation channel deepening (Simon et al. 2005; Boehlich and Strotmann 2019)(Bergemann and Gaumert 2010; Simon et al. 2005). The German Bight in the eastern North Sea receives oceanic water from the British Channel and the northwestern North Sea (Pohlmann 2006), with PO_4^{3-} concentrations of approximately 1.8 μM reported in September 2008 (Grunwald et al. 2010). The salinity ranges from below 30 in front of Elbe outlets to 31–32 approximately 30 km from the coast. At 50 km offshore at Helgoland Island, salinity varies between 31 and 32, whereas at 75 km offshore, salinity is higher than 33 (Williams, Tudor, and Gregory 2005; Heyen and Dippner 1998). Figure 7 shows the spatial distribution of salinity gathered during CTD casts. The results revealed a complex dispersal of lower salinity inputs into the North Sea from the Elbe River. Salinity ranged from 27.3 to 33, with the lowest salinity close to the Elbe Estuary and all over the periphery of the North Sea and higher salinity toward the centre.

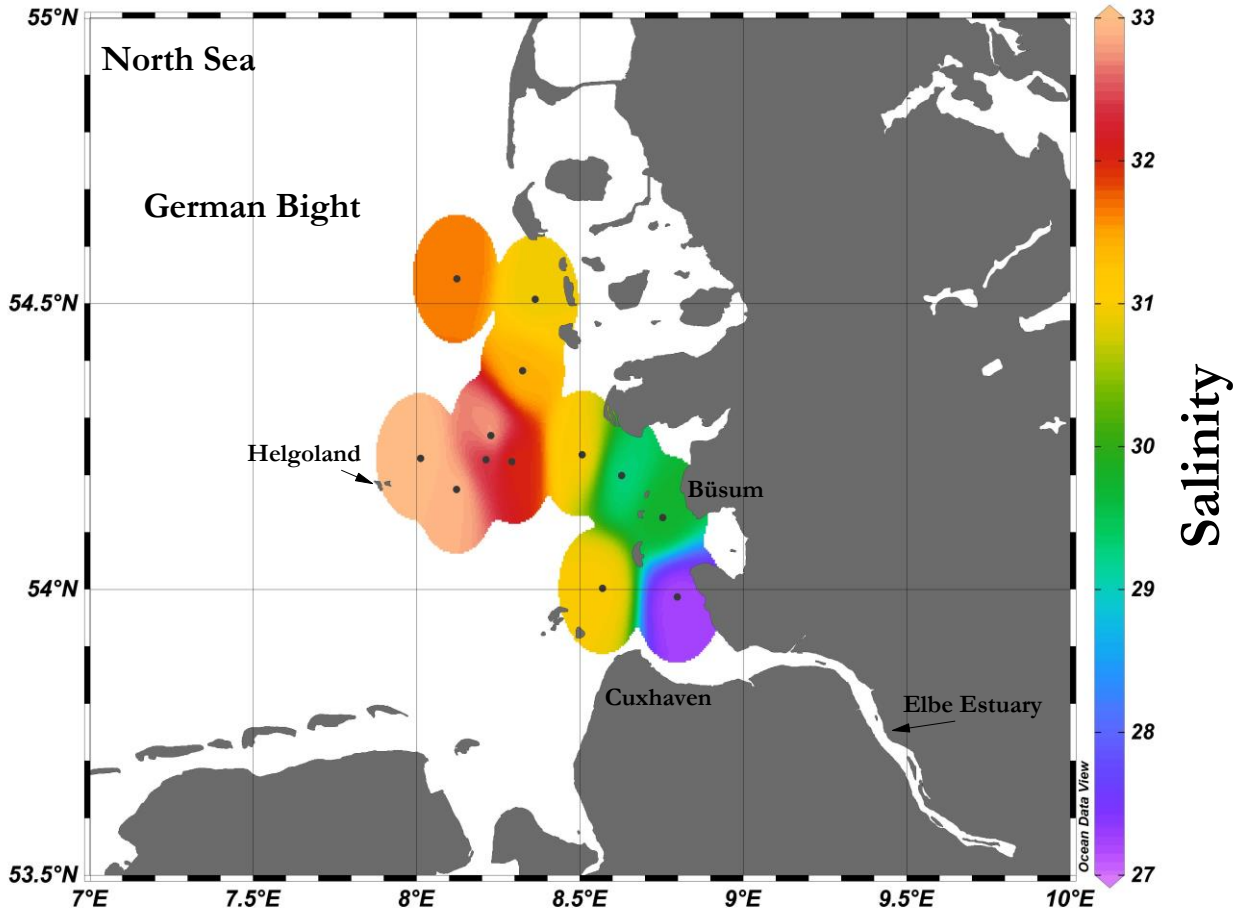

Figure 3.7 Overview of the sampling stations (red dots) in the German Bight (North Sea) at the outflow of the Elbe River. Locations of Helgoland Island and Elbe Estuary are denoted on the map. The map showed the regional overview of the study area reflecting the spatial distribution of seawater salinity. Map plotted using ODV 5.3.0 (Schlitzer 2020).

The PO_4^{3-} concentrations in the collected samples were analysed upon returning to the land-based laboratory using an electrochemical approach, discussed herein. A comparison with the classical colorimetric method was made for validation purposes. **Figures 3.8, A** and B show that the PO_4^{3-} concentrations obtained using the colorimetric and electrochemical approaches, respectively, against the variation of the salinity data gathered during CTD casts. Both methods show significant negative correlations ($p < 0.01$) with salinity. Although the electrochemical approach showed a weaker correlation ($R^2 = 0.4$) compared with the colorimetric method ($R^2 = 0.78$), significant differences exist between them at the 1% significance level (paired *t*-test, $df = 23$), with $p = 6.59 \times 10^{-29}$ for those obtained electrochemically and $p = 7.9 \times 10^{-29}$ for those obtained using the colorimetric method.

Considering all data, a mean accuracy of 93% (assessed as the average of the recovery values) for

electrochemical measurements compared to the colorimetric data was obtained, exhibiting a strong significant correlation with the Spearman correlation coefficient of 0.75 ($p < 0.01$, $n = 23$) (**Figure 3.8C & Figure 3.9**). The PO_4^{3-} concentrations determined using the colorimetric method were between 0.687 and 1.769 µM, with a mean PO_4^{3-} concentration of 1.189 ± 0.273 µM (n = 23). The proposed electrochemical method obtained minimum and maximum PO_4^{3-} concentrations of 0.624 µM and 1.83 µM, respectively, with a mean of 1.195 ± 0.367 µM (n = 24). Both methods showed no significant differences in the analytical results at 1 % significance level with (*t*-test, *p*-value = 0.74, *df* = 23).

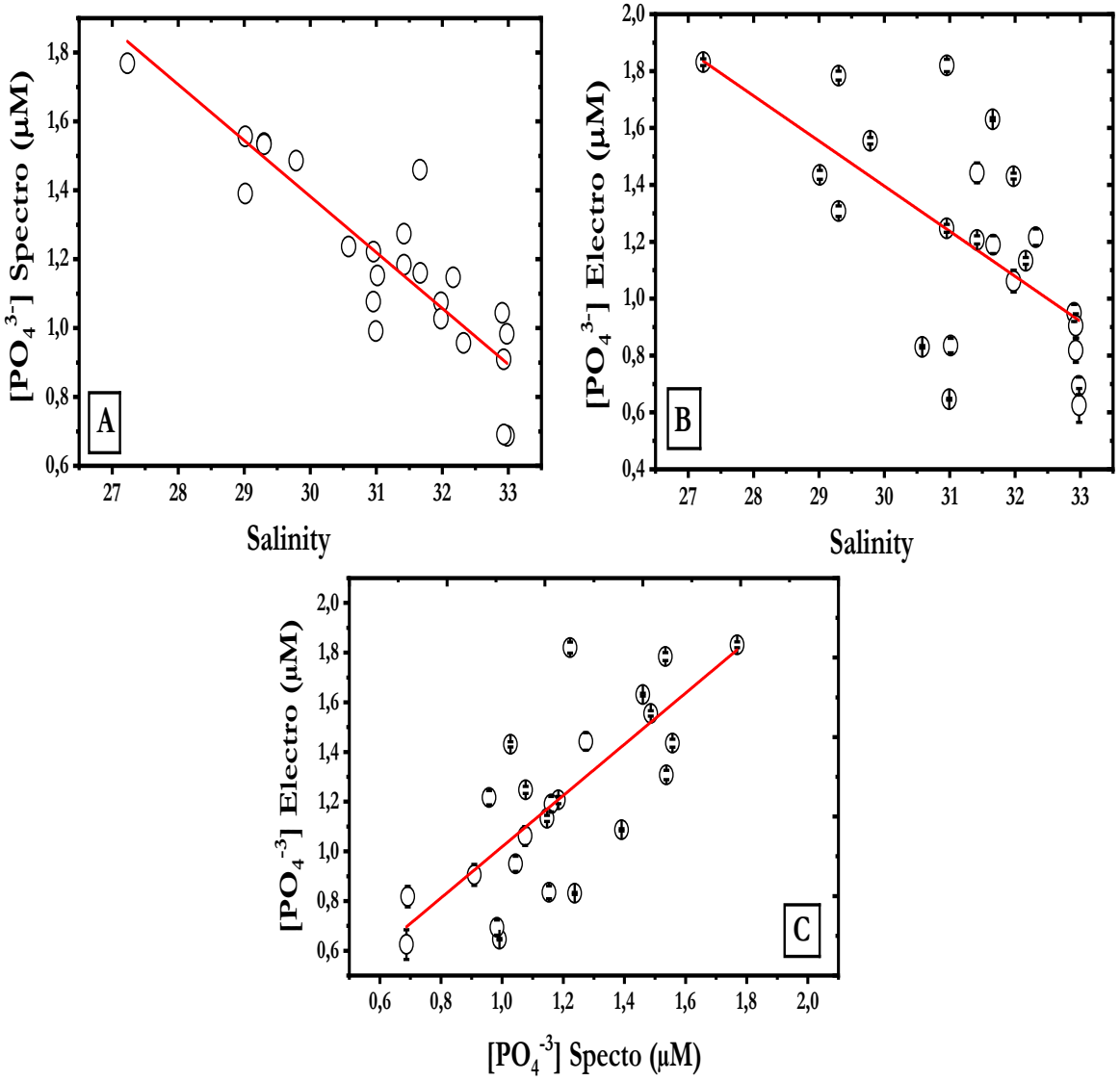

Figure 3.8 Property to property plots for the discrete samples collected. (A) PO_4^{3-} measured using the classical colourimetric method vs. salinity during CTD casts $y = -0.16259x + 6.259$, $R^2 = 0.78129$. (B) PO_4^{3-} measured electrochemically vs. salinity during CTD casts $y = -0.1586x +$

6.1539, R^2 = 0.4018. (C) PO_4^{3-} measured using the colorimetric method vs. PO_4^{3-} measured electrochemically y = 1.573x–− 0.8446, R^2 = 0.6812.

A Spearman correlation matrix (**Figure 3.9**) shows the relationships between the electrochemical determined PO_4^{3-} concentrations and other parameters determined in the discrete samples. For example, PO_4^{3-} concentrations significantly correlated with $\Sigma(NO_2^- + NO_3^-)$ and NO_3^- with positive correlation coefficients of 0.36 and 0.29; thus, the results show the relationship between the two main nutrients (N and P) required for primary production. The weak positive correlation with oxygen could refer to the enhanced PO_4^{3-} level due to riverine input and this could not be related to the biological activity. There is an anti-correlation with salinity, with a Spearman correlation coefficient of −0.629, which is related to the enhanced PO_4^{3-} concentrations from the freshwater Elbe River end-member.

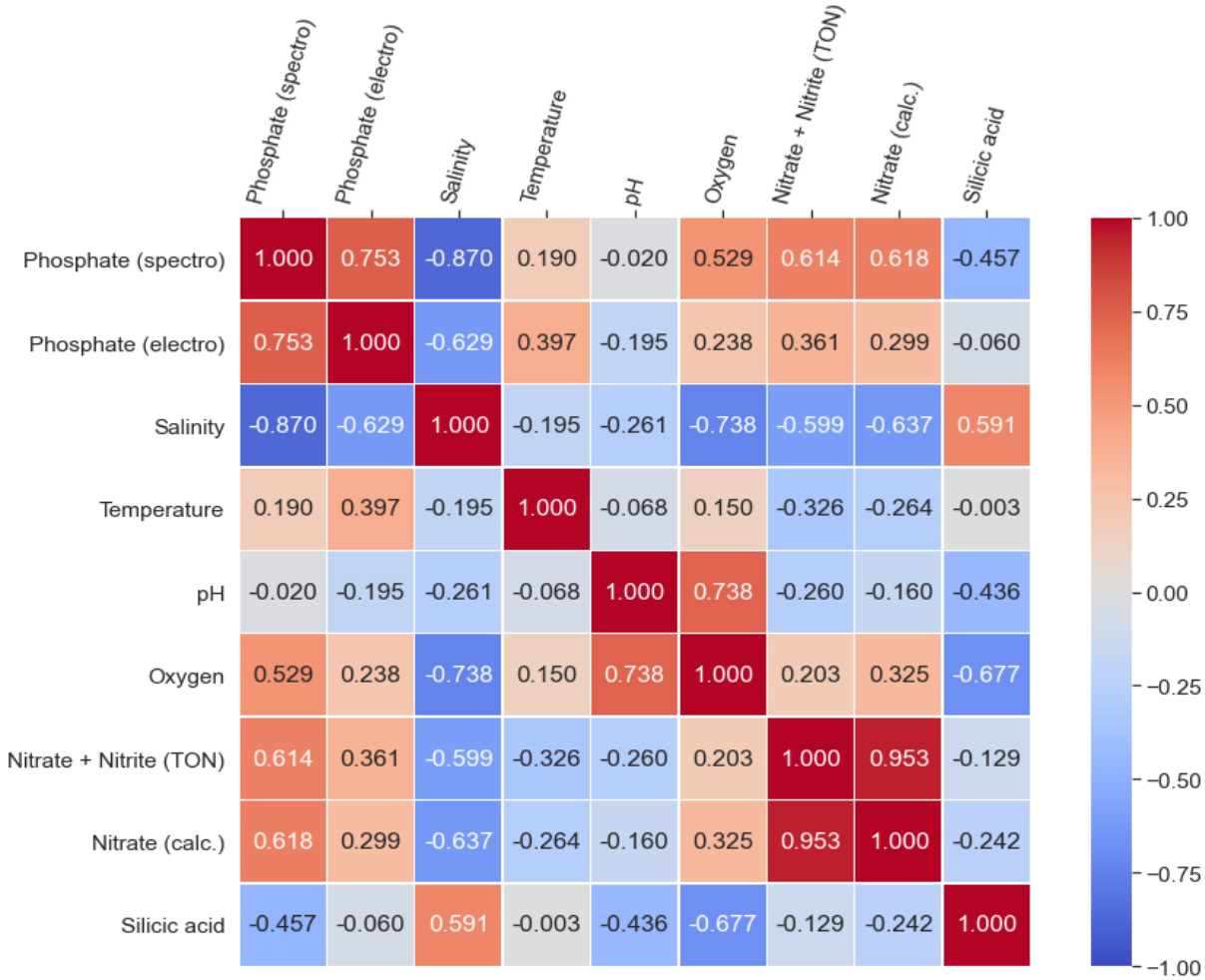

Figure 3.9 Spearman correlation matrix of different variables for the discrete samples collected off the North Sea. Positive correlation coefficients are shown in red boxes and negative correlation coefficients in blue boxes (p < 0.01).

3.4 Conclusion

In summary, a novel molybdate/CPE working electrode was presented for PO_4^{3-} sensing in seawater, which utilizes the formation of a phosphomolybdate complex to achieve high sensitivity and selectivity for PO_4^{3-} under acidic conditions. molybdate/CPE exhibited a wide detection range (0.01–3 μM) and a low detection limit of 0.003 μM at an RSD of 5.7% (for 0.2 μM, n = 10). In addition to the stability and reproducibility of the electrode, the sensor exhibited no interference from silicic acid, which is the most common interfering ion for PO_4^{3-} analysis in seawater. The proposed electrode was successfully utilized for real sample analysis and performed well as compared to the conventional colorimetric methods This study reveals the significant potential of the designed electrode to integrated into a portable electrochemical device for field testing PO_4^{3-} concentrations in marine waters.

Author Contributions: M.F.A.: investigation, methodology, data curation, visualization, writing—original draft. E.P.A.: funding acquisition, resources, supervision, writing—review and editing. A.G. A.: Formal analysis M.A. review and editing All authors have read and agreed to the published version of the manuscript.

Acknowledgment: All authors would like thank Prof. Dr. Amr Beltagi as he facilitated the EIS measurements on the VersaSTAT 4 Potentiostat in his laboratory at the Chemistry Department, Faculty of Science, Kafr El-Sheikh University, Egypt. M.F. Altahan wishes to thank the National Water Research Center (NWRC).

3.5 Supplementary information

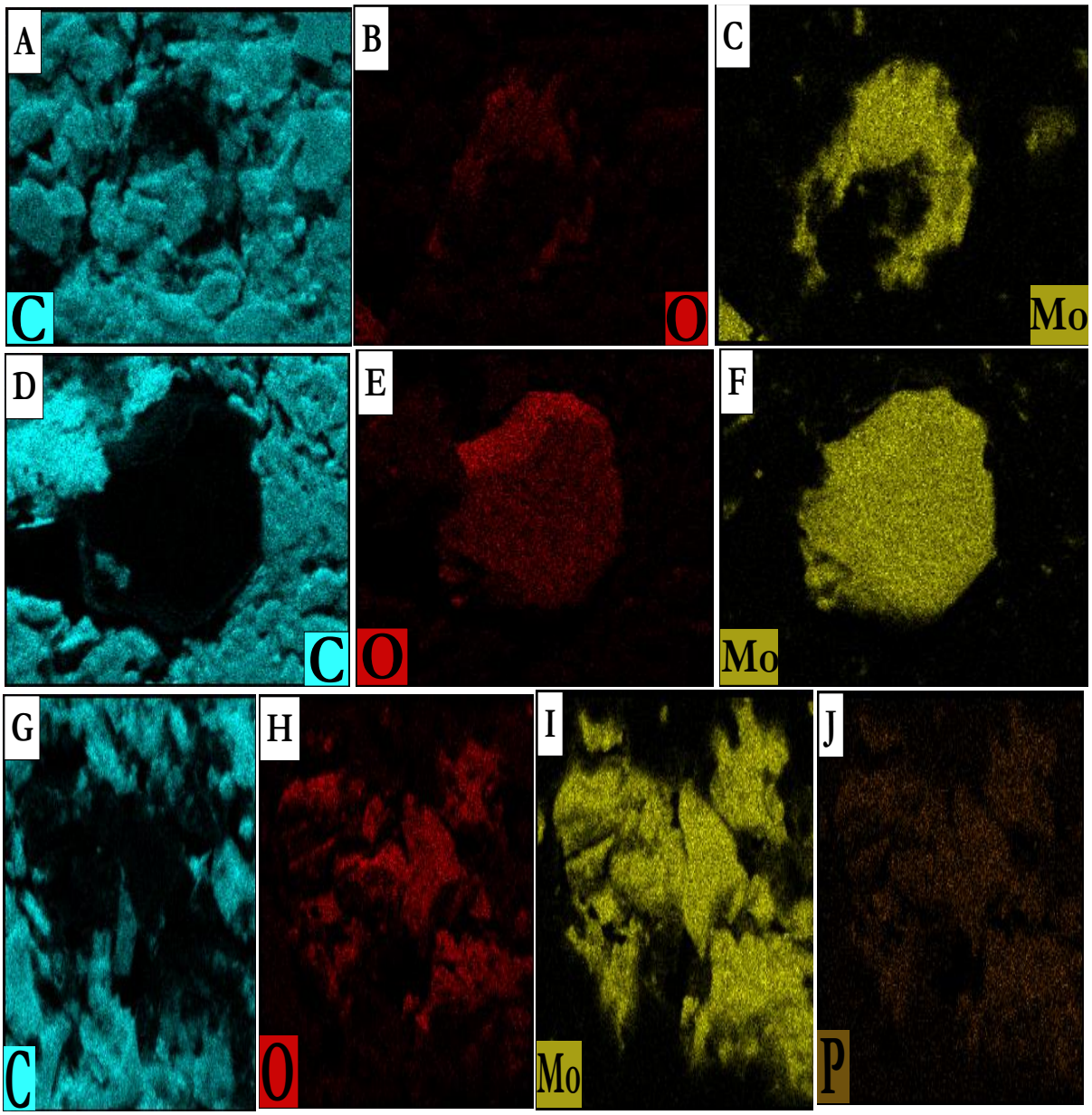

Figure S1.1 Mapping Analysis images of molybdate/ CPE without modification for (A) carbon, (B) oxygen and (C) molybdenum, molybdate/ CPE after CV into 0.1 M NaOH for (D) carbon,I) oxygen and (F) molybdenum and molybdate/CPE after SWV into 30 g/L NaCl (pH 0.8) with 1 M PO_4^{3-} for (G) carbon, (H) oxygen, (I) molybdenum and (J) phosphorus

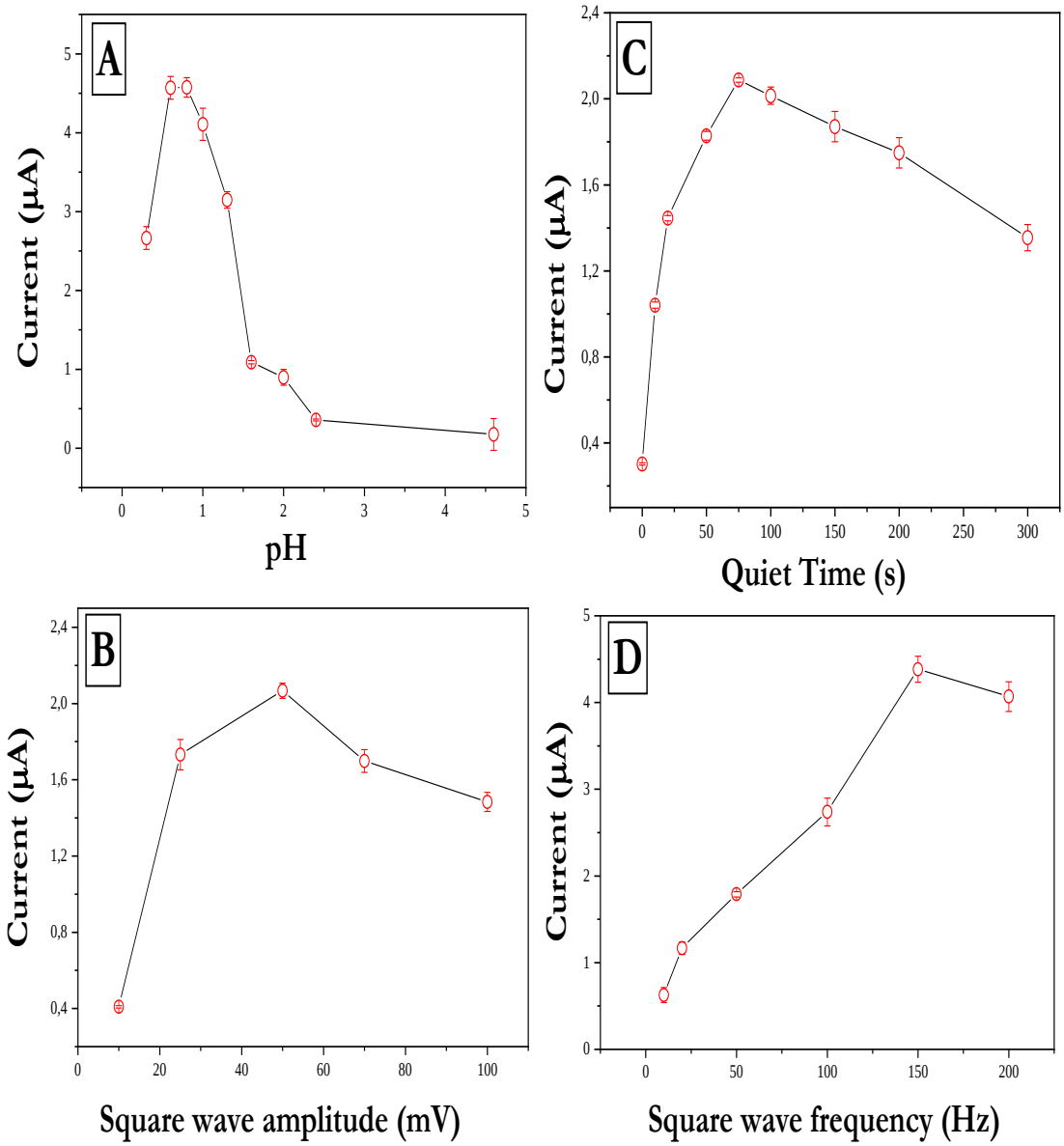

Figure S1.2 Square wave voltammetric peak current of 0.01 µM PO_4^{3-} in 30 g/L NaCl at (A) varying pH values including 4.6, 2.4, 2, 1.7, 1.3, 1, 0.8, 0.6, and 0.3; (B) varying complexation time from 0 to 300 seconds; (C) square wave amplitude variation from 10 to 100 mV; (D) square wave frequency variation from 10 to 200 Hz

.

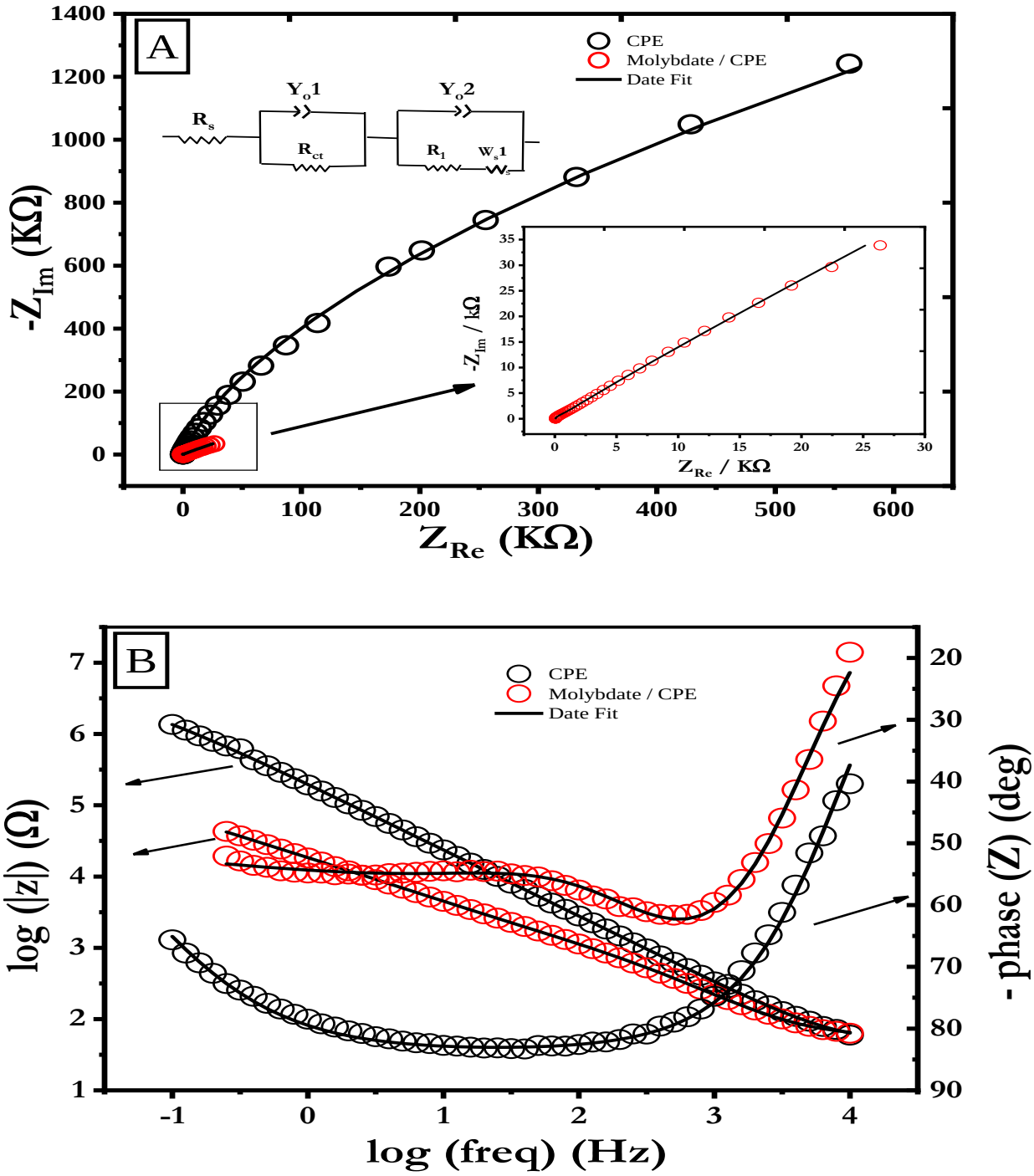

Figure S1.3 The impedance studies of the CPE and molybdate/CPE in a solution containing 35-g/L NaCl pH 0.8 at a 0.1 μM concentration of PO_4^{3-} in the frequency range 10^3–1 Hz. (A) Nyquist plot (Z(real) vs. Z(imaginary)), (B) Bode plots with bode' magnitude plot (log(frequency) in Hz vs. log |Z| in Ω) and bode phase angle plot (log(frequency) in Hz vs. (−phase angle) in degrees). The points denote the experimental data, whereas the lines are obtained using EC software fitting for the equivalent circuit depicted in (A, inset).

Table S1.1 Electrochemical impedance spectroscopy fitting data corresponding to Figure 3.3.

Parameters	**CPE**	**Molybdate/ CPE**
R_S (Ω cm^2)	46.06	48.3
R_{CT} (Ω cm^2)	1.838×10^{6}	1.73
Y_{O1} (F.s $^{-a1 - 1)}$)	0.9039×10^{-6}	3.639×10^{-6}
a_1	0.9287	0.8234
Y_{O2} (F.s $^{(a2 - 1)}$)	0.205×10^{-6}	1.708×10^{-9}
a_2	0.2528	0.271
R_f	9217	0.02316
W_{S1} (Ω. $S^{-1/2}$)	1.902×10^{6}	42086
X^2	8.185×10^{-4}	3.863×10^{-4}
Weighted $\Sigma(X^2)$	0.03891	0.02074

4 Use of bi-potentiostat as a simple and accurate electrochemical approach for the determination of orthophosphate in seawater

Mahmoud Fatehy Altahan[1,2], Mario Esposito[1], Boie Bogner[1], Eric P. Achterberg[1]

In preparation for submission……

[1] Chemical Oceanography Department, GEOMAR Helmholtz for Ocean Research Kiel, Kiel 24148, Germany.

[2] Central Laboratory for Environmental Quality Monitoring, National Water Research Center, El-Qanater El- Khairia 13621, Egypt.

Abstract

Autonomous *on-site* monitoring of orthophosphate (PO_4^{3-}) is urgently needed because of the importance of this nutrient- forprimary production in marine waters. Here, we report on the development and validation of an *on-site* autonomous electrochemical analyser for PO_4^{3-} in seawater. The new approach is based on the use of flow injection analysis in conjunction with a dual electrochemical cell (i.e., biopotentiostatic) detector (FIA-DECD) that uses two working electrodes sharing the same reference and counter electrode. Two working electrodes are used (molybdate/carbon paste electrode (CPE)) and CPE to correct for matrix effects. The proposed system was combined with a Python script for data processing. The effect of variation of square-wave voltammetry parameters (including step potential, amplitude, and frequency) on the analytical sensitivity was determined. Possible interferences from non-ionic surfactants and humic acid were investigated. The limit of quantification in artificial seawater (30 g/L NaCl, pH 0.8) was 0.014 μM for a linear concentration range of 0–02 - 3 μM. The proposed autonomous analyser was tested for ship-board PO_4^{3-} determination during a four-day research cruise in the North Sea. The analyser successfully measured 34 samples and achieved a good correlation (Pea'son' R = 0.91) with discretely collected samples which were analysed using a laboratory-based colorimetric reference analyser.

4.1 Introduction

Phosphorus (P) is one of the key elements required to maintain the stability of marine ecosystems. Like nitrogen, P is an important macronutrient for all living organisms and is essential for primary production and thus control of atmospheric oxygen levels (Van Cappellen and Ingall 1996; McDowell and Hamilton 2013). Phosphorus can be found in marine waters in dissolved and particulate forms. Orthophosphate (PO_4^{3-}), the major inorganic form of phosphorus, plays a critical structural and functional role in all marine organisms. Orthophosphate is released into waters following organic matter degradation by heterotrophic metabolic pathways and is available for either biological uptake, sorption onto mineral fractions, or incorporation into authigenic minerals (e.g., carbonate fluorapatite) (Canfield et al. 1993; Van Cappellen and Ingall 1996). High external P inputs into marine ecosystems, such as run-off from the widespread use of P fertilizer in agriculture, may lead to eutrophication and oxygen depletion. In oligotrophic regions, which account for about 40% of the w'rld's oceans, PO_4^{3-} concentrations are at nanomolar levels due to low supply and removal by primary production.

Since the early 1980s, research has been conducted into the development of on-line phosphate sensors (Puchades et al. 1990). Conventional laboratory methods based on classical colorimetric techniques are labour intensive and can only be used for the measurements of a limited number of discretely collected samples.

The Molybdenum Blue method is the most widely used laboratory technique for PO_4^{3-}. The method, first described by Murphy and Riley (Murphy and Riley 1962b) is based on the reaction of orthophosphate with molybdate under acidic conditions to form a yellow phosphomolybdate complex, which is readily reduced to a blue coloured complex by an excess of ascorbic acid in the presence of antimony (Sb) and organic acid (tartaric acid) in potassium antimony tartrate. The product complex is characterized by two spectral peaks at 720 nm and 880 nm, with a high intensity at 880 nm, and the complex is stable for several hours. The Molybdenum Blue method is limited by the stability of ascorbic acid, whose lifetime under dark conditions is only two months (Heidari-Bafroui et al. 2021).

The Molybdenum Yellow method was first described by Kriston and Mellon (Kitson and Mellon 1944) and is based on the addition of excess molybdate to an acidic solution of vanadate and PO_4^{3-} to form a yellow phosphomolybdate complex with a spectral peak at 340 nm, and the reagent mixture is stable for about one year.

A number of deployable sensors for PO_4^{3-} in seawater have been prepared based on the colorimetric Molybdenum Blue method. Hydrocycle-PO4 (Snazelle 2018a) is manufactured by

Sea-Bird Scientific (Philomath, Oregon, United States), Lab-On-Chip (LOC) by Clearwater Sensor Ltd. (Southampton, England) based on microfluidic technology (Beaton et al. 2022), WIZ is manufactured by SYSTEA SpA (Anagni, Lazio, Italy) based on a patented micro loop flow analysis (μLFA) (Bodini et al. 2015), and NuLAB is manufactured by Green Eyes LLC (Easton, United States) based on flow injection analysis (FIA)(Bohlen and Liebman 2019).

As reported for the NuLAB and LOC (Grand et al. 2017; 'Green Eyes, LLC'), an optical correction is performed using a reference channel to give the sensor high applicability in a variety of natural waters with high precision and accuracy. For this purpose, the analytical solution is passed through a reference channel to obtain the light intensity of the solution before the reagents are added to form the dye. This is very useful to correct for interferences caused by the sample matrix (e.g., salinity variations, coloured dissolved organic matter (CDOM)).

The long-term use of wet chemical sensors is limited by consumption of reagent solutions and instability of some of them (e.g., ascorbic acid). As an alternative, electrochemistry is a good candidate for miniaturized, ready-to-use sensors that minimize reagent and energy consumption and may be well suited for long-term environmental quality monitoring.

Several electrochemical sensors have been developed for the quantification of PO_4^{3-} in seawater, based on either amperometric or voltammetric techniques. Here, an electrochemical force potential is applied to the electrode or to the interface of a solution, causing a chemical reaction and consequently a current to flow, which is subsequently recorded (Mirceski and Gulaboski 2014). Almost all electrochemical probes for PO_4^{3-} are based on molybdate chemistry. However, there are a variety of electrochemical reactions.

The most common is the reduction of the phosphomolybdate complex. This complex can be formed in-situ via complexation between orthophosphate and ammonium molybdate, previously introduced into the solution. The determination of phosphomolybdate xomplex was done by cyclic voltammetry (Kolliopoulos, Kampouris, and Banks 2015).

There is also molybdate electrohydrolyzation by the molybdenum electrode. Where the determination was performed by amperometry (Jońca, Fernández, et al. 2011) or pulsed techniques such as differential pulse voltammetry (Jońca et al. 2013) or square-wave voltammetry (Barus et al. 2016)).

The second type of reaction is based on the oxidation of molybdate ions previously cast on the working electrode (screen-printed electrode) While the determination of the phosphmolybdate complex formed was performed by cyclic voltammetry (Cinti et al. 2016).

There are several reports in the literature on electroanalytical methods and promising prototypes for phosphate determination in seawater or freshwater. However, there are no reports of on-line deployment of these systems.

Previously, we reported the determination of orthophosphate in seawater by square wave voltammetry on carbon paste modified with ammonium molybdate and pretreated by cyclic voltammetry in sodium hydroxide (Altahan et al. 2021).

Here, we describe for the first time the application of a bi-potentiostat (i.e. double electrochemical cell) with two working electrodes based on carbon paste technology. The first working electrode contains the chemical reagent (molybdate reagent) in a carbon paste and the second working electrode, has no additive in the carbon paste base, and serves as a reference channel for matrix interference correction. The signal of the second working electrode is subtracted from that of the first working electrode. The bi-potentiostat approach was applied in a home-built analyser, for on-line determination of phosphate in seawater on a research vessel in the North Sea, using a Python script for automated data processing.

4.2 Materials and Methods

4.2.1 Chemicals

All reagents and calibration solutions used in this study were prepared with deionised water (resistivity 18.2 MΩ-cm, MilliQ, Millipore Water System) and reagent grade analytical salts. All glass and plastic wares were thoroughly cleaned before use. They were rinsed with deionised water and then immersed in an acid bath containing 10 % (v/v) concentrated HCl (37 %, reagent grade, Carl Roth, Germany) for > 24 hours and then rinsed again with deionised water.

All calibration solutions and standards for PO_4^{3-} and H_4SiO_4 were prepared in artificial seawater. Artificial seawater with a salinity of 30, was prepared from sodium chloride (Sigma Aldrich, Burlington, Massachusetts, USA) at 30 g/L. For on-line seawater samples acidification, 500 ml heat-resistant borosilicate glass laboratory bottles were filled with 50 % H_2SO_4 (98%, Carl Roth, Germany).

The stock solution of PO_4^{3-} (1 mM) was prepared by dissolving 0.136 g of potassium dihydrogensulphate (KH_2PO_4, Merck, Kenilworth, New Jersey, USA) in 1000 ml of deionised water. The stock solution of H_4SiO_4 (1 mM) was prepared from sodium metasilicate pentahydrate ($NaSiO_3.5H_2O$, Sigma Aldrich, USA) by dissolving 0.0212 g in 1000 ml of deionised water.

A stock solution of Triton x-100 was prepared at 50 % (v/v) (50 ml of Triton x -100 (Sigma Aldrich, USA) and 50 ml of isopropanol alcohol (C_3H_8OH, Fischer Scientific, USA). A stock solution for humic acid was prepared by dissolving 0.1 g of solid humic acid (Sigma Aldrich, USA) into 100 ml of a solution of 0.1 M NaOH and neutralized by 37 % HCl to pH ~ 7.5.

4.2.2 Description of Apparatus

The schematic diagram of the flow injection analyser- dual electrochemical cell detector (FIA-DECD), used for PO_4^{3-}, is described in **Figure 4.1**. The main hardware consists of two modules. The fluid transfer module consisted of a peristaltic pump (DYNAMAX RP -1, Rainin Instrument Co., US) that delivers the liquid to the electrochemical cell and is connected to a 10-way switching valve (Cheminert C25Z series, VICI, Texas, USA). Various samples and reagents are delivered to or withdrawn from the electrochemical cell by adjusting the pump direction (clockwise (CW) or counterclockwise (CC)) and switching the valve position. Both the peristaltic pump and the switching valve are controlled by software programmed in Python. The rotary fittings of the switching valve were equipped with finger-tight polyetheretherketone (PEEK) connectors to connect polytetrafluoroethylene (PTFE) tubing with an inner diameter of 0.8 mm for the transfer of standards and reagents. The same tubing and fittings were used for sample flow, connected to a Luer PEEK adapter (male-female) and a 0.45 μm syringe filter. For peristaltic pumping, pump tubing (Tygon LMT-55; green-green, inner diameter 1.85 mm) was used to deliver fluid to the electrochemical cell.

The measurement module consisted of the μStat 400 bi-potentiostat/galvanostat (Metrohm Dropsens, Spain) with 4 electrodes (2 working electrodes, reference electrode, counter electrode, and ground), cable connection with alligator clips with USB type-B connectors, and RS -232 cables. All electrochemical measurements were performed using Dropview software (Methrohm). The electrochemical cell consisted of four electrodes: 2 working electrode holders for carbon paste (BASi, US), a reference electrode of silver and silver chloride (Ag/AgCl) fed with saturated potassium chloride (3 M KCl), and a counter electrode of glassy carbon (BASi, US). A 50 ml glass beaker was used as electrochemical cell and covered with parafilm. The synchronisation between the measurement and fluid transfer modules was done through an I/O configuration (i.e., RS 232) with the bi-potentiostat and an Arduino board, which was preconfigured to control the states of the peristaltic pump and has the ability to exchange the digital signals with the bi-potentiostat. During the pumping step, the Arduino board was able to continuously send digital signals to the

bi-potentiostat and during the measurement step the bi-potentiostat was able to send signals to the Arduino board to stop pumping.

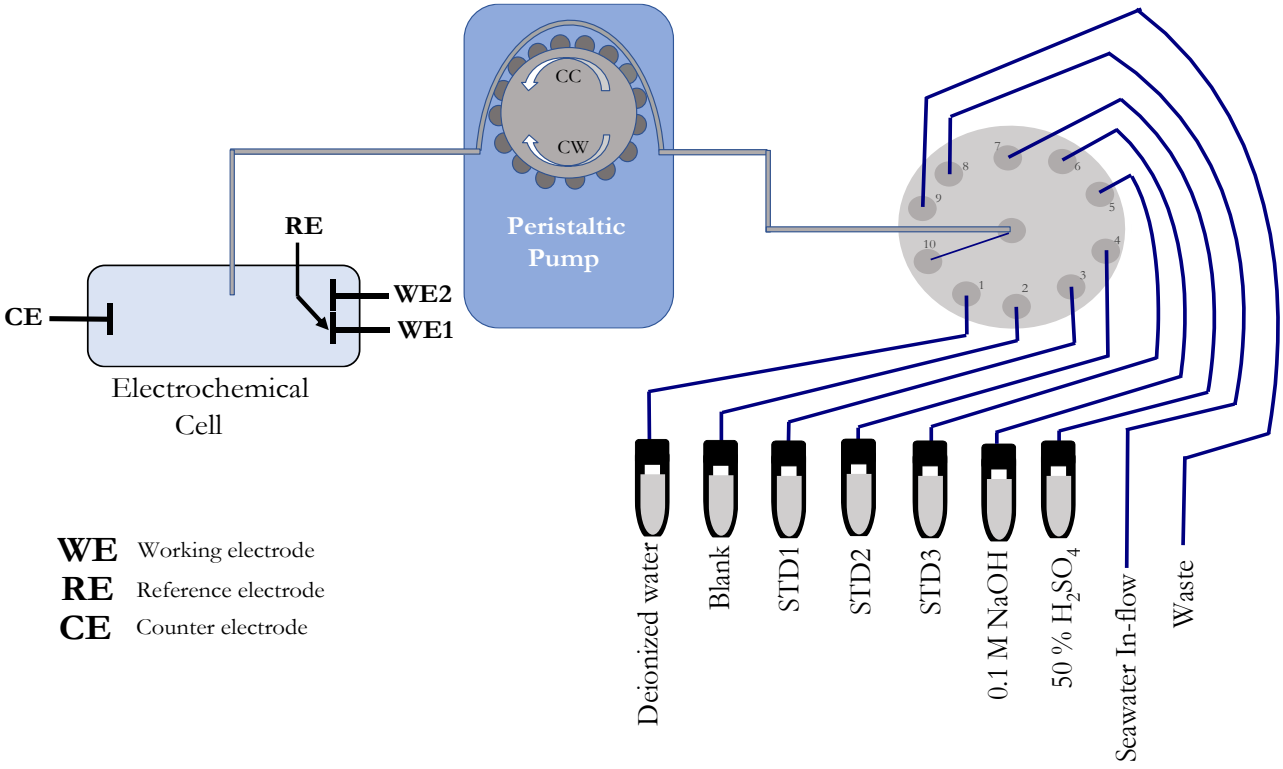

Figure 4.1 The schematic diagram for the FIA-DECD showing the peristaltic pump, electrochemical dual-channel cell and switching valve with the connections for all reagents, standard solutions and inflow of seawater

4.2.3 Preparations of modified electrodes

The preparation of molybdate/carbon paste electrode (CPE) and CPE was carried out in several steps. First, the carbon paste electrode holders were cleaned by placing them in plastic tubes filled with ethanol (CH_3OH ≥ 99.8%, ROTH, Germany) and sonicated at 30°C for 90 min in an ultrasonic bath. Then, the carbon paste mixtures were prepared as follows for molybdate/CPE; 0.6 g graphite powder (particle size < 20, Sigma Aldrich, USA) and 0.1 g ammonium molybdate tetrahydrate [$(NH_4)_6Mo_7O_{24}.4H_2O$] (≥ 99%, Sigma Aldrich, USA) were mixed in a mortar with 0.3 g paraffin oil (Sigma Aldrich, USA) for 10 minutes using a pestle to form a uniform carbon paste. The paste was stored into a 5 ml tube (Eppendorf) until use. A small amount of paste was pressed

into the cavity at the end of the electrode holder to produce the modified electrode. Later, an excess of the electrode material was removed by polishing using a piece of filter paper. Then, the modified electrode was rinsed with deionized water and inserted into the electrochemical cell. The carbon paste mixture for the CPE electrode was prepared by mixing 0.7 g graphite and 0.3 g paraffin oil, and the same procedure as outlined above was used. The CPE electrode was inserted into the electrochemical cell. Two electrochemical circuits were set up, where the two working electrodes, molybdate/CPE and CPE, shared the same auxiliary electrode and reference electrode and were immersed in a 50 ml glass vessel, which was then filled with a solution of 0.1 M NaOH; cyclic voltammetry was performed with a potential scan from – 0.5 to 0.5 V at a scan rate of 0.1 Vs^{-1} for 10 scan cycles. Deionized water was then introduced into the electrochemical cell for purification, followed by injection of a blank solution of artificial seawater.

4.2.4 Data Processing

Python software was used to process the raw data obtained from the Dropview software. **Figure 4.2** shows the flowchart for the steps of the protocol. The method is based on reading the raw data obtained via the Dropview script and producing the voltammograms of the two channels as an x, y Excel spreadsheet, where x is the current (μA) and y is the potential (V). The code is based on reading the files as column separated values (csv) (**step 1**) and dividing them into individual columns. The columns (Potential (V), Current (μA)) are divided into two parts; the first part is for molybdate/CPE (working electrode 1) and the second part is for CPE (working electrode 2) (**step 2**). Then, the two parts were merged into one csv spreadsheet. Smoothing of the resulting peak was performed by nonparametric regression, locally weighted scatterplot smoothing (LOWESS) with a frac value of 0.04 (**step 3**), which controls how narrow the window is for the local data; the 0.04 value makes the model more sensitive to the local data. Baseline correction was performed for background current subtraction using the PeakUtils Python package (Thompson 2018) (**step 4**), this package was used for peak quantification for each set of data with the indexes functions. Subtraction of the CPE current from the molybdate/CPE current was done (**step 5**) with subsequent determination of the peak height in μA using the Spciy Python module (Virtanen et al. 2020; Virtanen et al. 2018) which can detect peaks in the voltammogram (**step 6**). The obtained results were converted to the concentration in μM by constructing a calibration plot with the current in μA (y-axis) and concentration of PO_4^{3-} in μM (x-axis) using the linear regression model via the Python Statsmodels library (Seabold and Perktold 2010) .Calculating the concentration of the unknown sample in μM was done using the following equation.

$$\textbf{Concentration}\ (\mu\mathbf{M}) = (\boldsymbol{I} - \boldsymbol{B})/\boldsymbol{S} \qquad \textbf{Equation 4.1}$$

Where I is the peak current in μA of the sample, B is the intercept coefficient of the linear fit in μA and S is the slope coefficient of the linear fit in $\mu A.\mu M^{-1}$.

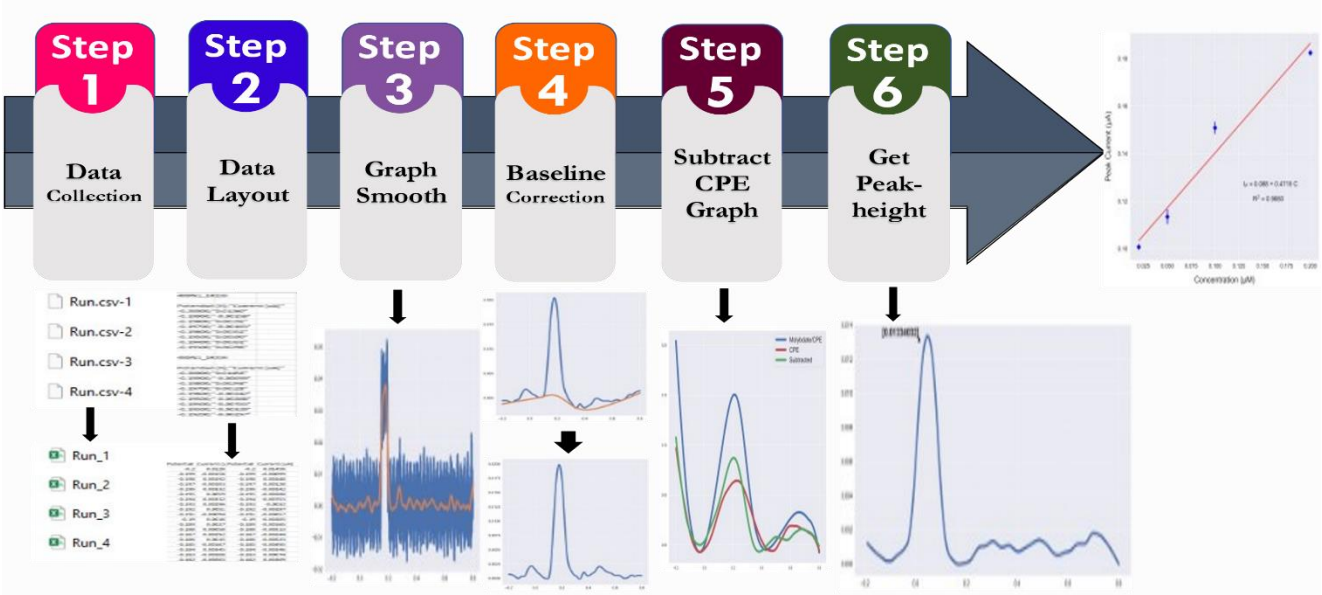

Figure 4.2 The description of the flow chart for the data processing in machine learning of the raw data obtained from Metrohm Dropview software.

4.2.5 Analytical procedure

The measurement cycle for PO_4^{3-} begins with a calibration consisting of a blank solution and three standard solutions with known PO_4^{3-} concentrations pre-acidified to pH 0.8 with 50 % sulfuric acid (H_2SO_4 98%, Carl Roth, Germany), followed by analysis of seawater samples also acidified online with 50% H_2SO_4. For the blank, standards, and seawater samples, PO_4^{3-} measurements were conducted by square wave voltammetry with a frequency of 10 Hz, a step potential of 2 mV, and an amplitude of 100 mV. Between measurements, a wash procedure was performed with cyclic voltammetry in a solution of 0.1 M NaOH for 20 scan cycles at a scan rate of 50 mV/s at a potential range of – 0.2 to 0.8 V, followed by rinsing of the flow cell with deionized water and subsequent discharge to waste. Before and after the measurements, deionized water was passed through the electrochemical cell to rinse the electrodes and glass vessel, and then discharged to waste. After the blank, standard, and wash step measurements, the peristaltic pump flow direction was reversed and the solution was returned to the vessel. After the seawater measurement, the solution was transferred directly to the waste container. For the blank, standards, and wash step

measurements, the peristaltic pump was set to a flow rate of 60% of the maximum speed (i.e., 48 rpm) for 170 s in a clockwise direction, and the same step was repeated in a counter clockwise direction after the measurement. For seawater analysis, the pump was configured at 60% of maximum speed for 155 s, followed by the addition of 50% H_2SO_4 for 25 s. **Figure S2.1** shows the graphical user interface for the control of the peristaltic pump, switching valve, and synchronization with the bi-potentiostat with a description of the components.

4.2.6 Field testing

A field trial was conducted in May-June 2022 on a research vessel in the German Bight of the North Sea, covering the the outflow of the Elbe estuary and the region between Cuxhaven, Helgoland and Büsum . The expedition transect of RV Littorina is shown in **Figure 4.3, top left**. The phosphate analyser was set up in the laboratory (**Figure 4.3, top right**) and supplied with a continuous seawater flow. The water was obtained from a 200 L tank which was supplied by surface seawater at a flow rate of 600 liters per hour (**Figure 4.3, bottom right and left**), and also housed several submersible sensors to collect additional hydrographic data. An YSI EXO2 probe was used to monitor salinity, temperature, and dissolved oxygen (DO) at a frequency of 1 minute. Sunburst SAMI pH and Trios Opus were used to monitor pH and nitrate (NO_3^-) at 15-minute and 1-minute intervals, respectively. Raw pH and NO_3^- data were corrected for salinity, temperature, and pressure data obtained from the EXO probe. The sample inlet for the analyser was fitted with a 0.45 μm syringe filter to remove particles. The analyser was equipped with a blank solution and three standard solutions (0.2, 1, 2 μM PO_4^{3-}), all prepared in artificial seawater (27 g/L) (pH 0.8). Discrete samples for validation of the analyser performance, were taken from the sampling line outlet, filtered through a 0.45 μm syringe filter attached to a 60 ml acid-washed syringe, and filled into pre-cleaned 15 ml low-density propylene tubes, and frozen (-20 °C) until analysis with anair-segmented multi-macronutrient Analyser (QuAAtro, Seal Analytical Ltd.). GPS coordinates (longitudes and latitudes) were obtained from NEMA data from the GEOMAR Littorina vessel and converted to comma separated values (csv) files.

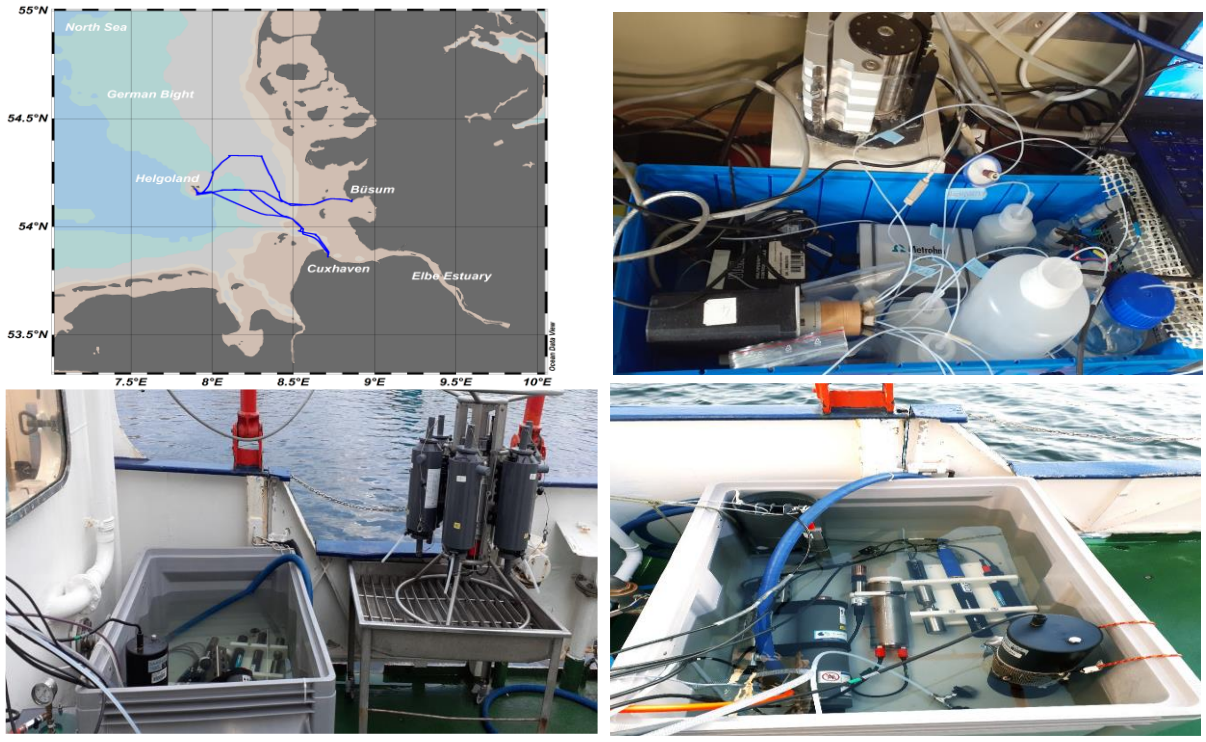

Figure 4.3 Map showing the track of RV Littorina in German Bight (southeastern North Sea) (top left), setup of the FIA-DECD during deployment on the research vessel (top right), 200-litre water tank with submerged sensors and which supplied the FIA-DECD analyser with surface seawater using a pump placed in the tank (bottom right and left).

4.3 Results and discussion

4.3.1 Dual-channels electrochemical PO_4^{3-} measurement

In this study we developed an improved electrochemical analyser for orthophosphate in marine water through the introduction of novel a dual electrochemical detector cell. The cell houses a first working electrode which contains the reagent molybdate in a CPE and acts as reagent channel, while the other working electrode only contains carbon paste and acts as a reference channel. The dual electrochemical cells detector uses a bi-potentiostat, where two working electrodes share the same reference and counter electrode. We applied the same potential range over both channels, with the two working electrodes exposed to the same conditions in the same aqueous medium. Previously, we tested the best conditions for the determination of orthophosphate in seawater(Altahan et al. 2021), which was previously acidified to 0.8 to ensure the exclusion of silicic acid, the main interference for orthophosphate analysis, as silicic acid has the ability to combines

with molybdate to form a silicomolybdate complex. The pH range of 0.4 – 0.9 was recommended to ensure a molybdate/proton ratio of 60 – 90, thus excluding the silicic acid interference (Directive 2000; Jońca, Comtat, and Garçon 2013a). The main principle of our method is based on the pretreatment of the molybdate-modified CPE with cyclic voltammetry in 0.1 M NaOH for 10 cycles to facilitate the formation of molybdate ions (MoO_4^{2-}), which are readily accessible to react with orthophosphate and form the phosphomolybdate complex, which is electrochemically detected with a characteristic peak at ~ 0.2 V. In the dual electrochemical detector mode, the second working electrode, which does not contain molybdate, is subjected to the same routine, and its voltammogram is subtracted from that of the reagent electrode (molybdate/CPE) to correct for the influence of the matrix interferences (**Figure 4.4**).

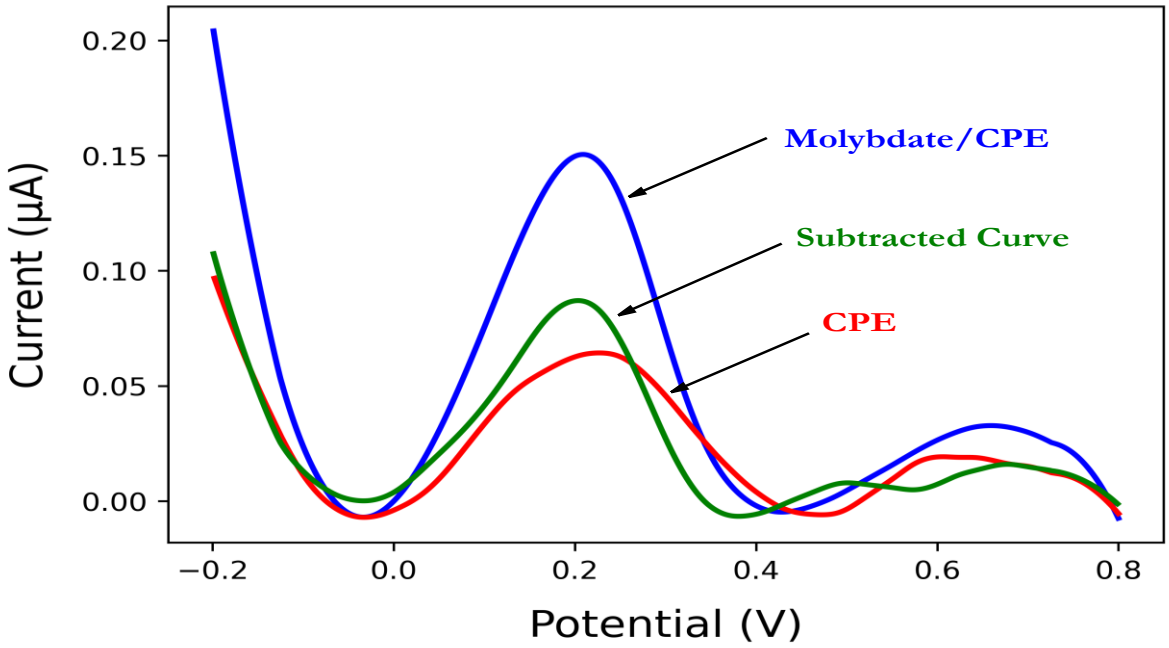

Figure 4.4 Square wave voltammograms of molybdate / CPE (blue line) and CPE (red line) in solution of 0.1 µM PO_4^{3-} in 35 g /L NaCl (pH 0.8)) obtained using step potential 2 mV, square amplitude 10 mV and square frequency 10 mV. The resulting voltammogram after subtraction of CPE signal from Molybdate/CPE signal is also shown(green line)

4.3.2 Influence of Square wave voltammetry parameters

The most effective way to increase the sensitivity of voltammetric measurements is to perform the analysis in such a way that the contribution of the charging current is reduced (Murray and Bard 1984; Mirceski, Komorsky-Lovric, and Lovric 2007). This is achieved by replacing cyclic

voltammetry (CV) techniques with a continuous potential ramp bysquare wave voltammetry (SWV) which employs a staircase potential time modulation with small potential pulses.

The reduction in charge current in SWV is achieved by measuring the current at the end of each potential step and these techniques are called current-sampled cyclic staircase voltammetry. The main tuning parameters of SWV are the sampling increment or step potential (ΔE) and the duration of the step potential ($\mathcal{T}$). For each potential step, two potential pulses are performed, where the duration of the potential pulses is equal and is denoted as $t_p = \mathcal{T}/2$, and the magnitude of each potential pulse is denoted as the square wave amplitude. The duration of the potential step $\mathcal{T}$ is expressed by the frequency in Hz (reciprocal of the second (s^{-1})) $f = \frac{1}{2t_p}$, and the sampling rate is expressed by the step potential and frequency as follows $v = f\Delta E$ (Mirceski et al. 2013; Mirceski and Gulaboski 2014). Previously, we investigated the effects of the three parameters (i.e., step potential, amplitude, and frequency) on the signal of a PO_4^{3-} measurement on molybdate/CPE applying a single electrochemical cell potentiostat. As we work in a dual electrochemical cells detector coupled with a flow injection analysis mode, which is different to the manual batch mode. In flow injection analysis, measurements are performed under hydrodynamic conditions, which differ from the manual batch mode where measurements were performed in a stationary sample solution. We now conducted the tests on the effect of these parameters on the slope with the bi-potentiostat, which can be referred to as the sensitivity of a calibration curve of 0, 0.5, and 1 µM PO_4^{3-} in 30 g/L NaCl (pH 0.8). **Figure 4.5, A** shows the effect of varying the frequency from 1 Hz to 20 Hz. The sensitivity increased from 1 Hz with a mean value of 0.0027 $\mu A.\mu M^{-1}$ to 10 Hz with a mean value of 0.0069 $\mu A.\mu M^{-1}$ ($\pm$ 0.0007), which further increased to a mean value of 0.0084 $\mu A.\mu M^{-1}$ with a standard deviation of 0.003 $\mu A.\mu M^{-1}$ at 20 Hz. The high standard deviation at 20 Hz could be due to noise which increases when the frequency increases above 10 Hz, as shown in **Figure S2.2**, where the voltammograms of 1 µM PO_4^{3-} at frequencies from 1 Hz to 20 Hz are shown. The step potential mainly controls how many points are sampled over the assigned potential range, and the number of points sampled decreased as the step potential is increased from 1 to 20 mV (**Figure S2.3**). **Figure 4.5, B** shows the effect of varying the step potential from 1 to 20 mV on the slope of the calibration. The slope increased from 0.0209 $\mu A.\mu M^{-1}$ at 1 mV to 0.0235 $\mu A.\mu M^{-1}$ at 2 mV and decreased to 0.01945 $\mu A.\mu M^{-1}$ at 5 mV. The amplitude of the square wave controls the width of the curve obtained. **Figure S2.4** shows the voltammograms of 1 µM PO_4^{3-} at different amplitudes of the square wave from 1 to 200 mV. **Figure 4.5, C** shows the effect of varying the square wave amplitude from 1 to 200 mV on the slope of the calibration curve, which increases 100-fold from 0.00103 $\mu A.\mu M^{-1}$ at 1 mV to 0.106 $\mu A.\mu M^{-1}$ at 50 mV, halving to

0.155 µA.µM^{-1} at 100 mV, and dropping to 0.12 µA.µM^{-1} at 200 mV, which can be attributed to the increasing peak width and opening over the potential range from - 0.2 to 0.8 V (**Figure 4.13**). Overall, optimal conditions were chosen for the square wave parameters: 10 Hz frequency, 2 mV step potential, and 100 mV amplitude.

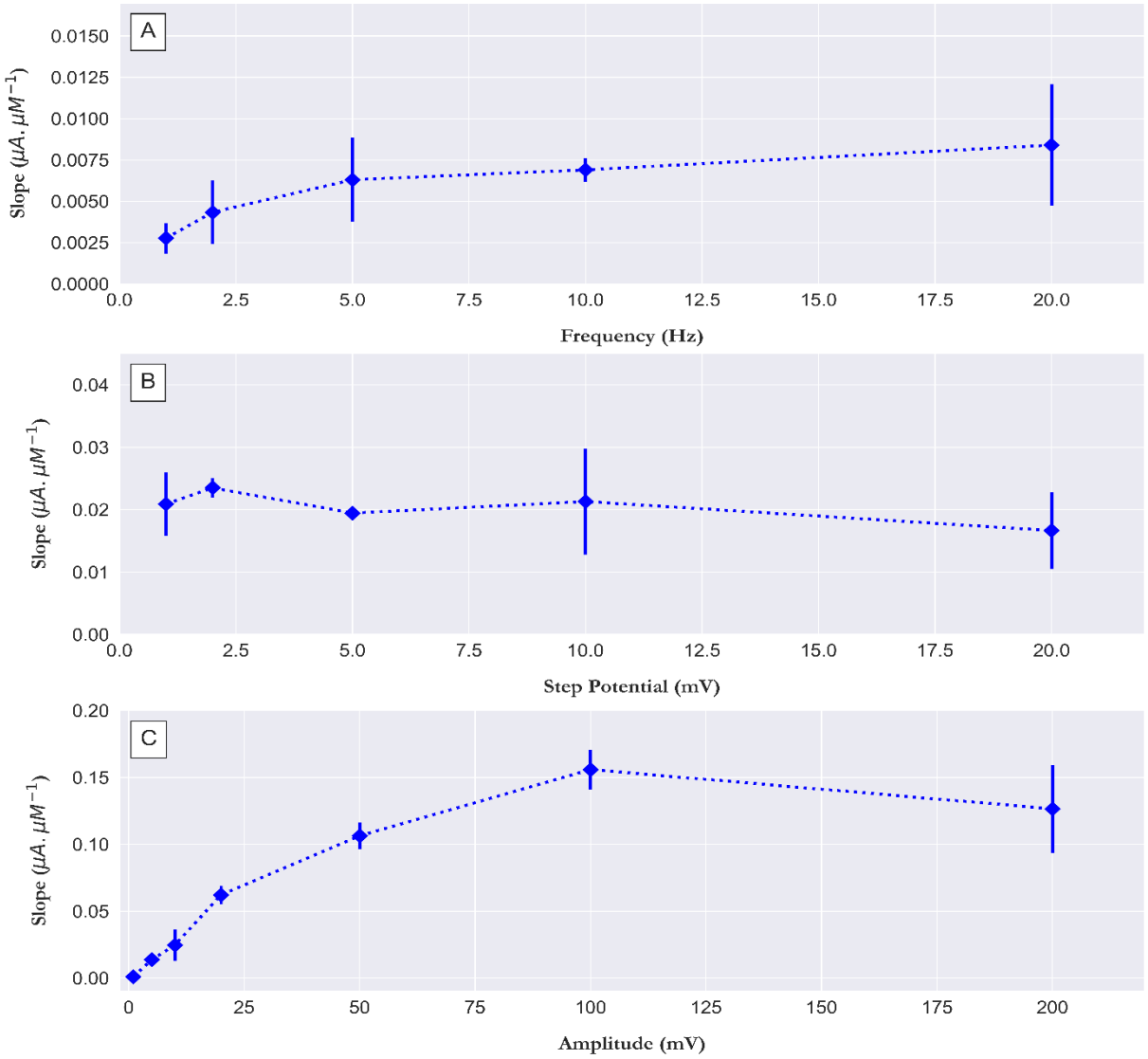

Figure 4.5 (A) effect of varying square wave frequency from 1 to 20 Hz, (B) effect of varying step potential from 1 to 20 mV and (C) effect of square wave amplitude from 1 to 200 mV on the slope of a calibration plot constructed from the corrected SWVs peak current of 0, 0.5 and 1 µM PO_4^{3-} in 30 g/L NaCl (pH 0.8). Error bar (n = 5).

4.3.3 Influence of Salinity variation

The effect of salinity on the peak signal was studied in detail, since salinity can vary strongly in estuaries and coastal waters, which is not the case in fresh waters and open ocean waters. The effect of salinity on electrochemical processes can be explained by the fact that the dominant salt sodium chloride is a strong supporting electrolyte. The effect of salinity was studied by measuring the peak current of a solution of 1 µM PO_4^{3-} (pH 0.8) at different salinities, for which different amounts of sodium chloride were dissolved in deionized water. The results were plotted against the peak signal of molybdate/CPE before and after applying the correction with CPE to investigate whether this correction has an effect on the correction of the influence of salinity variation. **Figure S2.5** shows the peak current of the square wave voltammogram for molybdate/CPE (uncorrected) in deionized water S = 0 (0.0012 µA), with the peak current increasing with increasing salinity S = 7 (0.09 µA). A slight increase in peak current with increasing salinity to S = 14 (0.113 µA), reaching a steady state with increasing salinity to S = 21 (0.116 µA). A high rise was obtained with increasing salinity to S = 28 (0.149 µA). In the corrected voltammogram after subtracting the CPE signal from the molybdate/CPE signal, the peak current in deionized water was S = 0 (0.00016 µA), which increased with increasing salinity S = 7 (0.038 µA). An increase in peak current was obtained with increasing salinity up to S = 14 (0.102 µA), and a steady state obtained at S = 21 (0.108 µA). A sharp increase in peak current was obtained by increasing the salinity to S = 28 (0.136 µA). The comparison between the two values showed that the values obtained from the corrected voltammogram were underestimated by 150% (S = 7) compared to the uncorrected voltammogram. The underestimation decreased with increasing salinity to S = 14 (10.9%), S = 21 (7.6%), and S = 28 (9.4%). Overall, the corrected voltammogram was not adequate to compensate for the variation in salinity. This is could be because with increasing sodium chloride concentration, high concentration of phosphomolybdate complexes can form at the molybdate/CPE. This is related to the fact that most of oxidation which refer here to the coupling between PO_4^{3-} and molybdate is mediated by the electrogenerated chloro-species (Saxena and Ruparelia 2019). This could not be happened at CPE which does not contain molybdate. This makes the correction (i.e., subtracting of CPE signal from molybdate/CPE signal) useless to correct for salinity variation. This leads to the recommendation to prepare calibration standards before field deployment with aa salinity close to that of the waters under investigation.

4.3.4 Interferences from Surfactant and Humic Acid

A surfactant is a substance with hydrophilic moieties as its head and hydrophobic moieties as its tail. A surfactant can alter the properties of the interface between the electrode and sample solution, affecting electrochemical processes and thus the peak signal. One of the non-ionic surfactants is Triton x-100, which is classified as a strongly hydrophobic surfactant with about 95 ethoxy groups (Shankar, Swamy, and Chandrashekar 2012). The influence of Triton x-100 on our peak currents was tested by a series of concentrations of Triton x-100 in a solution of 1 μM PO_4^{3-} (pH 0.8), and the peak current of molybdate/CPE and the corrected voltammogram were measured and compared to determine the improvement obtained by the application of our bi-potentiostat method. **Figure 4.6, A** shows the peak current of the voltammogram for molybdate/CPE (uncorrected). The results show that the addition of 2 mg/L Triton x-100 resulted in a 27% increase in peak current compared to a free surfactant standard solution of 1 μM PO_4^{3-} with a relative standard deviation (RSD) of 41%. For a solution of 10 mg/L Triton x-100, the increased peak current resulted in an overestimation of PO_4^{3-} by ~65% with an RSD of 14%. For 20 mg/L Triton x-100, an increase in peak current resulted in an overestimation of PO_4^{3-} of ~ 73% with an RSD of 28%. The peak current values obtained from the corrected voltammogram are shown in **Figure 4.6, B**. The peak current values showed a slight increase in peak current with the addition Triton x-100 compared to that of the free surfactant solution of 1 μM PO_4^{3-}. The increased peak current after the addition of Triton x-100 from 2 mg/L to 20 mg/L leads to a maximum overestimation of PO_4^{3-} of ~ 6 %, with RSD values in the range of 5 %.

The results show that our bi-potentiostat method is able to correct for interference caused by the surfactant (Triton x-100), which may be present in surface seawaters in the range of 0.1 to 2 ppm (Cosović and Vojvodić 1982).

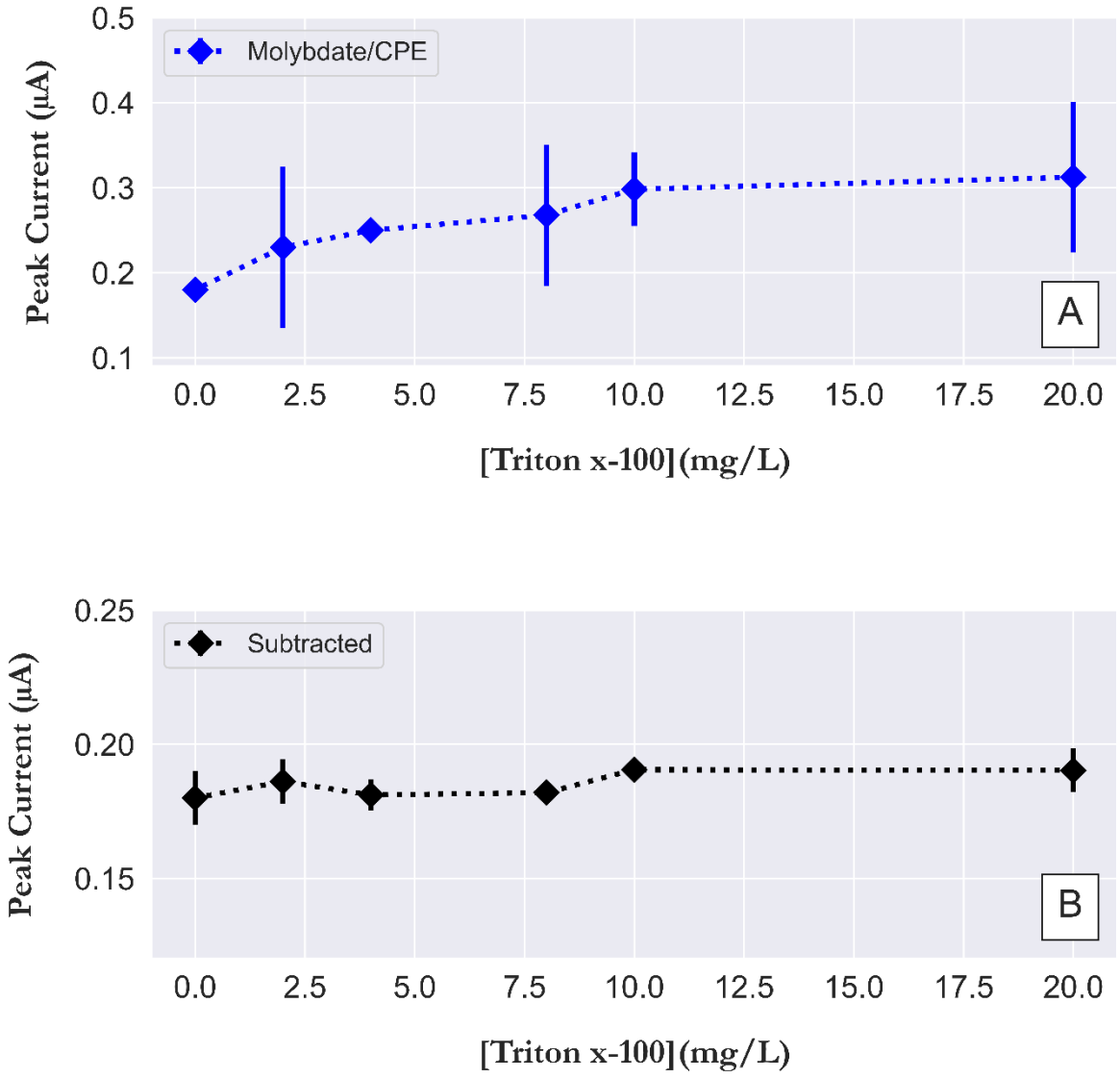

Figure 4.6 Interference effect from non-ionic surfactant (Triton x-100) on the square wave voltammograms peak current (µA) at (A) molybdate/CPE and (B) the resulting voltammogram obtained after subtraction of CPE signal from molybdate/CPE of 1 µM PO_4^{3-} in 30 g/L NaCl, pH 0.8. The parameters for SWV were step potential 2 mV, amplitude 50 mV and frequency 10 Hz. Error bar (n = 5).

Humic acid (HA) is classified as a surface-active compound that alters the electrochemical process and thus the voltammetric signal because HA affects the interface of the electrode surface like a surfactant (Piech, Baś, and Kubiak 2008). **Figure S2.6** indicates that at 1 mg/L HA suppresses the voltammetric signal of 1µM PO_4^{3-}, and the signal was tested in solution with concentration up to 20 mg/L.

The results showed the high effect of HA on the signal, this could be because of decreasing the functional activity of the carbon paste surface by adsorption of HA. This is because the high adsorption capacity of HA on carbon based electrode (Zghal et al. 2020).

4.3.5 Analytical performance

To investigate the analytical performance of the bi-potentiostat method, a series of standard solutions were measured. A series of standard solutions of 0.02, 0.05, 0.1, 0.2, 0.5, 1, 2, and 3 μM PO_4^{3-} was prepared in artificial seawater (30 g/L NaCl) (pH 0.8). Measurements were performed at a time interval of 30-minutes with a wash step between measurements (cyclic voltammetry in 0.1 M NaOH, scan rate 0.1 Vs^{-1} for 20 scan cycles). The SWV of the molybdate/CPE was corrected by the SWV of the CPE. As shown in **Figure 4.7**, two ranges of linear calibration plots were obtained, with a first linear range for concentrations of 0.02, 0.05, 0.1, 0.2 μM PO_4^{3-} and an analytical sensitivity of 0.4715 $\mu A.\mu M^{-1}$ and a detection correlation (R^2) of 0.968. The second linear range was for concentrations of 0.5, 1, 2 and 3 μM PO_4^{3-} with an analytical sensitivity of 0.0116 $\mu A.\mu M^{-1}$ and a detection correlation (R^2) of 0.989. The division of the two discrete linear regions was also observed in our previous work (Altahan et al. 2021), and due to adsorption of phosphomolybdate complex layers on the working electrode surface at high PO_4^{3-} concentrations. This could lead to the recommendation to prepare calibration standards with concentrations close to the concentration level of PO_4^{3-} in the water under study.

A similar behaviour was also noted in the colorimetric determination of PO_4^{3-} based on the molybdate blue method which suffers from the same limitations. This is illustrated by the fact that there is no report of a single instrument suitable for measuring PO_4^{3-} in a concentration range from nanomolar to micromolar levels (Ma et al. 2014; Deng et al. 2020).

The limit of detection (LOD) of our method was calculated as three times the standard deviation of the blank measurements (Long and Winefordner 1983; Belter, Sajnóg, and Barałkiewicz 2014), and was 0.014 μM PO_4^{3-}.

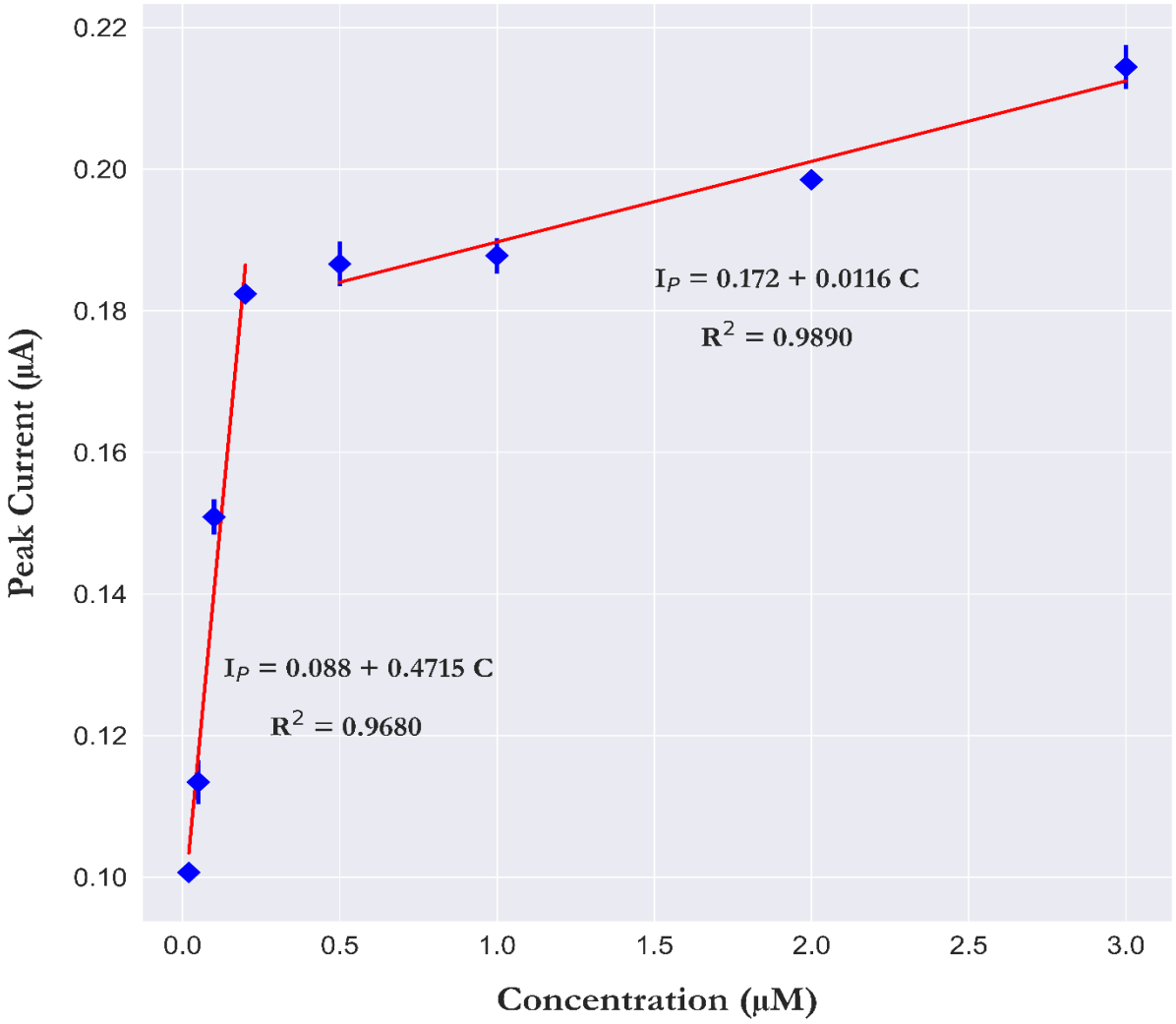

Figure 4.7 Calibration plots for two discrete ranges; low range (0.02, 0.05, 0.1 and 0.2 µM PO_4^{3-}) and high range (0.5, 1, 2 and 3 µM PO_4^{3-}) in 30 g/L NaCl (pH 0.8), step potential 2 mV, amplitude 50 mV and frequency 10 Hz. Error bar (± σ) (n = 5).

4.3.6 Field deployment

Validation of the new method took place during a research cruise with the vessel Littorina in the German Bight (southern North Sea). Field tests were conducted in the outflow plume of the Elbe estuary in the region of the North Sea between Helgoland (54.180327 N, 7.888944 E) and Cuxhaven (53.859336 N, 8.687906 E) and between Helgoland and Büsum (54.134622 N, 8.858591 E). The main source of nutrients to the shallow German Bight comes from the west, including the English Channel and via river discharge(e.g. Elbe, Rhine, Maas, Weser, Ems) (Los, Troost, and Van Beek 2014), but also from atmospheric deposition (Salomons et al. 2012). One of the main source of phosphate in North sea around Helogland is highly influenced by river discharge. This was clearly appeared with other previous studies in the same region where phosphate exhibit high

significant correlation with salinity (Raabe and Wiltshire 2009; Shchekinova et al. 2017). Typicaly, phosphate concentration is highly related to primary production and decomposition of organic matter. In north sea, phosphate exhibits a seasonal cycle, peaking in late summer and autum with an average concentration of 1 μM and bottoming out in April and May with an average concentration of 0.2 μM (Grunwald et al. 2010). In early summer through October/November, a gradual increase in phosphate concentration is observed. This is due to the fact that despite the uptake of phosphate by phytoplankton, the release of phosphate by the decomposition of organic matter exceeds the rate of consumption(van Beusekom, Loebl, and Martens 2009).

Figure 4.8,A shows the distribution of salinity obtained with the CTD EXO probe during the voyage of the Littorina, with a minimum and a maximum value of 15.5 at Cuxhaven and 30.26 at Helgoland, respectively. The data obtained show that salinity increased gradually as the vessel moved away from the coast of Cuxhaven, Büsum and the mouth of the Elbe River, and increases in the North Sea toward the island of Helgoland, where the maximum values are reached .. The distribution of dissolved oxygen (DO) (**Figure S2.8, A)**, indicates concentrations of 9.5 - 10 mg/L near Cuxhaven, and a decrease towards Helgoland (8.5 - 9 mg/L), including a clear minimum (< 8 - 7 mg/L). The pH values recorded by Sunburst SAMI sensor at a 15-minute time interval (see **Figure S2.8, B**) are consistent with the salinity data, with the lowest values (pH 8.106) measured near Cuxhaven, and an increase towards Helgoland (8.2 - 8.4). The distribution of nitrate (Trios OPUS sensor) mirrored salinity (**Figure 4.8, B)** with maximum values (>80 μM - 100 μM) near Cuxhaven and a decrease (< 20 μM - 5 μM) towards Helgoland. A similar patterns was obtained for $\Sigma(NO_3^- + NO_2^-)$ from the discretely collected samples that were analysed in the GEOMAR laboratory (**Figure S2.8, C**). A maximum concentration of 55.9 μM was reached near Cuxhaven, and levels gradually decreased and remained in the low range (< 10 μM - ~ 1 μM) towards Helgoland Island and also towards Büsum. A total of 36 measurements were conducted at sea for PO_4^{3-} with our analyser (FIA-DECD) at a time interval of 30 minutes. The distribution of PO_4^{3-} (**Figure 4.8, C)** where PO_4^{3-} shows a similar distribution as nitrate, with peak values near Cuxhaven (~ 1 μM), gradually decreasing towards Helgoland and slightly increasing towards Büsum. A similar distribution is seen for PO_4^{3-} from discretely collected samples with analysis by the standard spectrophotometric technique (34 discrete samples; **Figure 4.8, D**). . The distribution of H_4SiO_4 (see **Figure S2.8, D**) coincided with the PO_4^{3-} distribution, with maximum values (~ 15 μM) near Cuxhaven and a decreasing trend in an off shore direction with low concentrations (1 - 4 μM) near Helgoland and also near the coast towards Büsum.

To evaluate the suitability of the method for the determination of PO_4^{3-} in samples with high concentration of organic material. Since the voltammogram of the electrodes was greatly affected by the addition of humic acid, as previously described in subsection 4.3.4. Three on-site data points were taken in the Elbe Estuary and Kiel Canal watershed, as shown in **Figure S2.7**. The water in the channel is characterized by high turbidity, a high concentration of suspended solids, and an increasing concentration of organic matter (Schubert, Krebs, and Bergmann 2000). The voltammetric signal does not show any bias. However, the concentrations of PO_4^{3-} for the on-site data points were not reported because the concentration there (~ 2 µM) is higher than the maximal emium concentration in our calibration plot (1 µM).

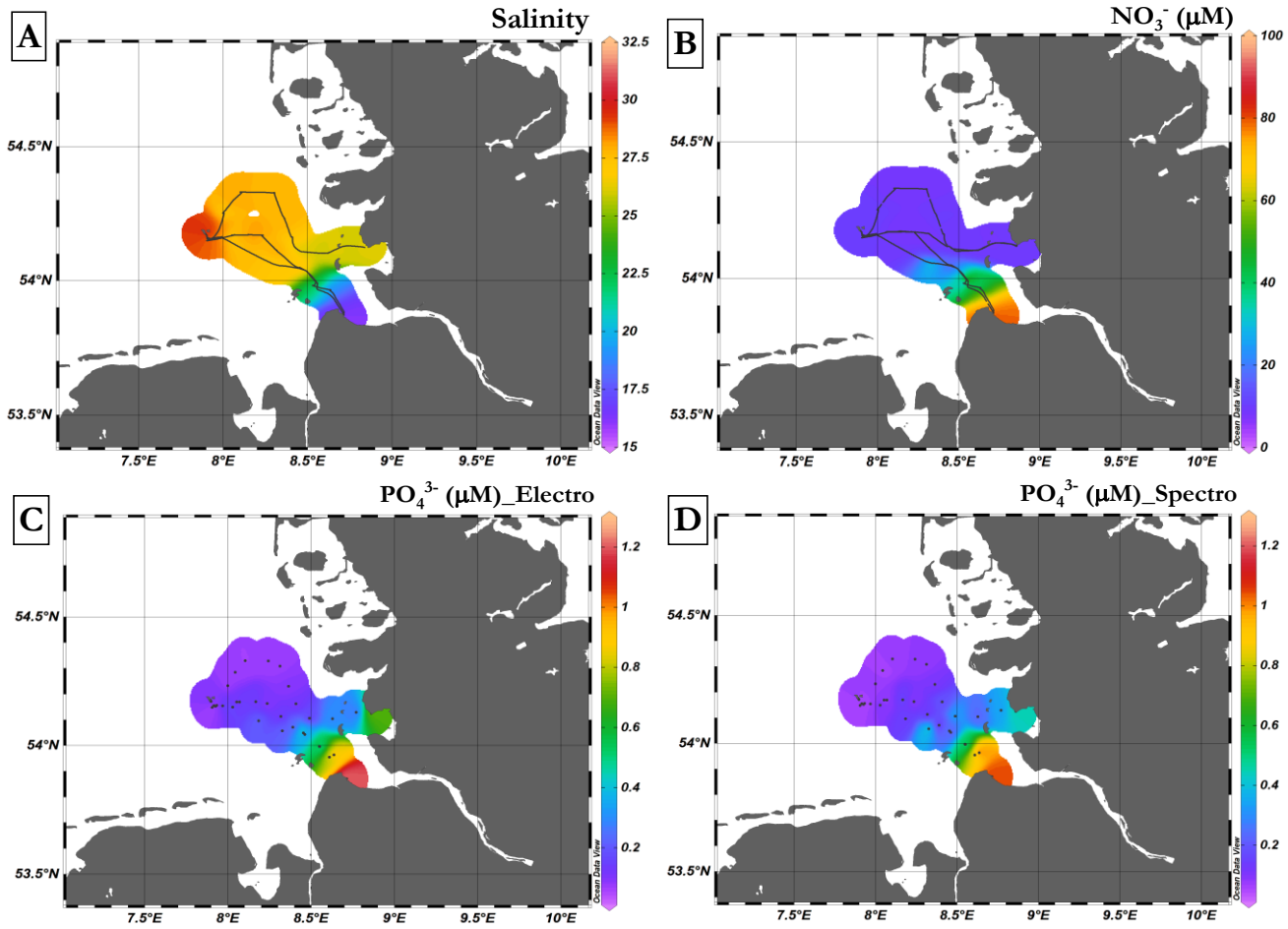

Figure 4.8 Contour plots of variables in study region (A) distribution of surface salinity, (B) distribution of NO_3^- concentration determined with the Trios sensor OPUS, (C) distribution of PO_4^{3-} concentration determined in discrete samples collected and analysed with electrochemical analyser (FIA-DECD) and (D)distribution of PO_4^{3-} concentration determined in discretely

collected samples and analysed at GEOMMAR using spectrophotometric analyser. Maps plotted via ODV 5.3.0 (Schlitzer 2020)

The electrochemical method was validated against the standard laboratory autoanalyzer technique The concentrations obtained by the new bi-potentiostat analyser averaged 0.26 µM, with minimum and maximum values of 0.018 µM and 1.2 µM, respectively. Concentrations obtained by the colorimetric analyser averaged 0.24 µM, with minimum and maximum values of 0.057 µM and 1.056 µM, respectively. Considering all data points, the mean accumulation level is 108% (evaluated as the average of the recovery values). The poor recoveries (~ 30 %) were obtained at values below 0.06 µM, which could be due to the deviation of the linearity of the calibration curve when measuring values in the nanomolar range (20 - 50 nM) and values in the micromolar range (0.2 - 3 µM), as shown in subsection 4.3.5.

The correlation plot between PO_4^{3-} concentrations obtained using the new analyser and standard laboratory technique **(Figure 4.9)** shows a good correlation coefficient (R^2) of 0.917 (n = 34), and also the paired t-test shows that there is no significant difference between the means at 1% level (p-value = 0,40597, *df* = 33) with the null hypothesis (mean (*on-site* data) = mean (discrete samples)) and the alternative hypothesis (mean (*on-site* data) - mean (discrete samples) < > 0).

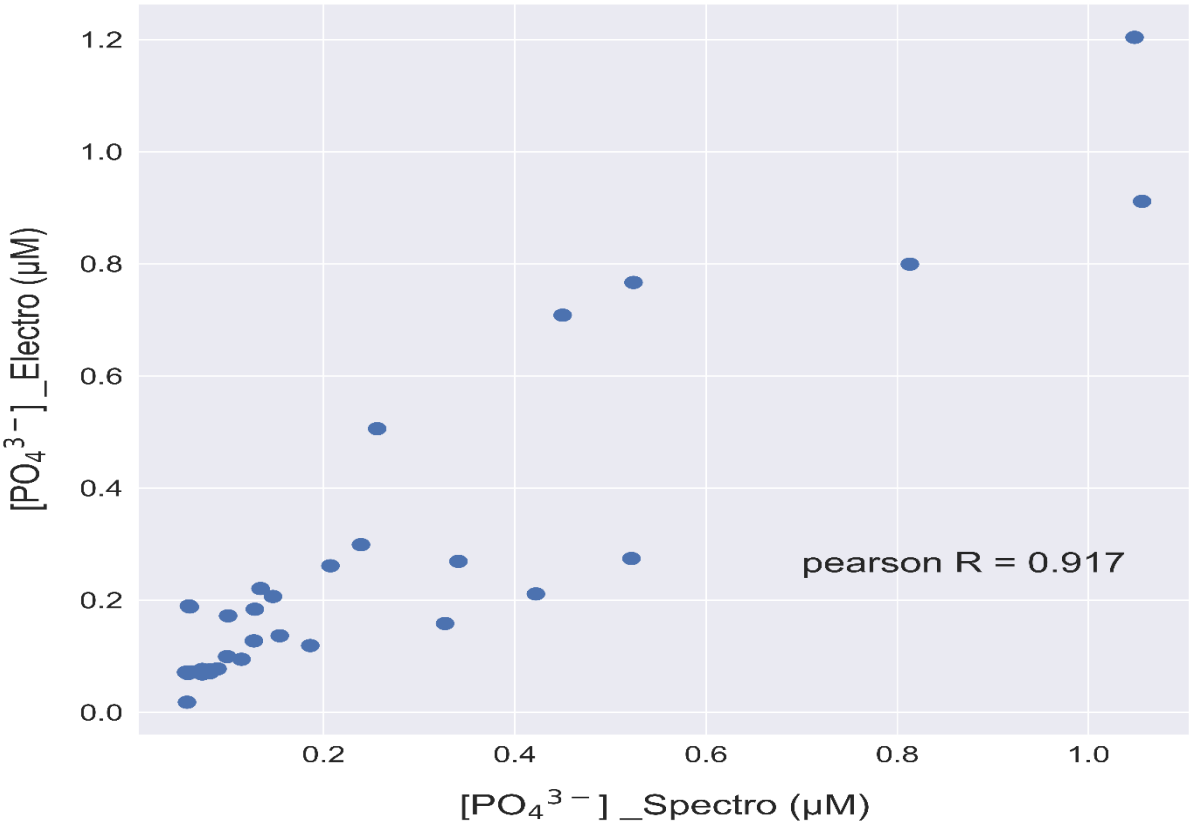

Figure 4.9 Property to property plot for *on-site* PO_4^{3-} concentrations (µM) measured electrochemically via FIA-DECD versus PO_4^{3-} concentrations (µM) measured in discrete samples collected and analysed via reference colorimetric laboratory-based analyser. Pearson' R = 0.917.

4.4 Conclusions and Suggestions for Future Work

Here we presented the application of a bi-potentiostat in an autonomous analyser for the electrochemical determination of PO_4^{3-}. The paper presented the application of our recently published method for *on-site* determination of PO_4^{3-} in seawater using molybdate/CPE after pretreatment with NaOH. Two working electrodes were used, molybdate/CPE and CPE, to correct matrix interference and increase the reliability of the method. The integration of the flow injection analyzer (peristaltic pump and switching valve) in conjunction with data processing using Python software allows full automation of the analyser. The method, with an analysis frequency of 30 minutes, exhibited a wide detection range of (0.2 - 3 µM) with a LOD of 0.14 µM. The method was validated for *on-site* determination of PO_4^{3-} at the coast and in open ocean seawater in North Sea on the track of RV Littorina with other sensors deployed beside our analyser. The analyser performed well compared to the laboratory colorimetric reference methods. Using the analyzer, the spatial distribution of PO_4^{3-} in the German Bight at the discharge plume of the Elbe estuary could be determined with patterns that correlate highly with other ancillary hydrographic data. To further improve the method, a commercial electrochemical flow cell with a low flow rate will be used to reduce reagent consumption and shorten measurement time. The use of a syringe pump instead of a peristatic pump, since the syringe pump is capable of delivering a small volume of solution (10 µL), will also help reduce reagents consumption.

Author Contributions: M.F.A.: conceptualization, investigation, methodology, visualization, writing—original draft. M.E.: software B.B.: software E.P.A.: funding acquisition, resources, supervision, writing—review and editing. All authors have read and agreed to the published version of the manuscript.

4.5 Supplementary information

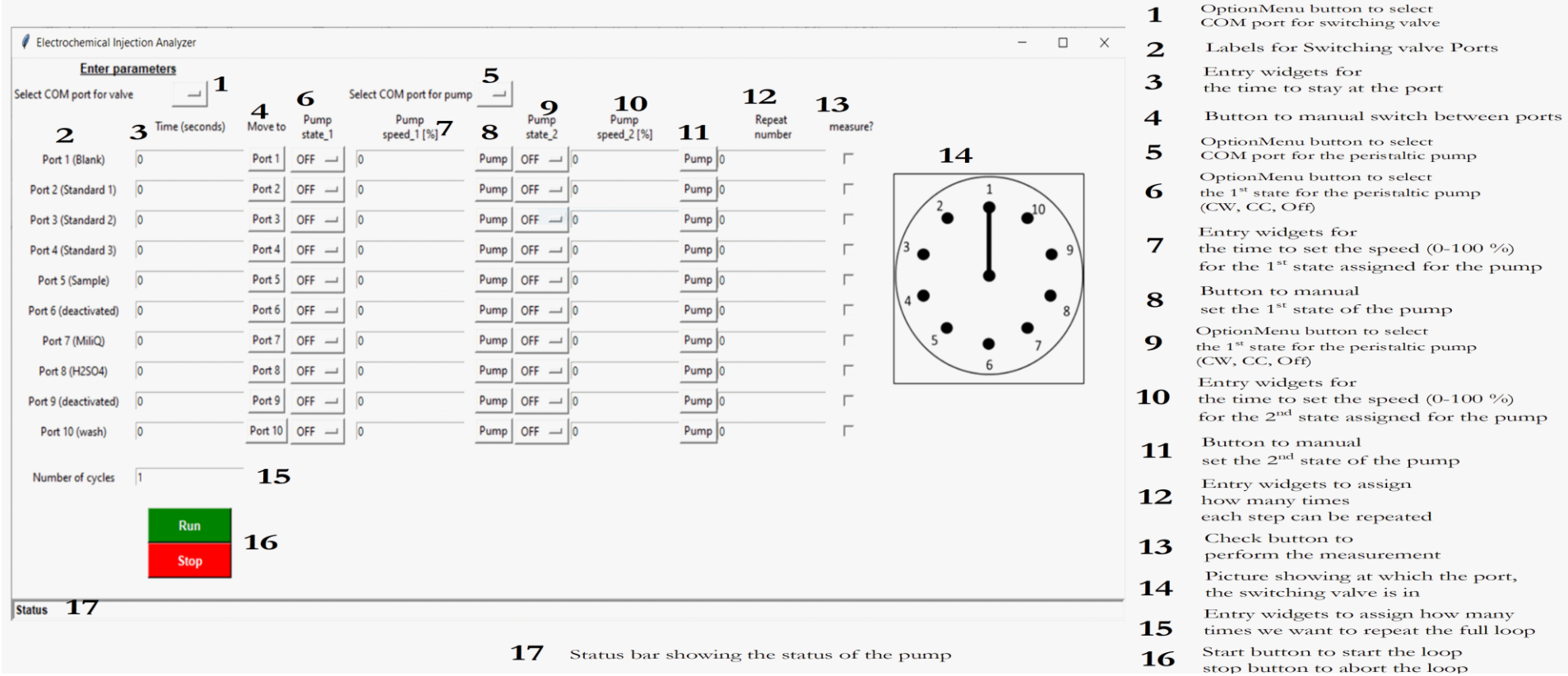

Figure S2.1 Detailed description of the Graphical User Interface (GUI) of the 'Electrochemical FIA.exe' to program the switching valve, the peristaltic pump and the synchronization with the Metrohm μStat 400 Bi-potentiostat.

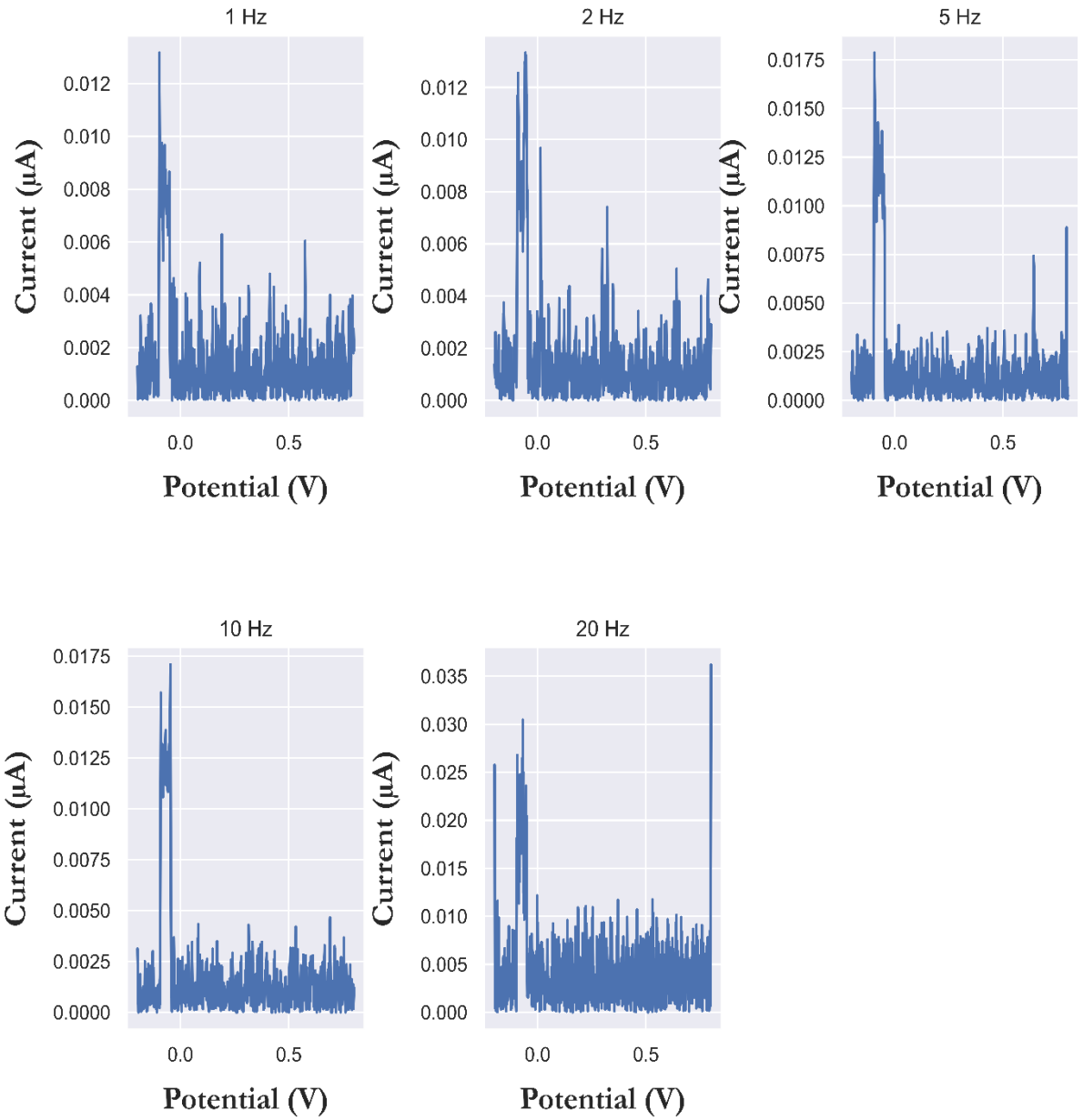

Figure S2.2 Square wave voltammograms of 0.5 µM PO_4^{3-} in 30 g/L NaCl (pH 0.8) (corrected voltammogram) at step potential of 1 mV, square wave amplitude 25 mV at frequencies 1 Hz, 2 Hz, 5 Hz, 10 Hz and 20 Hz.

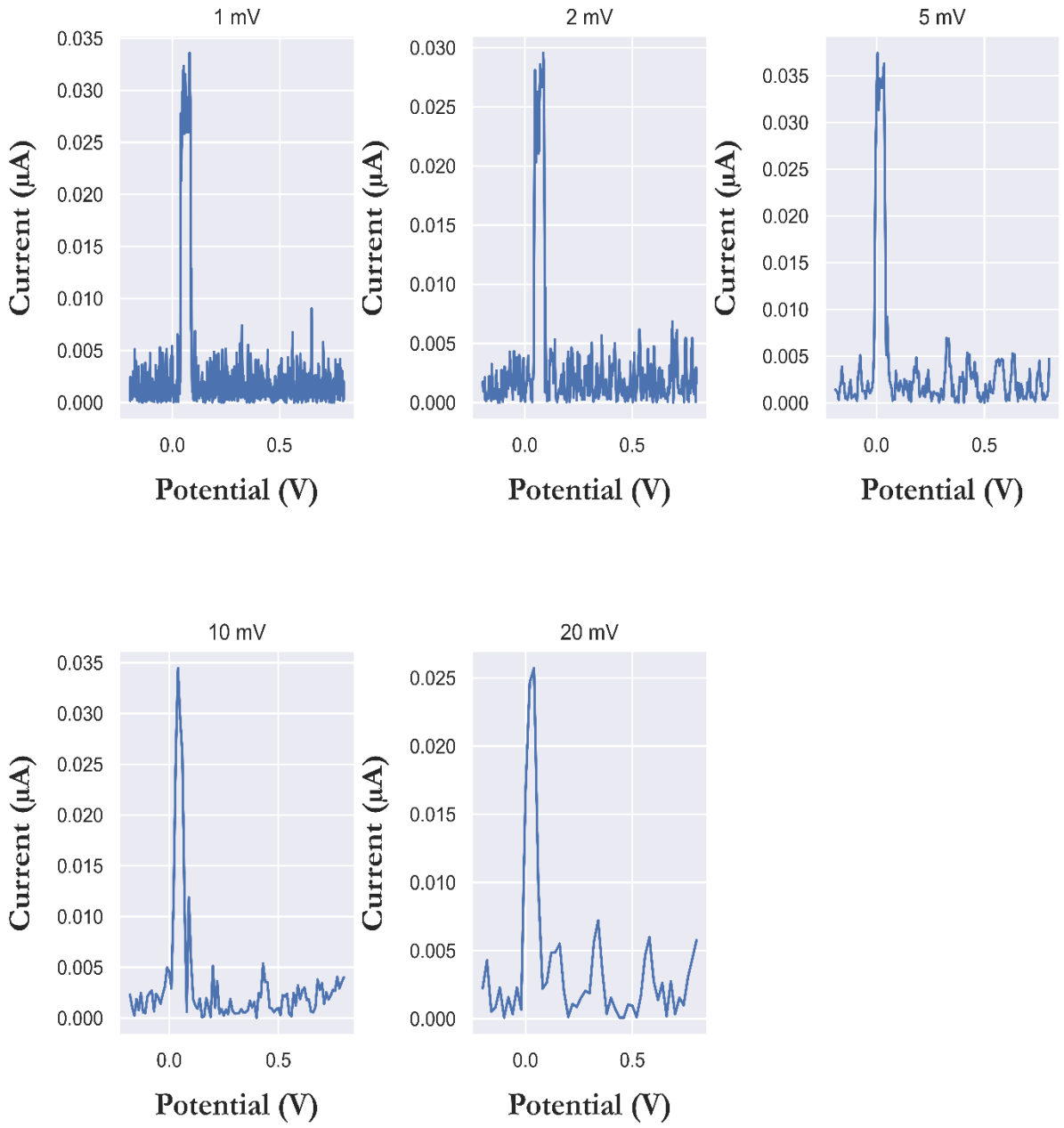

Figure S2.3 Square wave voltammograms of 0.5 µM PO_4^{3-} in 30 g/L NaCl (pH 0.8) (corrected voltammogram) at frequency of 10 Hz, amplitude 25 mV at step potential of 1 mV, 2 mV, 5 mV, 10 mV and 20 mV.

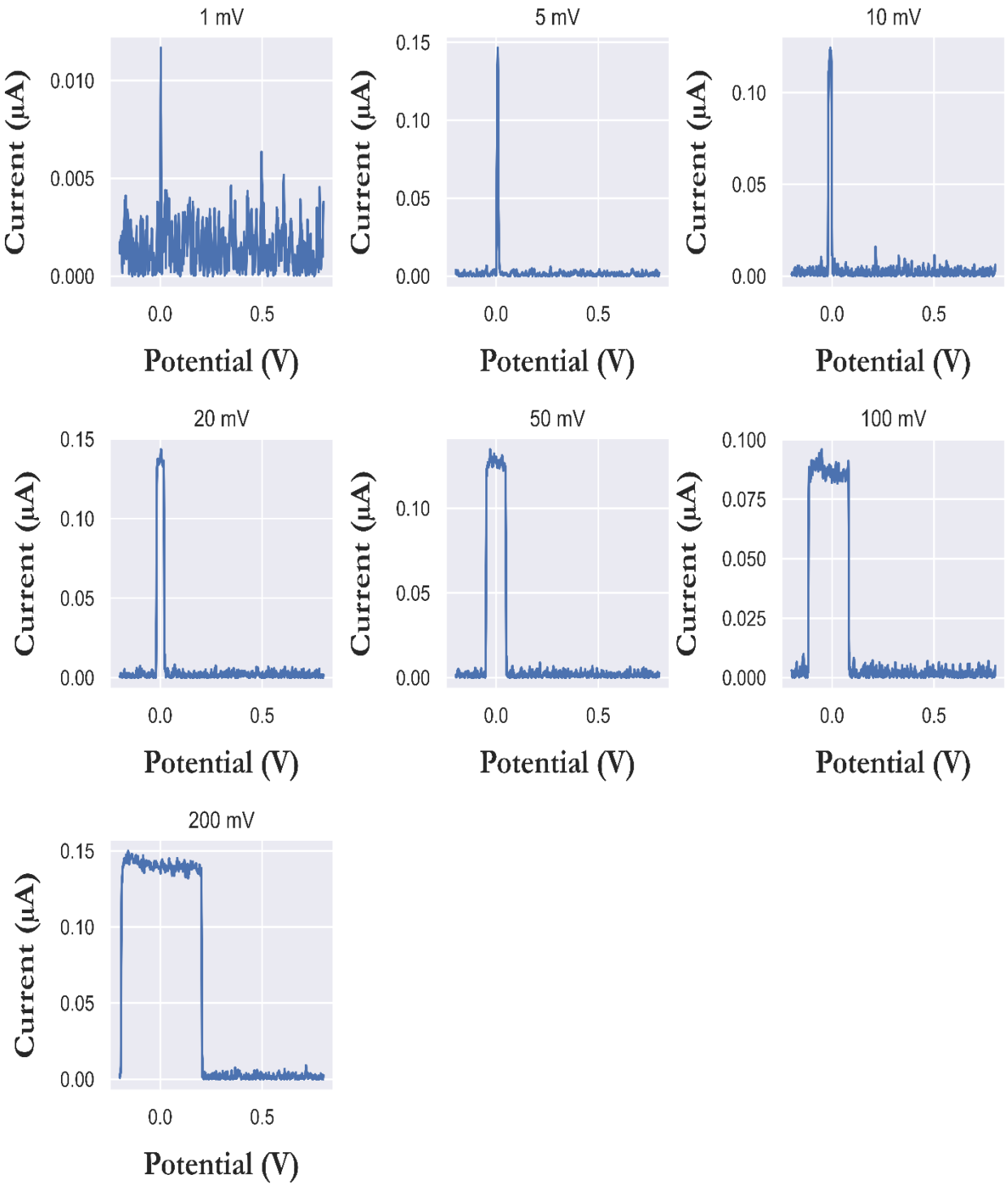

Figure S2.4 Square wave voltammograms of 0.5 µM PO_4^{3-} in 30 g/L NaCl (pH 0.8) (corrected voltammogram) at step potential of 1 mV and frequency of 10 Hz at square wave amplitudes of 1 mV, 5 mV, 10 mV, 20 mV, 50 mV, 100 mV and 200 mV.

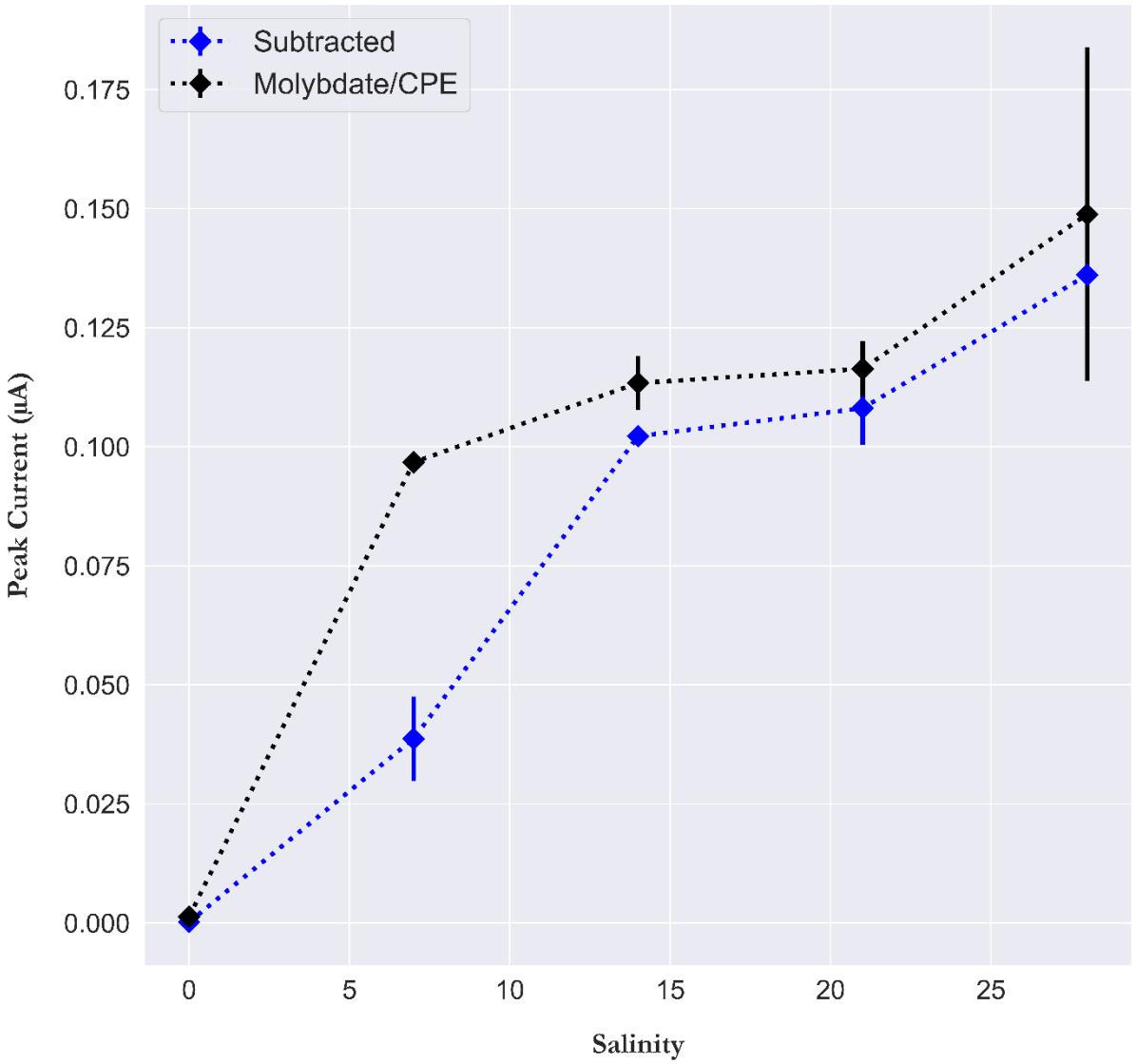

Figure S2.5 Effect of the variation of the salinity (0, 7, 14, 21 and 28) on the peak current of 1 µM PO_4^{3-} (pH 0.8) where the peak current of molybdate/CPE is shown as black circles and the peak current of corrected voltammogram is shown as blue circles. Error bar (n = 5).

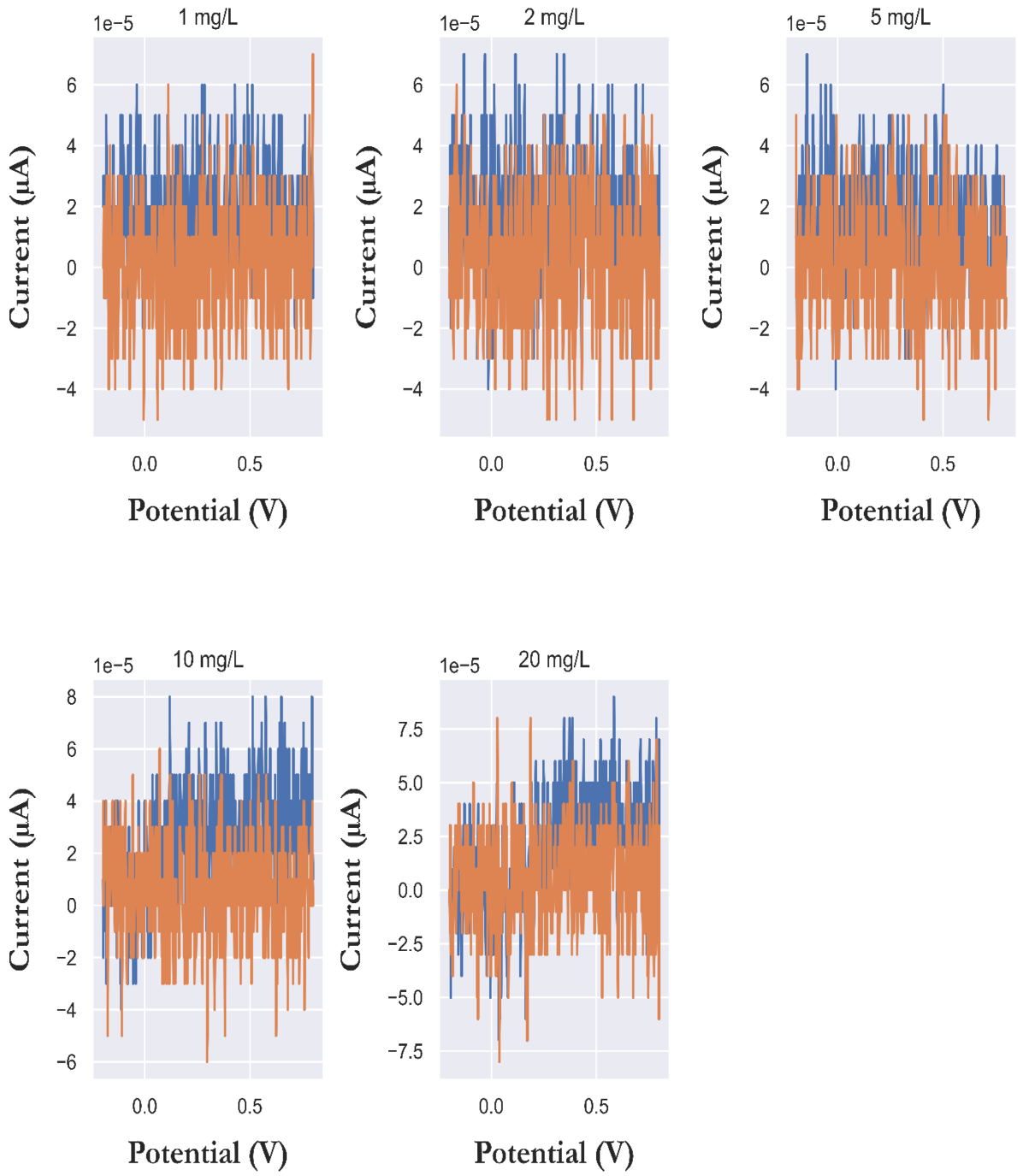

Figure S2.6 Square wave voltammograms of 1 µM PO_4^{3-} (30 g/L NaCl) pH 0.8 on molybdate/CPE (blue line) and CPE (orange line) in the presence of 1, 2, 5, 10, and 20 mg/L HA. Step potential 2 mV, frequency 10 Hz and amplitude of square wave 100 mV.

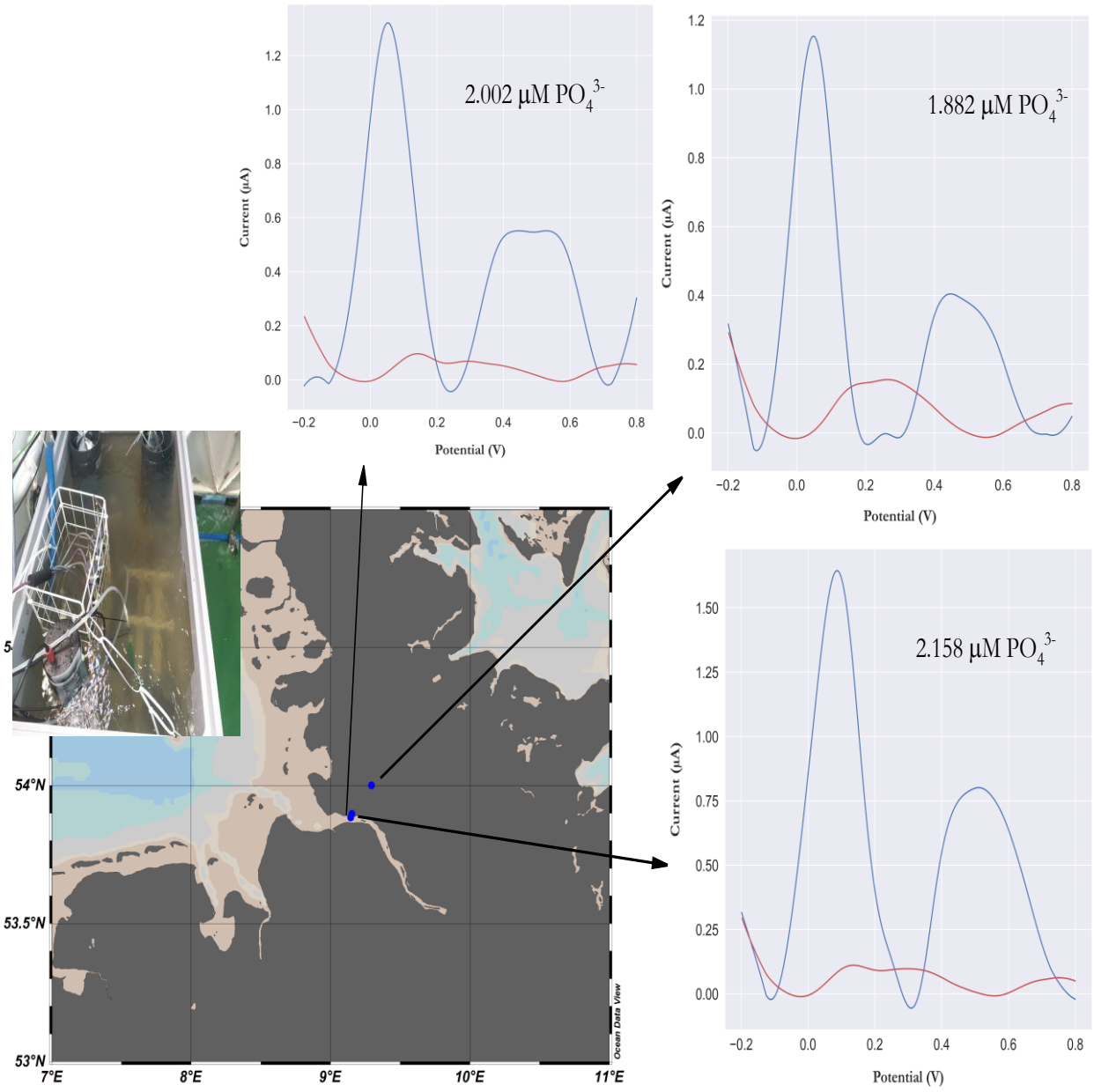

Figure S2.7 Location of three *on-site* data points taken at the Kiel Canal with square wave voltammograms at molybdate/CPE (blue line) and CPE (red line). The left inset shows the turbidity of the water entering the tank.

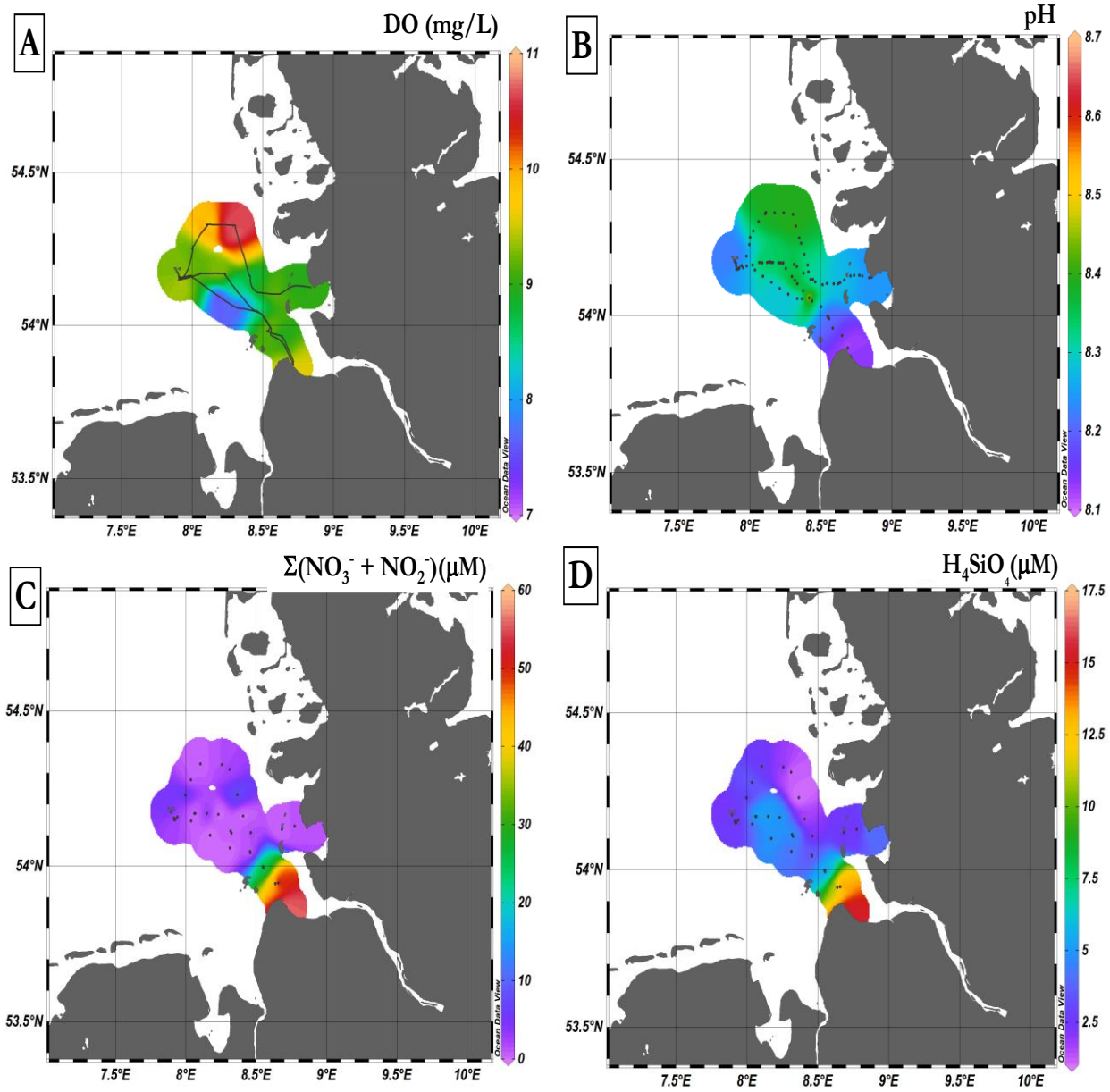

Figure S2.8 Overviews of (A) the distribution of surface dissolved oxygen (DO) in mg/L obtained from EXO sonde sensor, (B) distribution of pH obtained from sunburst SAMIpH and corrected for CTD salinity and temperature, (C) distribution of $\Sigma(NO_3^- + NO_2^-)$ in µM (bottom left panel) and (D) distribution of H_4SiO_4 in µM for the discrete samples collected from underway water supply and analyzed via QuAAtro air-segmented analyser.

5 Improvement of *on-site* sensor for simultaneous determination of phosphate, silicic acid, nitrate and nitrite in seawater

Mahmoud Fatehy Altahan[1,2], Mario Esposito[1], Eric P. Achterberg[1]

Published in *Sensors, MDPI*

DOI: 10.3390/s22093479

[1] Chemical Oceanography Department, GEOMAR Helmholtz for Ocean Research Kiel, Kiel 24148, Germany.

[2] Central Laboratory for Environmental Quality Monitoring, National Water Research Center, El-Qanater El- Khairia 13621, Egypt.

Abstract

Accurate, *on-site* determinations of macronutrients (phosphate (PO_4^{3-}), nitrate (NO_3^-), and silicic acid (H_4SiO_4)) in seawater in real time are essential to obtain information on their distribution, flux, and role in marine biogeochemical cycles. The development of robust sensors for long-term *on-site* analysis of macronutrients in seawater is a great challenge. Here, we present improvements of a commercial automated sensor for nutrients (including PO_4^{3-}, H_4SiO_4, and NO_2^- plus NO_3^-), suitable for a variety of aquatic environments. The sensor uses the phosphomolybdate blue method for PO_4^{3-}, the silicomolybdate blue method for H_4SiO_4 and the Griess reagent method for NO_2^-, modified with vanadium chloride as reducing agent for the determination of NO_3^-. Here, we report the optimization of analytical conditions, including reaction time for PO_4^{3-} analysis, complexation time for H_4SiO_4 analysis, and analyte to reagent ratio for NO_3^- analysis. The instrument showed wide linear ranges, from 0.2 to 100 µM PO_4^{3-}, between 0.2 and 100 µM H_4SiO_4, from 0.5 to 100 µM NO_3^-, and between 0.4 and 100 µM NO_2^-, with detection limits of 0.18 µM, 0.15 µM, 0.45 µM, and 0.35 µM for PO_4^{3-}, H_4SiO_4, NO_3^-, and NO_2^-, respectively. The Analyser showed good precision with a relative standard deviation of 8.9% for PO_4^{3-}, 4.8% for H_4SiO_4, and 7.4% for NO_2^- plus NO_3^- during routine analysis of certified reference materials (KANSO, Japan). The Analyser performed well in the field during a 46-day deployment on a pontoon in the Kiel Fjord (located in the southwestern Baltic Sea), with a water supply from a depth of 1 m. The system successfully collected 443, 440, and 409 *on-site* data points for PO_4^{3-}, $\Sigma(NO_3^- + NO_2^-)$, and H_4SiO_4, respectively. Time series data agreed well with data obtained from the analysis of discretely collected samples using standard reference laboratory procedures and showed clear correlations with key hydrographic parameters throughout the deployment period.

5.1 Introduction

Macronutrients such as phosphate (PO_4^{3-}), nitrate (NO_3^-), and silicic acid (H_4SiO_4) play key roles in the regulation of ocean productivity and thus the marine biogeochemical carbon cycle. In particular, PO_4^{3-} and NO_3^- are the bioavailable forms utilized by phytoplankton and autotrophic bacteria (Watson, Lenton, and Mills 2017; Altieri, Fawcett, and Hastings 2021), H_4SiO_4 exerts a strong influence on the productivity of silicifying phytoplankton such as diatoms, which are estimated to account for 40% of the total primary production in the oceans (Ragueneau et al. 2000; Field et al. 1998). However, excessive input of PO_4^{3-} and NO_3^- into estuaries and coastal waters leads to eutrophication, deoxygenation, and other processes that damage aquatic environment (Rabalais et al. 2014). In the open ocean, oligotrophic regions are subject to N and P limitation, which restricts biological productivity (Deutsch et al. 2007). In tropical and subtropical regions, H_4SiO_4 is depleted to low levels of ≈0.6 μM, which limits the diatom productivity and thus carbon export from the surface mixed layer (Krause et al. 2019). To study these biogeochemical processes, real-time and long-term monitoring of macronutrient concentrations is required to determine the spatial trends and temporal variations in their distributions (Blaen et al. 2016).

Nutrient data obtained from discrete samples usually collected at operational intervals and analyzed using laboratory techniques based on automated colorimetric approaches or ion chromatography. However, such methods are labor intensive, expensive, and yield datasets with a low temporal and spatial resolution (Rode et al. 2016).

Therefore, there is an urgent need for technologies that enable *on-site* measurements for long-term monitoring and are equipped to cope with challenging conditions during sporadic and transient environmental events. In the last 20 years, a number of studies have been conducted on *on-site* monitoring of nutrients in marine waters (Moscetta et al. 2009; Mills et al. 2004) using mainly three analytical approaches: optical, electrochemical, and wet chemical techniques. In particular, various ultraviolet (UV) optical sensors for routine measurement of NO_3^- have been developed and deployed on different platforms (Meyer et al. 2018; Nehir et al. 2021). These systems do not require chemical reagents, can measure over a wide range of concentrations, and are easy to use due to their small size and robustness (Daniel, Laës-Huon, Barus, Beaton, Blandfort, Guigues, Knockaert, Munaron, Salter, and Woodward 2020). Optical UV sensors have shown promise for long-term in situ deployment, but their application is limited by low sensitivity and accuracy due to optical interfering factors such as bromide and dissolved organic material (Pellerin et al. 2013).

Electrochemical techniques for nutrient measurements facilitate sensor miniaturization, require low power, and in some cases eliminate the need for reagents. Two electrochemical sensors have

been reported for H_4SiO_4 (Lacombe et al. 2008; Aguilar et al. 2015; Barus et al. 2018) and PO_4^{3-} (Jońca et al. 2013; Barus et al. 2016). In these sensors, molybdate (MoO_4^{2-}) ions are introduced into a working solution (NaCl solution (34.5 g L^{-1})) by electrochemical oxidation of a solid Mo wire. Then, either a silicomolybdate or a phosphomolybdate complex is electrochemically produced on an Au working electrode using cyclic voltammetry or square wave voltammetry. Although a short period of a few minutes is required for the electrochemical measurements, a longer period of 30 min is required for PO_4^{3-} measurements (Daniel, Laës-Huon, Barus, Beaton, Blandfort, Guigues, Knockaert, Munaron, Salter, and Woodward 2020). These techniques seem promising for long-term deployment due to absence of liquid reagents, but further development and investigation is needed for field applications.

Wet chemical methods, also known as reagent-based colorimetric methods, have been used in several *on-site* sensors deployed in rivers, estuaries, coastal waters, and oceans. These methods involve the formation of a light-absorbing dye that provides a robust measurement tool for nutrients with low detection limits and good precision. Among the more recent technologies used for in situ monitoring based on colorimetric assays is the implementation of microfluidics in lab-on-a-chip devices (LOC) (Beaton et al. 2011; Beaton et al. 2017). Although the LOC technology has shown better performance in terms of lower reagent consumption, lower power consumption, and smaller size compared to other commercially available in-situ analyzers, a multiparameter instrument LOC is not available, and the cost of sensors is relatively high.

Several colorimetric sensors based on flow injection analysis (FIA) have been reported. A submersible chemical analyzer known as Analyseur Chimique In Situ (ALCHIMIST) was installed on a remotely operated vehicle for in situ determination of $\Sigma(NO_3^- + NO_2^-)$ and total dissolved sulfide (Le Bris et al. 2000). NAS2E was used for monitoring of $\Sigma(NO_3^- + NO_2^-)$, and the NH4-Digiscan in situ analyzer was used for monitoring ammonium (NH_4^+) in coastal and estuarine waters. Other commercially available colorimetric in situ sensors and systems include the Autonomous Profiling Nutrient Analyzer (APNA) and ChemFIN (SubChem Systems, Inc., Narragansett, RI, USA) for NO_3^- and $\Sigma(NO_3^- + NO_2^-)$ analysis, and HydroCycle (Sea-Bird Scientific, Philomath, OR, U S) for PO_4^{3-}. Other systems are based on either the micro loop flow analysis (μLFA) (WIZ, SYSTEA S.p.A., Anagni, Latium, Italy) (Copetti et al. 2017; Bodini et al. 2015) or reverse flow analysis such as the autonomous nutrient analysis in situ (ANAIS) (Thouron et al. 2003).

Recently, new paper-based microfluidic devices for the determination of macronutrients in natural waters have been reported (Racicot et al. 2020; Charbaji et al. 2021). The techniques are based on fluid flow through paper by capillary action without the need for a pump. In principle, the device

consists of a sample port into which the water sample is introduced and transport channels connecting other parts of the device, such as the reaction zone, where the analyte solution mixes or reacts with the reagents. The signal (i.e., color formation) is subsequently formed in the detection zone and can be quantified using a cell phone or desktop scanner. Although the proposed systems offer promising applications for *on-site* observations of nutrients in natural waters, the technique does not allow for autonomous continuous monitoring.

All reported wet chemical in situ analyzers are designed to observe single nutrient, and therefore cannot perform multinutrient analysis with the same instrument. An exception is the WIZ probe, but there are no reports in the literature of long-term field testing of these multi-nutrient sensors. FIA systems based on a single syringe pump and a multiposition switching valve are excellent at compensating for the shortcomings of the continuous flow analyzers currently in use (Deng et al. 2020; 'FIALab Instruments, INC.' ; Hansen, Ruzicka, and Chocholous), as they are capable of delivering a small volume (at a level of 10 μL) of reagent without using peristaltic pumps (Ma et al. 2018). Automated syringe pump FIA instruments have been developed by EnviroTech LLC (Chesapeake, VA, USA) for *on-site* DNA in situ determination of $\Sigma(NO_3^- + NO_2^-)$, PO_4^{3-}, as well as H_4SiO_4 based on the Griess reaction (Griess 1879) using a Cd column as the reducing agent for NO_3^-, the classical blue phosphomolybdate method (Murphy and Riley 1962a), and the classical silicomolybdate method (Mullin and Riley 1955). The instruments perform routine chemical analyzes according to a preloaded protocol stored in their firmware. However, the protocols show a poor performance and precision, which limits their use for environmental applications in the field. In the stored protocol, only one standard was used for each nutrient. There is no matrix effect correction (i.e., no optical correction) in the sample concentration calculation, as described in the Data Processing Protocol section of the User's Guide, which limits the use of the analyzer in field deployments. The conventional cadmium column reduction procedure for nitrate determination, which requires regular regeneration, and the rate at which reagents and standards are consumed per measurement, also limit its use for long-term field use.

To the best of our knowledge, there are very few studies that have demonstrated multi-macronutrient analyzers for long periods of deployment. In the present work, we improve the performance of such an instrument by implementing a new nitrate method that uses vanadium chloride (VCl_3) for the reduction of NO_3^- to NO_2^-. This method has been used for a decade in flow analyzers for *on-site* monitoring of nitrate in natural waters (Wang et al. 2016; Fang et al. 2019; Nightingale et al. 2019). It showed more promising performance for long-term use than the classic copper-coated cadmium column or zinc particles reported by Ellis et al. in 2011, which must be replaced daily due to reduction efficiency degradation (Ellis et al. 2011). It also reduces the reagent

consumption, which increases the endurance of the sensor for longer deployment. The optimized method was tested during a deployment in coastal waters of the Kiel Fjord, Germany. The new method is validated by additional discrete sampling during the deployment and analysis using a reference air segmented flow analyzer.

5.2 Materials and Methods

5.2.1 Reagents and Standards Preparation

The reagents used in this study were analytical-grade salts prepared with deionized water (resistivity >18.2 MΩ-cm, Milli-Q, MilliporeSigma, Burlington, Massachusetts, USA). All glass and plasticware were routinely cleaned, rinsed with deionized water, soaked in 1 M HCl (37%, Carl Roth, Karlsruhe, Germany) for more than 24 h, rinsed with deionized water, and stored in plastic bags before use.

The reagents for PO_4^{3-} determination were prepared as follows.

- The acidic MoO_4^{2-} reagent (R1) was prepared by dissolving 12.8 g ammonium molybdate tetrahydrate ($(NH_4)_6Mo_7O_{24}$ $4H_2O$, Sigma Aldrich, Burlington, MA, USA) and 140 mL sulfuric acid (H_2SO_4, 98%, Merck, Kenilworth, NJ, USA) to obtain a concentration of 2.57 M (pH 0.6), 3.5 mL of a solution of potassium antimony (III) oxide tartrate trihydrate (PAT; $C_8H_4K_2O_{12}Sb_2$ $3H_2O$; Merck) (5.3 g/100 mL deionized water), and 1 mL of solution of sodium dodecyl sulfate ($C_{12}H_{25}OSO_2ONa$; Merck, Kenilworth, NJ, , USA) (30 g/L) in 1000 mL deionized water.
- Ascorbic acid reagent (R2) was prepared by dissolving 25 g of L(+)-ascorbic acid ($C_6H_8O_6$; ≥99%, Carl Roth, Karlsruhe, Germany) in 1000 mL of deionized water.

The reagents for H_4SiO_4 determination were prepared as follows:

- The MoO_4^{2-} reagent (R1) was prepared by dissolving 15 g of ammonium molybdate tetrahydrate, 5.4 mL of H_2SO_4, and 1 mL of sodium dodecyl sulfate solution in 1000 mL of deionized water.
- The oxalic acid reagent (R2) was prepared by dissolving 50 g of oxalic acid dihydrate ($C_2H_2O_4.2H_2O$; ≥99%, Carl Roth, Karlsruhe, Germany) into 1000 mL of deionized water.
- The ascorbic acid reagent (R3) was the same as that used for PO_4^{3-} determination.

The reagents for NO_3^- and NO_2^- determination were prepared as follows:

- The Griess reagent and VCl_3 reducing agent reagent were prepared by dissolving 5 g of VCl_3 (Sigma Aldrich, Burlington, MA, USA) in 200 mL of deionized water until the solution turned a dark brown color. Then, 15 mL of concentrated HCl (37%, trace-metal grade, Fisher Scientific,

Waltham, MA, USA) was added. After a dark-turquoise color appeared, 10 g of sulfanilamide ($H_2NC_6H_4SO_2NH_2$; Merck, USA) was added by dissolving 1 g of *N*-(1-naphthyl) ethylenediamine dihydrochloride ($C_{10}H_7NHCH_2CH_2NH_2.2HCl$; Merck, Kenilworth, NJ,USA) and 1 mL of a solution of Triton x-100 50% (*v*/*v*) (50 mL Triton x-100 (Sigma Aldrich, Burlington, MA, USA): 50 mL isopropanol (Fisher Scientific, Waltham, MA, USA) in 1000 mL of deionized water.

Stock solutions of PO_4^{3-} (1 mM) were prepared by dissolving 0.136 g of potassium dihydrogen sulfate (KH_2PO_4; Merck, Kenilworth, NJ, USA) into 1000 mL of deionized water. Stock solutions of H_4SiO_4 (1 mM) were prepared by dissolving 0.0212 g of sodium metasilicate pentahydrate ($Na_2SiO_3.5H_2O$; Sigma Aldrich, city, state, USA) into 1000 mL of deionized water. Stock solutions of NO_3^- (1 mM) were prepared by dissolving 0.0849 g of sodium nitrate ($NaNO_3$; Merck, Kenilworth, NJ, USA) into 1000 mL of deionized water. Stock solutions of NO_2^- (1 mM) were prepared by dissolving 0.0689 g of sodium nitrite ($NaNO_2$; Merck, Kenilworth, NJ,, USA) into 1000 mL of deionized water.

Standard PO_4^{3-}, H_4SiO_4, NO_3^-, and NO_3^- calibration solutions were prepared by further diluting the respective stock solutions with deionized water.

All reagent solutions were stored in brown 500 mL high-density polyethylene (HDPE) laboratory-grade bottles (Nalgene, Thermo Scientific, Waltham, MA, USA) and kept refrigerated when not in use. Blank, standard, and cleaning solutions were freshly prepared prior to field use and stored in 1000 mL HDPE Nalgene bottles.

5.2.2 Multinutrient Analyzer Description

The analyzer (AutoLAB, EnviroTech LLC, Chesapeake, VA, USA) was a multichannel *on-site* portable chemical analyser that automatically measures the concentrations of nutrients ($\Sigma(NO_3^- + NO_2^-)$, PO_4^{3-}, and H_4SiO_4) in natural waters using wet chemical techniques with colorimetric detection. The system consisted of four main parts, namely, a 16-way rotary valve, a stepper motor-driven syringe, 3 colorimetric detectors, and an electronic controller in a single housing (Figure 1). The rotary valve and the syringe (≈2.2 mL full motion) were driven by a stepper motor controlled by an internal program stored on a memory card and displayed on a terminal interface (Tera Term). A blank, sample, or standard is collected by the analyser by retracting the syringe plunger while the rotary valve is at the inlet position. Switching the rotary valve and retracting the plunger allows the reagent to be added to the analyte, causing a chemical reaction. This changes the colour of the solution contained in the syringe according to the concentration of the nutrient.

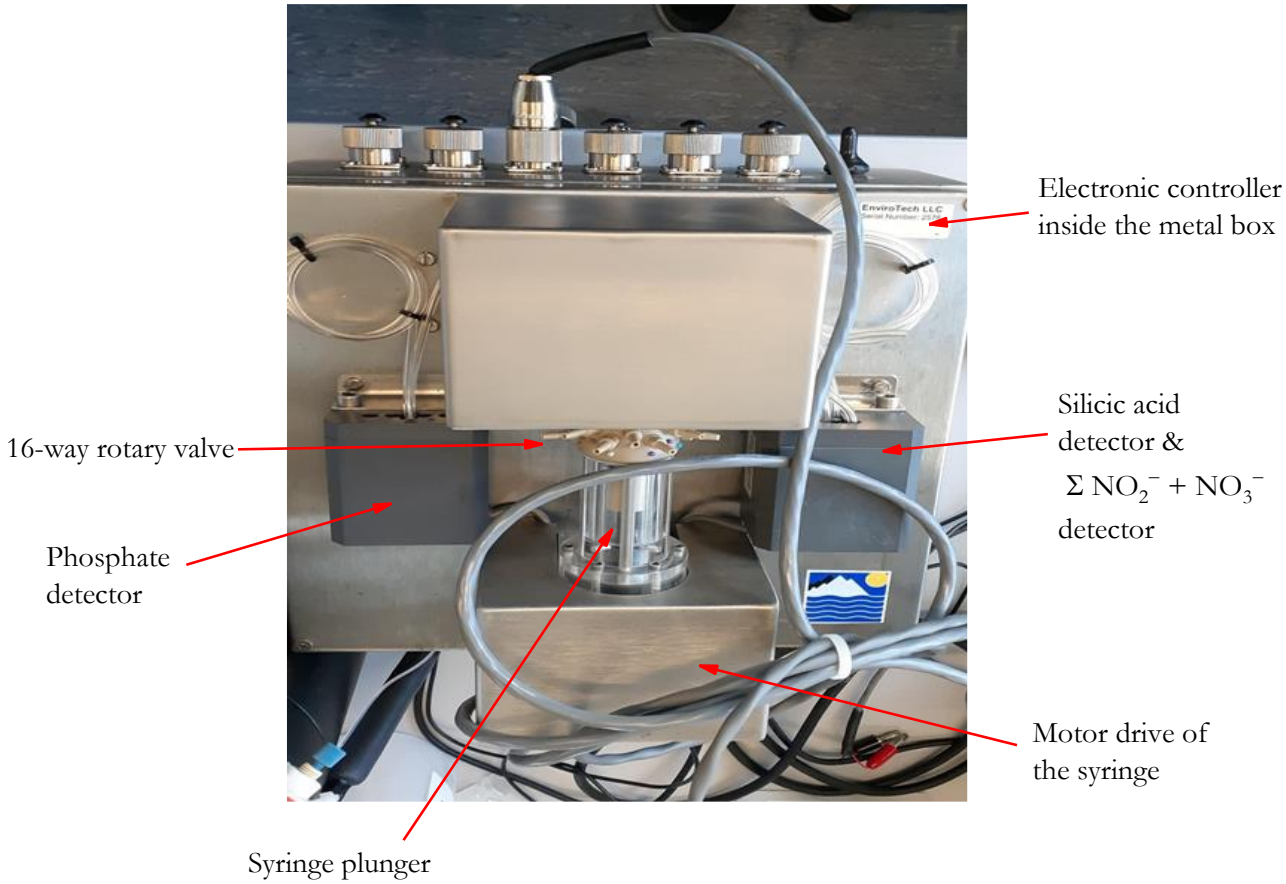

Figure 5.1 Hardware of multi-nutrient analyser (AutoLAB) showing the five major components, namely, the 16-way rotary valves, a motor drive of the syringe, the syringe plunger, three colorimetric detectors, and an electronic controller inside a metal box.

The colorimetric detector consisted of a narrow capillary flow cell made of high-grade glass (1 cm path length for the $\Sigma(NO_3^- + NO_2^-)$ and PO_4^{3-} detector and 2 cm path length for the H_4SiO_4 detector with a light-emitting diode (LED) as the light source on one side and a photodiode detector on the opposite side. An additional monitoring photodiode was positioned next to the LED to monitor the intensity of the light source. Green LED with a peak wavelength of 567 nm and a silicon photodiode with a peak intensity at a wavelength of 570 nm were used for $\Sigma(NO_3^- + NO_2^-)$. No information on LED or photodiodes of PO_4^{3-} or H_4SiO_4 detectors was given in the operating manual. To minimize light interference from the outside, the colorimeters were encapsulated in polyurethane. Inside the electronics housing was a series of electronic modules: the main control unit and the motor drivers and detector interfaces. Both the motor drivers and detector interfaces had their own microprocessors and were controlled by the main control unit via a link. Four devices (syringe motor, valve motor, phosphate detector, and (nitrate + nitrite) and

silicic acid detectors) were configured through an arrangement called a serial peripheral system (SPS), where the detectors and motors are referred to as SPS devices, and each device had its own SPS address, which is called in the internal scripting language.

The syringe had a polyetheretherketone (PEEK) plunger in a glass cylinder that was fitted with an O-ring. The valve was made of PEEK with a linear polytetrafluoroethylene (PTFE). The swivel fittings were provided with barbed adapters to connect the pump tubing (Tygon LMT-55; green-green, inner diameter 1.85 mm) for fluid transfer. The 0.5 mm PTFE tubing and 1/4 28" fittings were used to connect the valve to the detector. The same tubing and fittings were used for the sample, connecting via a 1/4 28" Luer adapter (female–male) PEEK.

5.2.3 Chemical Methods

5.2.3.1 Phosphate Chemical Assay

The conventional blue method was employed here to quantify PO_4^{3-} involving a direct reaction with orthophosphate in an acidic MoO_4^{2-} solution in the presence of PAT to form the yellow phosphomolybdate complex $H_3PO_4\ (MoO_3)_{12}$. This solution was then reduced by ascorbic acid as a reducing agent to form the deep blue-coloured phosphomolybdate complex $[H_4PMo_8^{(VI)}Mo_4^{(V)}O_{40}]^{3-}$, with extinction measured at a wavelength of 880 nm.

H_4SiO_4 has the same tendency to react with MoO_4^{2-} to form a silicomolybdate complex that adsorbs at 880 nm, interfering with PO_4^{3-} analysis in seawater. A pH of 0.4–0.9 with a proton/molybdate (H^+/MoO_4^{2-}) ratio of 60–80 minimizes the interference of H_4SiO_4 in the analysis of PO_4^{3-} (Jońca, Comtat, and Garçon 2013b; Directive 2000).

5.2.3.2 Silicic Acid Chemical Assay

The determination of the H_4SiO_4 is similar to that of PO_4^{3-}. In particular, it is based on the reaction of H_4SiO_4 with MoO_4^{2-} under acidic conditions of pH 1.5–2 to form the yellow complex $H_3SiO_4\ (MoO_3)_{12}$ after a complexation time of 180 s. The solution is then reduced by ascorbic acid in the presence of oxalic acid, which acts as a masking agent for PO_4^{3-} to form a deep blue colored product with maximum absorbance at a wavelength of 880 nm.

5.2.3.3 Nitrate and Nitrite Chemical Assay

The determination of NO_3^- and NO_2^- is based on the reduction of NO_3^- to NO_2^- using VCl_3 at elevated temperatures (≈50 °C) for 30 min. The reduced NO_3^- plus NO_2^- originally present in the

sample was quantified by using the Griess reagent method. This method is based on the diazotization of NO_2^- with sulfanilamide to form a diazonium salt, which is then reacted with the coupling agent *N*-(1-naphthyl) ethylenediamine dihydrochloride (NED) to form a pink azo dye with maximum absorbance at a wavelength of 540 nm. The mixed reagent (Griess reagent + VCl_3) allows for the determination of both NO_2^- and $\Sigma(NO_3^- + NO_2^-)$ and thus the calculation of NO_3^- with the same detector. The reaction mixture can be sent to the detector for NO_2^- determination before the heating step, while $\Sigma(NO_3^- + NO_2^-)$ is determined after the reduction and heating steps.

5.2.4 Analytical Protocol

The complete measurement cycle for each nutrient [PO_4^{3-}, H_4SiO_4, or $\Sigma(NO_3^- + NO_2^-)$] begins with a calibration that includes a blank and three mixed standards with known concentrations of PO_4^{3-}, H_4SiO_4, and NO_3^- followed by the analysis of the samples. For each nutrient cycle, after analysis of the highest concentrated standard and samples, a solution of 0.1 M NaOH + 0.5 mL L^{-1} 50 Triton X-100 was drawn into the syringe to wash the system and minimize carryover effects. During the washing step, the three detectors were used to assess the cleaning of the analyser. To prevent carryover between the solutions during sample analysis, the syringe and colorimeter were flushed twice with 2 mL of either the blank or the standard and six times with 2 mL of the seawater sample. For the PO_4^{3-} measurement, the analytical protocol involved the drawing of the analyte solution and the two reagents into the syringe in a volumetric ratio of 4:1:1. Mixing was performed by four consecutive back and forth movements of the syringe plunger, which allowed for the initial colour to develop. Then, the syringe injected the solution into the detector, allowing the colour development to fully develop for 180 s. Finally, the light intensity of the colour formed was measured. For the H_4SiO_4 measurement, the analyte solution was mixed with the three reagents in a ratio of 1:1:1:1. The analyte solution was mixed with the MoO_4^{2-} reagent in the syringe, and the flow was stopped for 180 s to allow the yellow complex to form before mixing with the other two reagents. Finally, the solution was transferred to the colorimeter for colour determination. For NO_3^- and NO_2^- measurement, the analyte solution was mixed with the modified Griess reagent at a volumetric ratio of 2:1. The solution was then passed into the PO_4^{3-} detector, where it was incubated at an elevated temperature (≈50 °C) for 30 min. The solution was then transferred to the $\Sigma(NO_3^- + NO_2^-)$ detector for colorimetric determination. For a single sample measurement, a total volume of 137 µL of reagents (i.e., mixed molybdate reagent and ascorbic acid) was used for PO_4^{3-} determination, a total volume of 396 µL of reagents (i.e., molybdate reagent, oxalic acid reagent, and ascorbic acid reagent) for H_4SiO_4 determination, and a total volume of 137 µL of Griess reagent containing vanadium chloride for $\Sigma(NO_3^- + NO_2^-)$ determination was required. A

schematic diagram of the syringe pump and the rotary valves is shown in **Figure 5.2.** The detailed steps for the nutrient measurement protocol are described in **Table S3.1** and Video S1 [42].

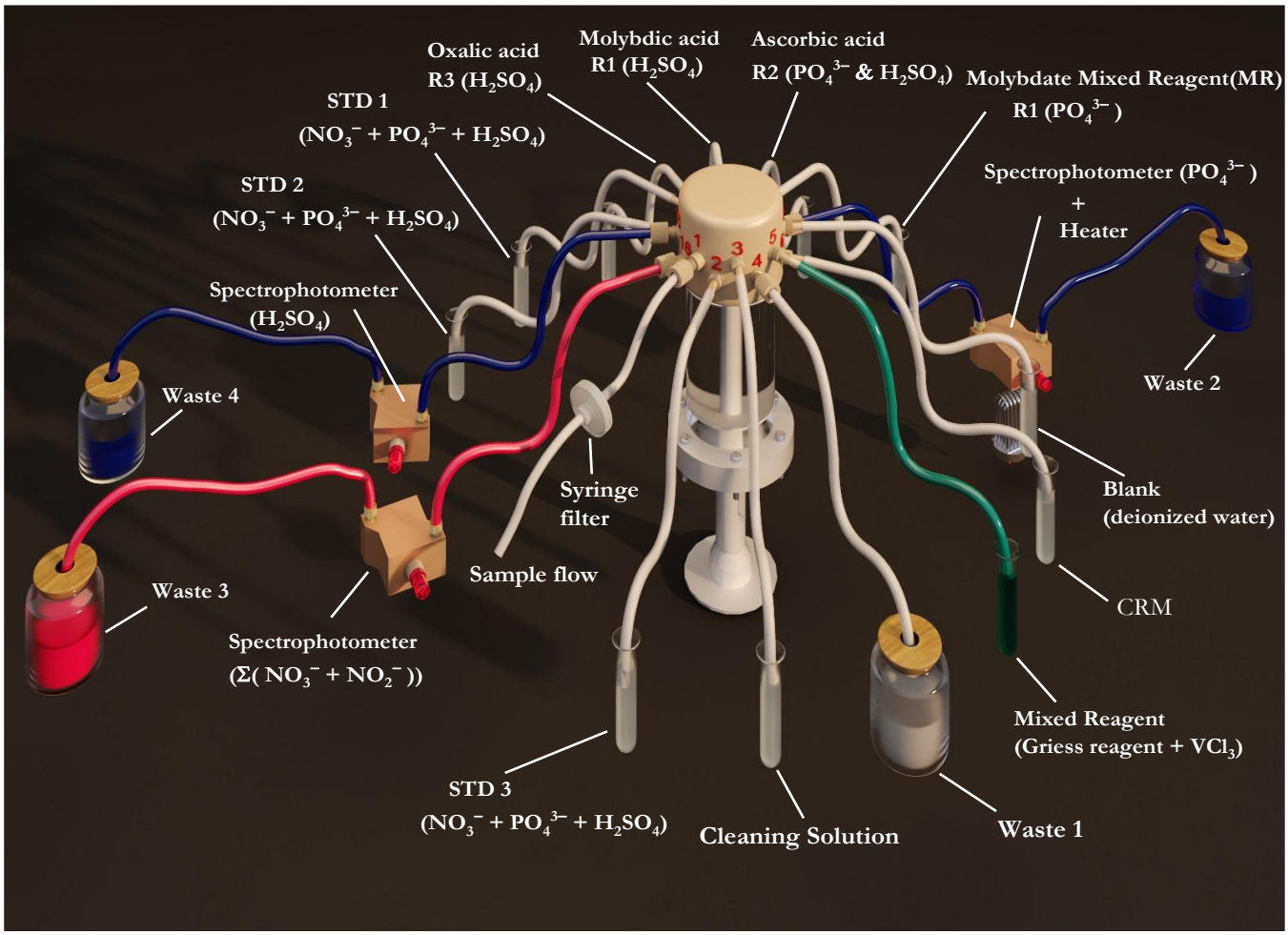

Figure 5.2 Three-dimensional schematic diagram of the AutoLab autoanalyzer (syringe and 16-way rotatory valve) for multinutrient determination. Standard solutions: STD; certified reference materials: CRM.

5.2.5 Data Processing

The absorbance of the blank, standard, and sample was calculated by using the following equation:

$$\textbf{Absorbance} = -log_{10}\left(\frac{V}{V^R} \times \frac{V_0^R}{V_0}\right) \qquad \textbf{Equation 5.1}$$

where V is the voltage of the measuring photodiode (intensity of transmitted light) and V_0 is the voltage of the monitoring photodiode (intensity of incident light) for the analyte solution after color formation, and V^R and V_0^R are the voltages of the measuring photodiode and the monitoring photodiode for the analyte solution before the reagent was added, respectively. A linear regression

between the absorbance of the blank and the three standards was assessed after every 10 measurements. The sample concentration (μM PO_4^{3-}, μM SiO_4^{4-}, or μM $\Sigma(NO_3^- + NO_2^-)$) was calculated by the following equation:

$$\text{Concentration (μM)} = (A - B)/S \qquad \textbf{Equation 5.2}$$

where A is the absorbance of the sample, B is the intercept of the linear fit in the absorbance unit (AU), and S is the slope of calibration curve (AU) μM^{-1}.

5.2.6 Field Deployment and Discrete Sampling

A field deployment was conducted on a pontoon in Kiel Fjord, southwestern Baltic Sea, Germany, in May–June 2021. The analyzer was housed in a weather-proof aluminum container (Zarges, Weilheim, Germany) that was placed on the pontoon (**Figure 5.3**). The analyzer was fed with a continuous water flow from a depth of 1 m using a submerged water pump with an output of 600 L/h and power consumption of 8 W (Eheim, Deizisau, Germany). The pump inlet was protected by a Cu net (mesh size ≈0.297 mm). The water flow was diverted to the analyzer's sample inlet through a 0.45 μm polyethersulfone syringe filter (Millipore). The analyzer was equipped with a blank solution and three standard solutions for NO_3^- (1, 5, and 10 μM), PO_4^{3-} (0.5, 1, and 2 μM), and H_4SiO_4 (1, 10, and 20 μM), all prepared in artificial seawater (17 g L^{-1} NaCl). After every 10 sample measurements, a calibration procedure was performed. A multiparameter sonde EXO2 (YSI, Yellow Springs, Ohio, USA) was deployed beside the analyzer to monitor salinity, temperature, and dissolved oxygen (DO). The EXO2 Sonde was deployed on 22 May at a depth of 1 m and sampling frequency of 1 min. Discrete samples were collected from the outlet of the pump filtered through a 0.45 μm syringe filter connected to a 60 mL acid-washed plastic syringe into acid pre-washed 15 mL low-density polypropylene tubes (SEAL Analytical Ltd., Southampton, UK) The collected samples were immediately frozen for later analysis using a QuAAtro continuous air segmented flow analyzer (SEAL Analytical Ltd.). Ancillary data such as wind speed, water temperature, rain precipitation, and solar radiation were obtained from the GEOMAR weather station positioned near the deployment site [43].

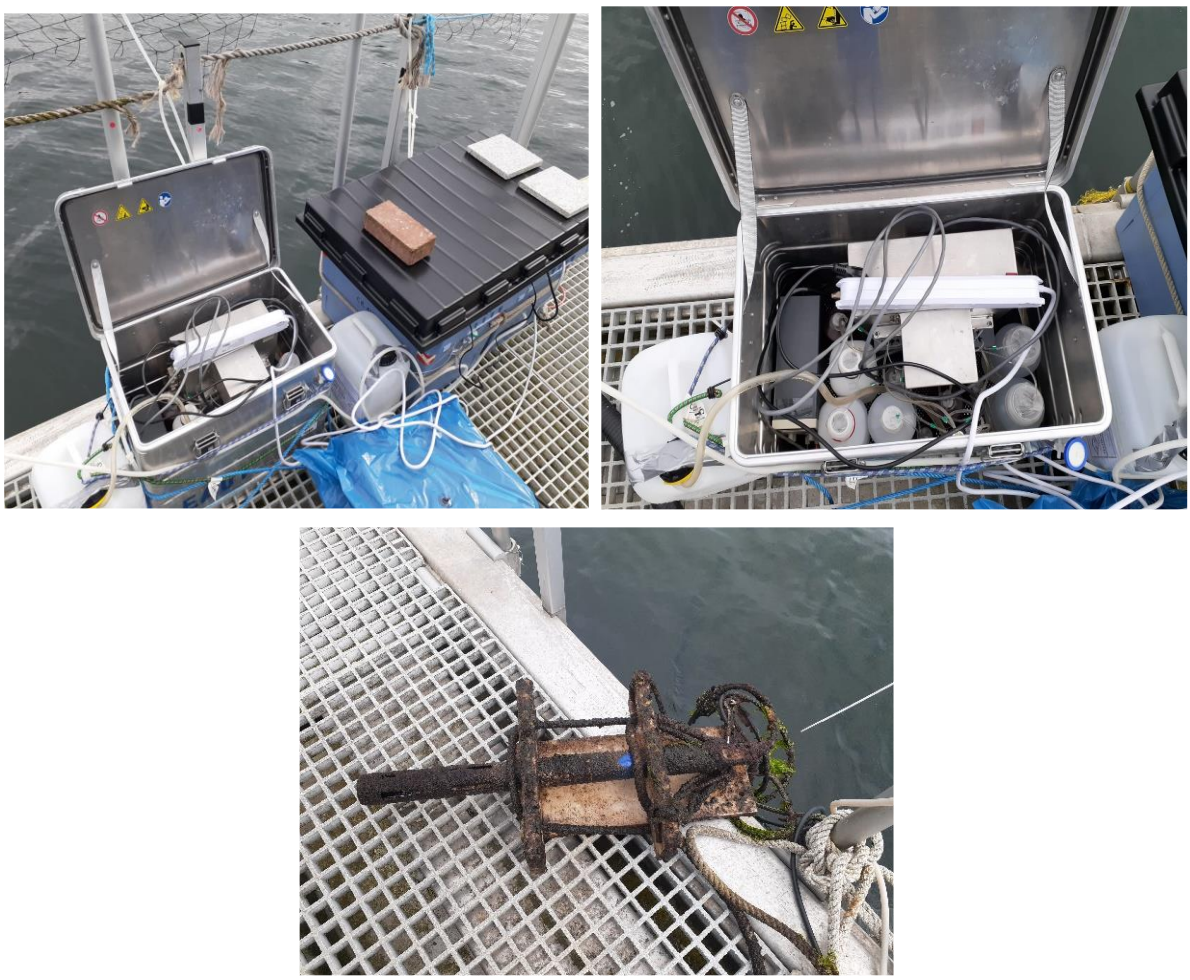

Figure 5.3 Deployment setup of the AutoLAB analyzer (upper) and the EXO2 Sonde after the deployment (bottom).

5.3 Results and Discussion

5.3.1 Optimization of Analytical Conditions

Different analytical conditions were studied to obtain the highest possible sensitivity for the nutrient measurements. The influence of key analytical parameters was evaluated, including reaction time for PO_4^{3-}, complexation time for H_4SiO_4, and analyte/reagent ratio for NO_3^-. For PO_4^{3-}, the reaction time was identified as the period between the stopping of the flow and the color development of the reaction mixture in the measurement flow cell. The reaction time varied from 0 to 300 s, and the analytical sensitivity was calculated from the absorbance values of the blank solution and two standard solutions (1 and 2 μM PO_4^{3-}) (**Figure 5.4, A**). With an increase in reaction times, the analytical sensitivity increased from 0.0058 (±0.0025) AU μM^{-1} and an RSD

of 43.9% for 0 s to 0.173 (±0.0002) AU μM^{-1} and 1.19% RSD for 120 s. Sensitivity continued to increase at 180 s with a mean value of 0.0181 (±0.0004) AU μM^{-1} and RSD of 2.41%. A slight decrease was observed at 240 s with a value of 0.0173 (±0.0011) AU μM^{-1} and an RSD of 6.22%. The maximum sensitivity was reached at 300 s with a mean value of 0.021 (±0.0045) AU μM^{-1} and an RSD of 21.9%. On the basis of the highest sensitivity value and the lower RSD value (5% level), 180 s was chosen as the optimal reaction time.

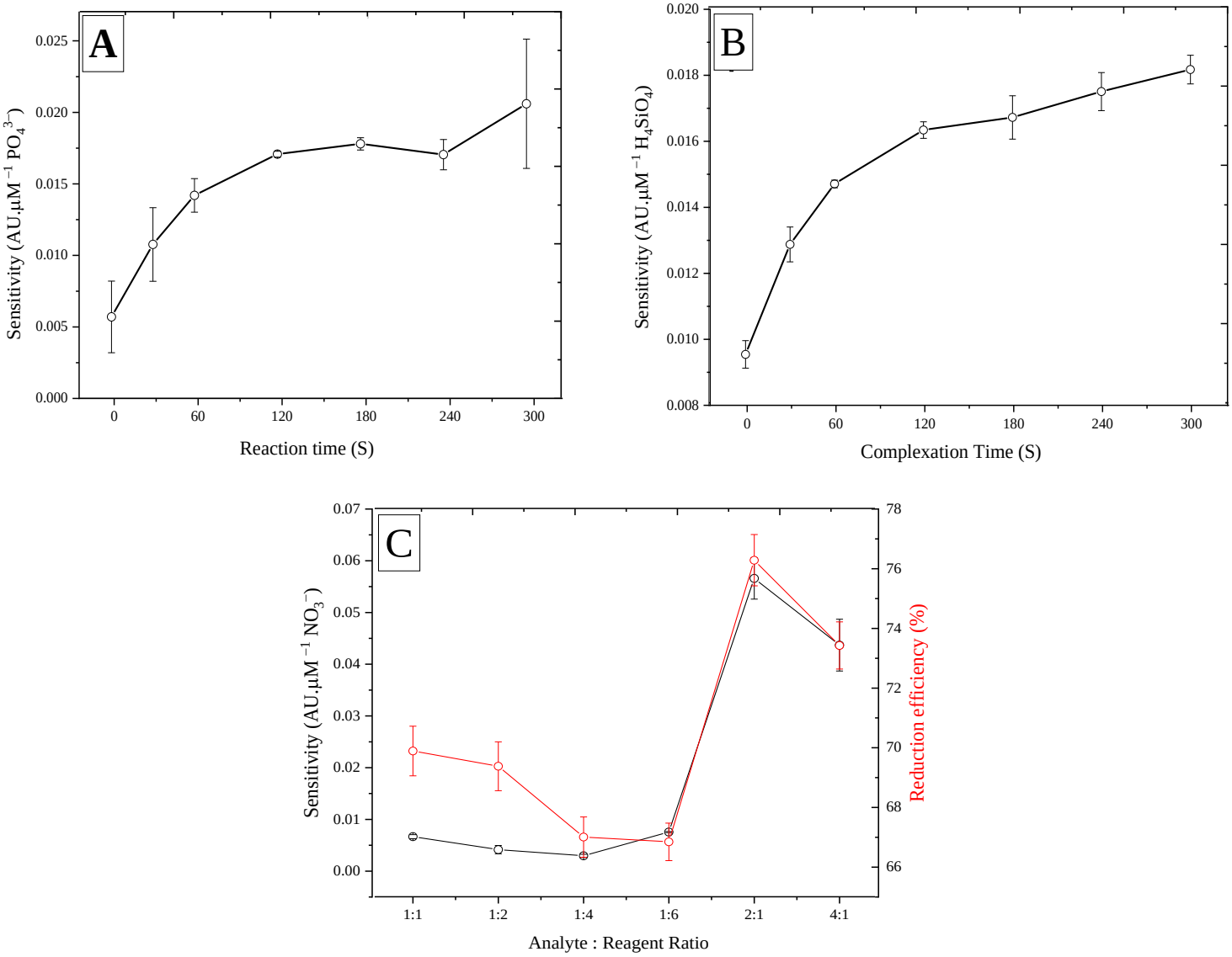

Figure 5.4 (**a**) Effect of the reaction time on the sensitivity (slope of the calibration curve: 0, 1, 2 µM PO_4^{3-}). (**b**) Effect of the complexation time on the sensitivity (slope of the calibration curve: 0, 1, 2 µM Si). (**c**) Effect of changing the analyte: reagent ratio on the sensitivity of the calibration curve (0, 1, 2 µM NO_3^-) (black lines) and on the reduction efficiency (%) (red lines). AU: absorbance unit. Error bar (±1 SD), n = 5.

For H_4SiO_4, the complexation time was identified as the time during which the analyte and Mo reagent reacted in the syringe and thus the time before the addition of the other two reagents (oxalic acid and ascorbic acid). Increased analytical sensitivity was observed with an increase in the complexation time from 0 s (0.0095 ± 0.00042) AU μM^{-1} and an RSD of 4.39% to 300 s (0.0181 ± 0.000436) AU μM^{-1} and an RSD of 2.4%. With an RSD value of 1.54%, and a change in analytical sensitivity (Δs) of 0.0068 AU μM^{-1} from 0 s to 120 s and Δs of 0.0018 AU μM^{-1} from 120 s to 300 s, 120 s was chosen as the optimal time for complexation. This shows good sensitivity with a low RSD for 120 s and no further improvement for complexation times of up to 300 s (**Figure 5.4, B**).

For NO_3^- measurements, the reaction temperature is crucial (García-Robledo, Corzo, and Papaspyrou 2014; Lin et al. 2019). We set the temperature to the maximum value (≈50 °C) and tested the reduction time from 20 min to 50 min (**Figure S3.1**). An improvement in reduction efficiency was obtained when we increased the reduction time from 20 min (61%) to 30 min (63%), while no further improvement was noted when the reaction time was increased to 50 min. Therefore, 30 min was chosen as the optimal reaction time. The analyte/reagent ratio was also investigated, and the maximum sensitivity was obtained at a ratio of 2:1 with a value of 0.054 AU μM^{-1}. The results were plotted against the ratio of absorbances values of NO_3^- and NO_2^- of the same concentration (to obtain reduction efficiency). As shown in **Figure 5.4, C**, the efficiency gradually decreased from a ratio of 1:1 (69%) to reach 66.8% at a ratio of 1:6, and then increased at a ratio of 2:1 (76.5%) and before decreasing again at a ratio of 4:1 (73.5%). On the basis of these results, a 2:1 ratio of analyte/reagent was chosen as optimal.

5.3.2 Effect of Salinity

Large variations in salinity were observed in estuaries and coastal waters compared to freshwater and open oceans, and these can affect the measurement of nutrients due to matrix differences. The effect of salinity on the analytical sensitivity of colorimetric measurements can be illustrated by two aspects. The first is the difference in refractive index between the saline sample and fresh water due to the salt effect, referred to as the Schlieren effect. The second is the effect of ionic strength on the analytical sensitivity. These effects occur at high salinity when the transmitted light is directed to the monitoring photodiode (Worsfold et al. 2013).

When the flow cell is filled with seawater, a lower voltage is measured by the photodiode than with deionized water. As a result, for the same analyte concentration, lower absorbance values were obtained for the samples in a seawater matrix compared to those in the deionized water matrix.

Equation (5.1) was used to calculate the absorbance offset, which was corrected by subtracting this offset from the sample absorbance after colour development.

Salinity variations have an effect on the chemistry used for each nutrient species. The Griess reaction, which involves reduction of nitrate based on VCl_3, is strongly affected by salinity fluctuations (Wang et al. 2016). To investigate the influence of the salinity variations on the analytical sensitivity, the determination of a standard solution of 5 µM NO_3^- was used for solutions with different salinity values that were prepared by dissolving different amounts of NaCl in deionized water. **Figure 5.5, A** shows an absorbance of 5 µM NO_3^- in deionized water S = 0 (0.14 AU), with absorbance values decreasing with increasing salinity from S = 7 (0.105 AU) to S = 14 (0.09 AU). A steady state was reached with increasing salinity to S = 23 (0.09 AU) and to S = 35 (0.09 AU).

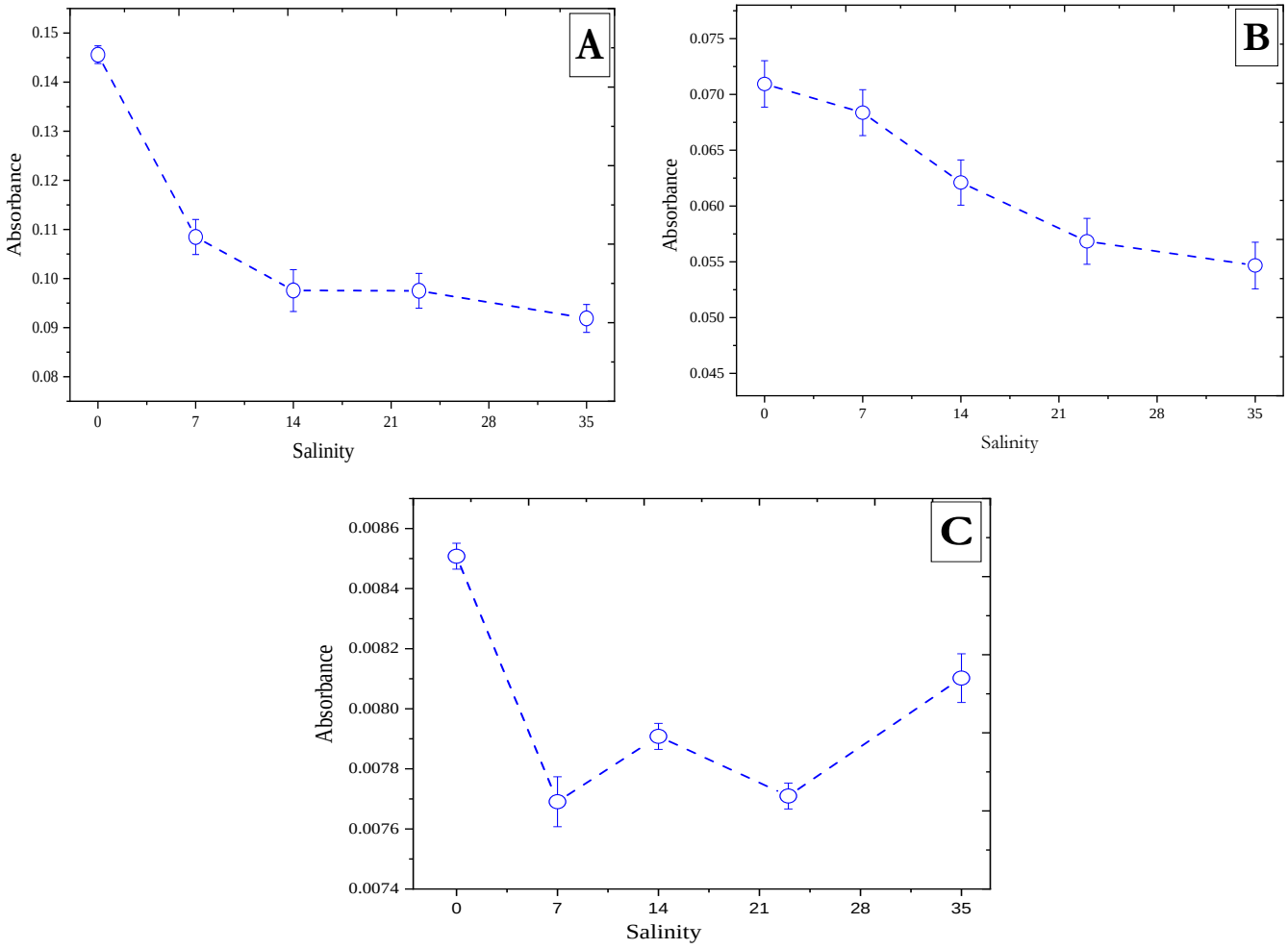

Figure 5.5 Effects of salinity (S = 0, 7, 14, 23, and 35) on the absorbances of a (**a**) 5 µM NO_3^- standard, (**b**) 5 µM H_4SiO_4 standard, and a (**c**) 1 µM PO_4^{3-} standard. Error bar (±1 SD), n = 10.

The influence of salinity variations on the analytical sensitivity in H_4SiO_4 measurements has been reported (Grasshoff, Kremling, and Ehrhardt 2009), with a reported molar absorptivity of the silicomolybdate blue complex in distilled water of 22×10^3 L mole^{-1} cm^{-1} and in oceanic seawater of 19×10^3 L mole^{-1} cm^{-1}. **Figure 5.5, B** shows the absorbance of 5 μM H_4SiO_4 in deionized water S = 0 (0.07 AU) with a higher value compared to salinities ranging from S = 23 (0.06 AU) to S = 35 (0.005 AU).

The analytical sensitivity of the Mo-Blue method for PO_4^{3-} is not affected by the variation in the salinity of the sample matrix (Murphy and Riley 1962b; Nagul et al. 2015). The Schlieren effect is the bias that generally occurs in the analytical signal when onboard blank and standard solutions with different salinities than the seawater samples used (Dias et al. 2006). This is evident when comparing the analytical sensitivity of 1 μM PO_4^{3-} standard in a solution of deionized water (S = 0) (0.008 AU) with that using a solution of S = 7 (0.008 AU). Although no large bias was observed when comparing samples with different salinities of S = 7–35 (**Figure 5.5, C**), an RSD value of 2.11% was noted. Variations in salinity had little effect on analytical sensitivity after applying the optical correction based on **Equation (5.1)** compared to values obtained without optical correlation (i.e., via the traditional Beer's law equation $A = -log_{10}(\frac{V}{V_0})$), where V is the voltage of the measuring photodiode (intensity of transmitted light) and V_0 is the voltage of the monitoring photodiode (intensity of incident light).

We attempted to correct for the salinity error during measurement by taking the photodiode measurement for the analyte solution before addition of the reagents. Figure S2 shows the measured concentrations of 5 μM NO_3^- (**Figure S3.2,A**), 5 μM H_4SiO_4 (**Figure S3.2, B**), and 1 μM PO_4^{3-} (**Figure S3.2, C**). The values obtained with the traditional Beer's law equation are shown as red circles, while those obtained with **Equation (5.1)** using the optical correction are shown as black circles. The comparison between the two values showed that the values obtained with the traditional Beer's law were underestimated by 3.95% (S = 0) for 5 μM NO_3^- compared to values obtained with the optical correction, with the underestimation increasing with increasing salinity to 40.6% (S = 23 and S = 35). An underestimation of 2.5% (S = 0) was found for 5 μM H_4SiO_4, increasing to 43.9% (S = 35) with increasing salinity. An underestimation of 1.42% (S = 0) was found for 1 μM PO_4^{3-}, increasing to 16.4% (S = 35) with increasing salinity. Despite the optical correction, it is recommended to use standards with salinity close to that of the studied waters for field work on board.

5.3.3 Analytical Performance

The analytical performance of the analyser was tested by evaluating a series of calibrations (**Figure 5.6**). The calibration plot showed measurements in deionized water spiked with 0.2, 0.5, 0.75, 1, 2, 5, 10, 20, 40, 60, and 100 µM PO_4^{3-}. The calibration plot showed an analytical sensitivity of 0.01211 AU μM^{-1}, indicating good linearity over a wide range (0.2–100 µM) of PO_4^{3-} with a coefficient of determination R^2 of 0.999. For H_4SiO_4, deionized water was spiked with a range of H_4SiO_4 standards (0.2, 0.5, 0.75, 1, 2, 5, 10, 20, 40, 60, and 100 µM H_4SiO_4). The calibration plot showed a sensitivity of 0.02377 AU μM^{-1} with a good linearity over a wide range (up to 100 µM) of H_4SiO_4 with R^2 = 0.992. For NO_3^- and NO_2^-, the calibration plots showed analytical sensitivities of 0.00614 and 0.01202 AU μM^{-1} for NO_3^- and NO_2^-, respectively, and broad linear ranges of 0.5 – 100 µM for NO_3^- and 0.4–100 µM for NO_2^- with R^2 = 0.998 and 0.995, respectively. The values of the intercepts and slopes of the corresponding calibration curves are presented in Table S2; standard deviation values, static t-values, and probabilities are also reported, and the data showed that all values were significant ($p < 0.01$), except for the intercept of the calibration curve for silicic acid, because the blank measurements for silicic acid in deionized water showed negative values (Arar 1997).

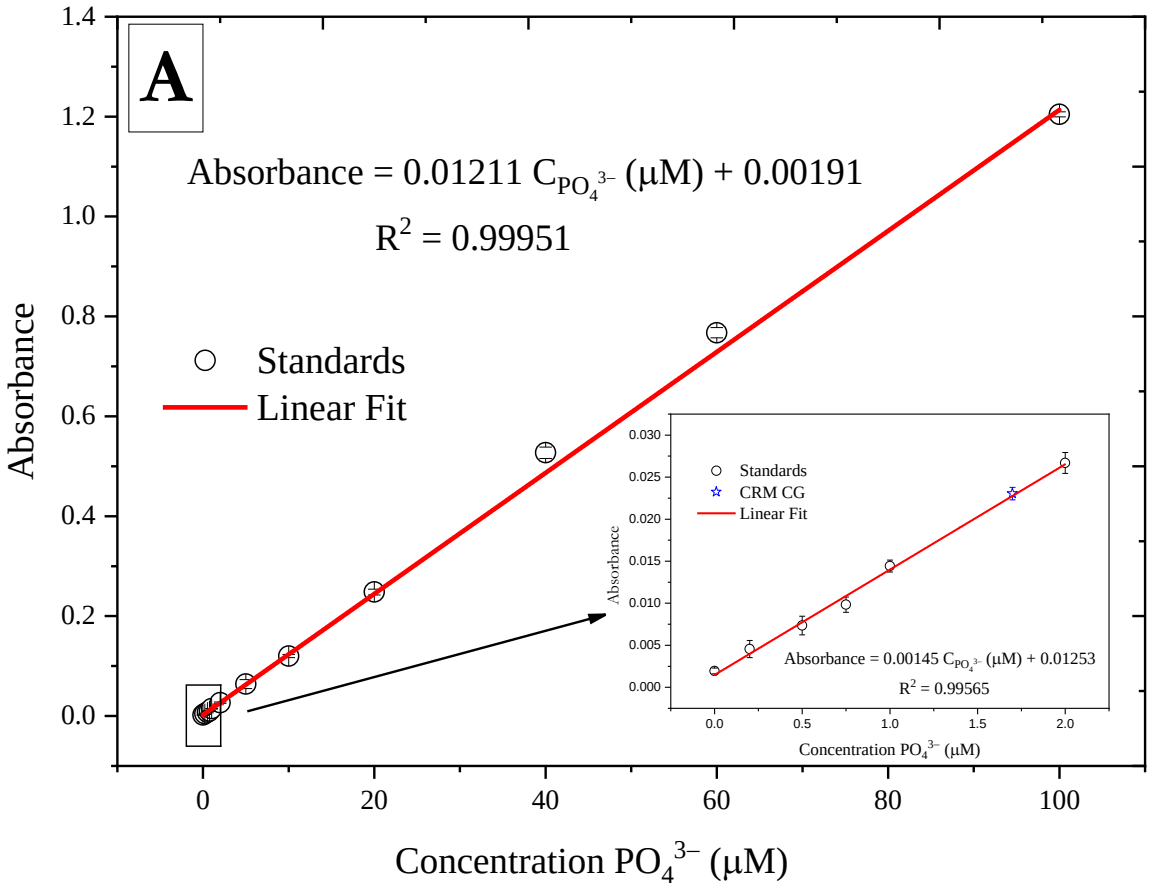

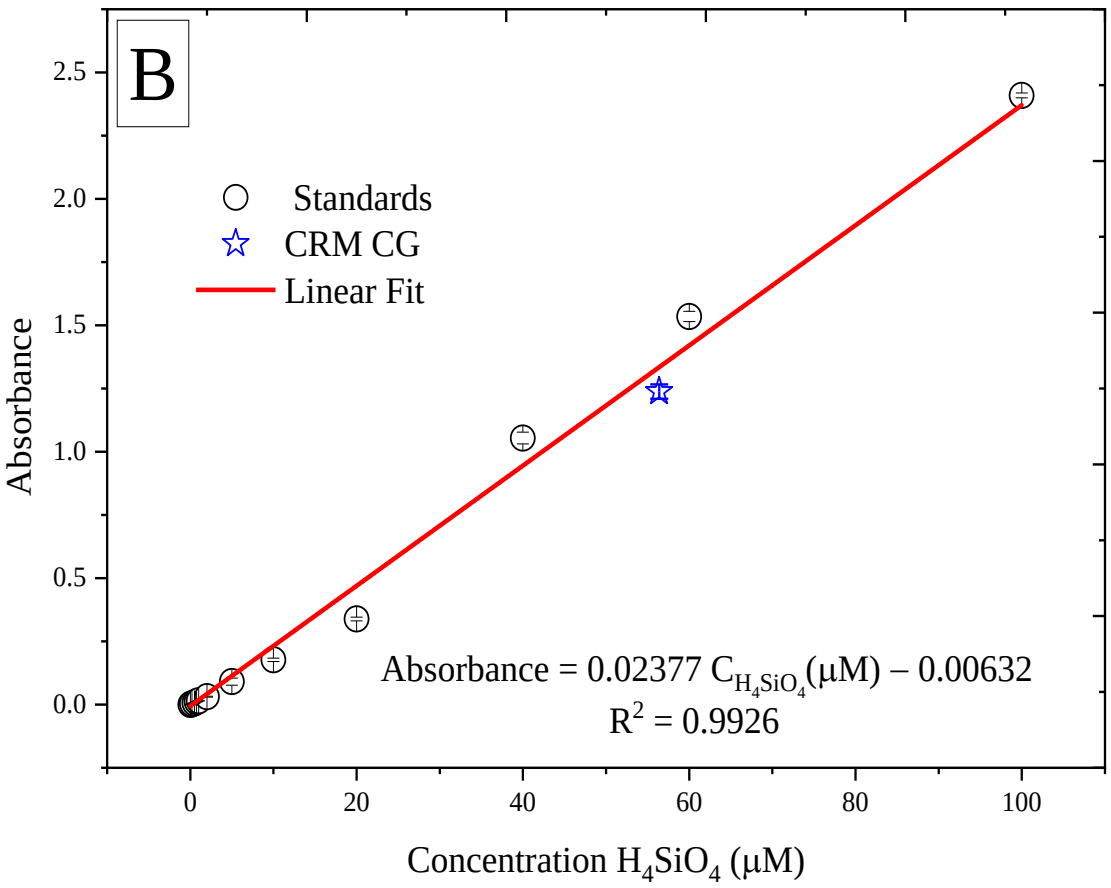
B
Standards
CRM CG
Linear Fit
Absorbance = 0.02377 $C_{H_4SiO_4}$(µM) – 0.00632
R^2 = 0.9926
Absorbance
Concentration H_4SiO_4 (µM)
0.0
0.5
1.0
1.5
2.0
2.5
0
20
40
60
80
100

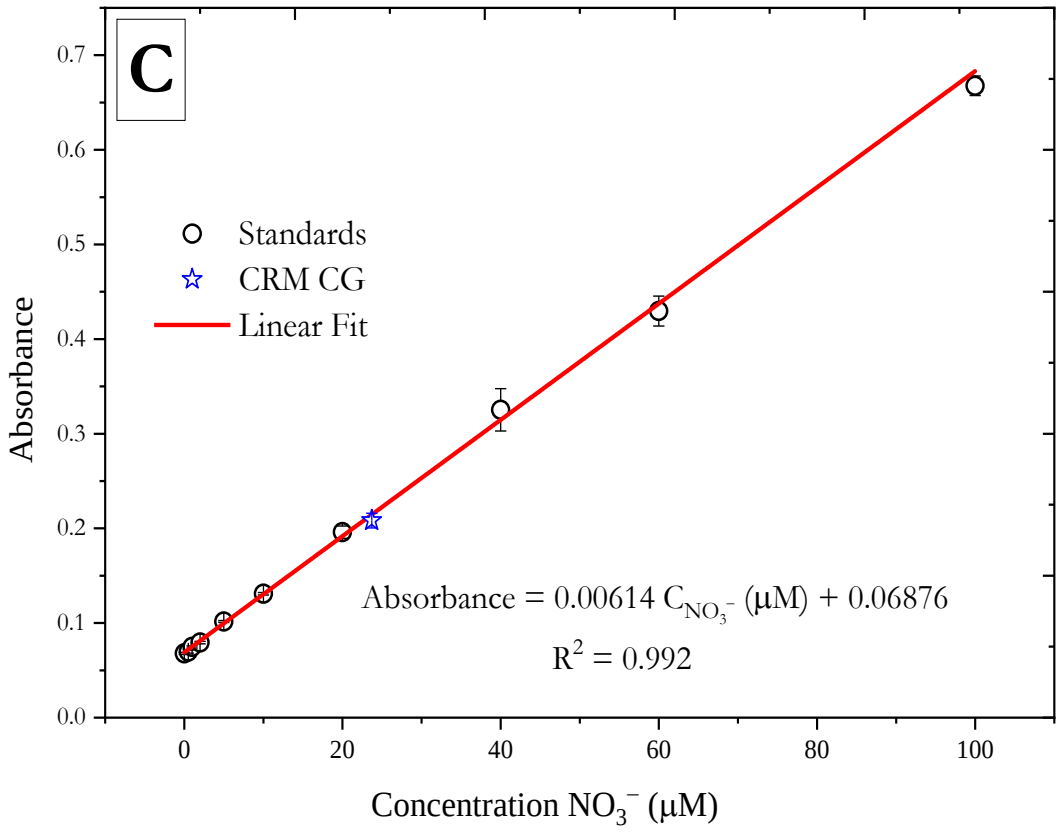
C
Standards
CRM CG
Linear Fit
Absorbance = 0.00614 $C_{NO_3^-}$ (µM) + 0.06876
R^2 = 0.992
Absorbance
Concentration NO_3^- (µM)
0.0
0.1
0.2
0.3
0.4
0.5
0.6
0.7
0
20
40
60
80
100

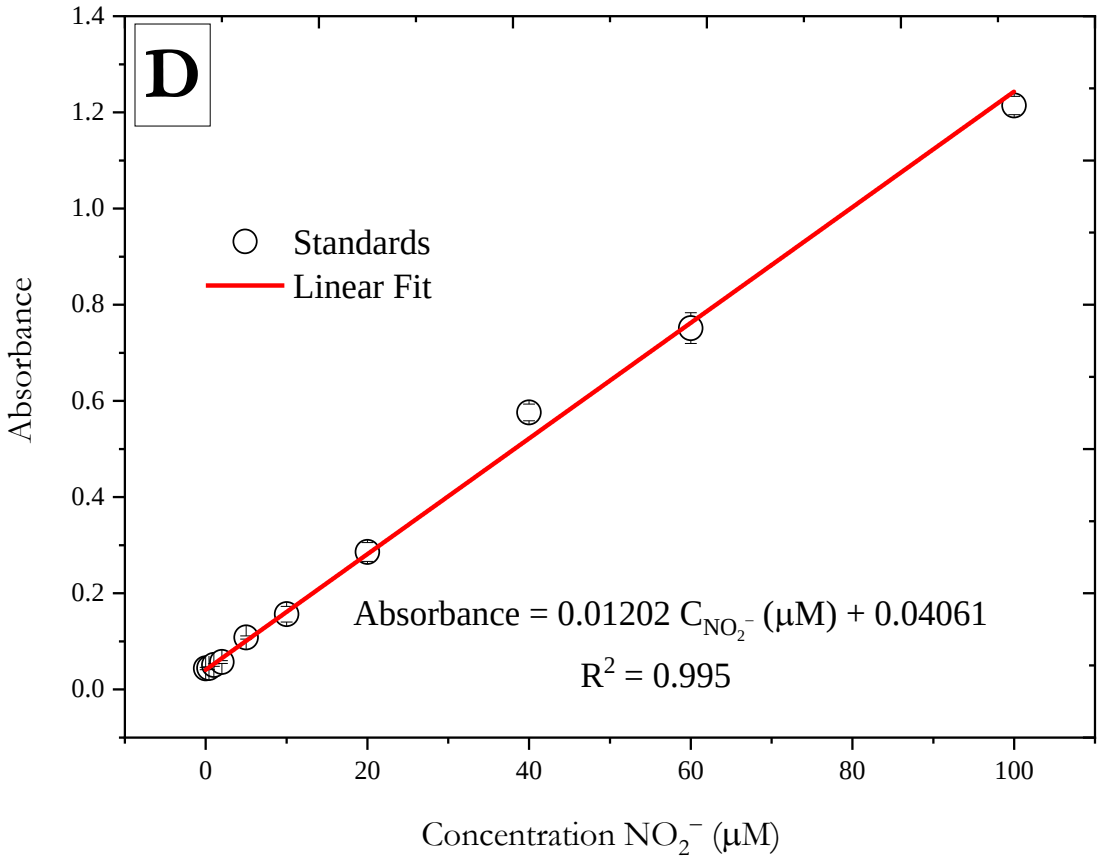

Figure 5.6 (**a**) Calibration curve for PO_4^{3-} standards (0, 0.2, 0.5, 0.75, 1, 2, 5, 10, 20, 40, 60, and 100 μM) in a 1 cm flow cell. (**b**) Calibration curve for H_4SiO_4 standards (0, 0.2, 0.5, 0.75, 1, 2, 5, 10, 20, 40, 60, 100 μM) into a 2 cm flow cell. (**c**) Calibration for NO_3^- standards (0, 0.5, 1, 2, 5, 10, 20, 40, 60, 100 μM) into a 1 cm flow cell. (**d**) Calibration curve for NO_2^- standards (0, 0.4, 1, 2, 5, 10, 20, 40, 60, 100 μM) into a 1 cm flow cell. Blue stars indicate the absorbance of the Kanso CRM CG. Error bar (±1 SD), n = 10.

The limit of detection (LOD) was calculated as 0.18 μM, 0.15 μM, 0.45 μM, and 0.269 μM, and the limit of quantification (LOQ) was calculated as follows: 0.6 μM 0.3 μM, 1.5 μM, and 0.89 μM for PO_4^{3-}, H_4SiO_4, NO_3^-, and NO_2^-, respectively, where LOD and LOQ were calculated according to IUPAC recommendation (Long and Winefordner 1983; Belter, Sajnóg, and Baralkiewicz 2014) using the following equations:

$$\boldsymbol{LOD = 3\,\sigma} \qquad \textbf{Equation 5.3}$$

$$\boldsymbol{LOD = 10\,\sigma} \qquad \textbf{Equation 5.4}$$

where σ is defined as the standard deviation of blank measurements (n = 10) (blank measurements were made by applying the associated calibration curves of the blank signals).

Technically, the analyser can detect nitrite in the field, as we described in the Materials and Methods. However, nitrite concentrations in natural waters are typically in the nanomolar range

and below our reported LOD, which limits the use of our analyser to detect nitrite and nitrate separately.

Table 5.1 indicates the figures of merit of the analyser following our analytical improvements and compares the performance with other portable *on-site* analysers reported in the literature and/or commercially available (WIZ (Bodini et al. 2015), APNA (Egli, Veitch, and Hanson 2009), Hydrocycle PO4 (Snazelle 2018b), NAS3X (Rong and Anson 1996), ANAIS (Thouron et al. 2003), ALCHEMIST (Le Bris et al. 2000), NuLAB ('Green Eyes, LLC'), and Lab on Chip (LOC) (Beaton et al. 2012; Grand et al. 2017; Clinton-Bailey et al. 2017), as well as other UV spectral sensors for NO_3^- such as SUNA (Bai et al. 2014), OPUS (Nehir et al. 2021; 'Trios '), and SUV-6 (Finch et al. 1998)). The WIZ, APNA, NAS3X, ANAIS, and NuLAB devices are the only multi-nutrient analysers reported to date. Although they have a number of advantages, there are some limitations to their application in the field. The sensitivity of WIZ analysers is limited by their high variability at low concentrations. APNA and ANAIS provide four separate units for PO_4^{3-}, H_4SiO_4, and NO_3^- or $\Sigma(NO_3^- + NO_2^-)$. APNA and ChemFIN are based on continuous flow injection analysis, in which the sample and reagent are introduced into a carrier stream, resulting in greater dispersion of the sample and affecting long-term sensitivity (Mansour and Danielson 2012). ANAIS is based on reverse injection analysis, in which the detection reagent is injected into the mobile phase of the sample, which reduces sample dispersion and ensures high sensitivity over a long period of time. However, this type of FIA still suffers from the fact that detection is performed under non-equilibrium conditions, which reduces sensitivity compared to manual methods (Cerdà, Avivar, and Cerdà 2012). NAS3X and NuLAB are based on the same type of FIA as the AutoLAB method, where a syringe pump and multi-position ports for reagent and sample delivery combine the features of continuous flow analysis with low reagent and sample consumption with the advantages of discrete (batch) sampling and high sensitivity, making them suitable for *on-site* applications (Monte-Filho et al. 2011).

NAS3X with four different units for the measurement of PO_4^{3-}, H_4SiO_4, $\Sigma(NO_3^- + NO_2^-)$, and ammonium and NuLAB are limited by the use of a cadmium column for NO_3^- reduction, which limits their application for long-term use as the cadmium column needs to be regenerated regularly to ensure stable analytical efficiency and thus sensitivity. Moreover, cadmium columns are toxic and decompose over time when they come into contact with organic matter in seawater (Schnetger and Lehners 2014a).

Table 5.1 Comparison of the AutoLAB (modified) and other available nutrient sensors reported in the literature and that are commercially available.

Analyzer	Method	Linear Range (μM)				LOD (μM)				Ref.
		PO_4^{3-}	NO_3^-	NO_2^-	H_4SiO_4	PO_4^{3-}	NO_3^-	NO_2^-	H_4SiO_4	
WIZ	μLFA [a]/ wet chemistry	0.19–32.2	0.28–71.4	0.15–19.2	-------	0.19	0.28	0.15	------	(Bodini et al. 2015)
APNA, ChemFIN	CFIA [b]/ wet chemistry	0.03–16	0.03–15	0.02 -10	0.05–50	0.03	0.03	0.02	0.05	(Egli, Veitch, and Hanson 2009)
Hydrocycle, Sea-Bird	FIA [c]/ wet chemistry	0–10	-------	-------	-------	0.075	------	------	------	(Snazelle 2018b)
NAS3X	FIA/ wet chemistry	0–6	0-300	-------	0–60	0.06	0.05	------	0.06	('Envirotech Instruments LLC')
ANAIS	rFIA [d]/ wet chemistry	0.1–5	0.1–40	-------	0.5–150	0.1	0.1	------	0.5	(Thouron et al. 2003)
ALCHEMIST	FIA/ wet chemistry	-------	0–40 [e]		-------	------	0.5		------	(Le Bris et al. 2000)
Lab-on-Chip	Micro-fluidics/ wet chemistry	-------	0.025–350	0–0.25	-------	------	0.05	0.02	------	(Beaton et al. 2012)
		0.14–10	-------	-------	-------	0.04	------	------	------	(Clinton-Bailey et al. 2017; Grand et al. 2017)
		-------	-------	-------	0–400	------	------	------	0.045	(Cao et al. 2017)
NuLAB	FIA/ wet chemistry	0.2–25	0.2–50 [e]	0.15-35	0.3–60	0.2	0.2	0.15	0.3	('Green Eyes, LLC')

SUNA	UV-spectral	-------	2.4–4000	-------	-------	------	2	-----	-----	('Sea-Bird Scientific')
OPUS	UV-spectral	-------	1–60	-------	-------	------	2	-----	-----	(Nehir et al. 2021)
SUV-6	UV-spectral	-------	0–400	-------	-------	------	0.21	-----	-----	(Finch et al. 1998)
ANESIS	Electro-chemistry	-------	-------	-------	1.63–132.8	------	------	-----	0.32	(Legrand et al. 2021)
AutoLAB (modified)	FIA/ wet chemistry	0.2–100	0.5–100	0.4–100	0.2–100	0.18	0.45	0.35	0.15	This work

[a] Micro loop flow analysis, [b] continuous flow injection analysis, [c] flow injection analysis, [d] reverse flow injection analysis, [e] $\Sigma(NO_3^- + NO_2^-)$.

As part of the evaluation of analytical performance, the accuracy of the analyser was determined in the laboratory using certified reference material (CRM CG, Kanso Co. Ltd., Osaka, Japan). Ten replicate measurements of CRM CG reference material for nutrients in seawater with an assigned PO_4^{3-} concentration of 1.7 ± 0.02 μM, assigned NO_3^- of 24.2 ± 0.2 μM and NO_2^- of 0.06 μM, and assigned H_4SiO_4 of 57.7 ± 0.5 μM. The means of the measured values were 1.4 ± 0.14 μM, 25.8 ± 2.7 μM, and 49.4 ± 2.8 μM for PO_4^{3-}, $\Sigma(NO_3^- + NO_2^-)$, and H_4SiO_4, respectively. The results show that the analyser is suitable for macronutrient analysis over a wide range of concentrations.

Ten replicate measurements of the CRM were taken over a 10-day period at a frequency of one measurement per day during the deployment to investigate both reproducibility and stability of the analyser (**Figure S3.3**). An RSD of 8.9% was obtained for PO_4^{3-} with maximum and minimum absorbance values of 0.023 and 0.018, respectively; an RSD of 7.4% was obtained for NO_3^- with maximum and minimum absorbance values of 0.25 and 0.2, respectively; and an RSD of 4.8% was obtained for H_4SiO_4 with maximum and minimum absorbance values of 0.58 and 0.5, respectively. The values of RSD are less than the extent reported by Gibbons et al. (10% RSD) (Gibbons and Coleman 2001), showing good precision of the analyser. These results demonstrate good applicability of the analyser for the analysis of seawater. The paired t-test was used to detect systematic error (bias) at a degree of freedom (*df*) of 9. No bias was observed for NO_3^- (t-value = 2.46, $t_{critical}$-value = 2.82, $p > 0.01$), which was not the case for PO_4^{3-} (t-value = 7.95, $t_{critical}$-value = 2.82, $p < 0.01$) and H_4SiO_4 (t-value = 6.163, $t_{critical}$-value = 2.82, $p < 0.01$), where there was a

significant difference between the assigned values and the measured values. This could have been due to the fact that only one CRM was tested.

5.3.4 Field Deployment

The performance of the analyser was demonstrated under environmental conditions during a field campaign in Kiel Fjord. The fjord is located on the southwestern coast of the Baltic Sea and is a mesohaline inner coastal water body that is a small extension of the Bay of Kiel. The Kiel Fjord is about 6 km wide at the mouth and has a length of 15 km; its mean and maximum depths are 10 m and 22 m, respectively. The hydrography of the Kiel Fjord is characterized by strong variability in salinity from S = 2.6–22.4 with a mean salinity of S = 14.3 (Schories et al. 2006). The higher salinity waters originate mainly from the North Sea, while the lower salinity waters originate from the eastern Baltic Sea with additional riverine inputs. The Baltic Sea is a transition zone between the high salinity water from the Kattegat and brackish water from its own central zone. The salinity in the fjord is strongly influenced by the salinity fluctuations in the Bay of Kiel. The water in the Kiel Fjord is well mixed; during strong wind conditions, the waters can be completely flushed (Javidpour et al. 2009). Temperatures in the fjord range from 0 °C to 22 °C with an annual mean value of 11 °C (Schories et al. 2006). Since the tidal range in the Baltic Sea is only 20 cm, the currents at the location of the measurement pontoon along the shore of Kiel Fjord are mainly determined by winds (Schröder, Kossel, and Lenz 2021; Healy, Wang, and Healy 2002). Overall, the water level in Kiel Fjord showed a nearly constant value during the deployment period (12 May to 28 June 2021). **Figure S3.4** shows the water level data obtained from the Kiel-Holtenau hydrological station. A mean water level of 502.8 ± 0.04 cm was obtained with minimum and maximum values of 460 cm and 541 cm, respectively. The datasets were obtained from the Federal Waterways and Shipping Administration (WSV) ('WSV-Wasserstraßen- und Schifffahrtsverwaltung des Bundes ' 2021).

Figure 5.7, A shows the hydrographic data of salinity, DO, and temperature obtained from the EXO2 Sonde during the period between 28 May and 27 June 2021, with two gaps on 12 June and 11–14 June due to a problem downloading data from the sensor. Water temperature showed a gradual increase from around 10 °C before reaching the maximum of 20.9 °C. Salinity fluctuated during the study period, with minimum and maximum values of 9.7 and 17.08, respectively (mean ± 1 SD; 13.5 ± 1.7). The DO showed a maximum value of 7.4 mg L^{-1} and a minimum of 12.07 mg L^{-1} (mean value of 9.6 ± 0.7 mg L^{-1}) throughout the study period (28 May–27 June). **Figure 5.7, B** shows timeseries data for water temperature obtained using a surface water temperature sensor from 28 May–27 June. Wind speed was obtained from a mast beside the deployment site.

Figure 5.7, C shows the time series data for dissolved carbon dioxide concentration (CO_2 partial pressure (pCO2)) obtained with the CONTROS HydroC-CO_2 sensor (4H Jena, Germany) mounted at the deployment site at a depth of 1 m adjacent to the sample intake of our analyzer. Two time series were obtained, the first from 3 June to 10 and the other from 17 June to 27 June, with a gap in between because the sensor was out of service. For the first period, the mean value was 599 ± 107 µatm with minimum and maximum values of 390 µatm and 1047 µatm, respectively. For the other time period, there was a a mean value of 479 ± 70 µatm with minimum and maximum values of 341 µatm and 807 µatm, respectively.

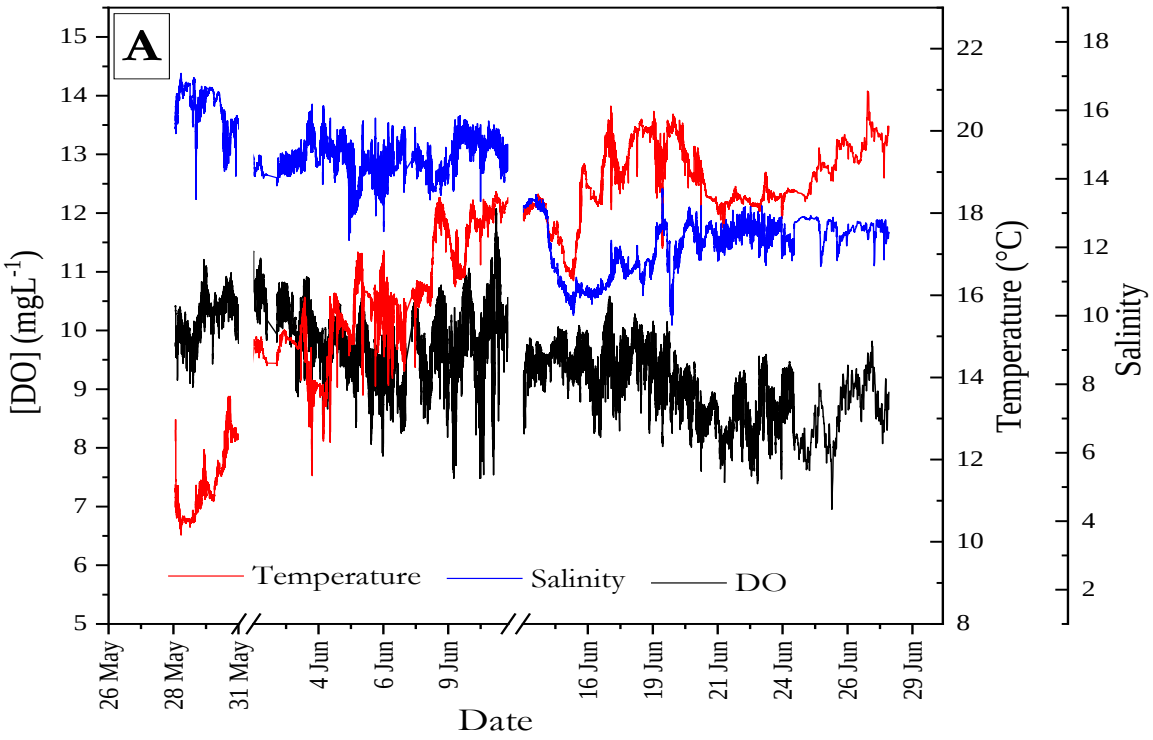

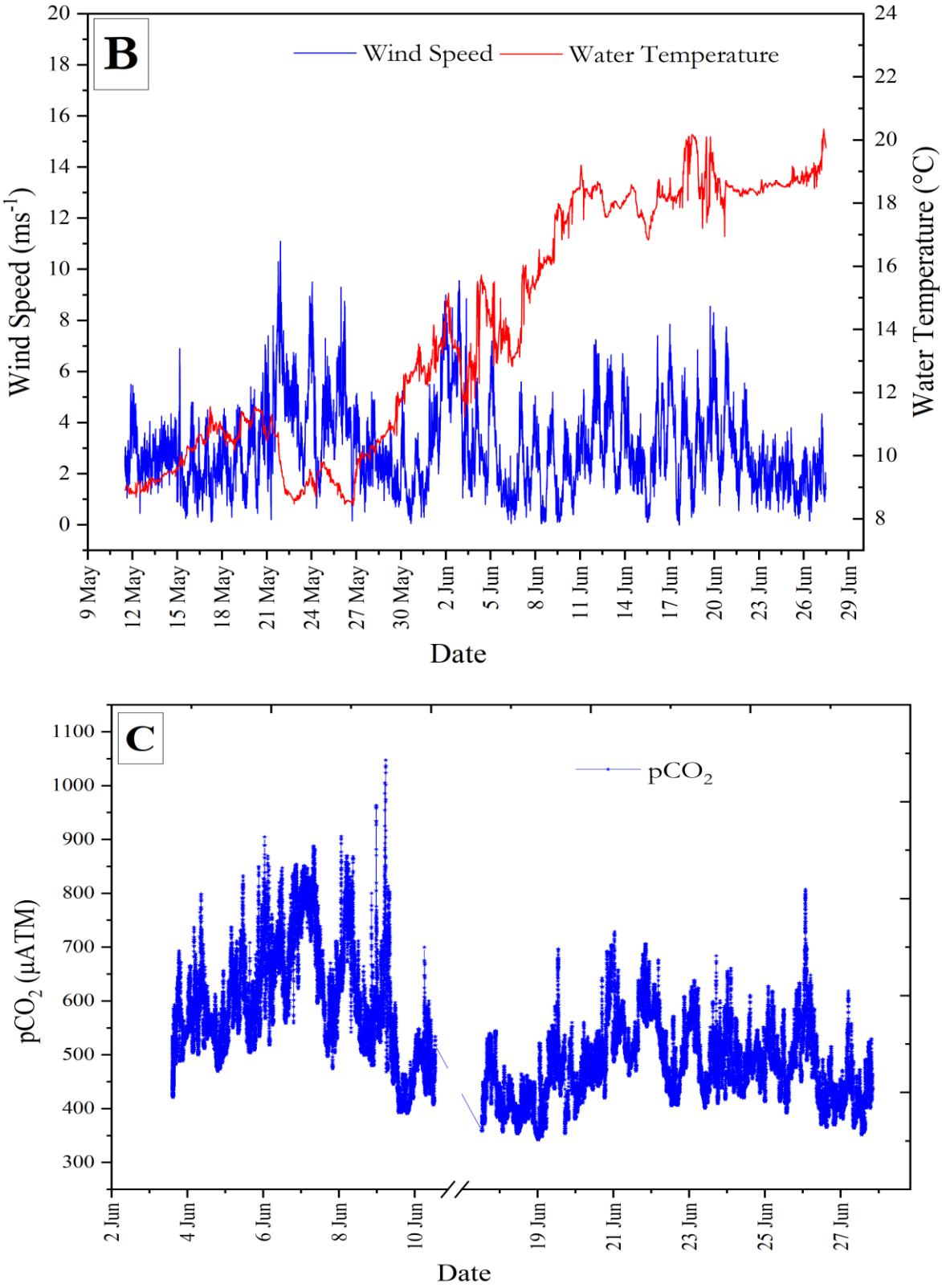

Figure 5.7 (**a**) Thirty-day time series (28 May to 28 June 2021) of the environmental parameters at Kiel Fjord including dissolved oxygen (DO) (black), salinity (blue), and temperature (red) at a 1 min sampling frequency (n = 32,820) recorded by the YSI sensor deployed near the AutoLAb

analyzer intake. (**b**) Time series data from the period 12 May to 26 June 2021, for wind speed (blue lines, left Y-axis) and water temperature (red lines, right Y-axis) obtained from GEOMAR weather metrological station. (**c**) Time series data from the period 28 May to 27 June 2021 from CONTROS HydroC-CO_2 for pCO_2 data.

Figure 5.8 shows the PO_4^{3-}, H_4SiO_4, and $\Sigma(NO_3^- + NO_2^-)$ data from the field deployment in Kiel Fjord over 46 days between May 12 and June 27. A total of 443 PO_4^{3-}, 440 Σ $(NO_3^- + NO_2^-)$, and 409 H_4SiO_4 *on-site* measurements at 66 min intervals was obtained. Outliers were mainly caused by trapped air bubbles in the flow cell and excluded from the time series. Bubbles formed either by clogging of the syringe membrane filter with sediments or by blockage in the copper net with large particles. The effect was evident from the low transmission values measured by the detector for the sample before reagent addition (i.e., before color formation). **Figure S3.5** shows the voltage readout of the photodiode detector over the whole period, wherein a reduction in values happened during some periods. One way to avoid fouling of the internal analyzer components problem is to use a tubing with a narrow inner diameter and a slow flow rate (the same approach is used for Sunburst devices (Lai, DeGrandpre, and Darlington 2018)). This was not possible with the aquarium pump used in our study as it was not possible to control the flow rate. In future applications, we will use a small pore size (e.g., 1 μm) syringe filter that will prevent internal fouling.

Rainfall data were monitored as the sum of the precipitation over a period of 12 h and measured three times per day at 0, 6, and 18 h UTC (**Figure 5.8, blue lines**).

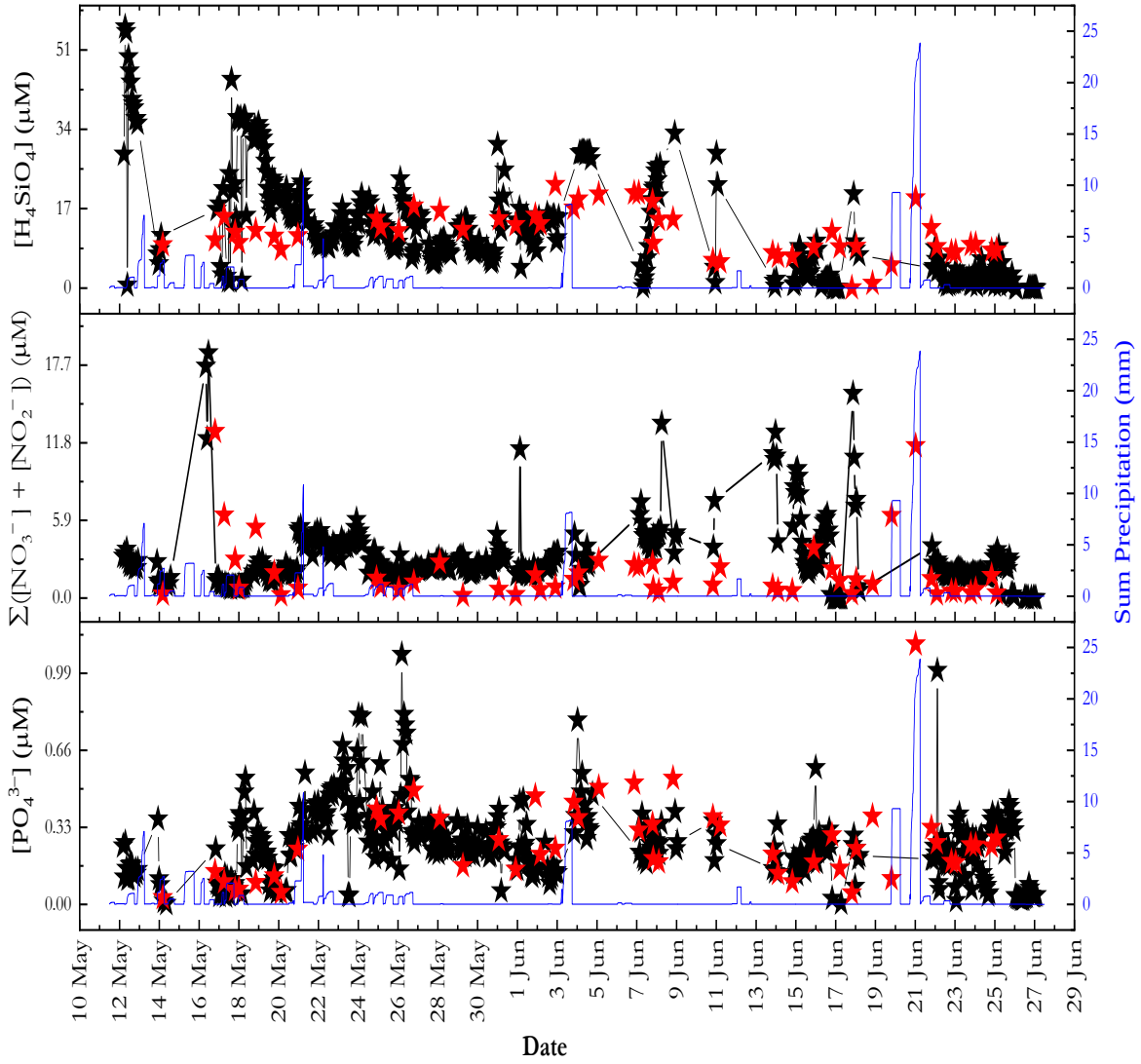

Figure 5.8 Time series data for the period of 12 May to 27 June 2021 of *on-site* PO_4^{3-}, $\Sigma(NO_3^- + NO_2^-)$, and H_4SiO_4 analyser measurements (black stars) obtained from an *on-site* analyser and from discrete samples analysed using a laboratory-based segmented flow analyser (red stars). Sum precipitation (i.e., rainfall data) were shown as blue lines. The nutrient concentrations were calculated by applying linear regression using four onboard standards.

Considering all the *on-site* data, the mean PO_4^{3-} concentration was 0.26 µM (±0.15); a minimum value of 0.0012 µM (<LOD), and a maximum value of 1.07 µM. The $\Sigma(NO_3^- + NO_2^-)$ concentrations ranged from 0.0025 (<LOD) to 18.6 µM, and the mean was 2.9 µM (±2.3). The H_4SiO_4 concentrations ranged from 0.001 µM (<LOD) to 55.9 µM; the mean was 12.2 µM (±10.4). For all data points of discrete samples (Figure 8, red stars**)**, PO_4^{3-} concentrations were in the range of 0.03–1.11 µM, and the mean was 0.27 ± 0.18 µM (n = 51). The $\Sigma(NO_3^- + NO_2^-)$ concentrations were in the range of 0.17–12.6 µM, and the mean value was 1.96 ± 2.51 µM. The H_4SiO_4 concentrations were between 0.007 µM

(<LOD) and 27.1 μM, and the mean value was 11.1 ± 4.9 μM. As one measurement cycle takes a total of 66 min, comparisons between the *on-site* data and the discrete samples (**Figure S3.6**) were made for the data points within a 30 min time interval. For PO_4^{3-} data points (n = 21) (**Figure S3.6, A**), a positive Pearson's correlation coefficient of 0.6534 was obtained. For $\Sigma(NO_3^- + NO_2^-)$ data points (n = 17) (**Figure S3.6, B**), two clear outliers were excluded from the correlation plot. A positive Pearson's correlation coefficient of 0.45 was obtained. A positive Pearson's correlation coefficient of 0.47 was determined for the H_4SiO_4 data points (n = 19) (**Figure S3.6, C**). Although no strong correlation was found between the PO_4^{3-} data points (in situ vs. discrete samples), there was no significant difference between the means at the 1% level (paired *t*-test, *p*-value = 0.729, *df* = 20), with the null hypothesis being mean (in situ) = mean (discrete samples). The same was true for the $\Sigma(NO_3^- + NO_2^-)$ data point, where a weak correlation but no significant difference between means was found (paired *t*-test, *p*-value = 0.04, *df* = 14). For H_4SiO_4, the difference between means was also not significant (paired *t*-test, *p*-value = 0.87, *df* = 18), with both the null and alternative hypotheses similar to those for PO_4^{3-} and $\Sigma(NO_3^- + NO_2^-)$. The analytical approaches appeared to be reliable to quantify nutrients under environmental conditions, as evidenced by comparison with values reported in the literature for the same time period. Fischer et al. (Fischer, Friedrichs, and Lachnit 2014) reported the concentration of macronutrients in samples collected at the institute pier at Kiel fjord at a depth of 2 m in May 2011. The mean value of H_4SiO_4 was 9.9 μM with maximum and minimum values of 14.5 μM and 5.8 μM, respectively. The mean value of PO_4^{3-} was 0.3 μM with minimum and maximum values of 0.2 μM and 0.4 μM, respectively. The mean value of NO_3^- was 0.1 μM with minimum and maximum values of 0 μM and 0.2 μM, respectively. Wasmund et al. (Wasmund et al. 2016) reported on the concentration of macronutrients in the Bornholm Basin. The Bornholm Basin is located east of the Arkona Basin on the southwestern coast of the Baltic Sea between Sweden and the island of Bornholm. For samples collected in surface waters at a depth of 5 m on 12 May 2016, the average concentrations of NO_3^-, PO_4^{3-}, and H_4SiO_4 were 0.31 μM, 0.35 μM, and 12.1 μM, respectively.

There are a variety of factors that influence the concentrations and distributions of nutrients in the water column of estuaries (e.g., fjords). The time scales of biogeochemical cycles depend on a variety of conditions, including freshwater inflow from rivers, which in turn depends on the morphology or topographic features of the fjord. Tidal flow controls the input of saline water and mixing processes. The biogeochemical cycles include microbial activity (remineralization), phytoplankton activity, grazing activity by zooplankton, and benthic exchange. In addition, anthropogenic inputs of domestic and industrial waste waters with high nutrient levels strongly affect the concentrations of macronutrients and phytoplankton growth in marine environments of densely populated urban centres (Nedwell et al. 1999; Statham 2012).

The main source of H_4SiO_4 in estuarine waters is the weathering of terrigenous rock minerals by naturally acidic rainwater (Marion 1998). Phosphorus has important anthropogenic sources (including wastewater), and following biological uptake in the surface waters is removed to subsurface waters and sediments by sinking phytoplankton debris, where it is released following remineralization. Sinking of phosphate associated with iron-oxyhydroxide particles transfers phosphate to sediments, where phosphate is released upon iron (III) reduction to iron (II) under anoxic conditions (Burdige 2021; Conley et al. 2009), and may be released to the overlying waters. A key source of nitrate to estuarine systems includes waste water discharges, but also run-off from agricultural lands of fertilizers (Nedwell et al. 1999; Latimer and Charpentier 2010).

The tidal amplitude in Kiel Fjord is low, and hence tidal currents have a low influence on the re-distribution of nutrients, which instead mainly depends on wind-driven processes [74]. **Figure S3.7** shows the relationship between the daily average concentrations of macronutrients analysed *on-site* using the analyser over the entire deployment period (12 May to 27 June) and the daily average of wind speed. A significant correlation coefficient was obtained for PO_4^{3-} ($r = 0.4$, $n = 37$), while two significant correlation coefficients ($r = 0.4$, $n = 33$) and ($r = 0.3$, $n = 31$) were obtained for $\Sigma(NO_3^- + NO_2^-)$ and H_4SiO_4, with nine points and seven points clear outliers being excluded, respectively. These outliers may be due to the fact that the distribution of nutrients in estuarine water is complicated and may be influenced by various environmental factors rather than just one factor (Statham 2012).

Remineralization of organic matter in subsurface fjord waters and sediments leads to an increase in pCO_2 (and macronutrients), with a subsequent transfer to surface waters by wind-driven mixing. As **Figure 5.9** shows, the increase in pCO_2 during the period from 03 to 10 June with a mean value of 591 μatm resulted in an increased supply of macronutrients through dissolution and respiration processes, leading to a concentration of H_4SiO_4 with a mean value of 18.1 μM, a concentration of $\Sigma(NO_3^- + NO_2^-)$ with a mean value of 3.8 μM, and a mean concentration of PO_4^{3-} of 0.3 μM. For the period from 17 June to 27, a mean value of 472 μatm was obtained for the pCO_2 value, with a mean concentration for H_4SiO_4 of 2.46 μM, a mean concentration for $\Sigma(NO_3^- + NO_2^-)$ of 2.12 μM, and a mean concentration for PO_4^{3-} of 0.2 μM (except for the clear outlier on 22 June). The slightly increased concentration of PO_4^{3-} between 17 June and 27 can be explained by the influx of freshwater, with a 2.6 decrease in salinity between the mean salinity from 2 June to 10 (mean salinity of 14.6) and 17 June to 27 (mean salinity of 11.98). Pearson's correlations were used to evaluate the relationship between pCO_2 data and the *on-site* macronutrients data, and three significant correlation models (**Figure S3.8**) were obtained over 11 days (from 4–9 June, 18 June and 22–27 June) with a correlation coefficient (r) of 0.3 ($n = 123$) between in situ pCO_2 data and *on-site* PO_4^{3-} data (*p*-value = 3.2×10^{-4}), correlation

coefficient (r) of 0.3 (n = 123) between in situ pCO_2 data and *on-site* $\Sigma(NO_3^- + NO_2^-)$ data (p-value = 8.14×10^{-4}), and correlation coefficient (r) of 0.3 (n = 108) between in situ pCO_2 data and *on-site* H_4SiO_4 (*p*-value = 0.001).

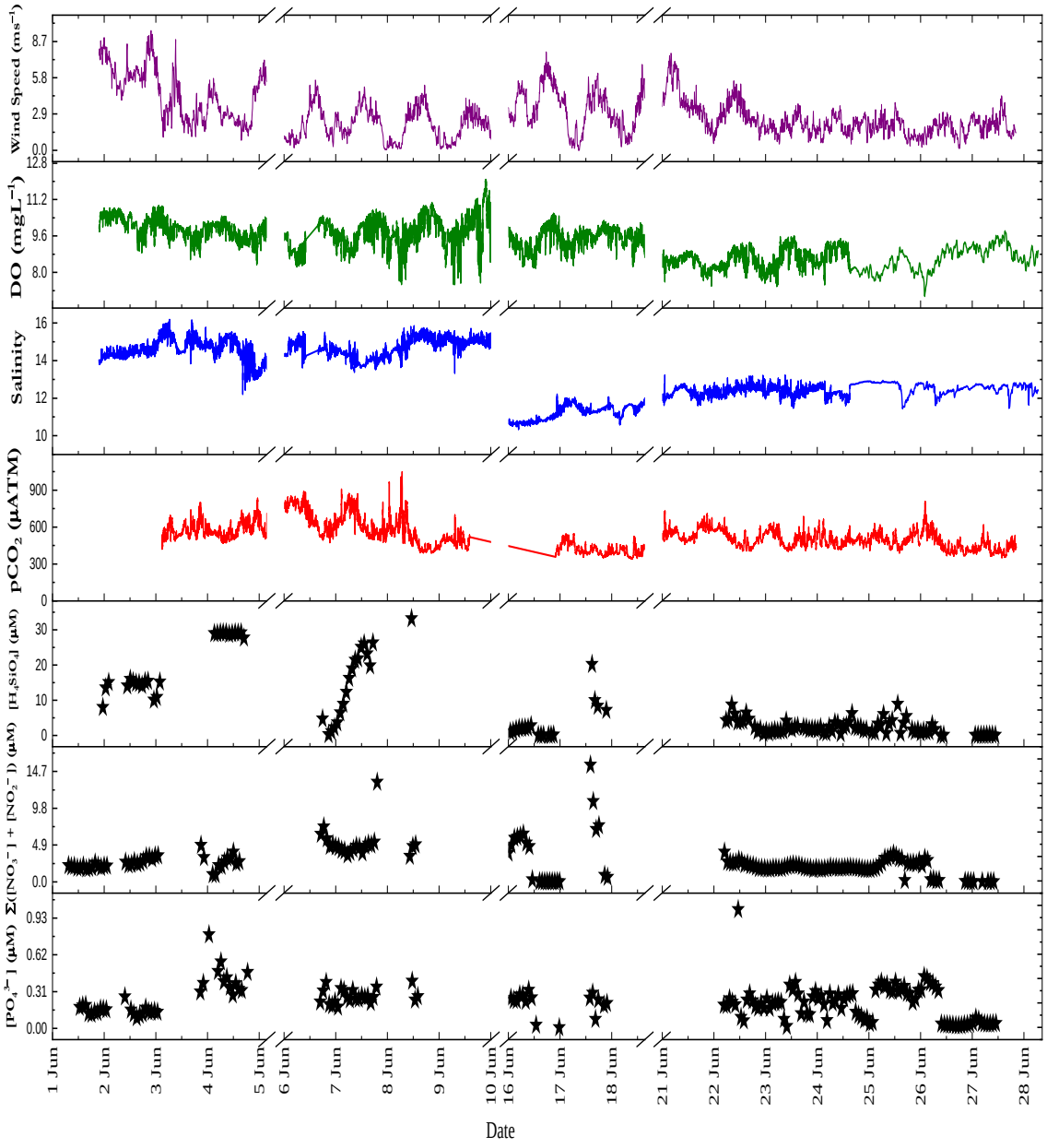

Figure 5.9 Time series data for the period from 2 June to 10 June 2021 and from 17 June to 27 June. June 2021 for PO_4^{3-}, $\Sigma(NO_3^- + NO_2^-)$, and H_4SiO_4 in µM represented by black stars; pCO_2 in µatm (red lines), DO in mgL^{-1} (green lines), salinity (blue lines), and wind speed in ms^{-1} (purple lines).

Overall, the time series data demonstrated that the *on-site* nutrient analyser was able to generate high-resolution data that helped to facilitate our ability to interpret biogeochemical processes of macronutrient cycling, benthic exchange, and water column mixing in Kiel Fjord.

5.4 Conclusions and Future Implications

This work highlights the ability of the AutoLAB multi-nutrient analyser, with optimized analytical protocols, to produce real-time, well-resolved measurements of macronutrients in the marine environment. The measurement procedure was improved by changing the measurement sequence, introducing the vandium chloride method for NO_3^- analysis and evaluating the effects of salinity fluctuations. Validations were performed by measurements of CRMs. The deployment in estuarine surface waters of the Kiel Fjord successfully captured the temporal distribution of macronutrients across a period of 46 days; the results were in good agreement with those obtained from the discrete samples analysed via a laboratory-based air-segmented flow analyser. Mean concentrations of 0.26 μM for PO_4^{3-}, 2.9 μM for $\Sigma(NO_3^- + NO_2^-)$, and 12.3 μM for H_4SiO_4 were measured in the Kiel Fjord from 12 May to 27 June 2021. The analyser successfully acquired temporal variations via 66 min time sampling intervals. The analyser was able to provide valuable information that helped to understand the nutrient dynamics of Kiel Fjord waters otherwise poorly captured via the discrete samples collection. The analyser allowed for the measurement of short-term fluctuations and also monitoring of long-term trends. Environmental variations were confirmed by other sensors placed next to the analyser at the site.

The LODs for the nutrient analysis by the analyser are indeed close to those reported in literature or for commercially available systems, but their applicability for long-term *on-site* monitoring of multiple nutrients in natural waters is limited by a range of drawbacks, including:

- The option to only determine a single nutrient by an analyzer.
- The use of a cadmium column for nitrate reduction, which may degrade by organic matter in the water, and also regular regeneration is typically needed. Our VCl_3 reduction approach therefore provides an important step forward.
- An absence of reports on long-term use or field testing in natural waters for some promising analyzers.

To further test the field application of the multi-macronutrient analyser, in situ deployments of the EnviroTech LLC's submersible units (NAS-2E) with the here-developed improved analytical protocol and vandium chloride method for NO_3^- quantification are planned in the near future.

Author Contributions: M.F.A.: investigation, methodology, visualization, writing—original draft. M.E.: validation, writing—review and editing. E.P.A.: conceptualization, funding acquisition, resources, supervision, writing—review and editing. All authors have read and agreed to the published version of the manuscript.

Funding: This research and the APC were funded by GEOMAR, Helmholtz for Ocean Research Centre, Kiel, Germany.

Acknowledgments: The authors would like thank GEOMAR for financially supporting this study. Andre Mutzberg is thanked for analysing the discrete nutrient samples. We are grateful to Truls Johannessen for providing us the AutoLAB analyser. We thank Ute Hecht for providing wind speed, water temperature, and rainfall data, and Christian Begler for providing pCO2 data. Many thanks to Bjoern Buchholz for allowing us to conduct our deployment at the GEOMAR institute pier. M.F. Altahan wishes to thank the National Water Research Center (NWRC). We also thank two anonymous reviewers for their useful comments on this manuscript.

Conflicts of Interest: The authors declare no-conflict of interest.

5.5 Supplementary Information

Table S3.1 Detailed Procedure for measurements during the analyzer deployment with the number of ports as mentioned in Figure 5.2

		Step		Port open	Linear movement[a]		Operation & Description
		1	a	3	4500 (r[b])		Draw up the cleaning solution into the syringe and all detectors, and set the light intensity for blank measurement.
			b	8	4500 (i[c])		
			c	3	4500 (r)		
			d	15	4500 (i)		
			e	3	4500 (r)		
			f	16	4500 (i)		
		2		4	4500 (i)		Initialize the syringe motor and detector, align the switching valve and ensure that the syringe plunger is fully retracted.
PO_4^{3-} Calibratio	Blank	3	a	7	4500 (r)	2x flushing	Washing the syringe and the PO_4^{3-} detector with deionized water
			b	8	4500 (i)		
		4	a	7	2700 (r)		Draw up the blank and set the light intensity for the reference (I^R, V^R)
			b	4	1350 (i)		

			c	8	1350 (i)		
		5	a	8	720 (r)		Withdraw the blank from the flow cell and add R1 (Molybdate mixed reagent) and R2 (Ascorbic Acid)
			b	9	180 (r)		
			c	10	180 (r)		
		6	a	8	450 (i) 450 (r)	4x mixing	Mixing the reagent with the blank and inject the reaction mixture inside the detector and waiting for 3 minutes for color development and set the light intensity for the measurement (V, I)
			b	4	180 (i)		
			c	8	900 (i)		
	Standard 1, 2, 3	7	a	7	4500 (r)	2x flushing	Washing the syringe and the PO_4^{3-} detector with deionized water
			b	8	4500 (i)		
		8	a	13(14, 2)[d]	4500 (r)	2x flushing	Washing the syringe and the PO_4^{3-} detector with STD1 (STD2, STD3)
			b	8	4500 (i)		
		9	a	13(14, 2)	2700 (r)		Draw up STD1(STD2, STD3) and set the light intensity for the reference (I^R, V^R)
			b	4	1350 (i)		
			c	8	1350 (i)		
		10	a	8	720 (r)		Withdraw STD1 from the flow cell and add R1 and R2
			b	9	180 (r)		
			c	10	180 (r)		
		11	a	8	450 (i) 450 (r)	4x mixing	Mixing the reagent with STD1 and inject the reaction mixture inside the detector and waiting for 3 minutes for color development and set the light intensity for the measurement (V, I)
			b	4	180 (i)		
			c	8	900 (i)		
washing		12	a	3	4500 (r)		Draw up the cleaning solution into the syringe and all detectors, and set the light intensity for blank measurement.
			b	8	4500 (i)		
			c	3	4500 (r)		
			d	15	4500 (i)		
			e	3	4500 (r)		
			f	16	4500 (i)		
Σ (NO_3^- + NO_2^-) Calibration	Blank	13		4	4500 (i)		Initialize the syringe motor and detector, align the switching valve and ensure that the syringe plunger is fully retracted.
		14	a	7	4500 (r)	2x flushing	Washing the syringe and the PO_4^{3-} detector with deionized water
			b	8	4500 (i)		
		15	a	7	4500 (r)	2x flushing	Washing the syringe and the Σ (NO_3^- + NO_2^-) detector with deionized water
			b	16	4500 (i)		
		16	a	7	2700 (r)		Draw up the blank and set the light intensity for the reference (I^R, V^R)
			b	4	700 (i)		
			c	16	2000 (i)		
		17	a	16	1440 (r)		Withdraw the blank from the flow cell and add mixed reagent (Griess reagent + VCl_3)
			b	5	360 (r)		
		18		16	450 (i) 450 (r)	4x mixing	Mixing the blank with the reagent

		19		8	1800 (i)		Waiting 30 minutes into PO_4^{3-} detector to allow NO_3^- reduction during incubation with VCl_3 reagent at maximum temperature (~ 50 °C).
		20	a	8	1800 (r)		Withdraw the reaction mixture from the PO_4^{3-} detector, waiting 2 min. inside the syringe housing to cool the mixture and open the Σ (NO_3^- + NO_2^-) detector, inject the mixture and set light intensity for the measurement (V, I)
			b	4	225 (i)		
			c	16	1575(i)		
	Standard 1, 2, 3	21	a	7	4500 (r)	2x flushing	Washing the syringe and the PO_4^{3-} detector with deionized water
			b	8	4500 (i)		
		22	a	7	4500 (r)	2x flushing	Washing the syringe and the Σ (NO_3^- + NO_2^-) detector with deionized water
			b	16	4500 (i)		
		23	a	13(14, 2)	4500 (r)	2x flushing	Washing the syringe and the Σ (NO_3^- + NO_2^-) detector with STD1 (STD2, STD3)
			b	16	4500 (i)		
		24	a	13(14, 2)	2700 (r)		Draw up STD1 (STD2, STD3) and set the light intensity for the reference (I^R, V^R)
			b	4	700 (i)		
			c	16	2000 (i)		
		25	a	16	1440 (r)		Withdraw STD1 (STD2, STD3) from the flow cell and add mixed reagent (Griess reagent + VCl_3)
			b	5	360 (r)		
		26		16	450 (i)	4x mixing	Mixing STD1 (STD2, STD3) with the reagent
					450 (r)		
		27		8	1800 (i)		Waiting 30 minutes into PO_4^{3-} detector to allow NO_3^- reduction during incubation with VCl_3 reagent at maximum temperature (~ 50 °C).
		28	a	8	1800 (r)		Withdraw the reaction mixture from the PO_4^{3-} detector, waiting 2 min. inside the syringe housing to cool the mixture and open the Σ (NO_3^- + NO_2^-) detector and inject the mixture and set light intensity for the measurement (V, I)
			b	4	225 (i)		
			c	16	1575(i)		
washing		29	a	3	4500 (r)		Draw up the cleaning solution into the syringe and all detectors, and set the light intensity for blank measurement.
			b	8	4500 (i)		
			c	3	4500 (r)		
			d	15	4500 (i)		
			e	3	4500 (r)		
			f	16	4500 (i)		
H_4O_4Si Calibration		30		4	4500 (i)		Initialize the syringe motor and detector, align the switching valve and ensure that the syringe plunger is fully retracted.
	Blank	31	a	7	4500 (r)	2x flushing	Washing the syringe and the H_4SiO_4 detector with deionized water
			b	15	4500 (i)		
		32	a	7	2700 (r)		Draw up the blank and set the light intensity for the reference (I^R, V^R)
			b	4	1350 (i)		
			c	15	1350 (i)		
		33	a	15	225 (r)		Withdraw the blank from the flow cell and add R1(molybdic acid)
			b	11	225 (r)		
					300 (i)		

		34		15	300 (r)	4x mixing	Mixing the blank and R1 and waiting 3 min for complexation
		35	a	12	225 (r)		Add R2 (Oxalic acid) and R3 (Ascorbic Acid) to the reaction mixture
			b	10	225 (r)		
		36		15	450 (i) 450 (r)	4x Mixing	Mixing the blank and the reagents
		37	a	4	225 (i)		Inject the reaction mixture into the H_4SiO_4 detector and set the light intensity for measurement (V, I)
			b	15	675 (i)		
	Standard 1, 2, 3	38	a	7	4500 (r)	2x flushing	Washing the syringe and the H_4SiO_4 detector with deionized water
			b	15	4500 (i)		
		39	a	13(14, 2)	4500 (r)	2x flushing	Washing the syringe and the H_4SiO_4 detector with STD1 (STD2, STD3)
			b	15	4500 (i)		
		40	a	13(14, 2)	2700 (r)		Draw up STD1 (STD2, STD3) and set the light intensity for the reference (I^R, V^R)
			b	4	1350 (i)		
			c	15	1350 (i)		
		41	a	15	225 (r)		Withdraw STD1 (STD2, STD3) from the flow cell add R1(molybdic acid)
			b	11	225 (r)		
		42		15	300 (i) 300 (r)	4x mixing	Mixing STD1 (STD2, STD3) and R1 and waiting 3 min for complexation
		43	a	12	225 (r)		Add R2 (Oxalic acid) and R3 (Ascorbic Acid) to the reaction mixture
			b	10	225 (r)		
		44		15	450 (i) 450 (r)	4x Mixing	Mixing STD1 (STD2, STD3) and the reagents
		45	a	4	225 (i)		Inject the reaction mixture into the H_4SiO_4 detector and set the light intensity for measurement (V, I)
			b	15	675 (i)		
washing		46	a	3	4500 (r)		Draw up the cleaning solution into the syringe and all detectors, and set the light intensity for blank measurement.
			b	8	4500 (i)		
			c	3	4500 (r)		
			d	15	4500 (i)		
			e	3	4500 (r)		
			f	16	4500 (i)		
CRM	PO_4^{3-} determination	47		4	4500 (i)		Initialize the syringe motor and detector, align the switching valve and ensure that the syringe plunger is fully retracted.
		48	a	7	4500 (r)	2x flushing	Washing the syringe and the PO_4^{3-} detector with deionized water
			b	8	4500 (i)		
		49		6	4500 (r)	2x flushing	Washing the syringe and the PO_4^{3-} detector with CRM
				8	4500 (i)		
		50	a	6	2700 (r)		Draw up CRM and set the light intensity for the reference (I^R, V^R)
			b	4	1350 (i)		
			c	8	1350 (i)		
		51	a	8	720 (r)		Withdraw CRM from the flow cell and add R1 (Molybdate mixed reagent) and R2 (Ascorbic Acid)
			b	9	180 (r)		
			c	10	180 (r)		
		52		8	450 (i) 450 (r)	4x mixing	Mixing the reagent with CRM and inject the reaction mixture inside the detector and waiting for

				4	180 (i)		3 minutes for color development and set the light intensity for the measurement (V, I)
				8	900 (i)		
	Σ (NO_3^- + NO_2^-) determination	53	a	7	4500 (r)	2x flushing	Washing the syringe and the PO_4^{3-} detector with deionized water
			b	8	4500 (i)		
		54	a	6	4500 (r)	2x flushing	Washing the syringe and the Σ (NO_3^- + NO_2^-) detector with CRM
			b	16	4500 (i)		
		55	a	6	2700 (r)		Draw up CRM and set the light intensity for the reference (I^R, V^R)
			b	4	700 (i)		
			c	16	2000 (i)		
		56	a	16	1440 (r)		Withdraw CRM from the flow cell and add mixed reagent (Griess reagent + VCl_3)
			b	5	360 (r)		
		57		16	450 (i)	4x mixing	Mixing CRM with the reagent
					450 (r)		
		58		8	1800 (i)		Waiting 30 minutes into PO_4^{3-} detector to allow NO_3^- reduction during incubation with VCl_3 reagent at maximum temperature (~ 50 °C).
		59	a	8	1800 (r)		Withdraw the reaction mixture from the PO_4^{3-} detector, waiting 2 min. inside the syringe housing to cool the mixture and open the Σ (NO_3^- + NO_2^-) detector and inject the mixture and set light intensity for the measurement (V, I)
			b	4	225 (i)		
			c	16	1575 (i)		
	H_4O_4Si determination	60	a	7	4500 (r)	2x flushing	Washing the syringe and the H_4SiO_4 detector with deionized water
			b	15	4500 (i)		
		61	a	6	4500 (r)	2x flushing	Washing the syringe and the H_4SiO_4 detector with CRM
			b	15	4500 (i)		
		62	a	6	2700 (r)		Draw up CRM and set the light intensity for the reference (I^R, V^R)
			b	4	1350 (i)		
			c	15	1350 (i)		
		64	a	15	225 (r)		Withdraw CRM from the flow cell and add R1(molybdic acid)
			b	11	225 (r)		
		65		15	300 (i)	4x mixing	Mixing CRM and R1 then waiting 3 min for complexation
					300 (r)		
		66	a	12	225 (r)		Add R2 (Oxalic acid) and R3 (Ascorbic Acid) to the reaction mixture
			b	10	225 (r)		
		67		15	450 (i)	4x Mixing	Mixing CRM and the reagents
					450 (r)		
		68	a	4	225 (i)		Inject the reaction mixture into the H4SiO4 detector and set the light intensity for measurement (V, I)
			b	15	675 (i)		
washing		69	a	3	4500 (r)		Draw up the cleaning solution into the syringe and all detectors, and set the light intensity for blank measurement.
			b	8	4500 (i)		
			c	3	4500 (r)		
			d	15	4500 (i)		

			e	3	4500 (r)			
			f	16	4500 (i)			
Sea water	PO_4^{3-} determination	70		4	4500 (i)		Initialize the syringe motor and detector, align the switching valve and ensure that the syringe plunger is fully retracted.	10 x (measurement loop)
		71	a	1	4500 (r)	6x flushing	Washing the syringe and the PO_4^{3-} detector with seawater	
			b	8	4500 (i)			
		72	a	1	2700 (r)		Draw up seawater and set the light intensity for the reference (I^R, V^R)	
			b	4	1350 (i)			
			c	8	1350 (i)			
		73	a	8	720 (r)		Withdraw seawater from the flow cell and add R1 (Molybdate mixed reagent) and R2 (Ascorbic Acid)	
			b	9	180 (r)			
			c	10	180 (r)			
		74	a	8	450 (i)	4x mixing	Mixing the reagent with seawater and inject the reaction mixture inside the detector and waiting for 3 minutes for color development and set the light intensity for the measurement (V, I)	
					450 (r)			
			b	4	180 (i)			
			c	8	900 (i)			
	$\Sigma (NO_3^- + NO_2^-)$ determination	75	a	1	4500 (r)	6x flushing	Washing the syringe and the $\Sigma (NO_3^- + NO_2^-)$ detector with seawater	
			b	16	4500 (i)			
		76	a	1	2700 (r)		Draw up seawater and set the light intensity for the reference (I^R, V^R)	
			b	4	700 (i)			
				16	2000 (i)			
		77	a	16	1440 (r)		Withdraw seawater from the flow cell and add mixed reagent (Griess reagent + VCl_3)	
			b	5	360 (r)			
		78		16	450 (i)	4x mixing	Mixing seawater with the reagent	
					450 (r)			
		79		8	1800 (i)		Waiting 30 minutes into PO_4^{3-} detector to allow NO_3^- reduction during incubation with VCl_3 reagent at maximum temperature (~ 50 °C).	
		80	a	8	1800 (r)		Withdraw the reaction mixture from the PO_4^{3-} detector, waiting 2 min. inside the syringe housing to cool the mixture and open the $\Sigma (NO_3^- + NO_2^-)$ detector and inject the mixture and set light intensity for the measurement (V, I)	
			b	4	225 (i)			
			c	16	1575 (i)			
	H_4O_4Si determination	81	a	1	4500 (r)	6x flushing	Washing the syringe and the H_4SiO_4 detector with seawater	
			b	15	4500 (i)			
		82	a	1	2700 (r)		Draw up seawater and set the light intensity for the reference (I^R, V^R)	
			b	4	1350 (i)			
			c	15	1350 (i)			
		83	a	15	225 (r)		Withdraw seawater from the flow cell and add R1(molybdic acid)	
			b	11	225 (r)			
		84		15	300 (i)	4x mixing	Mixing seawater and R1 then waiting 3 min for complexation	
					300 (r)			
		85	a	12	225 (r)		Add R2 (Oxalic acid) and R3 (Ascorbic Acid) to the reaction mixture	
			b	10	225 (r)			
					450 (i)	4x		

		86		15	450 (r)	Mixing	Mixing seawater and the reagents	
		87	a	4	225 (i)		Inject the reaction mixture into the H_4SiO_4 detector and set the light intensity for measurement (V, I)	

[a] maximum movement of the syringe is 4500 (~2.2 ml)

[b] r: retract; [c] i: inject

[d] port 13: STD1, port 14: STD2, port 2: STD3

Table S3.2 Slopes and intercepts including their standard deviations, t-values and the probabilities for the calibration curves in Figure 5.6.

		Value	Standard deviation	t-value	Probability
NO_3^-	**Int.**	0.06876	6.85×10^{-4}	100.42	1.079×10^{-13}
	Slp.	0.00614	9.76×10^{-5}	62.94	4.51×10^{-12}
NO_2^-	**Int.**	0.04061	0.00228	17.77	1.028×10^{-7}
	Slp.	0.01202	2.94×10^{-4}	40.87	1.414×10^{-10}
PO_4^{3-}	**Int.**	0.00191	4.88×10^{-4}	3.9	0.00294
	Slp.	0.01211	8.46×10^{-5}	143.1	5×10^{-10}
H_4SiO_4	**Int.**	-0.00632	0.00351	-1.8	0.10199
	Slp.	0.02377	6.48×10^{-4}	36.65	5.44×10^{-12}

Int.: Intercept, Slp. : Slope

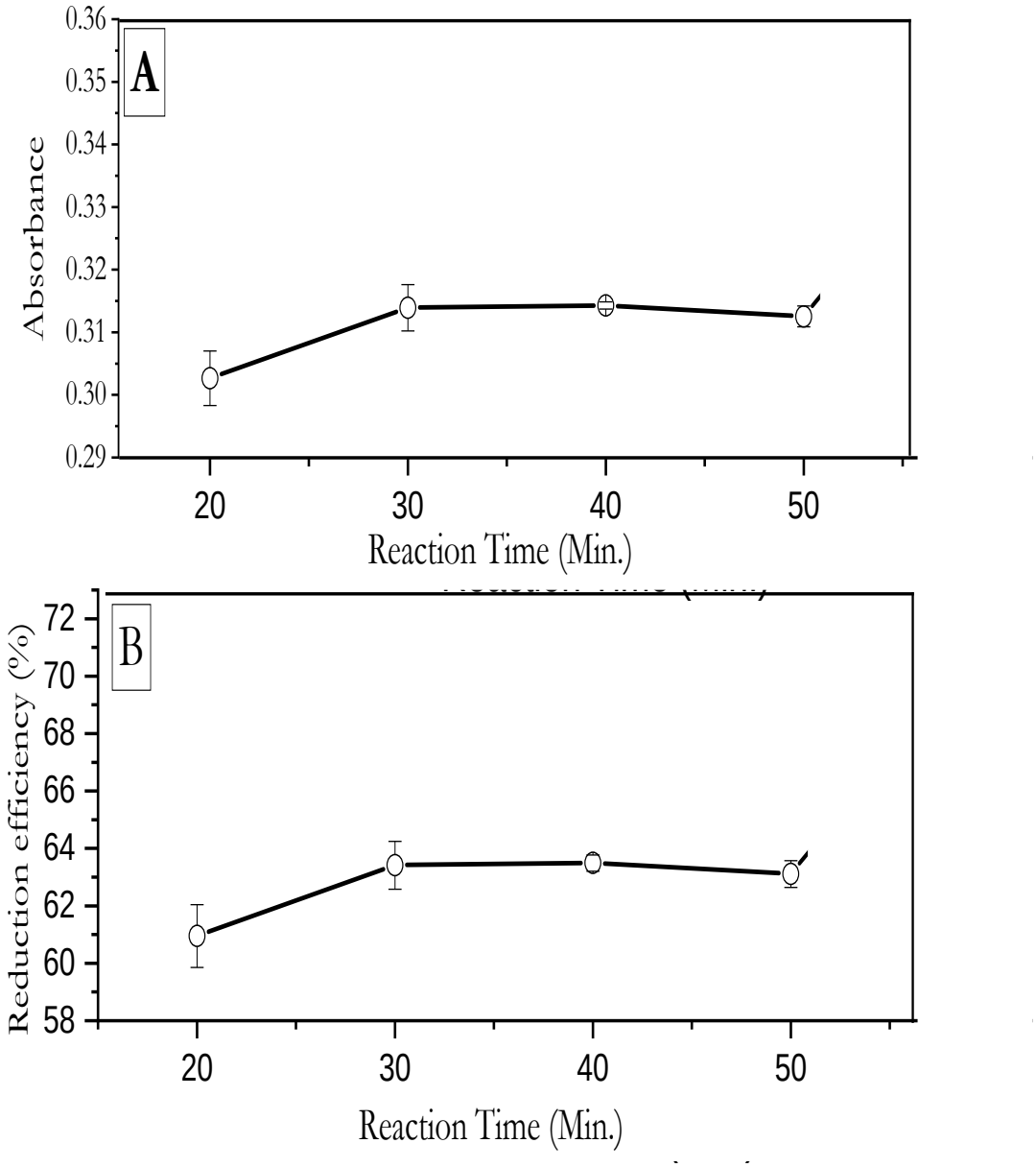

Figure S3.1 Effect of reaction time in minutes on (A) the absorbance of 10 μM NO_3^- and (B) the reduction efficiency (%) which defined as the ratio of the absorbance of 10 μM NO_3^- and the absorbance of 10 μM NO_2^-.

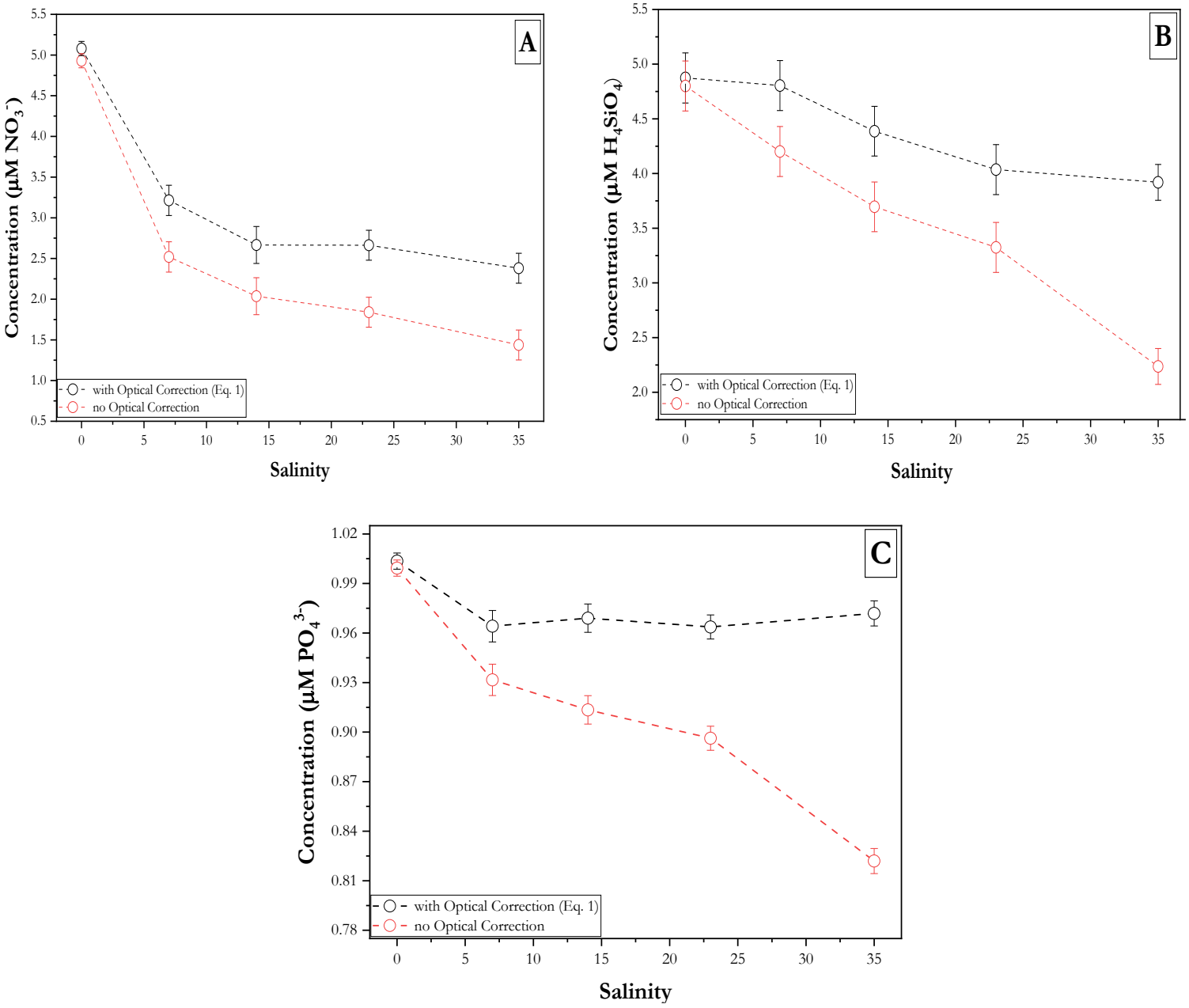

Figure S3.2 (A) calculated concentrations of 5 µM NO_3^-, (B) calculated concentrations of 5 µM H_4O_4Si and (C) calculated concentrations of 1 µM PO_4^{3-} samples with different salinity (0, 7, 14, 23, 35) based on calibration curves of (0, 1, 5 and 10 µM NO_3^-), (0, 1, 5, 10 µM H_4O_4Si) and (0, 0.5, 1, 2 µM PO_4^{3-}), respectively. The raw data were processed using equation 1 (black circles) and the red circles represent the data processed using the traditional Beer's Law equation ($A = -log_{10}(\frac{I}{I_0})$). Error bar (±1 SD), n = 10.

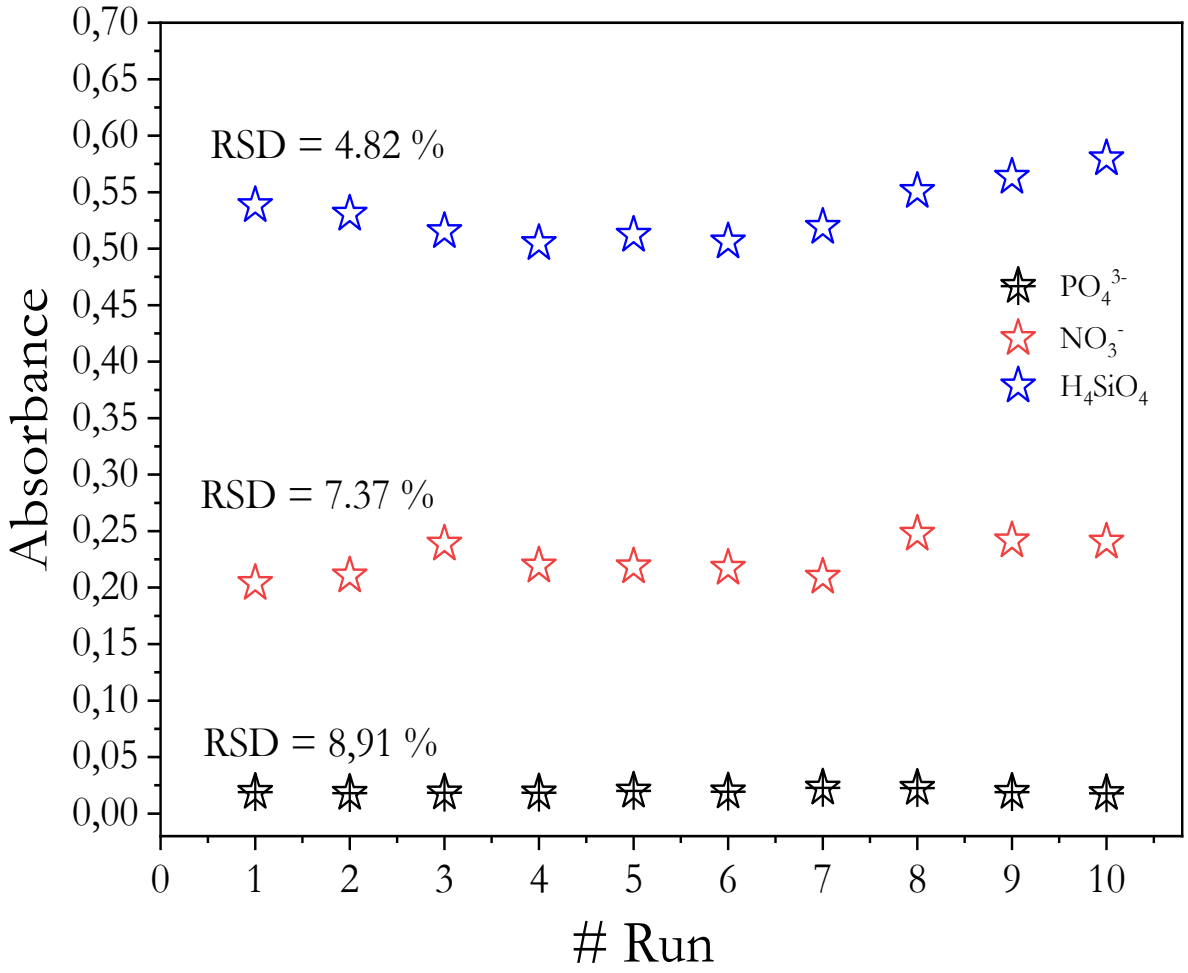

Figure S3.3 The measured absorbance value of KANSO CRM for nutrients for 6 consecutive runs of PO_4^{3-}, NO_3^-, and H_4O_4Si with RSD (relative standard deviation) value. The Certified value for CRM is 23.7 ± 0.2 µM for NO_3^-, 56.4 ± 0.5 µM for H_4O_4Si, and 1.7 ± 0.02 µM for PO_4^{3-}.

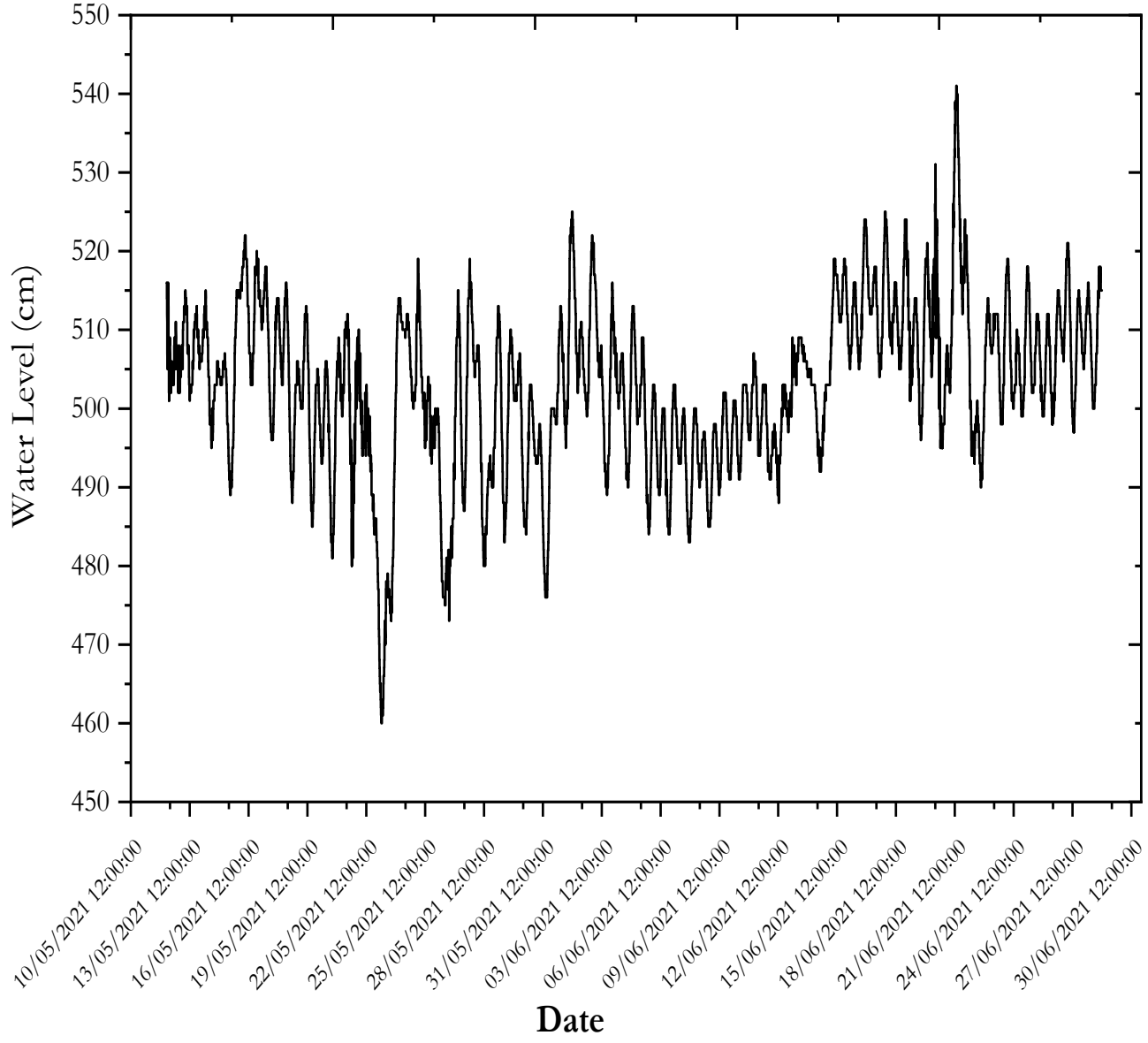

Figure S3.4 Time series data for the period from May 12 to June 28, 2021, for water level data at the kiel-Holtenau station obtained from the Federal Waterways and Shipping Administration (WSV).

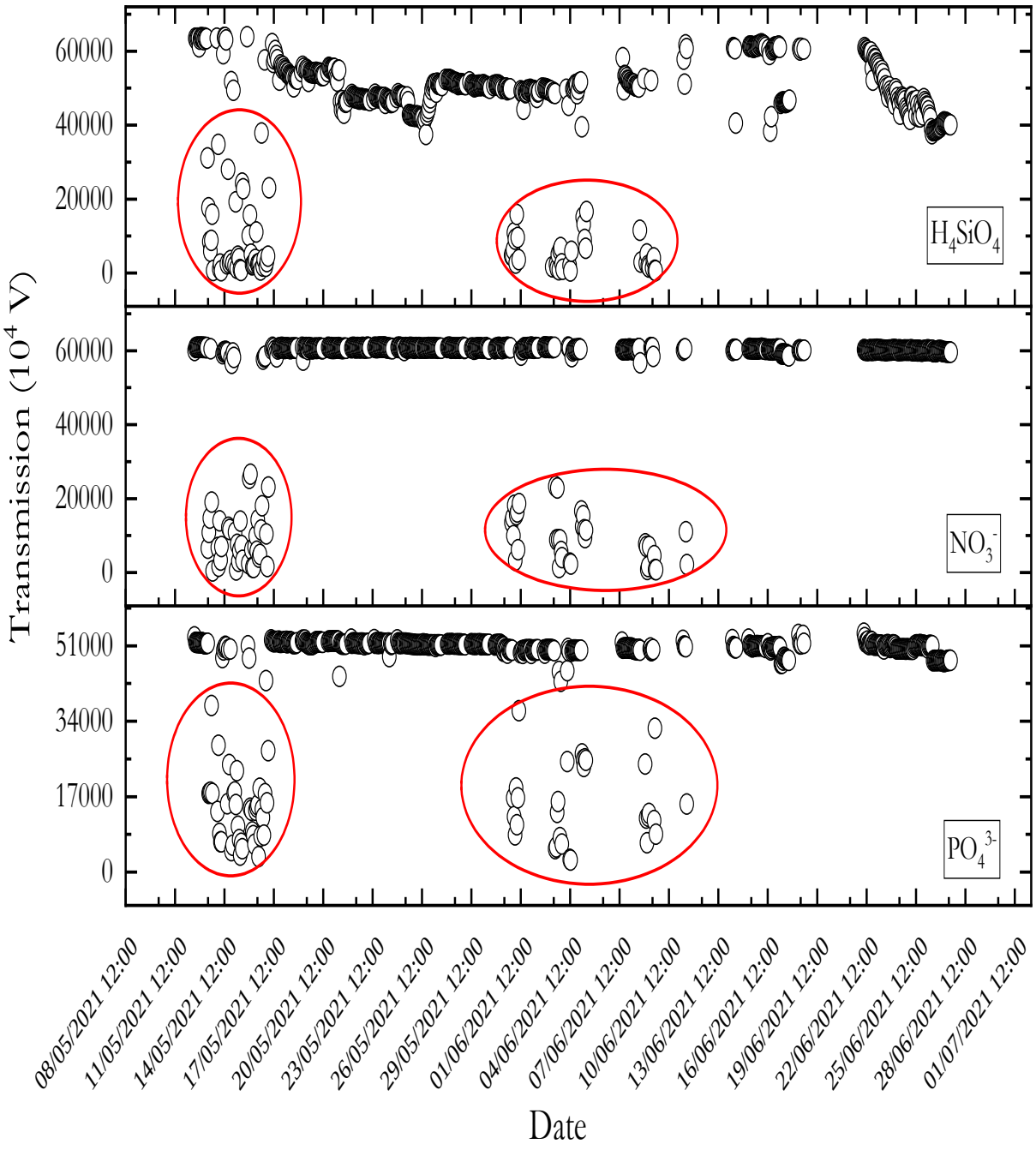

Figure S3.5 Time series data from May 12 to June 26, 2021, of PO_4^{3-}, NO_3^-, and H_4O_4Si photodiode detector readout; the points in red circles refer to the drop-down of the transmission values due to air bubbles trapped into the flow cell.

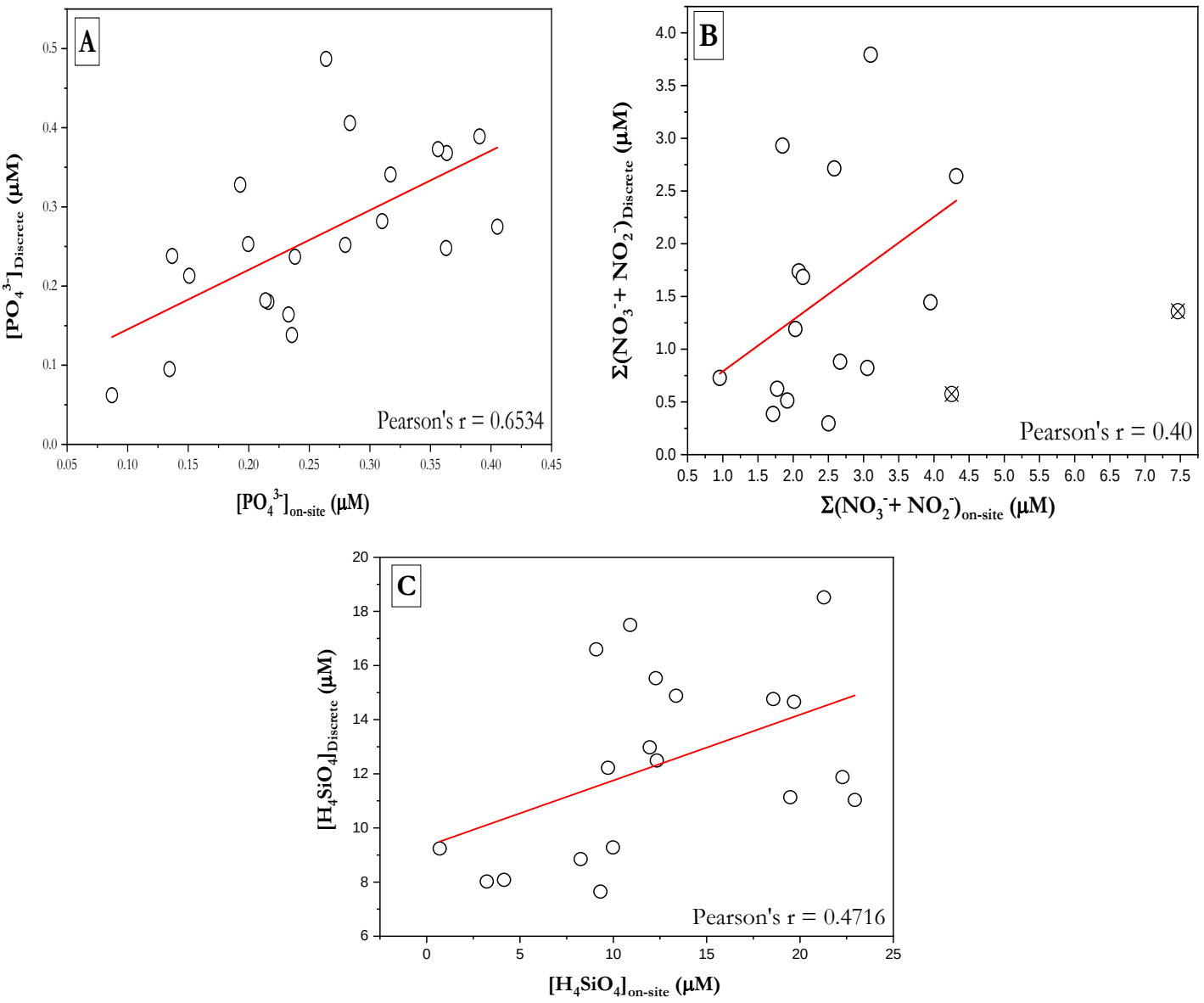

Figure S3.6 Property-to-property plots for (A) PO_4^{3-} in µM measured on-site with the AutoLAB analyser compared to synchronised PO_4^{3-} in µM measured with the air-segment analyser in the laboratory for discretely collected samples pearson'r = 0.6534, n = 21 , (B) $\Sigma(NO_3^- + NO_2^-)$ in µM measured on-site with the AutoLAB analyser compared to synchronised $\Sigma(NO_3^- + NO_2^-)$ in µM with the air-segment analyser in the laboratory for discretely collected samples, pearson'r = 0.4, n =17, two clear outliers (X) were removed and (C) H_4SiO_4 in µM measured on-site with the AutoLAB analyser compared to synchronised H_4SiO_4 in µM measured with the air-segment analyser in the laboratory for discretely collected samples, pearson'r = 0.4716, n = 19.

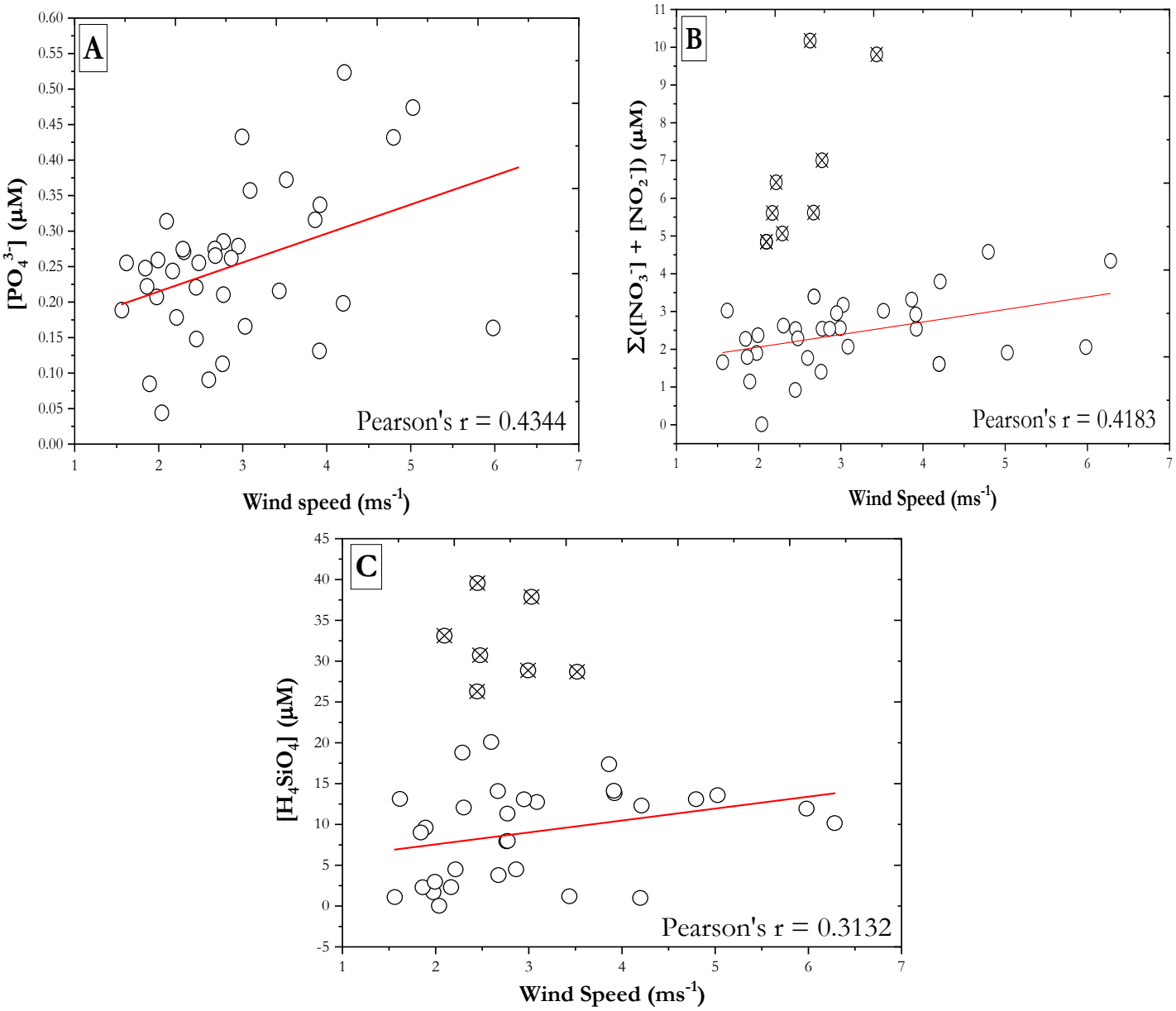

Figure S3.7 Plot-by-plot plots from 12 May to 27 June 2021 for (A) the daily average of on-site PO_4^{3-} concentration in µM versus the daily average of wind speed in ms^{-1}, (B) the daily average of on-site $\Sigma(NO_3^- + NO_2^-)$ concentration in µM versus the daily average of wind speed in ms^{-1}. the daily average of wind speed in ms-1, excluding clear outliers (9 points) (X), and (C) the daily average of H_4SiO_4 concentration in µM measured on site compared to the daily average of wind speed in ms^{-1}, excluding clear outliers (7 points) (X).

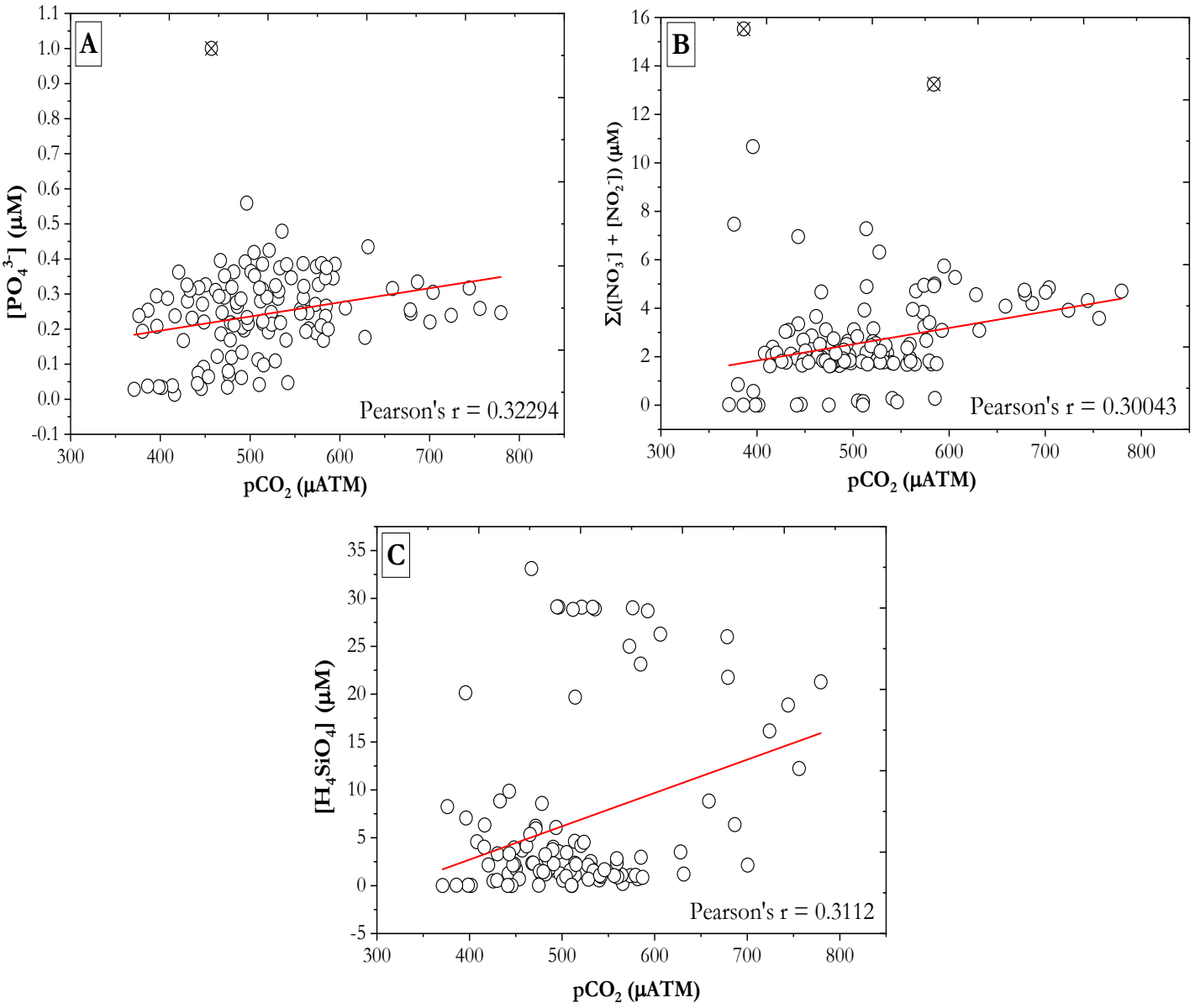

Figure S3.8 Plot-by-plot plots for the 11-day period from June 4 to June 9 and from June 18 and June 22 to June 27, 2021 for (A) in situ pCO_2 data compared to on-site PO_4^{3-} measured by AutoLab with a unique outlier (X) was excluded (pearson'r = 0.32294, n = 122), (B) in situ pCO_2 data compared with on-site $\Sigma(NO_3^- + NO_2^-)$ measured by AutoLab with two clear outliers (X) excluded (pearson'r = 0.30034, n = 122), and (C) in situ pCO_2 data compared with on-site H_4SiO_4 measured by AutoLab (pearson'r = 0.3112, n = 108).

6 Overall conclusions and future directions

This dissertation describes the development, improvement, and testing of analysers for macronutrients in marine waters. Concentrations of macronutrients such as phosphate, nitrite, nitrate, and silicic acid play a key role in biogeochemical processes in marine waters, controlling primary production and thus oxygen and carbon dioxide removal from the atmosphere, and playing a role in climate change. My aim was achieved through the following: (1) Development of a new electrochemical method for PO_4^{3-} in seawater, detailed description of laboratory-based characterization to exclude confounding effects and obtain the best sensitivity with further validation for analysis of discrete samples collected during a research cruise in the North Sea, (2) Deployment of our new electrochemical method in an autonomous flow injection analyser with application of a bi-potentiostat for a more reliable analysis with correction of matrix interferences and temporal variations of electrode sensitivity with further validation by on-board application of the analyser on a research cruise in the south-eastern North Sea.(3) Improvement of the field-available commercial sensor for macronutrients by adapting the measurement routine and applying a new vanadium chloride-nitrate reduction method and validation by analysis of CRMs and field tests over one month (46 days) in the Kiel Inner Fjord (southwestern Baltic Sea).

(1) Electrochemical determination of PO_4^{3-}

In Chapter 3, I first describe the development of a carbon paste electrode pre-treated with ammonium molybdate by cyclic voltammetry (CV) for 10 sampling cycles at a sampling rate of 0.1 Vs^{-1} in 0.1 M NaOH. During the pretreatment, the molybdate trioxide anion (MoO_4^{2-}) is formed on the surface of the working electrode, which can react with PO_4^{3-} to form the phosphomolybdate complex $[PMo_{12}O_{40}]^{3-}$. Scanning electron microscopy was used to characterise the modified electrode and to study the morphology, and energy dispersive electron microscopy was used to study the atomic composition of the electrode surface. Molybdate/CPE showed the following atomic composition (95.7% carbon: 3.42% oxygen: 0.85% molybdate). After CV in 0.1 NaOH, the atomic composition of the electrode surface changed as follows (89.9% carbon: 8.51% oxygen: 1.51% molybdate), demonstrating the high concentration of molybdate oxide. The interaction between MoO_4^{2-} and PO_4^{3-} in the phosphomolybdate complex was demonstrated by the distribution of phosphorus in the elemental analysis.

The modified electrode was used in square-wave voltammetry employing a Metrohm µ-AutoLab III potentiostat for PO_4^{3-} determination in artificial seawater (30 g/L NaCl) under strongly acidic conditions (pH 0.8) after a rest period (75 seconds) at a square-wave amplitude of 50 mV, a square-

wave frequency of 150 Hz, and a step potential of 1 mV. Optimization of the analytical conditions was studied in detail, including the pH of the medium, the square wave parameters, including amplitude and frequency, and the quiescent time. The pH of the medium is very important because the reaction of phosphate with molybdate should occur under acidic conditions. The highest peak current was obtained at pH 0.8 and pH 0.6, where pH 0.8 was chosen to reduce the sulfuric acid required for acidification. The quiet time is of great importance because it is the time between removal of the electrodes from a strongly basic medium (0.1 M NaOH, pH ~ 12.5) and inserting it to a strongly acidic medium (pH 0.8). The impedimetric performance was also studied to compare the CPE and molybdate/CPE in 0.1 M PO_4^{3-} in artificial seawater (30 g/L NaCl) pH 0.8, where the charge transfer resistance obtained from the equivalent circuit to fit the experimental impedimetric data for the CPE was 1.838 X 106 Ω and 1.173 Ω for molybdate/CPE, showing the fast kinetics of electrons in the presence of PO_4^{3-} on the working electrodes. A linear calibration plot with a linear inverse relationship between PO_4^{3-} concentrations and the charge transfer resistance was obtained over a concentration range of 0.1, 0.2, 0.3, 0.5, 0.8, and 1 M PO_4^{3-} with an analytical sensitivity of -431.6 $\mu M.\Omega^{-1}$ and a detection coefficient (R^2) of 0.981. The calibration plot was used for square wave voltammetry for a range of PO_4^{3-} concentrations (0.01 - 3 μM), obtaining two regions of linear behaviour, the first over a concentration range from 0.01 to 0.4 μM PO_4^{3-}, where the analytical sensitivity was 13.97 $\mu M.\mu A^{-1}$ and R^2 of 0.98, while the second over a concentration range from 1 to 4 μM with an analytical sensitivity of 0.30225 $\mu M.\mu A^{-1}$ and R^2 of 0.99, where the limit of determination (LOD) was 0.003 μM. Repeatability, reproducibility and stability of molybdate/CPE showed good values as evidenced by a relative standard deviation (RSD) of 5.76% and 4.32% for 0.2 and 5 μM PO_4^{3-}, respectively, for 10 repeated measurements. The RSD value of 5.46 % was obtained for 5 μM PO_4^{3-} over five sets of different newly modified electrodes, and the RSD value of 7.26% was obtained for 5 μM PO_4^{3-} measured on the same modified electrode over five days, indicating the degree to which our proposed electrode is stable with respect to the determination of PO_4^{3-}. Interference from non-ionic surfactants (Triton x-100) was investigated and no significant difference was obtained below 8 mg/L Triton x-100 in a solution of 0.01 μM PO_4^{3-} (30 g/L NaCl) pH 0.8, where an overestimation of ~ 40% and 55% occurred for 9 and 10 mg/L Triton x-100 than in a surfactant-free solution, respectively. However, this overestimation changes the linearity over a linear range of 0.01 - 0.05 μM PO_4^{3-} in a solution containing 10 mg/L Triton x-100 with R^2 of 0.99. Silicic acid had no interfering effect up to a concentration of 50 μM H_2SiO_4. Validation of the proposed method was performed for discrete samples collected from Niskin bottles of the CTD rosette frame during a research cruise in the North Sea. The PO_4^{3-} concentration in the samples was analysed electrochemically using our CPE

and compared to the PO_4^{3-} concentration analysed in the samples using a laboratory reference colourimetric Analyser.

In Chapter 4, the application of our autonomous on-site analyser for PO_4^{3-} was presented with the application of a bi-potentiostat where two working electrodes are used which sharie the same reference and auxiliary electrodes. The two working electrodes were molybdate/CPE and CPE. The bi-potentiostat approach was used to correct for the matrix interferences and correct for changes in analytical sensitivity. The portable bi-potentiostat from Metrohm Dropsense µ-Stat 400 was integrated in a continuous flow injection analyser employing a pumping module using a peristaltic pump and 10-port switching valve. The operation of the pumping module was performed by a Python script while communication with the potentiostat was conducted via an Arduino board and controlled via the Python script. Data processing was done via a Python script including 6 step which are data collection, data layout, data smoothing, baseline correction, subtraction of CPE current and plotting of peak current, in order to obtain the final data in µM. The analytical routine was described in chapter 3. Where CV firstly performed into 0.1 M NaOH, followed by square wave voltammetry into artificial seawater (30 g/L NaCl) acidified with H_2SO_4 to pH 0.8, and again CV in 0.1 NaOH as a cleaning step between measurements. Optimization of square wave voltammetry including the step potential, amplitude and frequency has been done where the influence of those parameters was investigated on the slope of a calibration plot of 0, 0.4 and 1 µM PO_4^{3-} in 30 g/L NaCl (pH 0.8). Square wave frequencies in the range of 1 to 20 Hz were studied and the slope of the calibration was recorded. The maximum sensitivity with lowest standard deviation was obtained at 10 Hz, and above 10 Hz the peak noise increased. The influence of the step potential in the range of 1 to 20 mV was investigated, and the best sensitivity was obtained at 2 mV. The influence of the amplitude of square wave voltammetry in the range of 1 to 200 mV was investigated, and the optimum amplitude was 100 mV in terms of high signal and low standard deviation. The effect of salinity variations was investigated in the range from 0 – 28 g/L NaCl. The peak current values increase with increasing salinity on molybdate/CPE and the corrected voltammogram. The results showed that the influence of salinity variation on peak current is very high and could not be corrected by our method. This leads to the recommendation to prepare calibration standards with a salinity close to that of the water under investigation.

Interferences from humic acid and a non-ionic surfactant were investigated which highlighted the effectiveness of our new method to correct for the interferences. A calibration plot was created for a concentration range from 0.02 to 3 µM PO_4^{3-} and two regimes of linear behaviour obtained. The first regime covered the concentration range 0.02 – 0.2 µM with an analytical sensitivity of

0.4715 μM.μA^{-1} and R^2 of 0.97, and the second the concentration range 0.5 – 3 μM with an analytical sensitivity of 0.0116 μA. μM^{-1} and R^2 of 0.98. with an LOD of 0.014 μA. Validation of our analyzer was performed during a field experiment with ship-board determination of PO_4^{3-} in seawater on a research cruise in the German Bight (southeastern North Sea). The analyser successfully analysed 34 samples which had been discreteky collected. Validation was conducted using a colorimetric reference analyser. The *on-site* data points help investigate the spatial distribution of PO_4^{3-}, which is highly inversely correlated with salinity and directly correlates with the *in-situ* real-time NO_3^- data acquired with the spectrophotometric analyzer OPUS, as well as the $\Sigma(NO_3^- + NO_2^-)$ and H_4SiO_4 data obtained from discrete samples analysed with a reference colorimetric method. Overall, the results obtained show the promise of our real-time analyser of PO_4^{3-} in seawater water, but its performance should be further investigated for long-term deployment in estuarine and coastal waters.

(2) Spectrophotometric determination of PO_4^{3-}, $\Sigma(NO_3^- + NO_2^-)$ and H_4SiO_4

Chapter 5 presented improvements to the commercially available autonomous multimacronutrient analyzer (AutoLAB). AutoLAB from Environtech LLC, USA. The analyser is, based on a sequential flow injection analysis using a single syringe pump and a multi-position rotary valve (16 ports) with three colorimetric detectors. The analytical method for PO_4^{3-} is based on the phosphomolybdate complex blue method (PMB), for H_4SiO_4 it is based on the blue silicomolybdate blue method (SiMB), and for $\Sigma(NO_3^- + NO_2^-)$ it is based on the classical Griess reagent method. We adapted the nitrate method by using the vanadium chloride as nitrate reduction method. The system was operated entirely by a scripting language stored on the memory card and displayed through a terminal interface (e.g. TeraTerm). The protocol of the measurement routine was modified to produce a calibration plot for a blank solution and three standard solutions for each nutrient every 10 sample measurements. In the PMB method, the analyte solution was mixed with a molybdate mixture (ammonium molybdate solution + potassium antimony tartrate) and an L(+)ascorbic acid solution in a 4:1:1 ratio, with the mixing reaction resulting in colour formation after a waiting period of 3 minutes. In the SiMB method, the analyte solution was mixed with ammonium molybdate solution, oxalic acid solution and ascorbic acid solution in the ratio of 1:1:1, with the reaction mixture allowing colour formation after a waiting time of 2 minutes. The Griess method test was based on the reaction of the analyte solution with a mixed reagent of sulfanilamide, N-1-naphthylethylenediamine dihydrochloride (NED) and vanadium chloride in the ratio 2:1; the reaction mixture allows colour formation after incubation at high temperature (~ 50 °C), whereupon a pink colour is formed, which is detected by the colorimetric $\Sigma(NO_3^- + NO_2^-)$

detector at a wavelength of 567 nm. For a single sample measurement, the total volume of reagent was adjusted to 137 µL for PO_4^{3-}, 396 µL for H_4SiO_4, and 137 µL for $\Sigma(NO_3^- + NO_2^-)$. The analytical conditions were optimised to achieve the best sensitivity, including the waiting time for colour formation for PO_4^{3-}, the waiting time for complexation of the analyte solution with the molybdate reagent for H_4SiO_4, and the ratio of analyte to reagent for $\Sigma(NO_3^- + NO_2^-)$. The influence of salinity was investigated because it potentially affects analytical sensitivity in two ways. The first aspect is the streaking effect caused by the difference in refractive index between salt water and fresh water, and the second is the effect of variation in ionic strength. The effect of salinity variation was studied in the range of 0, 7, 14, 21, 28, 35 on the absorbance of 1 µM PO_4^{3-}, 5 µM H_4SiO_4 and 5 µM NO_3^- where an equation with optical correction (**Equation 5.1**) was applied, help to correct for this variation at high extent comparing with the tradition Beer' law equation where underestimation was 3.95 % to 40.6 % for 5 µM.

Calibration plot were obtained for a wide linear range from 0.2 to 100 µM PO_4^{3-} with analytical sensitivity obtained was 0.01211 AU.μM^{-1} and R^2 of 0.999. While for H_4SiO_4, a calibration plot over a concentration range from 0.2 to 100 µM with analytical sensitivity of 0.02377 AU.μM^{-1} with R2 of 0.992. For NO_3^- and NO_2^-, calibration plots have been obtained for each of them where for NO3-, a calibration plot over a concentration range from 0.5 - 100 µM with an analytical sensitivity 0.00614 AU.μM^{-1} with R^2 of 0.998 while for NO_2^- a calibration plot was obtained for a concentration range from 0.4 to 100 µM with an analytical sensitivity of 0.01202 AU.µM-1 and R2 of 0.995. LOD were obtained as follow 0.18 µM, 0.15 µM, 0.45 µM and 0.269 µM for PO_4^{3-}, H_4SiO_4, NO_3^- and NO_2^-. Good repeatability was evident for 10 repeated measurements of CRM (Kanso, Japan) with RSD values of 8.9 % for PO_4^{3-}, 7.4 % for $\Sigma(NO_3^- + NO_2^-)$ and 4.8 % for H_4SiO_4 . Validation of the analyser with our method had been done under environmental conditions during a deployment over 46-days on a pontoon in inner Kiel fjord with a water supply from the depth 1 m. Discrete samples collected and analysed via reference laboratory-based colorimetric analyser, where no significant difference obtained with synchronized on-site data proven by paired t-test. The acquired on-site data success at a high extent to understand the biogeochemical processes with the help of other ancillary data obtained via other sensors deployed in-situ at a depth of 1 m.

(3) Further improvement of real-time monitoring analyser for macro-nutrients in seawater

Electrochemical measurements of nutrients in seawater are very promising for long-term use. The method I presented allows the determination of PO_4^{3-} with fewer reagents than

spectrophotometric determination. The electrochemical determination depends on the oxidation of PO_4^{3-} with molybdate at the working electrode to form the phosphomolybdate complex, which is detected by square-wave voltammetry. However, further improvements are needed to reduce the volume required for each measurement and also to reduce the consumption of sulfuric acid needed for acidification prior to analysis. A well-designed flow cell is needed to reduce the iR droplet that normally happens in the electrochemical cell.

The potential flow cell available on the market is from BASi, USA https://www.basinc.com/products/ec/flowcells, where the auxiliary electrode is made from a stainless steel block in a cross-flow mode.

The auxiliary electrode consists of a phenolic base, arms, a connection for a reference electrode (Ag/AgCl, 3M KCl), and inlet and outlet connections. The flow rate can be in the range of ~ 400 $ml.min^{-1}$ when connected to the pump (Ahluwalia et al. 2018). The proposed flow cell could help to bring the diffusion current to a steady state and compensate for the iR drop. Also, for the working electrode with microelectrode array such as screen-printed electrode prefabricated by the desired material could easily help for better performance for electrochemical measurements and this could be linked to their unique characteristics such as small capacitive charging current (i.e., low background current), also reduced iR drop and high-current density (Huang, O'Mahony, and Compton 2009).

Also, the application of sequential flow analysis using a syringe pump connected to a multi-position switching valve helps to eliminate the disadvantages of continuous flow injection analysis using a peristaltic pump and to miniaturize the autonomous analyser. One of the options available on the market is the Tecan Cavro syringe pumps https://partnering.tecan.com/cavro-syringe-pumps. Syringe pumps have several advantages over peristaltic pumps in that they can deliver solutions in the microliter range, are very accurate, and are easy to use. In addition, the syringe pump can be configured in a manifold with stopped flow, and samples and reagents are drawn into the syringe holder so that mixing can occur through sequential injections and withdrawals. The use of a syringe pump is useful to reduce the amount of analyte normally required for the proposed electrochemical flow cell or microelectrode arrays. Reducing the volume of analyte and reagent per measurement reduces the time required for the measurement. Software improvement could be achieved by integrating into the same software the packages and codes required for data processing, as well as the codes required for pump module control and potentiostat synchronization, so that peak current can be directly converted to concentration values during field deployment. To further validate the method in natural water, either freshwater or seawater, additional deployments should

be performed. An additional digestion step for the humic acid prior to analysis is strongly recommended to exclude interfering effects.

Spectrophotometric determination of macronutrients using the AutoLAB multi-nutrient analyser showed good results, highlighting its applicability in a wide range of waters. However, the limit of quantification is relatively high, limiting its applicability in oligotrophic regions where concentrations of PO_4^{3-} and NO_3^- are in the nanomolar range. Increasing the path length of the flow cell would increase the sensitivity of the analyser. Increasing the sensitivity of the nitrite detector would allow determination of $\Sigma(NO_3^-+NO_2^-)$ in seawater, where NO_2^- concentrations are usually in the nanomolar range, which could facilitate calculation of NO_3^- concentrations. The introduction of a new powerful heater would facilitate the reduction of NO_3^-, shorten the time required for the measurement, and improve the sensitivity of the method. However, in the available version of AutoLAB, there are three colorimetric spectrophotometers for PO_4^{3-}, H_4SiO_4, and $\Sigma(NO_3^-+NO_2^-)$, but the applicability for simultaneous determination is limited by the use of only one syringe pump, where a separate syringe pump setup allows simultaneous determination of the three nutrients, increasing the data points collected per hour. This setup is commercially available from NuLAB (GreenEyes, USA). Other additional parameters such as pH, alkalinity, iron, and manganese can be spectrophotometrically detected in a multiparameter configuration, contributing to a better understanding of biogeochemical processes. The field experiments reported have shown how the AutoLAB can capture temporal patterns of macronutrients using our proposed measurement routine. The use of this *on-site* analyser in the water supply on board a ship helps to capture not only the temporal variations but also the spatial distribution of macronutrients along the route of a research vessel.

7 References

Achterberg, Eric P, and Charlotte Braungardt. 1999. 'Stripping voltammetry for the determination of trace metal speciation and in-situ measurements of trace metal distributions in marine waters', *Analytica Chimica Acta*, 400: 381-97.

Adeloju, Samuel B. 2013. 'Progress and recent advances in phosphate sensors: A review', *Talanta*, 114: 191-203.

Adornato, L. R., E. A. Kaltenbacher, T. A. Villareal, and R. H. Byrne. 2005. 'Continuous in situ determinations of nitrite at nanomolar concentrations', *Deep Sea Research Part I: Oceanographic Research Papers*, 52: 543-51.

Aguilar, D, C Barus, W Giraud, E Calas, Emilie Vanhove, Adrian Laborde, Jérôme Launay, Pierre Temple-Boyer, N Striebig, and M Armengaud. 2015. 'Silicon-based electrochemical microdevices for silicate detection in seawater', *Sensors and Actuators B: Chemical*, 211: 116-24.

Ahluwalia, Rajesh K, Dionissios D Papadias, Nancy N Kariuki, Jui-Kun Peng, Xiaoping Wang, Yifen Tsai, Donald G Graczyk, and Deborah J Myers. 2018. 'Potential dependence of Pt and Co dissolution from platinum-cobalt alloy PEFC catalysts using time-resolved measurements', *Journal of The Electrochemical Society*, 165: F3024.

Allen, J Bard, and R Faulkner Larry. 2001. *Electrochemical methods fundamentals and applications* (John Wiley & Sons).

Altahan, Mahmoud Fatehy, Eric P Achterberg, Asmaa Galal Ali, and Magdi Abdel-Azzem. 2021. 'NaOH Pretreated Molybdate-Carbon Paste Electrode for the Determination of Phosphate in Seawater by Square Wave Voltammetry with Impedimetric Evaluation', *Journal of The Electrochemical Society*, 168: 127503.

Altieri, Katye E, Sarah E Fawcett, and Meredith G Hastings. 2021. 'Reactive Nitrogen Cycling in the Atmosphere and Ocean', *Annual Review of Earth and Planetary Sciences*, 49.

Amornthammarong, N., and J. Z. Zhang. 2009. 'Liquid-waveguide spectrophotometric measurement of low silicate in natural waters', *Talanta*, 79: 621-6.

Arar, Elizabeth J. 1997. 'Method 366.0 Determination of Dissolved Silicate in Estuarine and Coastal Waters by Gas Segmented Continuous Flow Colorimetric Analysis'.

Auflitsch, Stefan, Darren MW Peat, Paul J Worsfold, and Ian D McKelvie. 1997. 'Determination of dissolved reactive phosphorus in estuarine waters using a reversed flow injection manifold', *Analyst*, 122: 1477-80.

Bai, Yin, Jianhua Tong, Jinfen Wang, Chao Bian, and Shanhong Xia. 2014. 'Electrochemical microsensor based on gold nanoparticles modified electrode for total phosphorus determinations in water', *IET nanobiotechnology*, 8: 31-36.

Baker, AR, TD Jickells, M Witt, and KL Linge. 2006. 'Trends in the solubility of iron, aluminium, manganese and phosphorus in aerosol collected over the Atlantic Ocean', *Marine chemistry*, 98: 43-58.

Barus, C., I. Romanytsia, N. Striebig, and V. Garçon. 2016. 'Toward an in situ phosphate sensor in seawater using Square Wave Voltammetry', *Talanta*, 160: 417-24.

Barus, Carole, Dancheng Chen Legrand, Nicolas Striebig, Benoit Jugeau, Arnaud David, Maria Valladares, Praxedes Munoz Parra, Marcel E Ramos, Boris Dewitte, and Véronique Garçon. 2018. 'First deployment and validation of in situ silicate electrochemical sensor in seawater', *Frontiers in Marine Science*, 5: 60.

Beaton, Alexander D, Christopher L Cardwell, Rupert S Thomas, Vincent J Sieben, François-Eric Legiret, Edward M Waugh, Peter J Statham, Matthew C Mowlem, and Hywel Morgan. 2012. 'Lab-on-chip measurement of nitrate and nitrite for in situ analysis of natural waters', *Environmental Science & Technology*, 46: 9548-56.

Beaton, Alexander D, Allison M Schaap, Robin Pascal, Rudolf Hanz, Urska Martincic, Christopher L Cardwell, Andrew Morris, Geraldine Clinton-Bailey, Kevin Saw, and Susan E Hartman. 2022. 'Lab-on-chip for in situ analysis of nutrients in the deep sea', *ACS sensors*, 7: 89-98.

Beaton, Alexander D, Vincent J Sieben, Cedric FA Floquet, Edward M Waugh, Samer Abi Kaed Bey, Iain RG Ogilvie, Matthew C Mowlem, and Hywel Morgan. 2011. 'An automated microfluidic colourimetric sensor applied in situ to determine nitrite concentration', *Sensors and Actuators B: Chemical*, 156: 1009-14.

Beaton, Alexander D, Jemma L Wadham, Jon Hawkings, Elizabeth A Bagshaw, Guillaume Lamarche-Gagnon, Matthew C Mowlem, and Martyn Tranter. 2017. 'High-resolution in situ measurement of nitrate in runoff from the Greenland ice sheet', *Environmental Science & Technology*, 51: 12518-27.

Belter, Magdalena, Adam Sajnóg, and Danuta Barałkiewicz. 2014. 'Over a century of detection and quantification capabilities in analytical chemistry–Historical overview and trends', *Talanta*, 129: 606-16.

Bennett, Elena M, Stephen R Carpenter, and Nina F Caraco. 2001. 'Human impact on erodable phosphorus and eutrophication: a global perspective: increasing accumulation of phosphorus in soil threatens rivers, lakes, and coastal oceans with eutrophication', *BioScience*, 51: 227-34.

Berchmans, S., T. B. Issa, and P. Singh. 2012. 'Determination of inorganic phosphate by electroanalytical methods: a review', *Anal Chim Acta*, 729: 7-20.

Bergemann, M, and T Gaumert. 2010. 'Elbebericht 2008', *FGG Elbe, Hamburg*.

Berges, John A, and Margaret R Mulholland. 2008. 'Enzymes and nitrogen cycling', *Nitrogen in the marine environment*: 1385-444.

Bernard, CY, HH Dürr, C Heinze, J Segschneider, and E Maier-Reimer. 2011. 'Contribution of riverine nutrients to the silicon biogeochemistry of the global ocean–a model study', *Biogeosciences*, 8: 551-64.

Blaen, Phillip J, Kieran Khamis, Charlotte EM Lloyd, Chris Bradley, David Hannah, and Stefan Krause. 2016. 'Real-time monitoring of nutrients and dissolved organic matter in rivers: Capturing event dynamics, technological opportunities and future directions', *Science of the Total Environment*, 569: 647-60.

Bodini, S, L Sanfilippo, E Savino, and P Moscetta. 2015. "Automated micro loop flow reactor technology to measure nutrients in coastal water: State of the art and field application." In *OCEANS 2015-Genova*, 1-7. IEEE.

Boehlich, Marcus J, and Thomas Strotmann. 2019. 'Das Elbeästuar', *Die Küste, 87-Online First*.

Bohlen, Curtis, and Matthew Liebman. 2019. 'Quality Assurance Project Plan For Field Deployment of an Autonomous Nutrient Monitor in Casco Bay'.

Bojinov, M., I. Betova, and R. Raicheff. 1995. 'Transpassivity of molybdenum in H2SO4 solution', *Journal of Electroanalytical Chemistry*, 381: 123-31.

Bolin, Bert, and Robert B Cook. 1983. 'The major biogeochemical cycles and their interactions (Scope Report 21)'.

Boukamp, Bernard A. 1986. 'A nonlinear least squares fit procedure for analysis of immittance data of electrochemical systems', *Solid state ionics*, 20: 31-44.

Bowden, M., and D. Diamond. 2003. 'The determination of phosphorus in a microfluidic manifold demonstrating long-term reagent lifetime and chemical stability utilising a colorimetric method', *Sensors and Actuators B: Chemical*, 90: 170-74.

Boyd, Eric, and John W Peters. 2013. 'New insights into the evolutionary history of biological nitrogen fixation', *Frontiers in microbiology*, 4: 201.

Braman, Robert S., and Steven A. Hendrix. 1989. 'Nanogram nitrite and nitrate determination in environmental and biological materials by vanadium(III) reduction with chemiluminescence detection', *Analytical chemistry*, 61: 2715-18.

Brandes, Jay A, Nabil Z Boctor, George D Cody, Benjamin A Cooper, Robert M Hazen, and Hatten S Yoder. 1998. 'Abiotic nitrogen reduction on the early Earth', *Nature*, 395: 365-67.

Braungardt, Charlotte B, Eric P Achterberg, Bertil Axelsson, Jacques Buffle, Flavio Graziottin, Kate A Howell, Silvia Illuminati, Giuseppe Scarponi, Alan D Tappin, and Marie-Lou Tercier-Waeber. 2009. 'Analysis of dissolved metal fractions in coastal waters: An inter-comparison of five voltammetric in situ profiling (VIP) systems', *Marine chemistry*, 114: 47-55.

Bricker, Owen P. 1972. 'Earth Science: The Encyclopedia of Geochemistry and Environmental Sciences. Rhodes W. Fairbridge, Ed. Van Nostrand Reinhold, New York, 1972. xxii, 1322 pp., illus. $49.50. Encyclopedia of Earth Sciences Series, vol. IVA', *Science*, 178: 1277-77.

Bricker, Suzanne B, Ben Longstaff, William Dennison, Adrian Jones, Kate Boicourt, Caroline Wicks, and Joanna Woerner. 2008. 'Effects of nutrient enrichment in the nation's estuaries: a decade of change', *Harmful Algae*, 8: 21-32.

Broecker, Wallace S, and Tsung-Hung Peng. 1982. *Tracers in the Sea* (Lamont-Doherty Geological Observatory, Columbia University Palisades, New York).

Brzezinski, Mark A. 1985. 'THE Si:C:N RATIO OF MARINE DIATOMS: INTERSPECIFIC VARIABILITY AND THE EFFECT OF SOME ENVIRONMENTAL VARIABLES1', *Journal of Phycology*, 21: 347-57.

Brzezinski, Mark A., Jeffrey W. Krause, Matthew J. Church, David M. Karl, Binglin Li, Janice L. Jones, and Brett Updyke. 2011. 'The annual silica cycle of the North Pacific subtropical gyre', *Deep Sea Research Part I: Oceanographic Research Papers*, 58: 988-1001.

Brzezinski, Mark A., and David M. Nelson. 1986. 'A solvent extraction method for the colorimetric determination of nanomolar concentrations of silicic acid in seawater', *Marine chemistry*, 19: 139-51.

Bulen, WA, and JR LeComte. 1966. 'The nitrogenase system from Azotobacter: two-enzyme requirement for N2 reduction, ATP-dependent H2 evolution, and ATP hydrolysis', *Proceedings of the National Academy of Sciences of the United States of America*, 56: 979.

Burdige, David J. 2021. *Geochemistry of marine sediments* (Princeton university press).

Canfield, DE, R Wollast, FT Mackenzie, and L Chou. 1993. 'Interactions of C, N, P and S biogeochemical Cycles and Global Change', *NATO ASI Series (Series I: Global Environmental Change)*: 333.

Cao, X, SW Zhang, DZ Chu, N Wu, HK Ma, and Y Liu. 2017. "A design of spectrophotometric microfluidic chip sensor for analyzing silicate in seawater." In *IOP Conference Series: Earth and Environmental Science*, 012080. IOP Publishing.

Capone, Douglas G, Deborah A Bronk, Margaret R Mulholland, and Edward J Carpenter. 2008. *Nitrogen in the marine environment* (Elsevier).

Carpenter, Stephen R, Nina F Caraco, David L Correll, Robert W Howarth, Andrew N Sharpley, and Val H Smith. 1998. 'Nonpoint pollution of surface waters with phosphorus and nitrogen', *Ecological applications*, 8: 559-68.

Carstens, Marina, Ulrich Claussen, Michael Bergemann, and Thomas Gaumert. 2004. 'Transitional waters in Germany: the Elbe estuary as an example', *Aquatic Conservation: Marine and Freshwater Ecosystems*, 14: S81-S92.

Cerdà, Víctor, Jessica Avivar, and Amalia Cerdà. 2012. 'Laboratory automation based on flow techniques', *Pure and Applied Chemistry*, 84: 1983-98.

Chang, Byoung-Yong, and Su-Moon Park. 2010. 'Electrochemical impedance spectroscopy', *Annual Review of Analytical Chemistry*, 3: 207-29.

Charbaji, Amer, Hojat Heidari-Bafroui, Constantine Anagnostopoulos, and Mohammad Faghri. 2021. 'A New Paper-Based Microfluidic Device for Improved Detection of Nitrate in Water', *Sensors*, 21: 102.

Chen, Guohe, Dongxing Yuan, Yongming Huang, Min Zhang, and Maria Bergman. 2008. 'In-field determination of nanomolar nitrite in seawater using a sequential injection technique combined with solid phase enrichment and colorimetric detection', *Analytica Chimica Acta*, 620: 82-88.

Choi, Su-Hee, and Jong-Won Kim. 2009. 'Adsorption properties of Keggin-type polyoxometalates on carbon based electrode surfaces and their electrocatalytic activities', *Bulletin of the Korean Chemical Society*, 30: 810-16.

Cinti, Stefano, Daria Talarico, Giuseppe Palleschi, Danila Moscone, and Fabiana Arduini. 2016. 'Novel reagentless paper-based screen-printed electrochemical sensor to detect phosphate', *Analytica Chimica Acta*, 919: 78-84.

Clinton-Bailey, Geraldine S, Maxime M Grand, Alexander D Beaton, Adrian M Nightingale, David R Owsianka, Gregory J Slavik, Douglas P Connelly, Christopher L Cardwell, and Matthew C Mowlem. 2017. 'A lab-on-chip analyzer for in situ measurement of soluble reactive phosphate: improved phosphate blue assay and application to fluvial monitoring', *Environmental Science & Technology*, 51: 9989-95.

Conley, Daniel J., Svante Björck, Erik Bonsdorff, Jacob Carstensen, Georgia Destouni, Bo G. Gustafsson, Susanna Hietanen, Marloes Kortekaas, Harri Kuosa, H. E. Markus Meier, Baerbel Müller-Karulis, Kjell Nordberg, Alf Norkko, Gertrud Nürnberg, Heikki Pitkänen, Nancy N. Rabalais, Rutger Rosenberg, Oleg P. Savchuk, Caroline P. Slomp, Maren Voss,

Fredrik Wulff, and Lovisa Zillén. 2009. 'Hypoxia-Related Processes in the Baltic Sea', *Environmental Science & Technology*, 43: 3412-20.

Copetti, D, L Valsecchi, AG Capodaglio, and G Tartari. 2017. 'Direct measurement of nutrient concentrations in freshwaters with a miniaturized analytical probe: evaluation and validation', *Environmental monitoring and assessment*, 189: 144.

Cosović, Božena, and Vjeročka Vojvodić. 1982. 'The application of ac polarography to the determination of surface-active substances in seawater 1', *Limnology and Oceanography*, 27: 361-69.

Cotner, James B, and Bopaiah A Biddanda. 2002. 'Small players, large role: microbial influence on biogeochemical processes in pelagic aquatic ecosystems', *Ecosystems*, 5: 105-21.

Cotner Jr, James B, and Robert G Wetzel. 1992. 'Uptake of dissolved inorganic and organic bphosphorus compounds by phytoplankton and bacterioplankton', *Limnology and Oceanography*, 37: 232-43.

Cox, Robert D. 1980. 'Determination of nitrate and nitrite at the parts per billion level by chemiluminescence', *Analytical chemistry*, 52: 332-35.

Cruywagen, J. J., A. G. Draaijer, J. B. B. Heyns, and E. A. Rohwer. 2002. 'Molybdenum(VI) equilibria in different ionic media. Formation constants and thermodynamic quantities', *Inorganica Chimica Acta*, 331: 322-29.

Cuartero, Maria, Gaston A Crespo, and Eric Bakker. 2015. 'Tandem electrochemical desalination–potentiometric nitrate sensing for seawater analysis', *Analytical chemistry*, 87: 8084-89.

Cuartero, Maria, Gaston Crespo, Thomas Cherubini, Nadezda Pankratova, Fabio Confalonieri, Francesco Massa, Mary-Lou Tercier-Waeber, Melina Abdou, Jörg Schäfer, and Eric Bakker. 2018. 'In situ detection of macronutrients and chloride in seawater by submersible electrochemical sensors', *Analytical chemistry*, 90: 4702-10.

Cui, Jiewu, Edward E. Ogabiela, Jianing Hui, Yan Wang, Yong Zhang, Liang Tong, Jianfang Zhang, Samuel B. Adeloju, Xinyi Zhang, and Yucheng Wu. 2014. 'Electrochemical Biosensor based on Pt/Au Alloy Nanowire Arrays for Phosphate Detection', *Journal of The Electrochemical Society*, 162: B62-B67.

Daniel, Anne, Agathe Laës-Huon, Carole Barus, Alexander D Beaton, Daniel Blandfort, Nathalie Guigues, Marc Knockaert, Dominique Munaron, Ian Salter, and E Malcolm S Woodward. 2020. 'Toward a harmonization for using in situ nutrient sensors in the marine environment', *Frontiers in Marine Science*, 6: 773.

Daniel, Anne, Agathe Laës-Huon, Carole Barus, Alexander D. Beaton, Daniel Blandfort, Nathalie Guigues, Marc Knockaert, Dominique Munaron, Ian Salter, E. Malcolm S. Woodward,

Naomi Greenwood, and Eric P. Achterberg. 2020. 'Toward a Harmonization for Using in situ Nutrient Sensors in the Marine Environment', *Frontiers in Marine Science*, 6.

Deng, Yao, Peicong Li, Tengyue Fang, Yiyong Jiang, Jixin Chen, Nengwang Chen, Dongxing Yuan, and Jian Ma. 2020. 'Automated determination of dissolved reactive phosphorus at nanomolar to micromolar levels in natural waters using a portable flow analyzer', *Analytical chemistry*, 92: 4379-86.

Deshmukh, Rupesh K, Jian F Ma, and Richard R Bélanger. 2017. "Role of silicon in plants." In, 1858. Frontiers Media SA.

Deutsch, Curtis, Jorge L Sarmiento, Daniel M Sigman, Nicolas Gruber, and John P Dunne. 2007. 'Spatial coupling of nitrogen inputs and losses in the ocean', *Nature*, 445: 163-67.

Dias, Ana Cristi B., Eduardo P. Borges, Elias A. G. Zagatto, and Paul J. Worsfold. 2006. 'A critical examination of the components of the Schlieren effect in flow analysis', *Talanta*, 68: 1076-82.

Dijksma, M, Bernard A Boukamp, B Kamp, and WP Van Bennekom. 2002. 'Effect of hexacyanoferrate (II/III) on self-assembled monolayers of thioctic acid and 11-mercaptoundecanoic acid on gold', *Langmuir*, 18: 3105-12.

Directive, Water Framework. 2000. 'Water Framework Directive', *Journal reference OJL*, 327: 1-73.

Drummond, L., and W. Maher. 1995. 'Determination of phosphorus in aqueous solution via formation of the phosphoantimonylmolybdenum blue complex. Re-examination of optimum conditions for the analysis of phosphate', *Analytica Chimica Acta*, 302: 69-74.

Duce, RA, PS Liss, JT Merrill, EL Atlas, P Buat-Menard, BB Hicks, JM Miller, JM Prospero, RCTM Arimoto, and TM Church. 1991. 'The atmospheric input of trace species to the world ocean', *Global Biogeochemical Cycles*, 5: 193-259.

Dürr, HH, Michel Meybeck, Jens Hartmann, Goulven Gildas Laruelle, and Vincent Roubeix. 2011. 'Global spatial distribution of natural riverine silica inputs to the coastal zone', *Biogeosciences*, 8: 597-620.

Egli, Peter J, Scott P Veitch, and Alfred K Hanson. 2009. "Sustained, autonomous coastal nutrient observations aboard moorings and vertical profilers." In *OCEANS 2009*, 1-9. IEEE.

Ehlert, Claudia, Anja Reckhardt, Janek Greskowiak, Bianca TP Liguori, Philipp Böning, Ronja Paffrath, Hans-Jürgen Brumsack, and Katharina Pahnke. 2016. 'Transformation of silicon in a sandy beach ecosystem: insights from stable silicon isotopes from fresh and saline groundwaters', *Chemical Geology*, 440: 207-18.

Ellis, Peter S., Ali Mohammad Haji Shabani, Brady S. Gentle, and Ian D. McKelvie. 2011. 'Field measurement of nitrate in marine and estuarine waters with a flow analysis system utilizing on-line zinc reduction', *Talanta*, 84: 98-103.

Elser, James J., Matthew E.S. Bracken, Elsa E. Cleland, Daniel S. Gruner, W. Stanley Harpole, Helmut Hillebrand, Jacqueline T. Ngai, Eric W. Seabloom, Jonathan B. Shurin, and Jennifer E. Smith. 2007. 'Global analysis of nitrogen and phosphorus limitation of primary producers in freshwater, marine and terrestrial ecosystems', *Ecology Letters*, 10: 1135-42.

'Envirotech Instruments LLC'. *website;https://www.bodc.ac.uk/data/documents/nodb/pdf/envirotech_nas_nutrient_analyser.pdf*.

Estela, José Manuel, and Víctor Cerdà. 2005. 'Flow analysis techniques for phosphorus: an overview', *Talanta*, 66: 307-31.

Fabre, Sébastien, Catherine Jeandel, Thomas Zambardi, Michel Roustan, and Rafaël Almar. 2019. 'An Overlooked Silica Source of the Modern Oceans: Are Sandy Beaches the Key?', *Frontiers in Earth Science*, 7.

Fang, Tengyue, Peicong Li, Kunning Lin, Nengwang Chen, Yiyong Jiang, Jixin Chen, Dongxing Yuan, and Jian Ma. 2019. 'Simultaneous underway analysis of nitrate and nitrite in estuarine and coastal waters using an automated integrated syringe-pump-based environmental-water analyzer', *Analytica Chimica Acta*, 1076: 100-09.

Feng, Sichao, Min Zhang, Yongming Huang, Dongxing Yuan, and Yong Zhu. 2013. 'Simultaneous determination of nanomolar nitrite and nitrate in seawater using reverse flow injection analysis coupled with a long path length liquid waveguide capillary cell', *Talanta*, 117: 456-62.

'FIALab Instruments, INC.'. *website; https://www.flowinjection.com/hardware/sia-analyzers*.

Field, Christopher B, Michael J Behrenfeld, James T Randerson, and Paul Falkowski. 1998. 'Primary production of the biosphere: integrating terrestrial and oceanic components', *Science*, 281: 237-40.

Filippelli, Gabriel M, and Margaret Lois Delaney. 1996. 'Phosphorus geochemistry of equatorial Pacific sediments', *Geochimica et Cosmochimica Acta*, 60: 1479-95.

Finch, Miles S, David J Hydes, Charles H Clayson, Bernhard Weigl, John Dakin, and Pat Gwilliam. 1998. 'A low power ultra violet spectrophotometer for measurement of nitrate in seawater: introduction, calibration and initial sea trials', *Analytica Chimica Acta*, 377: 167-77.

Fischer, Matthias, Gernot Friedrichs, and Tim Lachnit. 2014. 'Fluorescence-based quasicontinuous and in situ monitoring of biofilm formation dynamics in natural marine environments', *Applied and environmental microbiology*, 80: 3721-28.

Follett, Christopher L, Daniel J Repeta, Daniel H Rothman, Li Xu, and Chiara Santinelli. 2014. 'Hidden cycle of dissolved organic carbon in the deep ocean', *Proceedings of the National Academy of Sciences*, 111: 16706-11.

Fowler, D., C. E. Steadman, D. Stevenson, M. Coyle, R. M. Rees, U. M. Skiba, M. A. Sutton, J. N. Cape, A. J. Dore, M. Vieno, D. Simpson, S. Zaehle, B. D. Stocker, M. Rinaldi, M. C. Facchini, C. R. Flechard, E. Nemitz, M. Twigg, J. W. Erisman, K. Butterbach-Bahl, and J. N. Galloway. 2015. 'Effects of global change during the 21st century on the nitrogen cycle', *Atmos. Chem. Phys.*, 15: 13849-93.

Fowler, David, Mhairi Coyle, Ute Skiba, Mark A Sutton, J Neil Cape, Stefan Reis, Lucy J Sheppard, Alan Jenkins, Bruna Grizzetti, and James N Galloway. 2013. 'The global nitrogen cycle in the twenty-first century', *Philosophical Transactions of the Royal Society B: Biological Sciences*, 368: 20130164.

Fowler, David, Claudia E Steadman, David Stevenson, Mhairi Coyle, Robert M Rees, UM Skiba, MA Sutton, J Neil Cape, AJ Dore, and Massimo Vieno. 2015. 'Effects of global change during the 21st century on the nitrogen cycle', *Atmospheric Chemistry and Physics*, 15: 13849-93.

Fuerst, John A. 2005. 'Intracellular compartmentation in planctomycetes', *Annu. Rev. Microbiol.*, 59: 299-328.

García-Robledo, Emilio, Alfonso Corzo, and Sokratis Papaspyrou. 2014. 'A fast and direct spectrophotometric method for the sequential determination of nitrate and nitrite at low concentrations in small volumes', *Marine chemistry*, 162: 30-36.

Geißler, Felix, Eric P Achterberg, Alexander D Beaton, Mark J Hopwood, Jennifer S Clarke, André Mutzberg, Matt C Mowlem, and Douglas P Connelly. 2017. 'Evaluation of a ferrozine based autonomous in situ lab-on-chip analyzer for dissolved iron species in coastal waters', *Frontiers in Marine Science*, 4: 322.

Georg, RB, AJ West, AR Basu, and AN Halliday. 2009. 'Silicon fluxes and isotope composition of direct groundwater discharge into the Bay of Bengal and the effect on the global ocean silicon isotope budget', *Earth and Planetary Science Letters*, 283: 67-74.

Gibbons, Robert D, and David E Coleman. 2001. 'Statistical methods for detection and quantification of environmental contamination'.

Gimbert, Laura J, Philip M Haygarth, and Paul J Worsfold. 2007. 'Determination of nanomolar concentrations of phosphate in natural waters using flow injection with a long path length liquid waveguide capillary cell and solid-state spectrophotometric detection', *Talanta*, 71: 1624-28.

Glenn, Craig R, Liliane Prévôt-Lucas, and Jacques Lucas. 2000. 'Marine authigenesis: from global to microbial'.

Glibert, Patricia M, Frances P Wilkerson, Richard C Dugdale, John A Raven, Christopher L Dupont, Peter R Leavitt, Alexander E Parker, JoAnn M Burkholder, and Todd M Kana. 2016. 'Pluses and minuses of ammonium and nitrate uptake and assimilation by phytoplankton and implications for productivity and community composition, with emphasis on nitrogen-enriched conditions', *Limnology and Oceanography*, 61: 165-97.

Grand, Maxime M., Geraldine S. Clinton-Bailey, Alexander D. Beaton, Allison M. Schaap, Thomas H. Johengen, Mario N. Tamburri, Douglas P. Connelly, Matthew C. Mowlem, and Eric P. Achterberg. 2017. 'A Lab-On-Chip Phosphate Analyzer for Long-term In Situ Monitoring at Fixed Observatories: Optimization and Performance Evaluation in Estuarine and Oligotrophic Coastal Waters', *Frontiers in Marine Science*, 4.

Grasshoff, Klaus, Klaus Kremling, and Manfred Ehrhardt. 2009. *Methods of seawater analysis* (John Wiley & Sons).

'Green Eyes, LLC'. *Available online: http://gescience.com/wp-content/uploads/2017/02/Green-Eyes-Data-Processing-Guide-1.pdf (accessed on 18 July 2022).*

'Green Eyes, LLC'. *website; http://gescience.com/wp-content/uploads/2017/02/NuLAB-4.pdf.*

Griess, JP, and ZAHH Bemerkungen. 1879. 'Ueber einige azoverbindungen', *Ber. Deutch Chem. Ges*, 12: 426-28.

Griess, P. 1879. 'Griess reagent: a solution of sulphanilic acid and α-naphthylamine in acetic acid which gives a pink colour on reaction with the solution obtained after decomposition of nitrosyl complexes', *Chem. Ber*, 12: 427.

Grunwald, Maik, Olaf Dellwig, Cora Kohlmeier, Nicole Kowalski, Melanie Beck, Thomas H Badewien, Stephan Kotzur, Gerd Liebezeit, and Hans-Jürgen Brumsack. 2010. 'Nutrient dynamics in a back barrier tidal basin of the Southern North Sea: Time-series, model simulations, and budget estimates', *Journal of Sea Research*, 64: 199-212.

Guanghan, Lu, Wu Xiaogang, Lan Yanhua, and Yao Shenlai. 1999a. 'Studies on 1:12 phosphomolybdic heteropoly anion film modified carbon paste electrode', *Talanta*, 49: 511-15.

———. 1999b. 'Studies on 1: 12 phosphomolybdic heteropoly anion film modified carbon paste electrode', *Talanta*, 49: 511-15.

Hansen, E.H., J. Ruzicka, and P. Chocholous. 'ADVANCES IN FLOW INJECTION ANALYSIS', *Website; https://www.flowinjectiontutorial.com/index.html.*

Hansen, HP, and F Koroleff. 1999. "Determination of nutrients In: Grasshoff K, Kremling K, Ehrhardt M, editors. Methods of seawater analysis." In.: Weinheim: Wiley-VCH.

Healy, Terry, Ying Wang, and J-A Healy. 2002. *Muddy coasts of the world: processes, deposits and function* (Elsevier).

Hedges, John I. 1992. 'Global biogeochemical cycles: progress and problems', *Marine chemistry*, 39: 67-93.

Heidari-Bafroui, Hojat, Amer Charbaji, Constantine Anagnostopoulos, and Mohammad Faghri. 2021. 'A Colorimetric Dip Strip Assay for Detection of Low Concentrations of Phosphate in Seawater', *Sensors*, 21: 3125.

Heyen, Hauke, and Joachim W Dippner. 1998. 'Salinity variability in the German Bight in relation to climate variability', *Tellus A*, 50: 545-56.

Hioki, A., J. W. H. Lam, and J. W. McLaren. 1997. 'On-Line Determination of Dissolved Silica in Sea water by Ion Exclusion Chromatography in Combination with Inductively Coupled Plasma Mass Spectrometry', *Analytical chemistry*, 69: 21-24.

Hoffman, Brian M, Dmitriy Lukoyanov, Zhi-Yong Yang, Dennis R Dean, and Lance C Seefeldt. 2014. 'Mechanism of nitrogen fixation by nitrogenase: the next stage', *Chemical reviews*, 114: 4041-62.

Holzer, M, M Frants, and B Pasquier. 1992. 'Global biogeochemical cycles'.

Howell, Kate A, Eric P Achterberg, Charlotte B Braungardt, Alan D Tappin, David R Turner, and Paul J Worsfold. 2003. 'The determination of trace metals in estuarine and coastal waters using a voltammetric in situ profiling system', *Analyst*, 128: 734-41.

Huang, Xing-Jiu, Aoife M O'Mahony, and Richard G Compton. 2009. 'Microelectrode arrays for electrochemistry: approaches to fabrication', *Small*, 5: 776-88.

Huang, Yuanfeng. 2017. 'An All-Solid-State Phosphate Electrode with H3PO4 Doped Polyaniline as the Sensitive Layer', *International Journal of Electrochemical Science*: 4677-91.

Hull, Michael N. 1972. 'On the anodic dissolution of molybdenum in acidic and alkaline electrolytes', *Journal of Electroanalytical Chemistry and Interfacial Electrochemistry*, 38: 143-57.

Hydes, D, M Aoyama, Alain Aminot, K Bakker, S Becker, S Coverly, Anne Daniel, A Dickson, O Grosso, and Roger Kerouel. 2010. 'Determination of dissolved nutrients (N, P, Si) in seawater with high precision and inter-comparability using gas-segmented continuous flow analysers'.

Ilangovan, G, and K Chandrasekara Pillai. 1997. 'Electrochemical and XPS characterization of glassy carbon electrode surface effects on the preparation of a monomeric molybdate (VI)-modified electrode', *Langmuir*, 13: 566-75.

Illuminati, Silvia, Anna Annibaldi, Cristina Truzzi, Mary-Lou Tercier-Waeber, Stéphane Nöel, Charlotte B Braungardt, Eric P Achterberg, Kate A Howell, David Turner, and Mauro Marini. 2019. 'In-situ trace metal (Cd, Pb, Cu) speciation along the Po River plume (Northern Adriatic Sea) using submersible systems', *Marine chemistry*, 212: 47-63.

Ingall, Ellery, and Richard Jahnke. 1994. 'Evidence for enhanced phosphorus regeneration from marine sediments overlain by oxygen depleted waters', *Geochimica et Cosmochimica Acta*, 58: 2571-75.

Ittekkot, Venugopalan, Daniela Unger, Christoph Humborg, and Nguyen Tac An. 2012. *The silicon cycle: human perturbations and impacts on aquatic systems* (Island Press).

Javidpour, Jamileh, Juan Carlos Molinero, Jesco Peschutter, and Ulrich Sommer. 2009. 'Seasonal changes and population dynamics of the ctenophore Mnemiopsis leidyi after its first year of invasion in the Kiel Fjord, Western Baltic Sea', *Biological Invasions*, 11: 873-82.

Johnson, Kenneth S, and Luke J Coletti. 2002. 'In situ ultraviolet spectrophotometry for high resolution and long-term monitoring of nitrate, bromide and bisulfide in the ocean', *Deep Sea Research Part I: Oceanographic Research Papers*, 49: 1291-305.

Jońca, J., M. Comtat, and V. Garçon. 2013a. 'In Situ Phosphate Monitoring in Seawater: Today and Tomorrow', 4: 25-44.

Jońca, Justyna, Carole Barus, William Giraud, Danièle Thouron, Véronique Garçon, and Maurice Comtat. 2012. 'Electrochemical behaviour of isopoly-and heteropolyoxomolybdates formed during anodic oxidation of molybdenum in seawater', *Int. J. Electrochem. Sci*, 7: 7325-48.

Jońca, Justyna, M Comtat, and V Garçon. 2013b. 'In situ phosphate monitoring in seawater: today and tomorrow.' in, *Smart Sensors for Real-Time Water Quality Monitoring* (Springer).

Jońca, Justyna, Violeta León Fernández, Danièle Thouron, Aurélien Paulmier, Michelle Graco, and Véronique Garçon. 2011. 'Phosphate determination in seawater: Toward an autonomous electrochemical method', *Talanta*, 87: 161-67.

Jońca, Justyna, William Giraud, Carole Barus, Maurice Comtat, Nicolas Striebig, Danièle Thouron, and Véronique Garçon. 2013. 'Reagentless and silicate interference free electrochemical phosphate determination in seawater', *Electrochimica Acta*, 88: 165-69.

Jońca, Justyna, Violeta León Fernández, Danièle Thouron, Aurélien Paulmier, Michelle Graco, and Véronique Garçon. 2011. 'Phosphate determination in seawater: Toward an autonomous electrochemical method', *Talanta*, 87: 161-67.

Kamp, Anja, Signe Høgslund, Nils Risgaard-Petersen, and Peter Stief. 2015. 'Nitrate storage and dissimilatory nitrate reduction by eukaryotic microbes', *Frontiers in microbiology*, 6: 1492.

Karl, D, R Letelier, L Tupas, Jo Dore, J Christian, and D Hebel. 1997. 'The role of nitrogen fixation in biogeochemical cycling in the subtropical North Pacific Ocean', *Nature*, 388: 533-38.

Karl, David M. 2014. 'Microbially mediated transformations of phosphorus in the sea: new views of an old cycle', *Annual review of marine science*, 6: 279-337.

Karl, David M, and Roger Lukas. 1996. 'The Hawaii Ocean Time-series (HOT) program: Background, rationale and field implementation', *Deep Sea Research Part II: Topical Studies in Oceanography*, 43: 129-56.

Karl, David M, and Georgia Tien. 1992. 'MAGIC: A sensitive and precise method for measuring dissolved phosphorus in aquatic environments', *Limnology and Oceanography*, 37: 105-16.

Karl, David M., and Karin M. Björkman. 2015. 'Chapter 5 - Dynamics of Dissolved Organic Phosphorus.' in Dennis A. Hansell and Craig A. Carlson (eds.), *Biogeochemistry of Marine Dissolved Organic Matter (Second Edition)* (Academic Press: Boston).

Kelso, B, Roger V Smith, Ronald J Laughlin, and S David Lennox. 1997. 'Dissimilatory nitrate reduction in anaerobic sediments leading to river nitrite accumulation', *Applied and environmental microbiology*, 63: 4679-85.

Kim, Guebuem, Jae-Woong Ryu, Han-Soeb Yang, and Seong-Taek Yun. 2005. 'Submarine groundwater discharge (SGD) into the Yellow Sea revealed by 228Ra and 226Ra isotopes: Implications for global silicate fluxes', *Earth and Planetary Science Letters*, 237: 156-66.

King, D, and DB Nedwell. 1985. 'The influence of nitrate concentration upon the end-products of nitrate dissimilation by bacteria in anaerobic salt marsh sediment', *FEMS Microbiology Ecology*, 1: 23-28.

King, SL, PN Froelich, and RA Jahnke. 2000. 'Early diagenesis of germanium in sediments of the Antarctic South Atlantic: in search of the missing Ge sink', *Geochimica et Cosmochimica Acta*, 64: 1375-90.

Kitson, R. E., and M. G. Mellon. 1944. 'Colorimetric Determination of Phosphorus as Molybdivanadophosphoric Acid', *Industrial & Engineering Chemistry Analytical Edition*, 16: 379-83.

Kodamatani, Hitoshi, Shigeo Yamazaki, Keiitsu Saito, Yu Komatsu, and Takashi Tomiyasu. 2011. 'Rapid method for simultaneous determination of nitrite and nitrate in water samples using short-column ion-pair chromatographic separation, photochemical reaction, and chemiluminescence detection', *Analytical Sciences*, 27: 187-87.

Kolliopoulos, Athanasios V, Dimitrios K Kampouris, and Craig E Banks. 2015. 'Rapid and portable electrochemical quantification of phosphorus', *Analytical chemistry*, 87: 4269-74.

Kounaves, Samuel P. 1997. "Voltammetric techniques." In, 709-26. Prentice Hall, Upper Saddle River, NJ, USA.

Kowalcze, Mateusz, and Małgorzata Jakubowska. 2018. 'Voltammetric determination of thujone in herbal matrices in the presence of Triton X-100', *Analytical biochemistry*, 543: 12-20.

Krause, Jeffrey W, Isabelle K Schulz, Katherine A Rowe, William Dobbins, Mie HS Winding, Mikael K Sejr, Carlos M Duarte, and Susana Agustí. 2019. 'Silicic acid limitation drives bloom termination and potential carbon sequestration in an Arctic bloom', *Scientific reports*, 9: 1-11.

Kumar, Deivasigamani Ranjith, Ganesh Dhakal, Jintae Lee, Yong Rok Lee, and Jae-Jin Shim. 2021. 'Ammonium heptamolybdate preloaded on flexible carbon-matrix film electrode for the electrochemical phosphate sensor in a river water sample', *Microchemical Journal*, 170: 106639.

Kuypers, Marcel MM, Hannah K Marchant, and Boran Kartal. 2018. 'The microbial nitrogen-cycling network', *Nature Reviews Microbiology*, 16: 263-76.

Lacombe, Marielle, Véronique Garçon, Danièle Thouron, Nadine Le Bris, and Maurice Comtat. 2008. 'Silicate electrochemical measurements in seawater: chemical and analytical aspects towards a reagentless sensor', *Talanta*, 77: 744-50.

Lai, Chun-Ze, Michael D DeGrandpre, and Reuben C Darlington. 2018. 'Autonomous optofluidic chemical analyzers for marine applications: Insights from the Submersible Autonomous Moored Instruments (SAMI) for pH and pCO2', *Frontiers in Marine Science*, 4: 438.

Laruelle, Goulven G, Vincent Roubeix, Agata Sferratore, B Brodherr, D Ciuffa, DJ Conley, HH Dürr, Josette Garnier, Christiane Lancelot, and Q Le Thi Phuong. 2009. 'Anthropogenic perturbations of the silicon cycle at the global scale: Key role of the land-ocean transition', *Global Biogeochemical Cycles*, 23.

Latimer, James S., and Michael A. Charpentier. 2010. 'Nitrogen inputs to seventy-four southern New England estuaries: Application of a watershed nitrogen loading model', *Estuarine, Coastal and Shelf Science*, 89: 125-36.

Launay, Jean Pierre, Rene Massart, and Pierre Souchay. 1974. 'Gradual reduction of molybdosilicates and related compounds', *Journal of the Less Common Metals*, 36: 139-50.

Le Bris, N, P-M Sarradin, D Birot, and A-M Alayse-Danet. 2000. 'A new chemical analyzer for in situ measurement of nitrate and total sulfide over hydrothermal vent biological communities', *Marine chemistry*, 72: 1-15.

Legiret, F. E., V. J. Sieben, E. M. Woodward, S. K. Abi Kaed Bey, M. C. Mowlem, D. P. Connelly, and E. P. Achterberg. 2013. 'A high performance microfluidic analyser for phosphate measurements in marine waters using the vanadomolybdate method', *Talanta*, 116: 382-7.

Legiret, François-Eric, Vincent J Sieben, E Malcolm S Woodward, Samer K Abi Kaed Bey, Matthew C Mowlem, Douglas P Connelly, and Eric P Achterberg. 2013. 'A high performance microfluidic analyser for phosphate measurements in marine waters using the vanadomolybdate method', *Talanta*, 116: 382-87.

Legrand, D Chen, S Mas, B Jugeau, A David, and C Barus. 2021. 'Silicate marine electrochemical sensor', *Sensors and Actuators B: Chemical*, 335: 129705.

Leigh, John A, and Jeremy A Dodsworth. 2007. 'Nitrogen regulation in bacteria and archaea', *Annu. Rev. Microbiol.*, 61: 349-77.

Letscher, Robert T, Dennis A Hansell, Craig A Carlson, Rick Lumpkin, and Angela N Knapp. 2013. 'Dissolved organic nitrogen in the global surface ocean: Distribution and fate', *Global Biogeochemical Cycles*, 27: 141-53.

Li, Hua-Bin, and Feng Chen. 2000. 'Determination of silicate in water by ion exclusion chromatography with conductivity detection', *Journal of Chromatography A*, 874: 143-47.

Li, L., G. Shang, and W. Qin. 2016. 'Potentiometric sensing of aqueous phosphate by competition assays using ion-exchanger doped-polymeric membrane electrodes as transducers', *Analyst*, 141: 4573-7.

Li, Qian P., Dennis A. Hansell, and Jia-Zhong Zhang. 2008. 'Underway monitoring of nanomolar nitrate plus nitrite and phosphate in oligotrophic seawater', *Limnology and Oceanography: Methods*, 6: 319-26.

Liang, Ying, Dongxing Yuan, Quanlong Li, and Qingmei Lin. 2007. 'Flow injection analysis of nanomolar level orthophosphate in seawater with solid phase enrichment and colorimetric detection', *Marine chemistry*, 103: 122-30.

Lin, Kunning, Peicong Li, Jian Ma, and Dongxing Yuan. 2019. 'An automatic reserve flow injection method using vanadium (III) reduction for simultaneous determination of nitrite and nitrate in estuarine and coastal waters', *Talanta*, 195: 613-18.

Long, Gary L, and James D Winefordner. 1983. 'Limit of detection. A closer look at the IUPAC definition', *Analytical chemistry*, 55: 712A-24A.

Longhurst, Alan, Shubha Sathyendranath, Trevor Platt, and Carla Caverhill. 1995. 'An estimate of global primary production in the ocean from satellite radiometer data', *Journal of Plankton Research*, 17: 1245-71.

López, X., J. M. Maestre, C. Bo, and J. M. Poblet. 2001. 'Electronic properties of polyoxometalates: A DFT study of α/β-[XM12O40]n- relative stability (M=W, Mo and X a main group element)', *Journal of the American Chemical Society*, 123: 9571-76.

Los, FJ, TA Troost, and JKL Van Beek. 2014. 'Finding the optimal reduction to meet all targets—applying Linear Programming with a nutrient tracer model of the North Sea', *Journal of Marine Systems*, 131: 91-101.

Ma, J., and R. H. Byrne. 2012a. 'Flow injection analysis of nanomolar silicate using long pathlength absorbance spectroscopy', *Talanta*, 88: 484-9.

Ma, Jian, Lori Adornato, Robert H Byrne, and Dongxing Yuan. 2014. 'Determination of nanomolar levels of nutrients in seawater', *TrAC Trends in Analytical Chemistry*, 60: 1-15.

Ma, Jian, and Robert H Byrne. 2012b. 'Flow injection analysis of nanomolar silicate using long pathlength absorbance spectroscopy', *Talanta*, 88: 484-89.

Ma, Jian, Peicong Li, Zhaoying Chen, Kunning Lin, Nengwang Chen, Yiyong Jiang, Jixin Chen, Bangqin Huang, and Dongxing Yuan. 2018. 'Development of an Integrated Syringe-Pump-Based Environmental-Water Analyzer (i SEA) and Application of It for Fully Automated Real-Time Determination of Ammonium in Fresh Water', *Analytical chemistry*, 90: 6431-35.

Ma, Jian, Dongxing Yuan, and Ying Liang. 2008. 'Sequential injection analysis of nanomolar soluble reactive phosphorus in seawater with HLB solid phase extraction', *Marine chemistry*, 111: 151-59.

Ma, Jian, Yuan Yuan, and Dongxing Yuan. 2017. 'Underway analysis of nanomolar dissolved reactive phosphorus in oligotrophic seawater with automated on-line solid phase extraction and spectrophotometric system', *Analytica Chimica Acta*, 950: 80-87.

MacIntyre, G, B Plache, MR Lewis, J Andrea, S Feener, SD McLean, KS Johnson, LJ Coletti, and HW Jannasch. 2009. "ISUS/SUNA nitrate measurements in networked ocean observing systems." In *OCEANS 2009*, 1-7. IEEE.

Mackey, Katherine RM, Kathryn Roberts, Michael W Lomas, Mak A Saito, Anton F Post, and Adina Paytan. 2012. 'Enhanced solubility and ecological impact of atmospheric phosphorus deposition upon extended seawater exposure', *Environmental Science & Technology*, 46: 10438-46.

Mansour, Fotouh R., and Neil D. Danielson. 2012. 'Reverse flow-injection analysis', *TrAC Trends in Analytical Chemistry*, 40: 1-14.

Marion, GM. 1998. 'The geochemistry of natural waters: Surface and groundwater environments', *Journal of Environmental Quality*, 27: 245.

Martin, John H, Steve E Fitzwater, and R Michael Gordon. 1990. 'Iron deficiency limits phytoplankton growth in Antarctic waters', *Global Biogeochemical Cycles*, 4: 5-12.

Massart, R, M Fournier, and P Souchay. 1968. 'Effect of stannous chloride on molybdosilicic acid: detection of reduced molybdostannosilicates', *CR Acad. Sci*, 267: 1805-08.

Mather, Rhiannon L., Sarah E. Reynolds, George A. Wolff, Richard G. Williams, Sinhue Torres-Valdes, E. Malcolm S. Woodward, Angela Landolfi, Xi Pan, Richard Sanders, and Eric P. Achterberg. 2008. 'Phosphorus cycling in the North and South Atlantic Ocean subtropical gyres', *Nature Geoscience*, 1: 439-43.

McDowell, Rich W, and David P Hamilton. 2013. "Nutrients and eutrophication: introduction." In, iii-vi. CSIRO PUBLISHING.

McElroy, Michael B. 2007. 'Ocean Biogeochemical Dynamics', *Physics Today*, 60: 65-65.

McLaughlin, Karen, Andrew Dickson, Stephen B Weisberg, Kenneth Coale, Virginia Elrod, Craig Hunter, Kenneth S Johnson, Susan Kram, Raphael Kudela, and Todd Martz. 2017. 'An evaluation of ISFET sensors for coastal pH monitoring applications', *Regional Studies in Marine Science*, 12: 11-18.

Meyer, David, Ralf D Prien, Louis Rautmann, Malte Pallentin, Joanna J Waniek, and Detlef E Schulz-Bull. 2018. 'In situ determination of nitrate and hydrogen sulfide in the Baltic Sea using an ultraviolet spectrophotometer', *Frontiers in Marine Science*, 5: 431.

Michalopoulos, Panagiotis, and Robert C Aller. 2004. 'Early diagenesis of biogenic silica in the Amazon delta: alteration, authigenic clay formation, and storage', *Geochimica et Cosmochimica Acta*, 68: 1061-85.

Mills, DK, N Greenwood, S Kröger, M Devlin, DB Sivyer, D Pearce, S Cutchey, and SJ Malcolm. 2004. "New approaches to improve the detection of eutrophication in UK coastal waters." In *2004 USA-Baltic Internation Symposium*, 1-7. IEEE.

Miranda, Katrina M., Michael G. Espey, and David A. Wink. 2001. 'A Rapid, Simple Spectrophotometric Method for Simultaneous Detection of Nitrate and Nitrite', *Nitric Oxide*, 5: 62-71.

Mirceski, Valentin, and Rubin Gulaboski. 2014. 'Recent achievements in square-wave voltammetry (a review)', *Macedonian Journal of Chemistry and Chemical Engineering*, 33: 1-12.

Mirceski, Valentin, Rubin Gulaboski, Milivoj Lovric, Ivan Bogeski, Reinhard Kappl, and Markus Hoth. 2013. 'Square-wave voltammetry: a review on the recent progress', *Electroanalysis*, 25: 2411-22.

Mirceski, Valentin, Sebojka Komorsky-Lovric, and Milivoj Lovric. 2007. *Square-wave voltammetry: theory and application* (Springer Science & Business Media).

Mitchell, B Greg, Eric A Brody, Osmund Holm-Hansen, Charles McClain, and James Bishop. 1991. 'Light limitation of phytoplankton biomass and macronutrient utilization in the Southern Ocean', *Limnology and Oceanography*, 36: 1662-77.

Monte-Filho, Severino S, Marcelo B Lima, Stéfani IE Andrade, David P Harding, Yebá NM Fagundes, Sergio RB Santos, Sherlan G Lemos, and Mario CU Araújo. 2011. 'Flow–batch miniaturization', *Talanta*, 86: 208-13.

Moorcroft, Matthew J, James Davis, and Richard G Compton. 2001. 'Detection and determination of nitrate and nitrite: a review', *Talanta*, 54: 785-803.

Moore, J Keith, Mark R Abbott, James G Richman, and David M Nelson. 2000. 'The Southern Ocean at the last glacial maximum: A strong sink for atmospheric carbon dioxide', *Global Biogeochemical Cycles*, 14: 455-75.

Morris, AW, and JP Riley. 1963. 'The determination of nitrate in sea water', *Analytica Chimica Acta*, 29: 272-79.

Moscetta, Pompeo, Luca Sanfilippo, Enrico Savino, Pietro Moscetta, R Allabashi, and Amara Gunatilaka. 2009. "Instrumentation for continuous monitoring in marine environments." In *OCEANS 2009*, 1-10. IEEE.

Motomizu, Shoji, and Zhen-Hai Li. 2005. 'Trace and ultratrace analysis methods for the determination of phosphorus by flow-injection techniques', *Talanta*, 66: 332-40.

Müller, A., and C. Serain. 2000. 'Soluble molybdenum blues - 'des pudels kern'', *Accounts of Chemical Research*, 33: 2-10.

Mullin, JoB, and JP Riley. 1955. 'The colorimetric determination of silicate with special reference to sea and natural waters', *Analytica Chimica Acta*, 12: 162-76.

Murphy, J, and JP Riley. 1962a. 'Colorimetric method for determination of P in soil solution', *Anal. Chim. Acta*, 27: 31-36.

Murphy, J., and J. P. Riley. 1962b. 'A modified single solution method for the determination of phosphate in natural waters', *Analytica Chimica Acta*, 27: 31-36.

Murray, a RW, and in: AJ Bard. 1984. 'Electroanalytical chemistry', *by AJ Bard, Marcel Dekker, New York*, 13: 191.

Nagul, Edward A, Ian D McKelvie, Paul Worsfold, and Spas D Kolev. 2015. 'The molybdenum blue reaction for the determination of orthophosphate revisited: opening the black box', *Analytica Chimica Acta*, 890: 60-82.

Nedwell, D. B., T. D. Jickells, M. Trimmer, and R. Sanders. 1999. 'Nutrients in Estuaries.' in D. B. Nedwell and D. G. Raffaelli (eds.), *Advances in Ecological Research* (Academic Press).

Nehir, Münevver, Mario Esposito, Christian Begler, Carsten Frank, Oliver Zielinski, and Eric P Achterberg. 2021. 'Improved Calibration and Data Processing Procedures of OPUS Optical Sensor for High-Resolution in situ Monitoring of Nitrate in Seawater'.

Nelson, David M., Robert F. Anderson, Richard T. Barber, Mark A. Brzezinski, Ken O. Buesseler, Zanna Chase, Robert W. Collier, Mary-Lynn Dickson, Roger François, Michael R. Hiscock, Susumu Honjo, John Marra, William R. Martin, Raymond N. Sambrotto, Frederick L. Sayles, and Daniel E. Sigmon. 2002. 'Vertical budgets for organic carbon and biogenic silica in the Pacific sector of the Southern Ocean, 1996–1998', *Deep Sea Research Part II: Topical Studies in Oceanography*, 49: 1645-74.

Nelson, David M., Paul Tréguer, Mark A. Brzezinski, Aude Leynaert, and Bernard Quéguiner. 1995. 'Production and dissolution of biogenic silica in the ocean: Revised global estimates, comparison with regional data and relationship to biogenic sedimentation', *Global Biogeochemical Cycles*, 9: 359-72.

Nevison, Cynthia, Peter Hess, Stuart Riddick, and Dan Ward. 2016. 'Denitrification, leaching, and river nitrogen export in the Community Earth System Model', *Journal of Advances in Modeling Earth Systems*, 8: 272-91.

Nightingale, Adrian M, Sammer-ul Hassan, Brett M Warren, Kyriacos Makris, Gareth WH Evans, Evanthia Papadopoulou, Sharon Coleman, and Xize Niu. 2019. 'A droplet microfluidic-based sensor for simultaneous in situ monitoring of nitrate and nitrite in natural waters', *Environmental Science & Technology*, 53: 9677-85.

Ogabiela, E., S. B. Adeloju, J. Cui, Y. Wu, and W. Chen. 2015. 'A novel ultrasensitive phosphate amperometric nanobiosensor based on the integration of pyruvate oxidase with highly ordered gold nanowires array', *Biosens Bioelectron*, 71: 278-85.

Otto, L, JTF Zimmerman, GK Furnes, M Mork, R Saetre, and G Becker. 1990. 'Review of the physical oceanography of the North Sea', *Netherlands Journal of Sea Research*, 26: 161-238.

Pagliano, E., M. Onor, E. Pitzalis, Z. Mester, R. E. Sturgeon, and A. D'Ulivo. 2011. 'Quantification of nitrite and nitrate in seawater by triethyloxonium tetrafluoroborate derivatization—Headspace SPME GC–MS', *Talanta*, 85: 2511-16.

Pagliano, Enea, Juris Meija, Ralph E. Sturgeon, Zoltan Mester, and Alessandro D'Ulivo. 2012. 'Negative Chemical Ionization GC/MS Determination of Nitrite and Nitrate in Seawater Using Exact Matching Double Spike Isotope Dilution and Derivatization with Triethyloxonium Tetrafluoroborate', *Analytical chemistry*, 84: 2592-96.

Pai, Su-Cheng, Yu-Ting Su, Mei-Chen Lu, Yalan Chou, and Tung-Yuan Ho. 2021. 'Determination of Nitrate in Natural Waters by Vanadium Reduction and the Griess Assay: Reassessment and Optimization', *ACS ES&T Water*, 1: 1524-32.

Pankratova, Nadezda, Maria Cuartero, Thomas Cherubini, Gaston A Crespo, and Eric Bakker. 2017. 'In-line acidification for potentiometric sensing of nitrite in natural waters', *Analytical chemistry*, 89: 571-75.

Patey, Matthew D, Micha JA Rijkenberg, Peter J Statham, Mark C Stinchcombe, Eric P Achterberg, and Matthew Mowlem. 2008. 'Determination of nitrate and phosphate in seawater at nanomolar concentrations', *TrAC Trends in Analytical Chemistry*, 27: 169-82.

Paulot, Fabien, Daniel J Jacob, Martin T Johnson, Tom G Bell, Alexander R Baker, William C Keene, Ivan D Lima, Scott C Doney, and Charles A Stock. 2015. 'Global oceanic emission of ammonia: Constraints from seawater and atmospheric observations', *Global Biogeochemical Cycles*, 29: 1165-78.

Paytan, Adina, and Karen McLaughlin. 2007. 'The oceanic phosphorus cycle', *Chemical reviews*, 107: 563-76.

Paytan, Adina, Gregory G Shellenbarger, Joseph H Street, Meagan E Gonneea, Kristen Davis, Megan B Young, and Willard S Moore. 2006. 'Submarine groundwater discharge: an important source of new inorganic nitrogen to coral reef ecosystems', *Limnology and Oceanography*, 51: 343-48.

Pellerin, Brian A., Brian A. Bergamaschi, Bryan D. Downing, John Franco Saraceno, Jessica D. Garrett, and Lisa D. Olsen. 2013. "Optical techniques for the determination of nitrate in environmental waters: Guidelines for instrument selection, operation, deployment, maintenance, quality assurance, and data reporting." In *Techniques and Methods*, 48. Reston, VA.

Pettersson, Lage, Ingegaerd Andersson, and Lars Olof Oehman. 1986. 'Multicomponent polyanions. 39. Speciation in the aqueous hydrogen ion-molybdate(MoO42-)-hydrogenphosphate(HPO42-) system as deduced from a combined Emf-phosphorus-31 NMR study', *Inorganic Chemistry*, 25: 4726-33.

Piech, Robert, Bogusław Baś, and Władysław W Kubiak. 2008. 'The cyclic renewable mercury film silver based electrode for determination of molybdenum (VI) traces using adsorptive stripping voltammetry', *Talanta*, 76: 295-300.

Pohlmann, Thomas. 2006. 'A meso-scale model of the central and southern North Sea: consequences of an improved resolution', *Continental Shelf Research*, 26: 2367-85.

Pondaven, Philippe, Olivier Ragueneau, Paul Tréguer, Anne Hauvespre, Laurent Dezileau, and Jean Louis Reyss. 2000. 'Resolving the 'opal paradox' in the Southern Ocean', *Nature*, 405: 168-72.

Pourbaix, Marcel. 1974. 'Atlas of electrochemical equilibria in aqueous solution', *NACE*, 307.

Presti, Massimo, and Panagiotis Michalopoulos. 2008. 'Estimating the contribution of the authigenic mineral component to the long-term reactive silica accumulation on the western shelf of the Mississippi River Delta', *Continental Shelf Research*, 28: 823-38.

Prodromidis, Mamas I. 2010. 'Impedimetric immunosensors—A review', *Electrochimica Acta*, 55: 4227-33.

Puchades, R, A Maquieira, J Atienza, and MA Herrero. 1990. 'State of the art in on-line techniques coupled to flow injection analysis FIA/on-line-a critical review', *Journal of Automatic Chemistry*, 12: 163-73.

Raabe, Thomas, and Karen Helen Wiltshire. 2009. 'Quality control and analyses of the long-term nutrient data from Helgoland Roads, North Sea', *Journal of Sea Research*, 1: 3-16.

Rabalais, Nancy N, Wei-Jun Cai, Jacob Carstensen, Daniel J Conley, Brian Fry, Xinping Hu, Zoraida Quinones-Rivera, Rutger Rosenberg, Caroline P Slomp, and R Eugene Turner. 2014. 'Eutrophication-driven deoxygenation in the coastal ocean', *Oceanography*, 27: 172-83.

Rabalais, Nancy N, R Eugene Turner, and William J Wiseman Jr. 2002. 'Gulf of Mexico hypoxia, aka" The dead zone"', *Annual Review of ecology and Systematics*: 235-63.

Racicot, Joan M., Teresa L. Mako, Alexander Olivelli, and Mindy Levine. 2020. 'A Paper-Based Device for Ultrasensitive, Colorimetric Phosphate Detection in Seawater', *Sensors*, 20: 2766.

Ragueneau, Olivier, P Tréguer, A Leynaert, RF Anderson, MA Brzezinski, DJ DeMaster, RC Dugdale, J Dymond, G Fischer, and R Francois. 2000. 'A review of the Si cycle in the modern ocean: recent progress and missing gaps in the application of biogenic opal as a paleoproductivity proxy', *Global and Planetary Change*, 26: 317-65.

Rahman, S, RC Aller, and JK Cochran. 2017. 'The missing silica sink: Revisiting the marine sedimentary Si cycle using cosmogenic 32Si', *Global Biogeochemical Cycles*, 31: 1559-78.

Rasmussen, Birger. 1996. 'Early-diagenetic REE-phosphate minerals (florencite, gorceixite, crandallite, and xenotime) in marine sandstones; a major sink for oceanic phosphorus', *American Journal of Science*, 296: 601-32.

Raymond, Jason, Janet L Siefert, Christopher R Staples, and Robert E Blankenship. 2004. 'The natural history of nitrogen fixation', *Molecular biology and evolution*, 21: 541-54.

Reuter, Rainer, Thomas H Badewien, Alexander Bartholomä, Axel Braun, Andrea Lübben, and Jürgen Rullkötter. 2009. 'A hydrographic time series station in the Wadden Sea (southern North Sea)', *Ocean Dynamics*, 59: 195-211.

Revsbech, Niels Peter, Lars Hauer Larsen, Jens Gundersen, Tage Dalsgaard, Osvaldo Ulloa, and Bo Thamdrup. 2009. 'Determination of ultra-low oxygen concentrations in oxygen minimum zones by the STOX sensor', *Limnology and Oceanography: Methods*, 7: 371-81.

Ridame, Céline, and Cécile Guieu. 2002. 'Saharan input of phosphate to the oligotrophic water of the open western Mediterranean Sea', *Limnology and Oceanography*, 47: 856-69.

Rimmelin-Maury, Peggy, Thierry Moutin, and Bernard Quéguiner. 2007. 'A new method for nanomolar determination of silicic acid in seawater', *Analytica Chimica Acta*, 587: 281-86.

Rimmelin, Peggy, and Thierry Moutin. 2005. 'Re-examination of the MAGIC method to determine low orthophosphate concentration in seawater', *Analytica Chimica Acta*, 548: 174-82.

Robertson, Lesley A, and J Gijs Kuenen. 1984. 'Aerobic denitrification: a controversy revived', *Archives of Microbiology*, 139: 351-54.

Rode, Michael, Andrew J Wade, Matthew J Cohen, Robert T Hensley, Michael J Bowes, James W Kirchner, George B Arhonditsis, Phil Jordan, Brian Kronvang, and Sarah J Halliday. 2016. "Sensors in the stream: the high-frequency wave of the present." In.: ACS Publications.

Rong, Chaoying, and Fred C Anson. 1996. 'Spontaneous adsorption of heteropolytungstates and heteropolymolybdates on the surfaces of solid electrodes and the electrocatalytic activity of the adsorbed anions', *Inorganica Chimica Acta*, 242: 11-16.

Ruzicka, Jaromir, and Elo Harald Hansen. 1988. *Flow injection analysis* (John Wiley & Sons).

Saji, Viswanathan S, and Chi-Woo Lee. 2012. 'Molybdenum, molybdenum oxides, and their electrochemistry', *ChemSusChem*, 5: 1146-61.

Sakamoto-Arnold, Carole M., Kenneth S. Johnson, and Carl L. Beehler. 1986. 'Determination of hydrogen sulfide in seawater using flow injection analysis and flow analysis1', *Limnology and Oceanography*, 31: 894-900.

Salomon, Markus, and Till Markus. 2018. *Handbook on Marine Environment Protection* (Springer).

Salomons, Wim, Brian L Bayne, Egbert K Duursma, and Ulrich Förstner. 2012. *Pollution of the North Sea: an assessment* (Springer Science & Business Media).

Satoh, Hisashi, Yuji Miyazaki, Shou Taniuchi, Mamoru Oshiki, Rathnayake M. L. D. Rathnayake, Masahiro Takahashi, and Satoshi Okabe. 2017. 'Improvement of a Phosphate Ion-selective Microsensor Using Bis(dibromophenylstannyl)methane as a Carrier', *Analytical Sciences*, 33: 825-30.

Saxena, Priya, and Jayesh Ruparelia. 2019. 'Influence of supporting electrolytes on electrochemical treatability of Reactive Black 5 using dimensionally stable anode', *Journal of The Institution of Engineers (India): Series A*, 100: 299-310.

Sayles, FL, WG Deuser, JE Goudreau, WH Dickinson, TD Jickells, and P King. 1996. 'The benthic cycle of biogenic opal at the Bermuda Atlantic Time Series site', *Deep Sea Research Part I: Oceanographic Research Papers*, 43: 383-409.

Schlesinger, William H., and Emily S. Bernhardt. 2013. 'Chapter 12 - The Global Cycles of Nitrogen and Phosphorus.' in William H. Schlesinger and Emily S. Bernhardt (eds.), *Biogeochemistry (Third Edition)* (Academic Press: Boston).

Schlitzer, R. 2020. "Ocean Data View, ODV 5.2. 1." In.

Schnetger, Bernhard, and Carola Lehners. 2014a. 'Determination of nitrate plus nitrite in small volume marine water samples using vanadium (III) chloride as a reduction agent', *Marine Chemistry*, 160: 91-98.

———. 2014b. 'Determination of nitrate plus nitrite in small volume marine water samples using vanadium(III)chloride as a reduction agent', *Marine chemistry*, 160: 91-98.

Schories, Dirk, Uwe Selig, Hendrik Schubert, K Jegzentis, M Mertens, M Schubert, and T Kaminski. 2006. 'Küstengewässer-Klassifizierung deutsche Ostsee nach EU-WRRL', *Teil A: Äußere Küstengewässer. Forschungsbericht.*

Schröder, Kevin, Elke Kossel, and Mark Lenz. 2021. 'Microplastic abundance in beach sediments of the Kiel Fjord, Western Baltic Sea', *Environmental Science and Pollution Research*, 28: 26515-28.

Schumann, Ulrich, and Heidi Huntrieser. 2007. 'The global lightning-induced nitrogen oxides source', *Atmospheric Chemistry and Physics*, 7: 3823-907.

'Sea-Bird Scientific'. *website; https://www.seabird.com/nutrient-sensors/suna-v2-nitrate-sensor/family-downloads?productCategoryId=54627869922/datasheet_SUNAV2.pdf*.

Seabold, Skipper, and Josef Perktold. 2010. "Statsmodels: Econometric and statistical modeling with python." In *Proceedings of the 9th Python in Science Conference*, 10.25080. Austin, TX.

Seefeldt, Lance C, Brian M Hoffman, and Dennis R Dean. 2009. 'Mechanism of Mo-dependent nitrogenase', *Annual review of biochemistry*, 78: 701-22.

Sequeira, Margaret, Michaela Bowden, Edel Minogue, and Dermot Diamond. 2002. 'Towards autonomous environmental monitoring systems', *Talanta*, 56: 355-63.

Shankar, S Sharath, BE Kumara Swamy, and BN Chandrashekar. 2012. 'Electrochemical selective determination of dopamine at TX-100 modified carbon paste electrode: A voltammetric study', *Journal of Molecular Liquids*, 168: 80-86.

Shchekinova, Elena, Sopha-Mith Kong, Maarten Boersma, and Karen Helen Wiltshire. 2017. 'Variations of annual turnover cycles for nutrients in the north sea, german bight nutrients turnover cycles in the north sea', *Oceanography & Fisheries Open access Journal*, 2.

Shipe, Rebecca F., and Mark A. Brzezinski. 2001. 'A time series study of silica production and flux in an eastern boundary region: Santa Barbara Basin, California', *Global Biogeochemical Cycles*, 15: 517-31.

Sieben, Vincent J, Cedric FA Floquet, Iain RG Ogilvie, Matthew C Mowlem, and Hywel Morgan. 2010. 'Microfluidic colourimetric chemical analysis system: Application to nitrite detection', *Analytical Methods*, 2: 484-91.

Simon, M, V Bekele, V Kulasova, C Maul, R Oppermann, and P Rehak. 2005. 'Die Elbe und ihr Einzugsgebiet. Ein geographisch-hydrologischer und wasserwirtschaftlicher Überblick', *Internationale Kommission zum Schutz der Elbe, Magdeburg*.

Slomp, Caroline P, and Philippe Van Cappellen. 2004. 'Nutrient inputs to the coastal ocean through submarine groundwater discharge: controls and potential impact', *Journal of Hydrology*, 295: 64-86.

Snazelle, Teri T. 2018a. "Laboratory evaluation of the Sea-Bird Scientific HydroCycle-PO4 phosphate sensor." In.: US Geological Survey.

Snazelle, Teri T. 2018b. "Laboratory evaluation of the Sea-Bird Scientific HydroCycle-PO4 phosphate sensor." In *Open-File Report*, 20. Reston, VA.

Sprong, PAA, Vera Fofonova, Karen Helen Wiltshire, Stefan Neuhaus, Kai-Uwe Ludwichowski, Laura Käse, Alexey Androsov, and Katja Metfies. 2020. 'Spatial dynamics of eukaryotic microbial communities in the German Bight', *Journal of Sea Research*, 163: 101914.

Statham, Peter J. 2012. 'Nutrients in estuaries—An overview and the potential impacts of climate change', *Science of the Total Environment*, 434: 213-27.

Stein, Lisa Y. 2019. 'Insights into the physiology of ammonia-oxidizing microorganisms', *Current opinion in chemical biology*, 49: 9-15.

Talarico, Daria, Fabiana Arduini, Aziz Amine, Danila Moscone, and Giuseppe Palleschi. 2015. 'Screen-printed electrode modified with carbon black nanoparticles for phosphate detection by measuring the electroactive phosphomolybdate complex', *Talanta*, 141: 267-72.

Tanaka, Nobuyuki, Kei Unoura, and Eiki Itabashi. 1982. 'Voltammetric and spectroelectrochemical studies of dodecamolybdophosphoric acid in aqueous and water-dioxane solutions at a gold-minigrid optically transparent thin-layer electrode', *Inorganic Chemistry*, 21: 1662-66.

Tegen, Ina, and Karen E Kohfeld. 2006. 'Atmospheric transport of silicon', *The silicon cycle: human perturbations and impacts on aquatic systems*, 66: 81.

Thompson, Nicole Lee. 2018. 'Total differential capacity plot analysis using data science methods'.

Thomsen, Jens, Kenneth S Johnson, and Robert L Petty. 1983. 'Determination of reactive silicate in seawater by flow injection analysis', *Analytical chemistry*, 55: 2378-82.

Thouron, Danièle, Renaud Vuillemin, Xavier Philippon, Antonio Lourenço, Christine Provost, Antonio Cruzado, and Véronique Garçon. 2003. 'An Autonomous Nutrient Analyzer for Oceanic Long-Term in Situ Biogeochemical Monitoring', *Analytical chemistry*, 75: 2601-09.

Topcu, Cihan, Bulent Caglar, Ahmet Onder, Fatih Coldur, Sema Caglar, Eda Keles Guner, Osman Cubuk, and Ahmet Tabak. 2018. 'Structural characterization of chitosan-smectite nanocomposite and its application in the development of a novel potentiometric monohydrogen phosphate-selective sensor', *Materials Research Bulletin*, 98: 288-99.

Tréguer, Paul J, and Christina L De La Rocha. 2013. 'The world ocean silica cycle', *Annual review of marine science*, 5: 477-501.

Treguer, Paul, David M Nelson, Aleido J Van Bennekom, David J DeMaster, Aude Leynaert, and Bernard Quéguiner. 1995. 'The silica balance in the world ocean: a reestimate', *Science*, 268: 375-79.

'Trios '. *website; https://www.trios.de/en/opus.html*.

Truesdale, Victor W, and Christopher J Smith. 1976. 'The automatic determination of silicate dissolved in natural fresh water by means of procedures involving the use of either α-or β-molybdosilicic acid', *Analyst*, 101: 19-31.

Udnan, Y., I. D. McKelvie, M. R. Grace, J. Jakmunee, and K. Grudpan. 2005. 'Evaluation of on-line preconcentration and flow-injection amperometry for phosphate determination in fresh and marine waters', *Talanta*, 66: 461-6.

Van Bennekom, AJ, and GW Berger. 1984. 'Hydrography and silica budget of the Angola Basin', *Netherlands Journal of Sea Research*, 17: 149-200.

van Beusekom, Justus EE. 2018. 'Eutrophication.' in, *Handbook on Marine Environment Protection* (Springer).

van Beusekom, Justus EE, Martina Loebl, and Peter Martens. 2009. 'Distant riverine nutrient supply and local temperature drive the long-term phytoplankton development in a temperate coastal basin', *Journal of Sea Research*, 61: 26-33.

Van Cappellen, Philippe, and Ellery D Ingall. 1996. 'Redox stabilization of the atmosphere and oceans by phosphorus-limited marine productivity', *Science*, 271: 493-96.

Van Kessel, Maartje AHJ, Daan R Speth, Mads Albertsen, Per H Nielsen, Huub JM Op den Camp, Boran Kartal, Mike SM Jetten, and Sebastian Lücker. 2015. 'Complete nitrification by a single microorganism', *Nature*, 528: 555-59.

van Veen, JA Rob, Olof Sudmeijer, Cornelis A Emeis, and Henk de Wit. 1986. 'On the identification of molybdophosphate complexes in aqueous solution', *Journal of the Chemical Society, Dalton Transactions*: 1825-31.

Virtanen, Pauli, Ralf Gommers, Evgeni Burovski, Travis E Oliphant, David Cournapeau, Warren Weckesser, Pearu Peterson, Stefan van der Walt, Nikolay Mayorov, and Josh Wilson. 2018. 'Scipy/Scipy: Scipy 1.1. 0Rc1', *Zenodo*.

Virtanen, Pauli, Ralf Gommers, Travis E Oliphant, Matt Haberland, Tyler Reddy, David Cournapeau, Evgeni Burovski, Pearu Peterson, Warren Weckesser, and Jonathan Bright. 2020. 'SciPy 1.0: fundamental algorithms for scientific computing in Python', *Nature methods*, 17: 261-72.

Wang, Baoxing, and Shaojun Dong. 1996. 'Electrochemical study of isopoly-and heteropoly-oxometallates film modified microelectrodes—vi. preparation and redox properties of 12-molybdophosphoric acid and 12-molybdosilicic acid modified carbon fiber microelectrodes', *Electrochimica Acta*, 41: 895-902.

Wang, Kang, Ying-Sing Li, and Peixin He. 1998. 'In situ identification of surface species on molybdenum in different media', *Electrochimica Acta*, 43: 2459-67.

Wang, Shu, Kunning Lin, Nengwang Chen, Dongxing Yuan, and Jian Ma. 2016. 'Automated determination of nitrate plus nitrite in aqueous samples with flow injection analysis using vanadium (III) chloride as reductant', *Talanta*, 146: 744-48.

Wang, X. H., M. R. Gartia, J. Jiang, T. W. Chang, J. L. Qian, Y. Liu, X. R. Liu, and G. L. Liu. 2015. 'Audio jack based miniaturized mobile phone electrochemical sensing platform', *Sensors and Actuators B-Chemical*, 209: 677-85.

Warwick, C., A. Guerreiro, and A. Soares. 2013. 'Sensing and analysis of soluble phosphates in environmental samples: a review', *Biosens Bioelectron*, 41: 1-11.

Wasmund, Norbert, Jörg Dutz, Falk Pollehne, Herbert Siegel, and Michael L Zettler. 2016. 'Biological assessment of the Baltic Sea 2015', *Meereswiss. Ber*, 98.

Watson, Andrew J, Timothy M Lenton, and Benjamin JW Mills. 2017. 'Ocean deoxygenation, the global phosphorus cycle and the possibility of human-caused large-scale ocean anoxia', *Philosophical Transactions of the Royal Society A: Mathematical, Physical and Engineering Sciences*, 375: 20160318.

Wei, Hong, Dawei Pan, Zhengwen Zhou, Haitao Han, and Rilong Zhu. 2021. 'On-site electrochemical determination of phosphate with high sensitivity and anti-interference ability in turbid coastal waters', *Ecotoxicology and Environmental Safety*, 221: 112444.

Wheat, C Geoffrey, and James McManus. 2005. 'The potential role of ridge-flank hydrothermal systems on oceanic germanium and silicon balances', *Geochimica et Cosmochimica Acta*, 69: 2021-29.

Williams, AT, DT Tudor, and MR Gregory. 2005. "Marine debris—onshore, offshore, seafloor litter. Encylopedia of Coastal Science (Encyclopedia of Earth Sciences Series)." In.: Berlin, Germany: Springer.

Wollast, R, and FT Mackenzie. 1983. 'The global cycle of silica', *Silicon geochemistry and biogeochemistry*: 39-76.

Wood, Elwyn Devere, FAJ Armstrong, and Francis A Richards. 1967. 'Determination of nitrate in sea water by cadmium-copper reduction to nitrite', *Journal of the marine Biological Association of the United Kingdom*, 47: 23-31.

Worsfold, Paul J., Robert Clough, Maeve C. Lohan, Philippe Monbet, Peter S. Ellis, Christophe R. Quétel, Geerke H. Floor, and Ian D. McKelvie. 2013. 'Flow injection analysis as a tool for enhancing oceanographic nutrient measurements—A review', *Analytica Chimica Acta*, 803: 15-40.

'WSV-Wasserstraßen- und Schifffahrtsverwaltung des Bundes '. 2021. *Pegel Kiel-Holtenau website; https://www.pegelonline.wsv.de/gast/stammdaten?pegelnr=9610066*.

Xu, Guohua, Xiaorong Fan, and Anthony J Miller. 2012. 'Plant nitrogen assimilation and use efficiency', *Annual review of plant biology*, 63: 153-82.

Yang, Yanyan, Stefanos Banos, Gunnar Gerdts, Antje Wichels, and Marlis Reich. 2021. 'Mycoplankton biome structure and assemblage processes differ along a transect from the Elbe River down to the river plume and the adjacent marine waters', *Frontiers in microbiology*, 12: 640469.

Yin, Tianya, Stathys Papadimitriou, Victoire MC Rérolle, Martin Arundell, Christopher L Cardwell, John Walk, Martin R Palmer, Sara E Fowell, Allison Schaap, and Matthew C Mowlem. 2021. 'A novel lab-on-chip spectrophotometric pH sensor for autonomous in situ seawater measurements to 6000 m depth on stationary and moving observing platforms', *Environmental Science & Technology*, 55: 14968-78.

Yuan, Zengwei, Songyan Jiang, Hu Sheng, Xin Liu, Hui Hua, Xuewei Liu, and You Zhang. 2018. 'Human Perturbation of the Global Phosphorus Cycle: Changes and Consequences', *Environmental Science & Technology*, 52: 2438-50.

Zakem, Emily J, Alia Al-Haj, Matthew J Church, Gert L van Dijken, Stephanie Dutkiewicz, Sarah Q Foster, Robinson W Fulweiler, Matthew M Mills, and Michael J Follows. 2018. 'Ecological control of nitrite in the upper ocean', *Nature communications*, 9: 1-13.

Zehr, Jonathan P, and Raphael M Kudela. 2011. 'Nitrogen cycle of the open ocean: from genes to ecosystems', *Annual review of marine science*, 3: 197-225.

Zeldvich, Ya B. 1946. 'The oxidation of nitrogen in combustion and explosions', *J. Acta Physicochimica*, 21: 577.

Zghal, Sabrine, Ilyes Jedidi, Marc Cretin, Sophie Cerneaux, and Makki Abdelmouleh. 2020. 'One-step synthesis of highly porous carbon graphite/carbon nanotubes composite by in-situ growth of carbon nanotubes for the removal of humic acid and copper (II) from wastewater', *Diamond and Related Materials*, 101: 107557.

Zhang, J-Z, Charles J Fischer, and Peter B Ortner. 1999. 'Optimization of performance and minimization of silicate interference in continuous flow phosphate analysis', *Talanta*, 49: 293-304.

Zhang, J, GS Zhang, and SM Liu. 2005. 'Dissolved silicate in coastal marine rainwaters: comparison between the Yellow Sea and the East China Sea on the impact and potential link with primary production', *Journal of Geophysical Research: Atmospheres*, 110.

Zhang, Jia-Zhong, and JIE Chi. 2002. 'Automated analysis of nanomolar concentrations of phosphate in natural waters with liquid waveguide', *Environmental Science & Technology*, 36: 1048-53.

Zhang, Min, Dongxing Yuan, Yongming Huang, Guohe Chen, and Zhen Zhang. 2010. 'Sequential injection spectrophotometric determination of nanomolar nitrite in seawater by on-line preconcentration with HLB cartridge', *Acta Oceanologica Sinica*, 29: 100-07.

Zhang, Xinning, Bess B Ward, and Daniel M Sigman. 2020. 'Global nitrogen cycle: critical enzymes, organisms, and processes for nitrogen budgets and dynamics', *Chemical reviews*, 120: 5308-51.

Zui, OV, and JW Birks. 2000. 'Trace analysis of phosphorus in water by sorption preconcentration and luminol chemiluminescence', *Analytical chemistry*, 72: 1699-703.

Declaration

I, Mahmoud Fatehy Abdalqader Altahan, herbey declare that I have written this dissertation independently and in compliance with the scientific rules of the German Research Foundation. I have used only those sources, data and the support that I have clearly indicated. Furthermore, I assure that this dissertation has not been submitted for the award of any other academic degree and that none of my academic degrees have been withdrawn. All published manuscripts have been addressed in the appropriate places.

Kiel, October 2022

Mahmoud Fatehy Abdalqader Altahan